Computer Simulation of 3D Turbulent Wind Effects on Buildings

APPUPILLAI BASKARAN

A Thesis
in
the Centre
for
Building Studies

Presented in Partial Fulfillment of the Requirements
for the Degree of Doctor of Philosophy at
Concordia University
Montreal, Quebec, Canada

September 1990

ISBN 0-315-90819-X

Canada

COMPUTER SIMULATION OF 3D TURBULENT WIND EFFECTS ON BUILDINGS

ABSTRACT

APPUPILLAI BASKARAN, Ph.D.
CONCORDIA UNIVERSITY, 1990.

A systematic research has been performed to evaluate the wind effects on buildings through numerical modelling techniques. A new modular structure computer code named **TWIST** - **T**urbulent **WI**nd **S**imulation **T**echnique - has been developed by using the Control Volume technique. Preliminary computations have been made in evaluating wind effects on a single building exposed to normal wind flow conditions.

Only limited studies attempted to evaluate wind directionality effects on buildings as well as modelling wind environmental conditions for more than one building. To examine the feasibility of the developed computer code, TWIST has been modified and computations as well as comparisons with experimental data are performed for different wind directions. Progress has also been made in predicting the pedestrian level wind conditions for a typical downtown location of Montreal. For the considered multiple building configuration, experimental work has also been carried out in the BLWT at the Centre for Building Studies of Concordia University.

Previous studies have used the standard $k-\varepsilon$ turbulence model for creating turbulence in the flow. However, the validity of the $k-\varepsilon$ models and involved constants are questionable for recirculating and separating flows. To improve the computed results,

two simple modifications on the standard k-ε turbulence models namely, streamline curvature correction and preferential dissipation correction are identified and included in the calculations. Eventhough boundary conditions play a major task on the numerical modelling process, a suitable boundary treatment method for wind flow conditions around buildings has not been formulated. So far the standard wall functions are used as boundary conditions for all variables (u, v, w, k, ε) involved in the computation. In the present study a new zonal treatment procedure has been developed for the turbulence variables (k and ε) to bridge the solid boundary nodes with the computational domain. Extensive computations have been performed after implementing both the above mentioned modifications and the new zonal treatment method. Computed results appear improved and they also agree well with the measured data from BLWTs.

*N*umerical solutions are sensitive to the changes of some input parameters. A systematic sensitivity study has been carried out by considering three parameters, namely, the number of computational nodes, the size of the computational domain and the criteria of convergence. Software evaluating wind effects on buildings would be an attractive tool for the design process particularly if appropriate for microcomputer environment. As a first step towards this approach and as a practical application of the present research, a version of TWIST, for the evaluation of wind effects on buildings is developed and implemented in various microcomputers.

ACKNOWLEDGEMENTS

On October 9th, 1984, I met a scholar. He has been guiding me academically and personally, supporting me morally and financially, encouraging me and supervising me. He is Dr. **TED Stathopoulos** and my sincere thanks to him.

There is always a woman behind every successful man and it is my pleasure to give that credit to my dear wife **Shanthi.**

The author is indebted to Drs. D. A. Paterson and R.Basu for their help during the early stage of this research. Always, the faculty of Centre for Building Studies encouraged me, in particular, I would like to thank Drs. D.Feldman and M. Zaheer-Uddin.

DEDICATION

Dedicating this thesis to the lotus feet of **SWAMI SRI SATHYA SAI BABA**

Oh Lord !!

May all be happy

May all be healthy

May all see auspiciousness

May none suffer

Let there be peace peace peace.

TABLE OF CONTENTS

List of Tables x

List of Figures xi

CHAPTER 1 01
INTRODUCTION

1.1 General 01
1.2 Methods for Predicting the Wind Effects on Buildings 04
1.3 Thesis Organization 09

CHAPTER 2 11
LITERATURE REVIEW

2.1 Introduction 11
2.2 Literature Survey 12
2.3 Justifications for the Present Study 19

CHAPTER 3 23
NUMERICAL PROCEDURE

3.1 Introduction 23
3.2 Necessary Differential Equations 23
3.2.1 Momentum Equations 23
3.2.2 Turbulence Models 26
3.2.3 Compact Form of the Necessary Equations 28
3.3 Discretization Procedure 30
3.3.1 Discretization Methods 30
3.3.2 Discretization of the Momentum Equations 33
3.3.3 Discretization of the Continuity Equation 38
3.4 Boundary Conditions 40
3.4.1 Free Boundary 42
3.4.2 Symmetrical Boundary 42
3.4.3 Solid Boundary 42

CHAPTER 4 45
DESCRIPTION OF THE DEVELOPED COMPUTER CODE

4.1 Introduction 45
4.2 Essential Features of the Code 47
4.2.1 Structure of Module 1 47
4.2.2 Structure of Module 2 49
4.2.3 Structure of Module 3 52

CHAPTER 5 59
COMPUTATION OF WIND FLOW CONDITIONS AROUND A BUILDING

5.1 Computing for Normal Wind Flow Conditions 60
5.1.1 Comparisons of the Velocities with Measured Data 60
5.1.2 Comparisons of the Pressures With Measured Data 69
5.2 Computing the Wind Directionality Effect 74
5.2.1 Modifications on the Present Code 78
5.2.2 Predicted Flow Behaviour 81
5.2.3 Comparison of the Computed Results with Measured Data 89

CHAPTER 6 97
COMPUTATION OF WIND EFFECTS FOR MULTIPLE BUILDING CONFIGURATION

6.1 Specification of the Selected Configuration 98
6.2 Computed Results and Discussion 104
6.3 Experimental Measurements and Comparisons 106

CHAPTER 7 115
IMPROVEMENTS ON THE TURBULENCE MODELS AND BOUNDARY CONDITIONS

7.1 Modification on the Turbulence Models 116
7.1.1 Streamline Curvature Correction 116
7.1.2 Preferential Dissipation Correction 118
7.1.3 Results and Discussion 122

7.2 Zonal Treatment method for Solid Boundaries 125
7.2.1 Treatment for kinetic energy 127
7.2.2 Treatment for Dissipation Rate of Kinetic energy 128

7.3 Predicted Flow Behaviour 130
7.4 Comparisons of the Computed Results with Measured Data 143

CHAPTER 8 155
SENSITIVITY STUDY FOR NUMERICAL SOLUTION

8.1 Influence of the Domain Size on the Computed Results 156
8.2 Influence of the Number of Nodes on the Numerical Solution 165
8.3 Effect of Error Level on the Computed Solution 175

CHAPTER 9 181
APPLICATION OF THE PRESENT COMPUTER CODE

9.1 Evaluation of the Wind-Effects on Microcomputers 181
9.2 Computed Results and Discussion 185

CHAPTER 10 196
CONCLUSIONS AND RECOMMENDATIONS

10.1 Summary of the Present Contributions 196
10.2 Recommendations for Future Research 199

REFERENCES 201
APPENDIX 222
1 Derivation of Difference Equation from Differential Equation 222
2 Steps Involved in TDM Algorithm 230
3 List of Symbols and Notations 233
4 Computer Code Utilization 236

List of Tables

Table	Description	Page
1.1	Comparison of Computational Times for Different Computers (Gentzsch, 1987)	07
1.2	Estimated Computing Time for the Elliptic Boundary Value Problem (Wacker, 1987)	08
3.1	PDE's Representing Wind Flow Conditions Around Buildings	29
7.1	Modified PDE's Representing Wind Flow Conditions Around Buildings	121
8.1	Specification of the Different Computational Domain Considered in the Present Study	160
8.2	Specification of the Different Computational Grid Distribution Considered in the Present Study	167
9.1	Performance Improvements in Microcomputers	182
9.2	Comparison of CPU Time for FDBFAP (Filiatrault and Cherry,1989)	184
9.3	Specification Details for the Computer System Used in the Present Study	186
A.4.1	Numerical Values for the Sample Input	240
A.4.2	Computed Grid Distribution Data	244
A.4.3	Samples of the Output for u-velocities	246
A.4.4	Samples of the Output for v-velocities	247
A.4.5	Samples of the Output for w-velocities	248
A.4.6	Samples of the Output for Kinetic Energy	249
A.4.7	Samples of the Output for Dissipation Rate of k	250
A.4.8	Samples of the Output for Pressure	251

List of Figures

Figure	Descriptions	Page
1.1	Perspective of Wind-Induced Effects on Buildings	02
1.2	Trend of Relative Computational Cost for Numerical Flow Simulation on Large Computers (Chapman,1979)	06
3.1	A Typical xy- Face of a Control Volume	34
3.2	A Typical xz Face of a Control Volume	35
3.3	Non-Uniform Staggered Grid Arrangement with u and v Locations...	37
3.4	Boundary Locations for 3-D Wind Flow Conditions Around a Building	41
4.1	The Three Modules of TWIST	46
4.2	Structure of Module 2	50
4.3	Structure of Module 3	53
4.4	Flow Chart to Analyze the Grid System	54
4.5	Flow Chart to Analyze the Velocity Field	56
4.6	Flow Chart to Analyze the Pressure Field	57
5.1	Side view of Flow Pattern Around a Building	61
5.2	Comparison of the Upstream Longitudinal Wind Velocities (u) with and without Turbulence models	62
5.3	Comparison of the Downstream Longitudinal Wind Velocities (u) with and without Turbulence models	64
5.4	Comparison of the Upstream Lateral Wind Velocities (v) with and without Turbulence models	66
5.5	Comparison of the Downstream Lateral Wind Velocities (v) with and without Turbulence models	67
5.6	Comparisons of the Wind Speed Amplification Factors Measured around a Building and Computed by using the Standard Turbulence Models (H = 60 m)	68

5.7 Comparisons of the Wind Speed Amplification Factors Measured around a Building and Computed by using the Standard Turbulence Models (H = 180 m) 70
5.8 Wind-Induced Wall Pressures on a Building Computed by using the Standard Turbulence Models (H = 55 m) 71
5.9 Wind-Induced Wall Pressures on a Building Computed by using the Standard Turbulence Models (H = 120 m) 73
5.10 Measured and Computed Pressure Coefficients on a Flat Roof (L/H = 6) 75
5.11 Measured and Computed Pressure Coefficients on a Flat Roof (L/H = 3) 76
5.12 Plan View of the Grid Arrangement for Oblique Flow Modelling 82
5.13 Initial Assumed Flow Distribution for Oblique Wind Condition 83
5.14 Vector plots of the Computed Velocity Field Around a Building for Different Wind Directions, (h = 2 m) 85
5.15 Streamline plots of the Computed Velocity Field around a Building for Different Wind Directions, (h = 2 m) 86
5.16 Vector plots of the Computed Velocity Field around a Building for Different Wind Directions, (h = 10 m) 87
5.17 Streamline plots of the Computed Velocity Field around a Building for Different Wind Directions, (h = 10 m) 88
5.18 Comparison of the Computed Velocity Ratios with Measured Data for Different Wind Directions (h = 10 m) 90
5.19 Comparison of the Computed Velocity Ratios with Measured Data for Oblique Wind Direction (h = 2 m) 92
5.20 Comparisons of the Pressure Coefficients for the Windward Wall of a Building 94
5.21 Comparisons of the Pressure Coefficients for the Leeward Wall of a Building 95

6.1 Downtown Montreal Highlighting the Region of the Building Under Consideration 99

6.2 Probability Distributions of Hourly Mean Wind Speed at 300 m over Montreal for Daylight Hours (07:00 - 19:00) During the Winter. (Derived from Data Obtained at 10 m Height at Dorval Airport for the Period 1974 - 1983). 100

6.3 Computational Domain, Proximity Region and Buildings Considered 101

6.4 Plan and Side view of the Computational Grid 103

6.5 Vector Plots of the Computed Velocity Field around the Buildings of the Selected Configuration 105

6.6 Computed Velocity Ratios around the Buildings of the Selected Configurations 107

6.7 Experimental Set - up for Velocity Measurements 108

6.8 Velocity and Turbulence intensity Profiles for a Simulated Suburban Exposure in the Boundary Layer Wind Tunnel 110

6.9 Comparisons of the Computed and Measured Velocity Ratios at 2 m from the Ground Level for Various Locations around the Buildings .. 112

6.10 Relation Between Measured and Computed Velocity Ratios 113

7.1 Wind - Induced Wall Pressures on a Building Computed by using the Modified Turbulence Models (H = 55 m) 123

7.2 Wind - Induced Wall Pressures on a Building Computed by using the Modified Turbulence Models (H = 120 m) 124

7.3 Computed Turbulence Intensity around a Building (Side view, H = 55 m) 131

7.4 Computed Turbulence Intensity around a Building (Side view, H = 120 m) 132

7.5 Computed Dissipation rate of kinetic energy around a Building (Side view, H = 55 m) 134

7.6 Computed Dissipation Rate of Kinetic Energy around a Building (Side view, H = 120 m) 135
7.7 Computed Pressure Field around a Building (Side view, H = 55 m) 136
7.8 Computed Pressure Field around a Building (Side view, H = 120 m) 137
7.9 Comparison of the Velocity Vectors around a Building (Side view, H = 55 m) 139
7.10 Comparison of the Velocity Vectors around a Building (Side view, H = 120 m) 140
7.11 Comparison of the Streamline Plots around a Building (Side view, H = 55 m) 141
7.12 Comparison of the Streamline Plots around a Building (Side view, H = 120 m) 142
7.13 Comparisons of the Computed Velocity Profiles with Measured Data 144
7.14 Comparisons of the Computed Turbulence Intensities with Measured Data 145
7.15 Computed and Measured Pressure Coefficients on the Windward Wall of Different Buildings 147
7.16 Computed and Measured Pressure Coefficients on the Leeward and Side Walls of Different Buildings 148
7.17 Computed and Measured Pressure Coefficients on the Roof of Different Buildings 150
7.18 Computed and Measured Average Pressure Coefficients on the Walls of Buildings with Different Aspect Ratios 152
7.19 Computed and Measured Average Pressure Coefficients on the Roofs of Buildings with Different Aspect Ratios 153
8.1 Computational Mesh Distributions and Co-ordinate System used (only velocity nodes are shown) 157

8.2 Side view of Streamline Plots for Different Computational Domains 161
8.3 Exploded view of the Flow Distribution for DD2 and DD4 Computational Domain 163
8.4 Computed Pressure Coefficients on the Building Walls with Different Computational Domains 164
8.5 CPU Time or Iteration Requirements for Different Computational Domains 166
8.6 Computed Vector Plots with Different Number of Computational Nodes 169
8.7 Computed Longitudinal Velocity on the Building Upstream for Different Number of Computational Nodes 170
8.8 Computed Turbulence Intensity on the Building Upstream for Different Number of Computational Nodes 171
8.9 Computed Pressure Coefficients on the Building Walls with Different Number of Computational Nodes 173
8.10 CPU Time or Iteration Requirements with Different Number of Computational Nodes 174
8.11 Reduction in the Normalized Error Level for Different Variables of Computation 177
8.12 Effect of Normalized Error on the CPU Time or on the Number of Iterations 179
9.1 CPU Time Requirements for BLAST in Various Computer System (BLAST, 1988) 183
9.2 CPU Time taken by TWIST for Test Runs with Different Grids 187
9.3 CPU Time taken by TWIST for Test Runs with Different Number of Iterations 189
9.4 Variation of Longitudinal Velocity for Test Runs with Different Grids in Micros 191
9.5 Variation of Turbulence Intensity for Test Runs with Different Grids in Micros 192

9.6 Wall Pressure Coefficients Measured and Computed (with Different Grids) in Micros 194
A.1.1 Typical Grid Point Cluster for a One-Dimensional Problem 223
A.1.2 Piece-wise Linear Profile for the Variation of the variable 225
A.4.1 Parameters of the Computational Domain for Wind Flow Conditions around Buildings 241
A.4.2 Distance of the First Grid Node from Solid Boundaries 243
A.4.3 Available Options for Post-Processing the Numerical Output 252
A.4.4 Post-Processed Views of the Grid Arrangement 253
A.4.5 Contour Plots of the u Velocity Values after Post-Processing 254
A.4.6 Contour Plots of the Turbulence Intensity Values after Post-Processing 255
A.4.7 Vector Plots of the Post-Processed u and w Velocity Components 256
A.4.8 Post-Processed Pressure Coefficient Values on the Building Envelope 257

CHAPTER 1

INTRODUCTION

" Wind Engineering Integrates Traditional Fields of Science and Engineering - Meteorology, Fluid Dynamics, Structural Mechanics and Numerical Analysis - to Minimize the Unfavorable Effects of Wind and to Maximize the Favorable ones " - J . CERMAK

1.1 General

A systematic approach is necessary to understand the products of nature and their consequences in human life. Wind is not only an integral part of human survival but it also has significant effects when it flows around buildings. Only about three decades ago, a relatively young interdisciplinary engineering area named " ***Wind Engineering*** " was identified to address the interaction of wind in the atmospheric boundary layer with the man-made structures and natural geographical features. This new discipline has grown rapidly to accommodate the urgent need for wind engineering information by practicing engineers and its international growth can be clearly verified from the overwhelming success of the past seven international conferences. The participation of engineers and scientists from both research institutions and industries has been increasing continuously from one conference to the next as increased interest continues to evolve.

Three major wind induced effects on buildings referring to structural, environmental and energy aspects are listed in Fig.1.1 along with a few inherent details. It is the responsibility of a building engineer to design a safe and economical building against these effects. The recent trend in architecture is towards irregularly shaped buildings

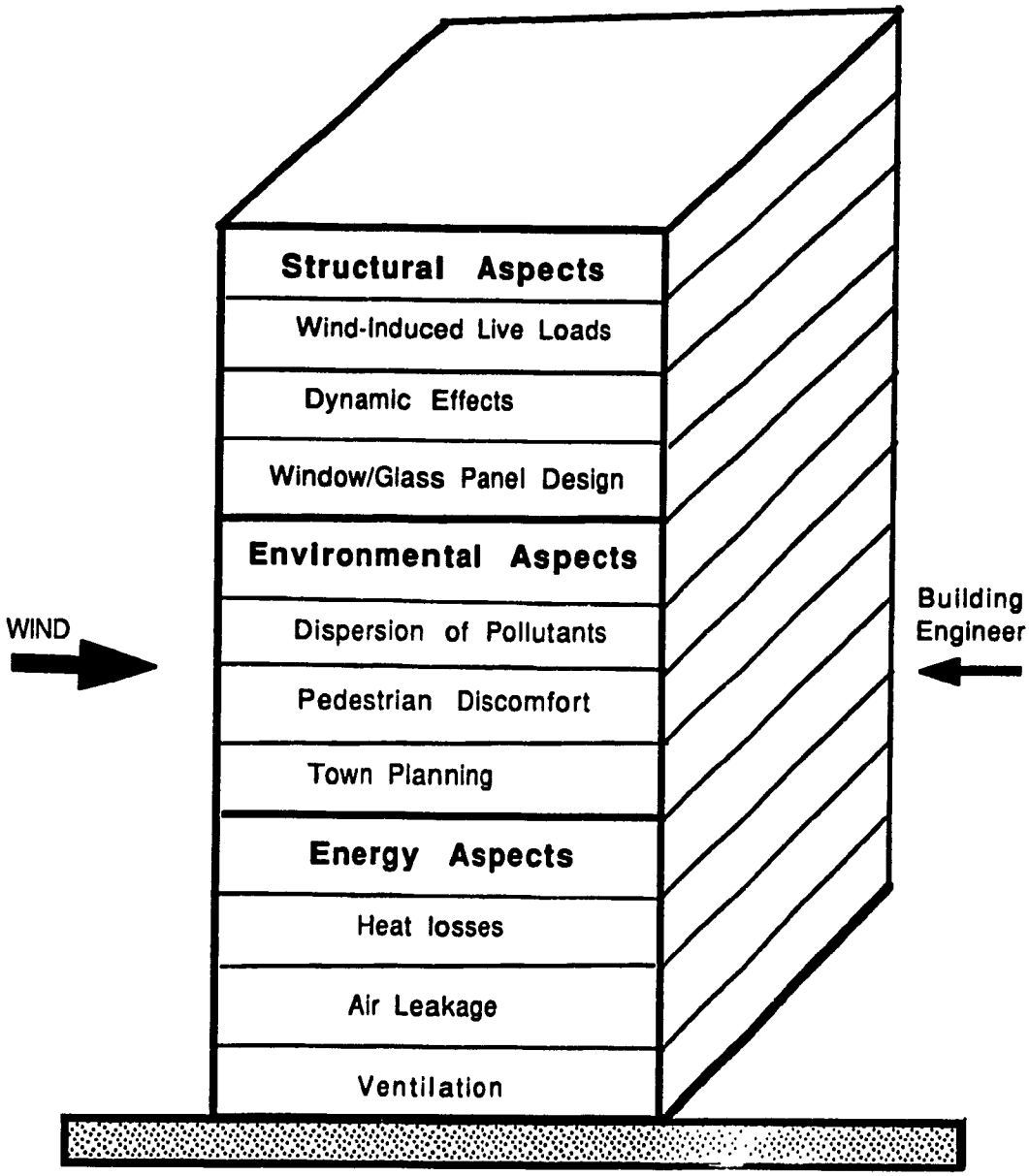

Fig.1.1: Perspective of Wind-Induced Effects on Buildings

with often severe departures from symmetry. Evaluation of local mean and fluctuating pressures is critical during the design process. Building Codes - and in particular the National Building Code of Canada - have attempted to adjust to these changes and there have been remarkable improvements in the code guidelines for wind induced loads and effects. However, advancement in construction technology and adaptation of new materials for buildings and structures favours the risk of wind - induced failures. The use of glass window and light weight cladding for exterior structural skin has increased the vulnerability of tall buildings towards wind loading. The well known John Hancock Tower glass window failure in Boston is an ideal example.

Among other emerging applications of wind engineering is the problem of air pollution. Environmental concerns urge the government officials to increase research funding for the understanding of the wind influence on the dispersion of dense gases and also scientists and researchers from other disciplines such as chemical engineering and toxicology are added to the discipline of wind engineering. Another important issue that demands clear understanding of wind engineering aspects is the increased attention by city planners and engineers to public safety and human comfort due to buffeting of pedestrians by gusting winds, soil and snow drifting. In modern cities older low buildings are usually replaced by tall residential and commercial buildings. This replacement, changes not only the outlook of a city but also creates local wind environmental conditions which are unpleasant and some times dangerous for the pedestrians walking around the new buildings. By-laws have already been implemented in some cities and the developers may have to carry out wind tunnel model studies or to consult with a wind engineer for any new construction, in order to ensure that the proposed buildings will not induce unpleasant or dangerous pedestrian level wind conditions in their vicinity.

Air infiltration causes significant energy losses in buildings. An excellent review on the influence of wind in building energy consumption is given by Arens and Williams (1977). From the review it is clear that there are mainly three ways that wind influences energy consumption in buildings, namely air infiltration and exfiltration, surface heat transmission and mechanical system efficiency.

From the above discussion it is clear that a thorough understanding and reliable quantification of wind is vitally important. Various tools available to characterize the wind effects will be presented in the following section.

1.2 Methods for Predicting the Wind Effects on Buildings

First, man attempted to measure the wind speed and thereby quantify the wind effects on buildings. Thus full scale measurements provide the basic information about real - life conditions which is essential for solving the wind loading problems. Extensive research efforts have been made towards the full scale measurements of wind effects on tall buildings (Dalgliesh and co-workers, 1975,1980). Recently a unique facility has been constructed at Texas Tech University, U.S.A to carry out research on wind effects on buildings by using a rotating low-rise building in the field. Even though full scale measurements have been successful, many disadvantages, such as long duration to obtain data, expenses involved in the process and, most importantly, the need to build the structure before measurements can be carried out made researchers think for better alternatives. However, the data from full scale wind load measurements are most urgently needed to validate the results obtained from physical and numerical modelling techniques.

Model - scale buildings and structures have also been tested in simulated flows established in Boundary Layer Wind Tunnels (BLWT). In 1956, the first successful

attempt was achieved by Cermak and tests were performed on the World Trade Center model - the first use of BLWT for building design. Physical modelling techniques were also extended to the solution of various problems such as the study of wind-wave interactions (Davenport, 1985) and mountain-valley winds (Cermak, 1984). These advancements made many appreciable contributions to the field of wind engineering. Building Codes and Standards of Practice are benefited and updated using the results from wind tunnel studies (Cermak,1987). Nevertheless, the examination of different building shapes along with their actual environmental conditions is expensive to elaborate.

On the other hand, advances in Computational Fluid Dynamics (CFD) and the trend towards Numerical Modelling provide a new tool for the solution of wind flow problems around buildings. The vigorous simulation of wind flow over a building is an ambitious and challenging undertaking. It holds the promise that the implementation of a mathematical model can be worked out for almost any practical problems. When comparing the computer speed and cost for numerical flow simulation the latter has been reduced by a factor of 10 every eight years (Fig. 1.2). For a 2-D problem requiring the solution of the Navier - Stokes Equation (NSE), Table 1.1 indicates the significant decrease in computational time achieved with the progress in computer technology. The estimated computing time for the elliptic boundary value problem is compared in Table 1.2 and it is evident that the computing speed has also been increased significantly.

Improvements in computer hardware technology also made revolutions in the storage capacity of the computers. Computer memory capabilities are translated nearly directly to the number of considered grid points during the numerical simulation. In 1950 computer memory permited the usage of only 250 grid points and this has been changed to 500,000 points during the early 1980's - see Chapman (1979). At present numerical simulations would be feasible even if one could consider meshes with 10^8 to 10^9 grid points (Kutler,1985).

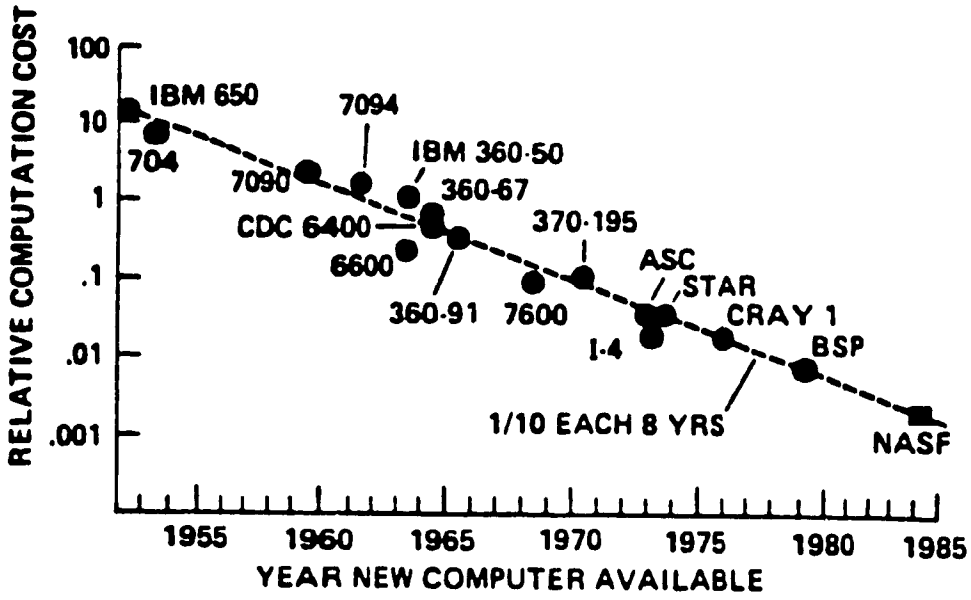

Fig.1.2: Trend of Relative Computational Cost for Numerical Flow Simulation on Large Computers (Chapman,1979)

Computer	CPU-time	
UNIVAC 1106	100	days
ICL 2980	25	"
CDC CYBER 175	4	"
IBM 3081K	3	"
CDC 7600	2	"
CDC STAR 100	1	"
ICL DAP	13	hours
HITACHI S9/IAP	10	"
FUJITSU 7890	10	"
ILLIAC IV	6	"
CRAY-1S	4	"
CYBER 205	4	"
CRAY-XMP	3	"

Table.1.1 Comparison of Computational Times for Different Computers (Gentzsch, 1987)

YEAR	DIMENSION	NODES		
		10	100	1000
1968 IBM 360-91 2 MFLOPS	1	0.01 SEC.	0.6 SEC.	40 SEC.
	2	0.03 SEC.	40 SEC.	10 HR.
	3	0.6 SEC.	2 HR.	5 WEEKS
1987 CRAY-2 100MFLOPS	1	0.0002 SEC.	0.01 SEC.	1 SEC.
	2	0.0006 SEC.	0.7 SEC.	12 MIN.
	3	0.01 SEC.	2 MIN.	15 HR.

Table.1.2 Estimated Computing Time for the Elliptic Boundary Value Problem (Wacker, 1987)

From the proceeding there is no doubt that affordable computer resources exist and can be well utilized for the numerical simulation of wind effects on buildings and structures. Therefore, this approach forms the choice, task or challenge for the present research generation.

The computer simulation approach has many apparent attractive advantages in comparison to the conventional wind tunnel and full scale methods. For instance:

* In most applications, the computational cost is many orders of magnitude lower than the cost of a corresponding experimental investigation.
* It may be easier to simulate the full scale boundary conditions analytically with computational methods rather than physically in a wind tunnel.
* The problems of scale effect and fabrication of expensive models for wind tunnel are eliminated.

1.3 Thesis Organization

The thesis, which is mainly oriented towards evaluating the wind flow conditions around buildings and wind induced effects on buildings by using the computer modelling technique, is organized in ten chapters along with three appendices. Only a few studies have been made in this field of research and chapter 2 is dedicated to their review. In chapter 3 the numerical procedure for the computer modelling of wind flow conditions is discussed. Necessary mathematical equations are grouped into a compact form. Details for the numerical discretization of the differential equations, existing methodologies for the solution of difference equations and their inter-related terms are included with their derivation. Chapter 4 describes the developed computer code which has three modules performing pre-processing, main computation and post-processing respectively.

Computation of wind flow conditions around a single building forms the subject of Chapter 5. Both velocities and pressures are computed for buildings exposed to normal as well as angled flow conditions. Description of the predicted flow behaviour and comparisons of the computed results are also included. Chapter 6 addresses the issue of numerical modelling for multiple building configurations. A typical downtown location of Montreal is selected for this exercise and wind environmental conditions are evaluated. Experiments are also carried out in the boundary layer wind-tunnel of the Centre for Building Studies of Concordia University and this chapter contains the experimental details as well as the comparisons of the experimental data with computational results.

The improvements made on the standard turbulence models and the development of a new zonal treatment method for boundary specifications of turbulence variables are described in chapter 7. Modified expressions of the turbulence model and the derivation of the zonal treatment method is given. Extensive computations and comparisons are made by implementing these modifications and the zonal treatment method. The developed new approach is also tested for different building heights .

Chapter 8 systematically examines the sensitivity of the numerical solution for changes in the computational parameters, namely, the number of computational grid nodes, the size of the flow domain and the criteria of convergence used. Results from the repetitive computer runs that are made to obtain an optimum solution are presented. A version of the computer code is developed and implemented in various microcomputers and chapter 9 analyses the results of the considered test cases. Finally, chapter 10 summarizes the achievements of the present study and identifies various problems for further research in this area.

CHAPTER 2

LITERATURE REVIEW

" Historically the study of turbulence has motivated a number of important mathematical developments. Despite this long and otherwise very fruitful effort, turbulence in fluids has removed something of a mystery and has recently begun to yield some of its secrets "
- A. CHORIN

2.1 Introduction

The previous chapter has addressed the importance of wind loads on buildings and other wind related problems. In this chapter the salient features of the previous studies are reviewed and the urgent need for additional research work is identified with justification. Conventionally, the researchers in fluid mechanics have undertaken the task of numerical modelling of fluid flow. Only very recently, a few studies were made by the wind engineering group. Prediction of wind flow around buildings is the objective of the present work. Therefore, only those studies which are directly related to this aim have been surveyed. This chapter does not discuss the studies which clearly fall into the fluid mechanics aspect - say Chorin (1978, 1980), Benodekar et al. (1985), Djilali (1987.a) and Simpson (1989). For the same reason studies which are totally devoted to numerical methods or schemes - say Raithby (1976.a,b) Patel (1982), Vandoormaul and Raithby (1984) and Jang et al. (1986) are also not reviewed.

Numerical simulation techniques have been applied in modelling indoor air movements as well. Several studies, focussing on the issue of identifying an efficient ventilation

system were carried out by Gosman et al. (1980), Chio et al. (1988) and Awbi (1989). Nevertheless, the present review excludes these studies in order to concentrate more on outdoor air environments. For the last 25 years, numerous experimental studies are carried out in the field of wind engineering and some of those data are also used by the present study to validate the computed results. The essential experimental features are explicitly presented with the comparisons.

2.2 Literature Survey

One of the early attempts in numerical modelling of turbulent flow over bluff bodies was made by Vasilic-Melling (1977). The major contribution of this work is on two-dimensional problems with the dual aim of gaining familiarity with the numerical solution procedure and of comparing the computed predictions with the available experimental data. The same procedure is extended for three-dimensional flows on surface-mounted cubes. Sensitivity analysis of the numerical solution was made by using a uniform upstream velocity profile. Experiments on flow visualization and velocity measurements were also undertaken. Comparisons of the computed results were then made with the measured data only for mean pressures. The study concluded that the numerical simulation did not faithfully represent the shear layer and recirculating flow which develops on the downstream side of the obstacle. A better treatment of the turbulence model parameters and the use of more suitable, instead of one - dimensional, wall functions has been suggested for future work. The significance of the study by Vasilic-Melling lies in the formation of a basic solution algorithm which has been subsequently modified on several occasions in order to solve the complicated nature of the interaction between wind flow and building.

Hanson et al. (1984) investigated the possibilities of developing a numerical model for wind flow problems around buildings. Their attempts include both the Random Vortex Method (RVM) and the Control Volume Method (CVM) for two - dimensional laminar flow of wind without adding the effect of turbulence intensity. The employed RVM has been developed by Chorin (1973) whereas the used CVM originated from Caretto et al. (1972). Both methods were briefly narrated and applied only to buildings with a symmetrical roof of arbitrary pitch. Attempts have not been made to compare results with other studies or with experimental data. However, the approach of this study brings out the advantages of CVM over RVM. The latter is not compatible with turbulence models and appears inefficient and expensive for the wind flow problems around three-dimensional sharp edged buildings.

Results of three - dimensional simulation of wind flow around buildings were reported by Hanson et al. (1986). The discretized non - linear equations of each cell have been solved by using Tri - Diagonal Matrix (TDM) algorithm with a successive over relaxation factor of 1.5. No direct attempts were made to include the effects of turbulence. However, the viscosity of the incoming flow was increased by using an effective term in the numerical modelling. Since the study is interested in the reverse - vortex flow which could develop between parallel buildings, only wind velocities are computed and compared with another study (Borges and Saraiva,1979) which measured the reverse wind velocity by using sand erosion technique. The computed wind speed ratios are also compared with a wind tunnel study (Penwarden and Wise,1973). From the comparison it has been noted that the deficiency of the simulation - its failure to reproduce the compactness of the wake - could be improved by the introduction of a more detailed treatment of the turbulence. Semi - empirical turbulence models such as the well - known k-ε model have been suggested for further work in this area.

As a step toward validating the results obtained from mathematical models, Summers et al. (1986) used the wind tunnel data of Everett and Lawson (1984). From the various comparisons it is clear that better computational tools are needed for the evaluation of wind effects around building configurations. Furthermore, the computed velocities at greater heights from the ground level agree better than those computed at lower heights with respect to wind tunnel measured velocity values. This provides an indication that computational methods may provide better results for wind effects on high rise buildings than for low buildings which are sitting at greater distortion of turbulence. Note that wind tunnels are also encountering the same problem in the measurement of wind effects on low buildings.

By averaging the Navier-Stokes Equation (NSE) with respect to time one can obtain the Reynolds Equation (RE). Paterson (1986.b) has made a successful attempt in solving the RE. The effect of turbulence in the flow has been conveniently accounted by means of the standard k- ε turbulence models developed by Launder and Spalding (1974). The CVM was employed to discretize the non-linear Partial Differential Equations (PDE). Algebraic equations were derived by using the Hybrid Difference Scheme (HDS). The Alternative Direction Implicit (ADI) method was applied for the solution of the resulting linear algebraic equations and the SIMPLE algorithm of Patankar (1980) was used to fulfill the condition of continuity. The computed results were compared extensively with three sets of wind tunnel experimental data (Castro and Robins, 1977, Woo, Peterka and Cermak, 1977, Davies, Quincey and Tindall, 1979) as well as with two full scale measurement results (Joubert et al., 1967 and Melbourne and Joubert, 1971). All computations and comparisons were made for a single building square or rectangular in plan form, placed in a continuous flow stream. The approaching flow has always been maintained normal to the obstacle which brings the advantage of symmetry along the main axis to the computational modelling. Due to the discretization of the RE, only mean pressures were computed and compared. For all cases compared, neither the recirculation zone nor the pressure on sides of the buildings seem to be acceptable in

comparison to wind tunnel data or full scale values. Even for such simple cases like single objects with normal incidence of wind flow, the predicted parameters need improvements, particularly at separation of the flow and in the wake.

Mathews (1987.a) also attempted to compute the wind generated pressure coefficients on a single building. A two - dimensional grid arrangement has been utilized and empirical values are used for the length scale and for the intensity of turbulence. Mean pressure coefficients are computed for two buildings having different geometry. The velocity of the approaching flow has been assumed uniform with height and normal to the predominant building dimension. The set of turbulence constants which have been proposed for the atmospheric boundary layer by Yeung and Kot (1985) is used by Mathews and Meyer (1987.b,1987.c) for the computation of pressure coefficients on a semi-circular greenhouse. The dependence of the pressure coefficients on the Reynolds number and on the exposure factor is evaluated. It has been reported that the pressure coefficients are independent of Reynolds number for Re greater than $3x10^3$. Computations are also performed for different inlet boundary layer profiles and only a small variation is noted on the computed pressure coefficients.

The wind flow conditions around a cube has been studied by Baetke (1986) on a super computer in order to evaluate the efficiency of vector codes and it has been found that the CRAY machine requires only 1/10 of the computing time in comparison to the scalar machine CDC CYBER 175. The developed code can run on any machine with architecture similar to that of the CRAY and to evaluate its accuracy, an elementary cubic shape building is used. Extensive efforts were made in predicting the wind-induced pressure values for various grid arrangements. The quadratic upstream interpolation scheme of Leonard (1979) was utilized for the numerical discretization of the momentum equations. Comparisons of the computed results with the experimental data reveal significant differences for turbulent inflow conditions (Baetke et al.,1987). Inclusion

of a better alternative method than the wall function approach is recommended to predict the wall shear stress at boundaries of separating and recirculating flow regions.

By taking 5-10 hours in a supercomputer HITAC 810-20, Murakami et al. (1987.a,1987.b) predicted wind velocities and turbulence intensities around a cubic model along with the pressure field of the flow. The time dependent NSE have been solved by using the Marker-And-Cell (MAC) method. All spatial derivatives were approximated by central difference scheme. The specialty of this approach lies in using the highly sophisticated turbulence models viz, Large Eddy Simulation (LES). Thus Reynolds stress components were replaced by the LES as explained in Ferziger (1979) along with two Smagorinsky constants whose values are given by Laurence (1987). The LES solves the NSE in time dependent form and yields the fluctuating motions of turbulence. It is also possible in the simulation to analyze the turbulence statistics of the flow field at any instant of time.

The predictions were made in two steps. First, the solution procedure develops the boundary layer and then the effect of air flow around a cubic model is analyzed. Tangential velocity components are assumed to obey a power - law profile having an exponent of 0.25. The time interval used for time marching is 0.005 on a time scale which is normalized by building height, $(\Delta t/H)$. The computed flow pattern and various turbulence statistics were compared with the measured wind tunnel data. The numerical modelling by using the LES can also predict the instantaneous wind-induced parameters. The computed turbulence intensities are found to be smaller than the measured data, near ground level. Nevertheless, this study demonstrates the capability the supercomputers of solving the complexities of unsteady NSE. The time-averaged pressure and velocity are generally the first level information required by any designer. Unfortunately, however, designers also do not have frequent access to supercomputers.

By using the standard k-ε turbulence model, Murakami and Mochida (1988,1989.a) computed the steady wind conditions around a cubic model. The standard wall functions of Launder and Spalding (1974) are used to bridge the boundary cell with the outer domain for all variables. Repeated computer runs are made with different grid arrangements for a simple building geometry. The influence of the number of nodes has also been studied as mentioned already in the work of Baetke (1986). Only mean pressure coefficients are computed for normal wind flow conditions and compared with the measured data.

Bui and Oppenheim (1987) presented some simulated results for the air flow over a scale model in a wind tunnel using the Random Vortex Method (RVM). The two-dimensional computational flow domain is divided into two regions, one inside the boundary layer where vortex sheets simulate the potential flow and the other outside the boundary layer where vortex bulbs develop in the flow. Mean wind velocity vectors are evaluated for a two-dimensional square model sitting inside a channel with a uniform approaching velocity. Attempts were not made for comparison with any measured data. This study differs from others in this field by simulating the wind tunnel environment rather than the actual atmospheric wind environment directly.

Along the lines of RVM, the flow around bluff bodies can also be represented by the Discrete Vortex Method (DVM). Inamerro and Saito (1985) used DVM to study the unsteady flow around 2D bodies having different aspect ratios. By applying the DVM, Bienkiewicz and Kutz (1989) also computed Strouhal numbers for square and rectangular prisms and compared them with respective measured wind-tunnel data. However, the expansion of RVM or DVM for turbulent three dimensional wind flow around buildings is not a trivial one (Chorin 1980, Hanson et al. 1984, Wilson 1985, Mathews 1987.a and Murakami 1989.b). So the RVM algorithm is not likely to help the

representation of the wind flow conditions around buildings in the atmospheric environment.

Some studies were also made by using commercially available software. One such general purpose computer code is called PHOENICS and it has been developed and marketed by Spalding (1981). Details of the philosophy underlying its creation and distribution policies can be found in Rosten and Spalding (1986). PHOENICS has a wide range of applications such as flow calculation in internal combustion engines (Markatos and Shan, 1985) and computation of flow in turbine cascade (Olovsson, Lofdahl and Classon, 1986). However, as previously mentioned, only studies that used PHOENICS related to air flow around buildings are reviewed here.

Haggkvist et al. (1986) predicted qualitatively the wind flow conditions around a gable roof building. The main purpose of this study was to evaluate the features of PHOENICS numerical computation of flow around buildings. Computed results for a single building configuration were compared with the measured data in their recent work (Haggkvist et al.,1989). Jansson (1987) also used PHOENICS for the evaluation of wind - induced effects on square buildings of different heights. From the comparison of the computed results with the measured data, a weak estimate of the inlet turbulence profile by the numerical modelling has been noticed. Due to this underestimation of the turbulence conditions, high suction values were predicted on the upstream part of the building roof. No comparisons were made with wind-induced pressures on the walls or velocities around the building.

Recently, Richards (1989) used PHOENICS for computer modelling of wind flow conditions around a low-rise building. Body - fitted grid systems which are generated by distorting the regular rectangular grids were used in this study to match the building

boundaries with the grid locations. Computations were performed for a variety of 2-D cases and a few pressure values were computed under 3-D analysis. The comparisons include data from a full scale study.

Another commercially available code called SOLA (SOLution Algorithm) has been developed by Hirt and co-workers (1976) based on the numerical procedure of Amsden and Harlow (1970) and Hirt and Cook (1972). Applications of this code for 3-D flow around bluff bodies were made by Hirt, Ramshaw and Stein (1978) without including any turbulence models.

2.3 Justification for the Present Study

From the review it is clear that Computational Wind Engineering (CWE) emerging from Computational Fluid Dynamics (CFD) has a high potential for further research. The idea of using the existing codes is excluded due to two reasons. First the codes are found to be expensive for long term research (Summers et al, 1986). Second most of the commercial codes do not allow any modification to their internal structure. Nevertheless, the area of CWE not only needs further work in terms of applications but it also urgently demands detailed examination of some fundamental issues. Thus a new modular structure computer code named **TWIST** - Turbulent WInd Simulation Technique - has been developed based on the Control Volume Method (CVM) as part of this current research. The main advantage of modular structure coding is that the user can extend the code for any problems of interest, by adding new modules to the existing ones. In addition, stand alone tests for debugging are also easier in modular fashion coding.

Preliminary computations have been performed to evaluate the wind effects on a single building exposed to normal wind flow conditions with the dual aim of gaining familiarity with the computer algorithm and validating the newly developed code. Most of the previous studies considered only normal flow conditions for the modelling. However, wind flow depends on the local topography and the surrounding buildings. Moreover, the information about the wind flow distribution around a building for various directions may be useful for architects and designers. To examine the feasibility of computing the wind directionality effect, TWIST has been modified and computations have been performed for different wind directions. Comparisons of the computed results with the measured data reveal that the TWIST can also predict the basic characteristics of the angled flow conditions.

Developing a software tool that can be used by architects and practicing engineers to evaluate wind environmental conditions around buildings appears to be attractive and a potential alternative tool for the expensive and time consuming measurements in the wind-tunnel. As a first step towards this approach, a cluster of buildings typically representing a downtown location of Montreal is modelled in the computer and wind velocities around the buildings are computed. To validate the computed results, experimental works were also conducted in the Boundary Layer Wind Tunnel (BLWT) at the Centre for Building Studies of Concordia University for the same configuration as that of the numerical modelling. Both the computed and measured data were converted into conventional velocity (amplification or reduction) ratios for comparison purposes.

All the previous studies considered the standard k- ε turbulence model of Launder and Spalding (1974) along with its so-called universal constants, for the creation of turbulence conditions in the numerical modelling. However, the validity of the standard k - ε turbulence models and its constants is questionable for recirculating and separating flows (Rodi 1975, Hanjalic and Launder, 1979, 1980 and Rodi and Scheuerer, 1986).

The calculated turbulent shear stress is found to be insensitive to the streamline curvature of the flow and hence the turbulent viscosity is not affected by the local flow behaviour. In addition only a low rate of dissipation of turbulent kinetic energy is computed when standard k- ε turbulence models are used. To account for these effects and to improve the predictions two simple modifications on the standard k- ε turbulence models namely streamline curvature correction and preferential dissipation correction are identified and applied in the present study.

Studies have not been initiated in the past to identify a suitable boundary treatment method for the wind flow conditions around buildings. On the other hand, specification of boundary conditions plays a major task in the numerical modelling process. Previous studies used the conventional wall-functions to bridge the solid boundary control volumes with the outer cells. When wall-functions are applied for all the five variables of the computation (u, v, w, k, ε), the near wall turbulence properties are underestimated. This is due to the fact that the wall functions are developed (Van Der Berg,1975) based on 1-D Couette flow assumptions and they are valid only for the velocity variables, (Patel et al., 1985 and Launder and Shima, 1989). Thus for the turbulence variables (k and ε) a new effective zonal treatment method is developed during the current research and implemented in the computer code. In the new procedure the local Reynolds number is used to monitor the near wall flow region and expressions derived based on the Taylor series expansion technique are applied for the computation. It has been shown that the results of the new approach agree well with the measured data once the specifications are properly implemented in the code.

Numerical solutions are always sensitive to the computational parameters, mainly the number of grid nodes on the computational domain, the extent of the computational boundary and the criteria used for convergence. A systematic sensitivity study is carried out to identify the influence of the above parameters on the output of the system.

carried out to identify the influence of the above parameters on the output of the system. The computational speed and the storage capacity of micros are increasing day by day, so as well their usage by the engineering community. To make use of this present research for the professional engineers, a version of the TWIST is developed and implemented in various microcomputer systems.

CHAPTER 3

NUMERICAL PROCEDURE

" Four factors which influence the accuracy of the predictions are the degree to which the solution satisfies the differential equation, the degree to which it satisfies the finite difference equation, the conditions imposed at the boundaries and the adequacy of the turbulence model " - D.VASILIC - MELLING

3.1 Introduction

This chapter will present and discuss the numerical procedure used for the simulation of the 3-D turbulent wind flow conditions around buildings. Here, numerical procedure, implies:

1) grouping the necessary equations (section 3.2)
2) discretizing the differential equations into difference form (section 3.3)
3) identifying and discussing the various steps involved in the specification of the boundary conditions (section 3.4)

For each section, a complete set of derivation from basic principles is provided either in the sections or in an appendix to enable the reader to follow the procedure without much assistance from further literature.

3.2 Necessary Differential Equations

3.2.1 Momentum Equations

The flow of wind around buildings is assumed to be :
- incompressible, i.e., the density of the flow is constant.

- slightly viscous, i.e., the effect of Reynolds number is large.
- continuous, i.e., it fulfils the law of conservation of mass.

In fluid mechanics, the wind flow around buildings is analogous to incompressible flow around bluff bodies. By applying Newton's second law of motion, Navier and then Stokes derived the set of equations for conservation of momentum (Hinze,1975), called the Navier-Stokes Equations (- hereafter abbreviated as NSE). For wind flow conditions around buildings, the NSE are described as:

$$\frac{\partial \hat{q}_i}{\partial t} + \hat{q}_j \frac{\partial \hat{q}_i}{\partial x_j} = -\frac{1}{\rho}\frac{\partial \hat{p}_i}{\partial x_i} + \nu \frac{\partial^2 \hat{q}_i}{\partial x_j \partial x_j} \qquad (3.1)$$

The conservation of mass can be expressed as:

$$\frac{\partial \hat{q}_i}{\partial x_i} = 0 \qquad (3.2)$$

Where:

ν is the kinematic viscosity
$\hat{q}$ is the instantaneous velocity vector
$\hat{p}$ is the fluid pressure
ρ is the density and
t is the time

The movement of air particles can be conveniently expressed by using the laws of conservation of momentum (Eq. 3.1) and mass, (Eq. 3.2). However, the wind flow around buildings is turbulent in nature. Turbulent flow motion is an irregular flow in

which the various quantities show random variation with respect to time and space. In the mathematical description of turbulent flow, it is convenient to assume that the fluid motion consist of a mean flow and a fluctuating component superimposed on the mean value. Thus, averaging NSE with respect to time over a coarse grid flow domain represents the characteristics of wind flow around buildings in space. The time-averaged NSE are called Reynolds Equations (- hereafter abbreviated as RE) and are written as follows:

$$U_j \frac{\partial u_i}{\partial x_j} = \frac{\partial}{\partial x_j}(\nu_t \frac{\partial u_i}{\partial x_j}) - \frac{\partial p}{\partial x_i} \qquad (3.3)$$

where:

U_j is the velocity vector

ν_t is the turbulent viscosity and

i , j are components in the 3D field

The turbulent viscosity is calculated by using the eddy-viscosity concept as follows:

$$\nu_t = C_\mu \frac{k^2}{\varepsilon} \qquad (3.4)$$

In the above equation, C_μ is a constant, having value 0.09. The k and ε are the kinetic energy and its dissipation rate respectively. To evaluate the value of these new variables (k and ε), the so called "Turbulence Models" are also included in the computation which will be discussed in the following subsection.

The condition for continuity of steady incompressible flow can be written as:

$$\frac{\partial u}{\partial x} + \frac{\partial v}{\partial y} + \frac{\partial w}{\partial z} = 0 \qquad (3.5)$$

3.2.2 Turbulence Models

Turbulence models will not simulate the details of the turbulent motion but only the effect of turbulence on the mean flow behaviour. One could have zero - equation or one - equation or two - equation models depending on the number of equations employed in the calculation. The zero - equation model uses only the PDE's for the mean flow fields and no differential equations for turbulence properties. In that case, the turbulence values are evaluated based on the mean flow condition for each grid point (Prandtl, 1925). The one - equation model contains a PDE for the kinetic energy, k, and it requires input of a length scale distribution based on experimental observations (Spalding, 1967).

In addition to the kinetic energy, exact transport equations can also be derived from the NSE for the dissipation rate of turbulent kinetic energy (ε), the product of kinetic energy and length scale (kl) and the vorticity (ω), as shown in Batchelor (1967), Spalding (1983) and Rodi (1984). Thus the two - equation turbulence models can be grouped by selecting the respective PDE of k and ε or k and kl or k and ω. These equations are based on the hypothesis of turbulent process and involve empirical constants or empirical functions with constants or both (Roach, 1979). A comparison was performed by Launder and Spalding (1972) who showed that the best among them was the k - ε model of turbulence based on the economy of computation, degree of universality and accuracy of the prediction. Summaries of turbulent models with various practical applications are also given by Rodi (1982,1984) and Markatos (1986). The k - ε turbulence model has been generally utilized in the current study and the equations are written as follows:

$$U_j \frac{\partial k}{\partial x_j} = \frac{\partial}{\partial x_j}\left(\frac{\nu_t}{\sigma_k}\frac{\partial k}{\partial x_j}\right) + G - \varepsilon \qquad (3.6)$$

$$U_j \frac{\partial \varepsilon}{\partial x_j} = \frac{\partial}{\partial x_j}\left(\frac{\nu_t}{\sigma_\varepsilon}\frac{\partial \varepsilon}{\partial x_j}\right) + C_1 G\frac{\varepsilon}{k} - C_2\frac{\varepsilon^2}{k} \qquad (3.7)$$

where:

$G = \nu_t \frac{\partial U_i}{\partial x_j}\left(\frac{\partial U_i}{\partial x_j} + \frac{\partial U_j}{\partial x_i}\right)$, is the generation term

$C_1 = 1.44$
$C_2 = 1.92$
$\sigma_k = 1.00$ } universal constants
$C_\mu = 0.09$
$\sigma_\varepsilon = 1.30$

Note that the values given to the so-called "universal constants" are those recommended by Launder and Spalding (1972). The values were determined mostly from experimental data of turbulent flow and in particular the value of C_μ was obtained from shear layer equilibrium. Values for C_1 and C_2 are obtained from equilibrium of wall layer and decay of grid turbulence respectively. The other constants are fixed based on computer optimization.

Complicated models have been developed and used to describe the basic features of turbulence (Ferziger,1983 and Hunt,1988). Stress equation models and algebraic stress models are some of them. The models with less restrictions in assumptions are eventually the most difficult to apply in practice. One method frequently used to describe the turbulent nature of the flow is the Large Eddy Simulation (LES). The basic idea behind this technique is to filter out scales of turbulence that are smaller than the

dimensions of the grid in which the flow is calculated. The small scale turbulence is then modelled using some simplified assumptions. Murakami et al (1987.a,1987.b) showed that by applying the LES for wind flow problems, one can predict the instantaneous pressures and velocities. Inclusion of the LES in the computational procedure demands more computational time and storage than the $k-\varepsilon$ model. In the present study it is decided to compute the wind flow around buildings by using the $k-\varepsilon$ model of turbulence.

3.2.3 Compact Form of the Necessary Equations

In developing the finite difference version for a number of equations, it is much more convenient to deal with a single general equation for any dependent variable. A compact form for the above discussed differential equations can be expressed as:

$$U_j \frac{\partial \phi}{\partial x_j} = \frac{\partial}{\partial x_j}\left[\Gamma_\Phi \frac{\partial \phi}{\partial x_j}\right] + S \qquad (3.8)$$

in which the left hand side represents the transport of ϕ by convection. In the right hand side, the first term stands for the diffusion of ϕ with the proportionality factor , Γ_ϕ whereas the second term (source term) is related to the generation or destruction of ϕ as well as any other factors that are not accounted by the convection and diffusion expression. Thus ϕ may represent both vector (u, v, w) and scalar (k, ε) properties of the flow.

Table 3.1 groups all the equations that are used to model the wind flow around buildings. It has three second order partial differential equations representing the velocities in three directions along with the fluid pressure gradient. Also there are two second order partial differential equations with empirical constants to characterize the

Viscosity	$\nu_t = C_\mu \frac{k^2}{\epsilon}$	3.4
Continuity	$\frac{\partial u}{\partial x} + \frac{\partial v}{\partial y} + \frac{\partial w}{\partial z} = 0$	3.5
Compact Form	$U_j \frac{\partial \phi}{\partial x_j} = \frac{\partial}{\partial x_j} [\Gamma_\phi \frac{\partial \phi}{\partial x_j}] + S$	3.8
x-Momentum	$U_j \frac{\partial u}{\partial x_j} = \frac{\partial}{\partial x_j} [\nu_t \frac{\partial u}{\partial x_j}] - \frac{\partial p}{\partial x_1}$	3.9
y-Momentum	$U_j \frac{\partial v}{\partial x_j} = \frac{\partial}{\partial x_j} [\nu_t \frac{\partial v}{\partial x_j}] - \frac{\partial p}{\partial x_1}$	3.10
z-Momentum	$U_j \frac{\partial w}{\partial x_j} = \frac{\partial}{\partial x_j} [\nu_t \frac{\partial w}{\partial x_j}] - \frac{\partial p}{\partial x_1}$	3.11
Kinetic Energy	$U_j \frac{\partial k}{\partial x_j} = \frac{\partial}{\partial x_j} [\frac{\nu_t}{\sigma_k} \frac{\partial k}{\partial x_j}] + G - \epsilon$	3.12
Dissipation Rate	$U_j \frac{\partial \epsilon}{\partial x_j} = \frac{\partial}{\partial x_j} [\frac{\nu_t}{\sigma_\epsilon} \frac{\partial \epsilon}{\partial x_j}] + C_1 G \frac{\epsilon}{k} - C_2 G \frac{\epsilon^2}{k}$	3.13

Table. 3.1: PDE's Representing Wind Flow Conditions Around Buildings

turbulence nature of the flow. Note that these equations are non-linear and have strong inter-linkages. This can be clearly seen from Eq. 3.13 in which ε incorporates functions of ε itself, via the source term. In addition, one more partial differential equation is listed to fulfil the condition of continuity.

3.3 Discretization Procedure

In the previous section the necessary equations which will adequately represent the wind flow conditions around buildings have been identified. The solution of these equations can be achieved only if they are discretized into the form of linear algebraic equations. What follows are the various methods of discretization and their relative merits and demerits as well as the selection of a suitable method for the solution of the problem of interest.

3.3.1 Discretization Methods

There are many methods available in the literature for numerical discretization of the non linear PDE's. The Finite Difference Method (FDM) or the Finite Element Method (FEM) is used to convert a set of PDE's into a set of algebraic equations. The FEM provides more flexibility in fitting irregular domains and in specifying the boundary conditions. However, freedom is restricted in applying the various numerical techniques such as HDS and SIMPLE (Zienkiewicz, 1972, Patankar, 1980 and Raithby et al., 1986) for FEM. Furthermore, the extension of this method into three dimensional problems is still in the research stage and needs refinements (Habashi and Peeters, 1987 , Peeters and Habashi, 1987) for the solution of problems of wind flow around buildings.

In FDM there are different techniques such as Taylor series expansion, Fourier series method and the method of weighted residuals for the discretization of the PDE. Nevertheless, it is evident from the literature (Pearson 1976, Gosman and Lai 1982, Patankar 1980, Wilson 1985, Mathews 1987.a and Murakami, 1989. b) that these methods are not suitable for the application of wind flow problems. Thus it is decided to select the Control Volume Method (CVM) as a suitable tool for the wind flow problems. However, the Random Vortex Method (RVM) which had been used for the solution of incompressible fluid flow equations, was also examined.

The RVM for the solution of the 2-D NSE was first developed and presented by Chorin (1973). The incompressible flow of a slightly viscous fluid around a bluff body can be often characterized by three main flow regimes (Summers et al. , 1985). Away from the body, the flow is largely irrotational and may thus be formulated in terms of potential flow theory. In the immediate neighbourhood of solid surfaces a boundary layer is formed in which the Prandtl boundary layer approximation is assumed to be valid. Beyond this boundary layer and in the downstream wake of the obstacle, the flow is complicated. This area has concentrated vorticity generated by the viscous interaction of the fluid with the obstacle. This representation has been numerically dealt with the following steps:

1) solve the numerical equations for the entire flow field without the effect of viscosity. The inviscid flow with scalar vorticity field, ζ, has been described by Chorin (1979) as:

$$\frac{\partial \zeta}{\partial t} + U\frac{\partial \zeta_i}{\partial x_j} = 0 \qquad (3.14)$$

The above equation can be solved by first order differential equation procedures.

2) inject the effect of viscosity into flow regimes as a random component to the motion. This can be indirectly achieved by assuming a Gaussian random distribution having zero mean and the variance as a function of Reynolds number. i.e.

$$\sigma^2 = 2\frac{\Delta t}{R_e} \qquad (3.15)$$

where Δt is the time step and Re is the Reynolds number.

3) evaluate the pressure by coupling the equation of motion with a suitable stream function (Summers et al., 1985).

The RVM is extremely good for fluid flow problems due to its grid free character. There is no need for any initial guess of the pressure field or flow separation points. Furthermore, the bluff body may have any arbitrary shape and its edges should not necessarily be sharp. As discussed in the previous chapter, a systematic application of RVM for two - dimensional wind flow problems is given by Bui and Oppenheim (1987). However, the extension of this method to three dimensional problems is not trivial. The other major drawback of this method is that it is not compatible with any standard turbulence models. This creates many difficulties in predicting the recirculation zones of the turbulent flow field.

The RVM has been improved over the years. One important improvement is the random sheet method presented by Chorin (1978). In this method the Prandtl boundary layer equation was utilized instead of the NSE in order to eliminate singularity problems. Nevertheless, the non-rotating vortex sheets cannot be valid for turbulent boundary layer flows (Chorin 1986). With all the above mentioned drawbacks, the wind flow field for three dimensional buildings with high Reynolds numbers cannot be solved successfully by the RVM. Further discussion on these matters are given by Baetke (1986), Chorin (1980, 1986), Hanson et al. (1986) and Wilson (1985).

From the above discussion, it is clear that based on both economical and computational grounds the CVM is the best tool for the solution of the problem of interest.

3.3.2 Discretization of the Momentum Equations

The basic idea of the control volume formulation is easy to understand and lends itself to direct physical interpretation. In this method, the computational domain is divided into a number of non - overlapping imaginary control cells such that each grid point or point of interest is surrounded by one control volume to compute the grid point properties. Piecewise profiles or functions expressing the variation between two adjacent grid points are used to evaluate the required integrals.

Consider a rectangular grid in order to derive the finite difference form for the differential equations. Figure 3.1 shows a typical xy face of the control volume. The node "P", with its neighbors labelled E, W, N, and S, represents the location at which the scalar variables (k, ε and p) are calculated. The three velocity components (u, v and w) are calculated at points e, w, n, and s which lie mid-way between the grid nodes. Similar notations are also provided for the xz control volume face shown in Fig. 3.2. This grid arrangement, which allocates vectors at different locations from those of scalars is known as a" *staggered grid* " configuration and has two main advantages. First, velocities lie mid-way between the locations of pressure which drive them. Thus the specification of pressure values on boundaries is not required by placing the boundaries of the computational domain and the boundaries of the building envelope on the velocity nodes of the staggered grid. Secondly, the velocities are directly available for the calculation of convective fluxes across the face of the imaginary control volume surrounding the central node. This eliminates the profile assumption of the relevant velocity values between the grid nodes. These advantages have its own price. A computer program based on the staggered grid must carry all the indexing and geometrical information about the locations of the vectors and the scalars. It must also perform

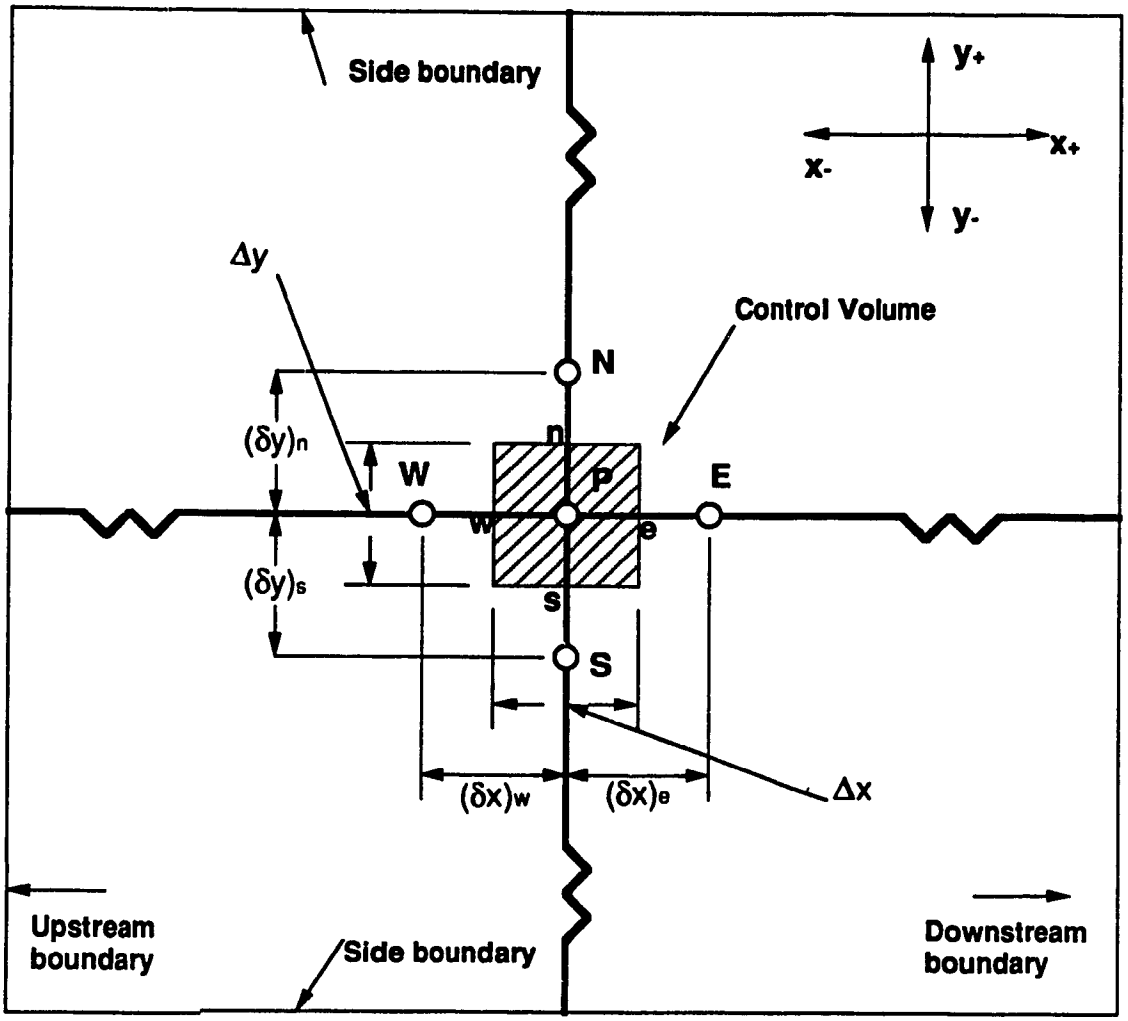

Fig.3.1: A Typical xy Face of a Control Volume

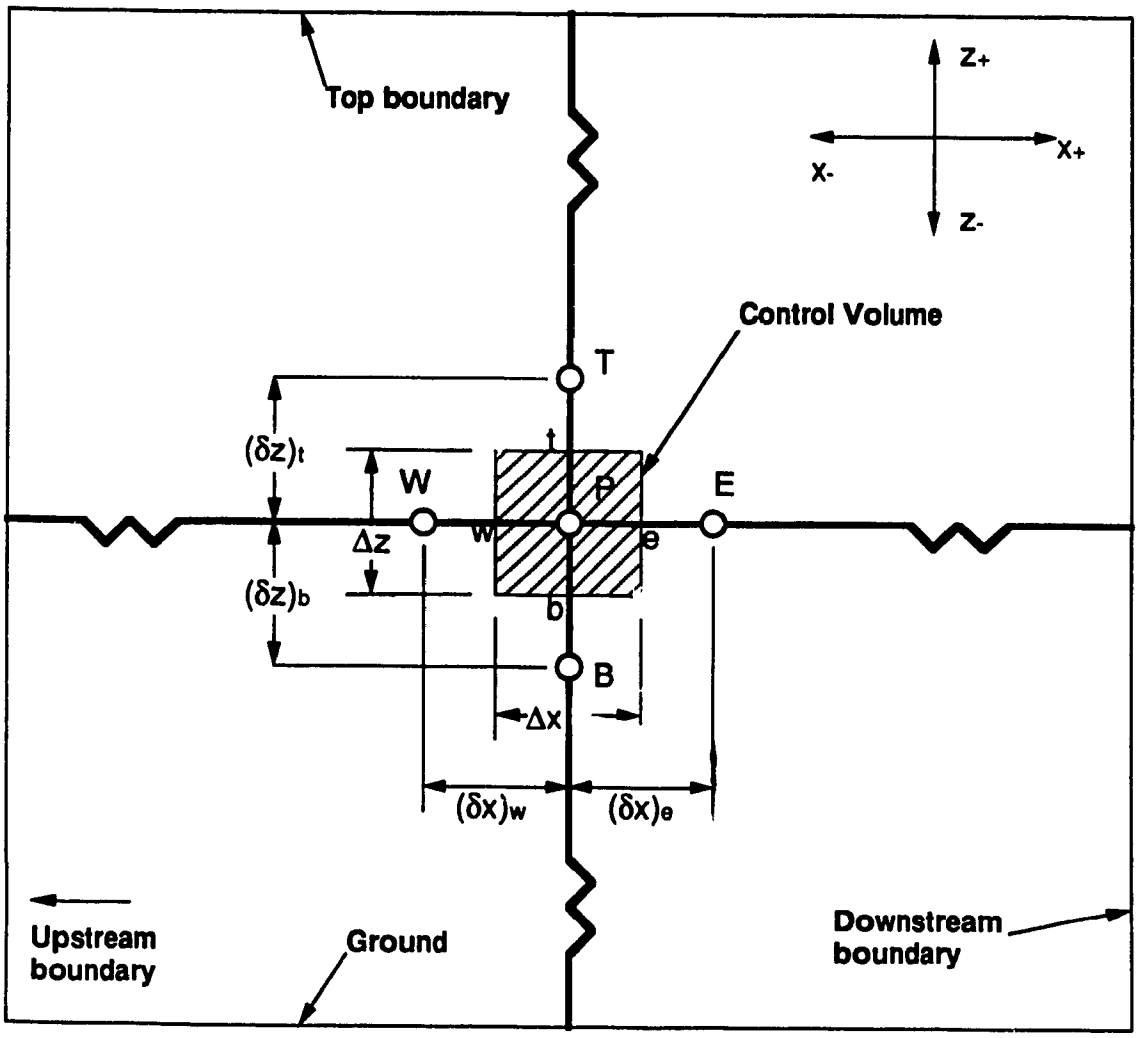

Fig.3.2: A Typical xz Face of a Control Volume

certain rather tiresome interpolations. However, the benefits of the staggered grid outright the disadvantages of this method (Vasilic-Melling, 1977, Patankar, 1980, Paterson, 1986.b, Murakami, 1989.b).

For most practical situations, the grid is not uniform as shown in Fig. 3.3. Then the pressure will not lie mid-way between the velocity components. This means that velocities will not in general lie at the center of their own control volumes. However, to keep the accuracy of the results high, it is important not to have a larger grid interval next to a smaller interval. The number of neighbors for a grid point will depend on the dimensionality of the problem. For the two dimensional situation shown in Fig. 3.3., four u neighbors are shown outside the control volume whereas if the problem of interest is three dimensional as in the case of the present study, then u would hold six neighbors instead of four.

For simplicity a one - dimensional control volume is considered and the differential equations are discretized into difference form. The various steps involved in the discretization process are given in Appendix 1. Application of the Hybrid Difference Scheme (HDS) is also shown in detail. In compact form, Eq. A.1.17 is written as:

$$a_P \ \phi_P = \left[\sum_{m=1}^{n_p} a_m \ \phi_m \right] + S_L \qquad (3.16)$$

in which:

P is the grid node where the dependent variable ϕ is computed;

n_P is the number of nodes surrounding P;

a_P is the hybrid difference scheme coefficient and

S_L is the linearized source term.

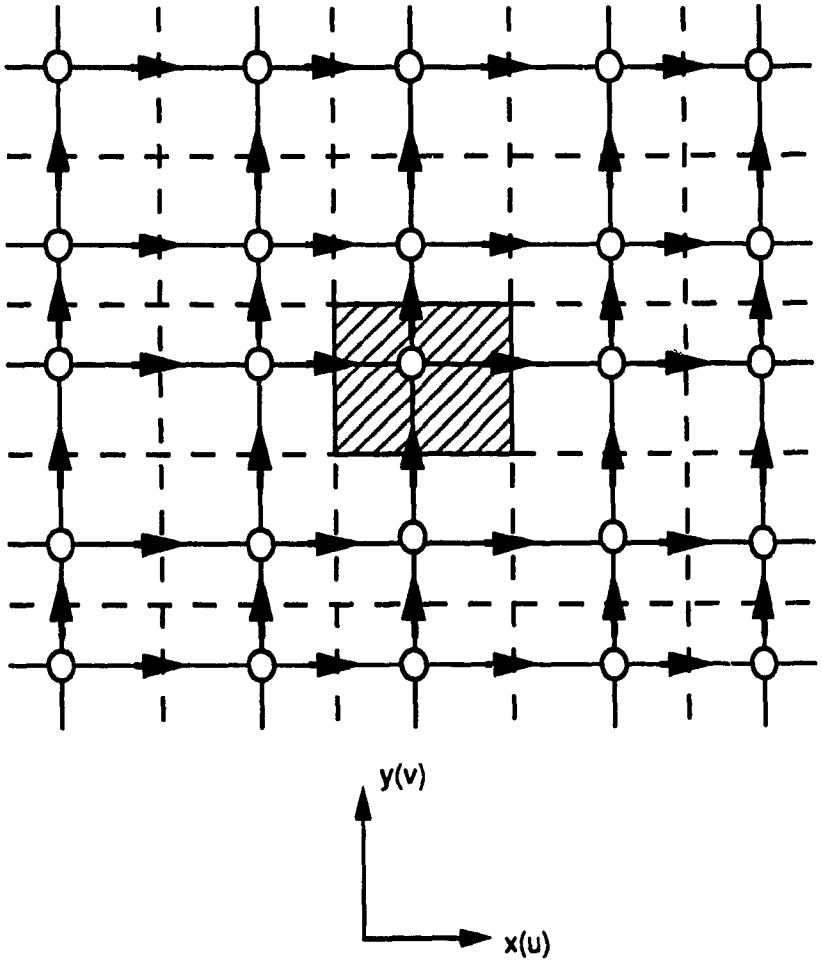

Fig. 3.3 Non-Uniform Staggered Grid Arrangement with u and v Locations. (Patankar, 1980)

3.3.3 Discretization of the Continuity Equation

In the previous section, the method for transforming five out of six PDE equations is given. The remaining equation is the one that fulfils the condition of continuity and the unknown to be found is the pressure field. However, before discussing the discretization form for continuity, it is worth referring to the inherent problems in the first three equations viz., momentum equations. This may be used to establish a link among the equations.

For the momentum equation

$$U\frac{\partial u}{\partial x} = \frac{\partial}{\partial x}\left(\Gamma_{\phi}\frac{\partial u}{\partial x}\right) + S \qquad (A.1.1)$$

the source term, S is represented by:

$$S = -\frac{\partial p}{\partial x} \qquad (3.17)$$

If the pressure field is known then there is no particular difficulty in solving Eq. A.1.1. However, determination of the pressure field seems rather obscure and there is no clear direct method available for obtaining pressure (Vasilic-Melling, 1977, Patankar, 1980, Paterson, 1986.b and Mathews, 1987.a). The unknown pressure field can be estimated by the following relationship:

Actual pressure = guessed pressure + pressure correction; or

$$p = p^{*} + p' \qquad (3.18)$$

Then the response in velocity field can be written as:

$$u = u^* + u'$$
$$v = v^* + v'$$
$$w = w^* + w' \qquad (3.19)$$

where u^*, v^* and w^* stand for the imperfect velocity field based on the guessed pressure field p^* and u', v' and w' are respective velocity correction factors.

These factors can be derived from the pressure corrections as follows:

$$u'_e = (p'_P - p'_E)d_e \qquad (3.20)$$

where:

u'_e is the velocity correction along the direction of east due to the difference in pressure between nodes P and E and

d_e is the proportionality factor $= \dfrac{\Delta y \Delta z}{a_e}$

Correction factors for other velocity components (v and w) are derived in similar fashion. Obviously these velocities will not satisfy the continuity Eq. 3.5 and its one - dimensional version

$$\frac{\partial u}{\partial x} = 0 \qquad (3.21)$$

$$(u_e - u_w)\Delta y \Delta z = 0 \qquad (3.22)$$

By combining Eq 3.19 and 3.20:

$$u_e = u^*_e + d_e(p'_P - p'_E)$$
$$u_w = u^*_w + d_w(p'_w - p'_P) \qquad (3.23)$$

Using these expressions in the above discretized continuity equation, grouping and rearranging, the following equation is obtained

$$a_P p' = a_E p'_E + a_W p'_W + S_L \qquad (3.24)$$

where:

$$\begin{aligned} a_E &= d_e \Delta y \Delta z \\ a_W &= d_w \Delta y \Delta z \\ a_P &= a_E + a_W \\ S_L &= (u^*_w - u^*_e)\,\Delta y \Delta z \end{aligned} \qquad (3.25)$$

The derivation given above is for the one dimensional situation. Three - dimensional forms can be obtained by following the same procedure. The final discretization equation for the condition of continuity or the pressure correction equation can be written as:

$$a_P p'_P = a_E p'_E + a_W p'_W + a_S p'_S + a_N p'_N + a_T p'_T + a_B p'_B + S_L \qquad (3.26)$$

Note that the above equation can also be transformed in a compact form as Eq. 3.16 in which Φ becomes the pressure correction.

3.4 Boundary Conditions

Treatment of boundaries is one of the most important modelling tasks during the numerical evaluation of wind effects on buildings. Figure 3.4 shows the various boundary locations for the calculation of 3-D turbulent wind flow conditions around a

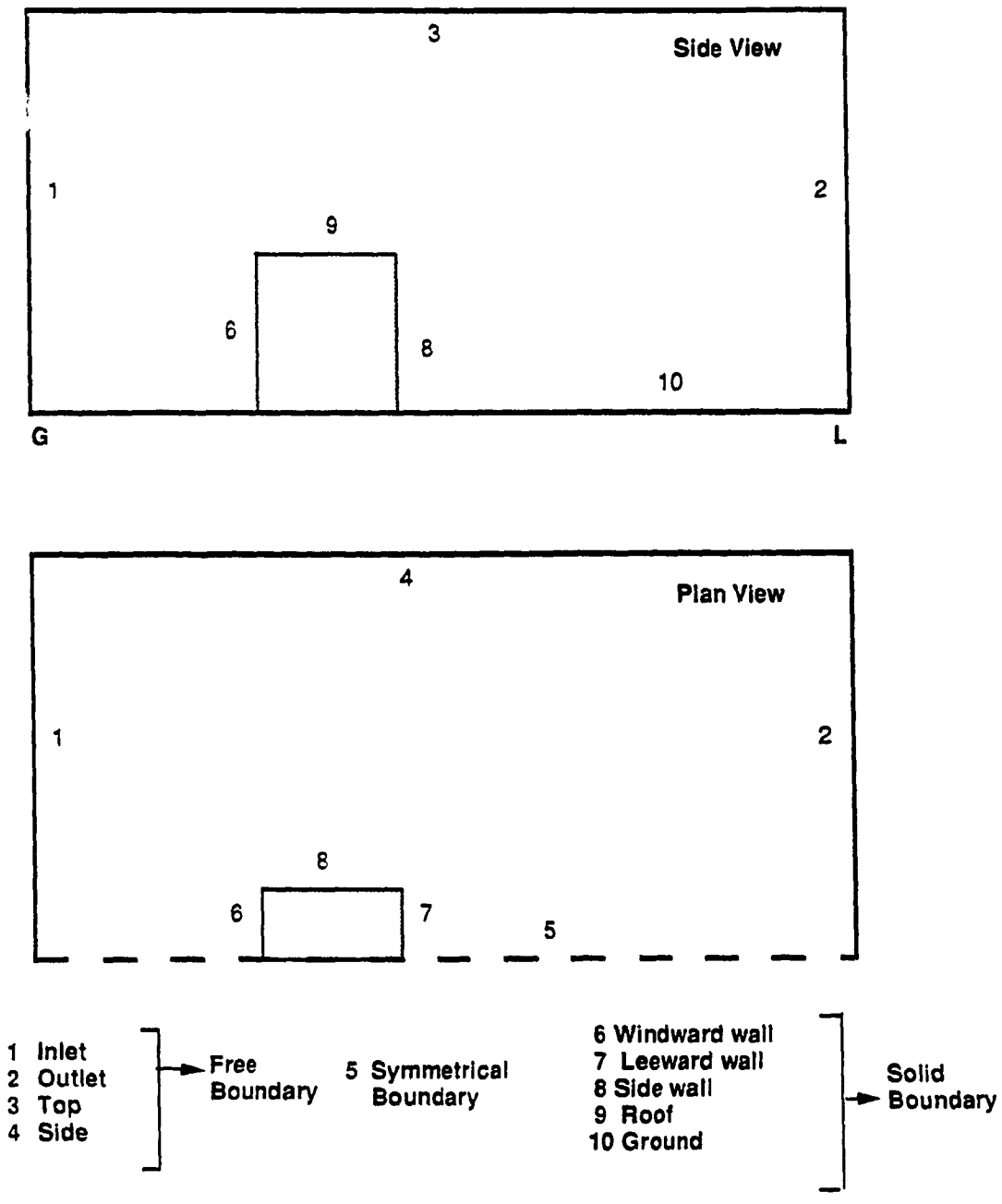

Fig.3.4: Boundary Locations for 3-D Wind Flow Conditions Around a Building

building. In total there are ten locations where information of the variables has to be transformed into the computational domain. However, based on their characteristic the boundaries can be grouped under three categories - namely free boundaries {1, 2, 3, 4}, symmetrical boundaries {5} and solid boundaries {6, 7, 8, 9, 10}. In most of the previous studies, a common approach is followed for the free and symmetrical boundaries whereas differences in treatment are found for the solid boundary.

3.4.1 Free Boundary

Dirichlet boundary conditions are applied for the air-to-air boundaries during the computational procedure. This can be easily done by transforming the values of the variable from IMAX-1 to IMAX, JMAX-1 to JMAX and KMAX-1 to KMAX, if IMAX, JMAX and KMAX are the total number of grid nodes in x, y and z directions respectively. A similar exercise will also be performed for the values of all variables on the first node.

3.4.2 Symmetrical Boundary

The normal velocity v and the normal gradient for the other quantities (u, w, k, ε) at the axis of symmetry are assumed to have zero value.

3.4.3 Solid Boundary

Researchers follow a variety of approaches for the different variables in order to identify the presence of the solid boundary in the computational procedure. For the velocity variables (u, v, w) Vasilic-Melling (1977), Murakami and Mochida, (1988,1989.a) and the present study use the wall-function approach of Launder and Spalding (1974) to bridge the Viscous Sub - Layer - hereafter abbreviated as VSL - with the outer region. In accordance with this method, the linearized source term of Eq. 3.16 is modified based on the wall shear stress calculated by:

$$\frac{U_P}{\left(\frac{\tau}{\rho}\right)_w} C_\mu^{.25} k_P^{.5} = \frac{1}{\kappa} \ln\left[E_L d_P \frac{C_\mu^{.25} k_P^{.5}}{\nu}\right] \qquad (3.27)$$

in which:

U_P is the velocity at node P

k_P is the kinetic energy at node P

d_P is the distance between P and the solid boundary

E_L is the boundary layer constant, approximately equal to 9.0 for smooth wall

κ is the Von-Karman constant and

ν is the kinematic viscosity of the fluid.

Equation 3.27 assumes a region where local production and dissipation of the flow are balanced, shear stress is uniform and the log-law of the wall

$$\frac{U_P}{U_*} = \frac{1}{\kappa} \ln\left(E_L Y^+\right) \qquad (3.28)$$

applies. This is valid for $11.5 < Y^+ < 10^3$, in which Y^+ is the local Reynolds number or normalized wall distance given by:

$$Y^+ = \frac{C_\mu^{.25} k_P^{.5}}{\nu} d_P \qquad (3.29)$$

For $0 < Y^+ < 11.65$, a linear velocity profile is appropriate, i.e.

$$\frac{U_P}{U_*} = Y^+ \qquad (3.30)$$

Thus the wall shear stress is calculated based on the local flow behaviour and as well its interaction with the solid surface.

For the turbulence kinetic energy k, the turbulence generation term, G of Eq. 3.12 is calculated after Vasilic-Melling (1977) by:

$$G = \frac{1}{vol}\int_{vol} \lambda \frac{\partial}{\partial y}\left(\sqrt{u^2 + w^2}\right) d(vol) \qquad (3.31)$$

in which, vol is the boundary control volume.

On the solid boundary, the dissipation rate of kinetic energy is evaluated by assuming a linear variation of length scale of turbulence with distance from the boundary. Using U* the wall turbulent viscosity can be written as:

$$\nu_t = \kappa U_* d_P \qquad (3.32)$$

and by using the above relation in Eq. 3.4, the rate of dissipation of kinetic energy becomes:

$$\varepsilon = \frac{C_\mu^{.75} k^{1.5}}{\kappa d_P} \qquad (3.33)$$

Thus Eqs. 3.28 to 3.33 are used as boundary conditions for all the solid boundary nodes during the computational procedure.

CHAPTER 4

DESCRIPTION OF THE DEVELOPED COMPUTER CODE

" Too much generality makes the program voluminous and inconvenient to apply for simple problems. Too little generality restricts its use to a very few situations. Initially, it is probably best to develop a rather restricted version of the program with, however, a flexible frame-work so that the scope of the program can be enlarged " - S.V.PATANKAR

4.1 Introduction

This chapter presents and discusses the details of computer code used in the present study. The computer code has been developed as part of this current research and it has been given the name **TWIST** to represent **T**urbulent **WI**nd **S**imulation **T**echnique. TWIST is composed of modular structure. The main advantage of modular coding is that the user can easily extend or modify the code for other problems of interest by adding new modules. Stand alone test for debugging are also easier in modular fashion coding. In fact there are three main modules in TWIST performing pre-processing, main computation and post-processing respectively, as shown in Fig. 4.1. These three modules can run individually or in sequence. ANSI Fortran-77 is used for coding of all three modules, however, the post-processing module 3 frequently calls the NCAR graphics subroutines (Clare et al.,1987) during its operations. Modules 2 and 3 need more storage in comparison with module 1 whereas, module 2 takes the highest CPU time among the three for its operations.

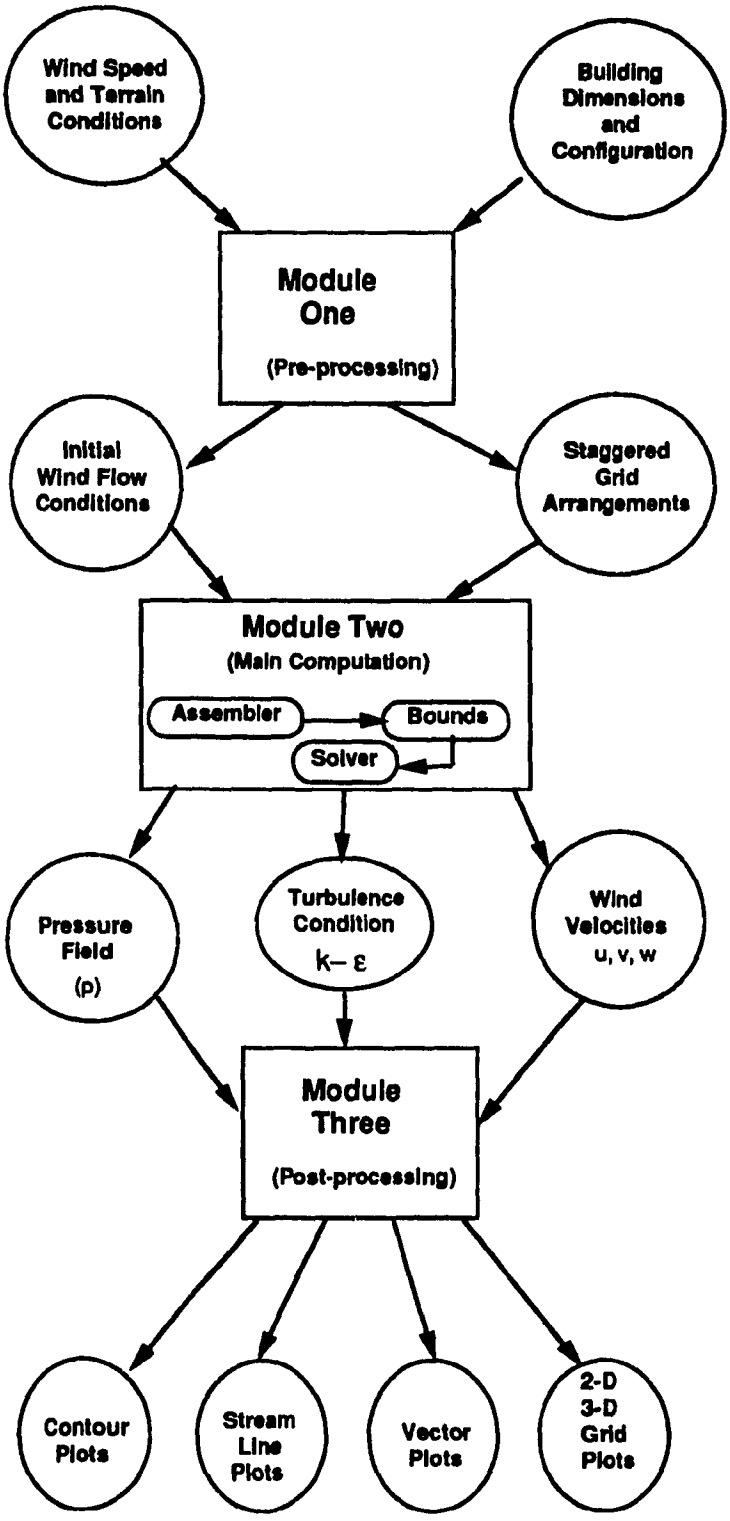

Fig.4.1: The Three Modules of TWIST

Throughout this study, TWIST has been modified and used for various problems of interest such as the case of wind blowing normal and at an angle to a single building and the study of wind environmental conditions around a group of buildings exposed to normal wind. The applicability of TWIST is also extended to various computer systems. In fact versions of TWIST can run under VAX/6.3, VAX/1.2, AST Premium 386/20, Dell 286/20 and IPC 286/12. However, the following discussion is directly applicable to the case of a single building exposed to normal wind conditions and running in the VAX/1.2 computer system. The necessary modifications for the other cases are presented in the respective chapters.

4.2 Essential Features of the Code

4.2.1 Structure of Module 1

Module 1 performs the necessary pre-processing for the computation and produces a 3-D staggered grid arrangement, the initial velocity and turbulence distributions. The need for a staggered grid arrangement is presented in the previous chapter and further details are well documented elsewhere (Patankar,1980). The unidirectional geometric progression algorithm is used for computing the grid system. In this procedure the intervals between each grid node expand in geometric progression away from the faces of the building (Paterson, 1989.b). The module needs the dimension of the computational domain in each of the three directions and the number of grid nodes required in each direction as well as on the building envelope. Having this information the program calculates the grid arrangement and stores the co-ordinates of the location of the nodes. Revisions of the computed values are always possible.

Module 1 also needs the wind speed, u_g, at gradient height, z_g, and the power law exponent appropriate for the roughness characteristics of the terrain system and the building. Based on these known parameters the longitudinal wind velocity component at height z is calculated by using a power law profile as follows:

$$\frac{u}{u_g} = \left\{\frac{z}{z_g}\right\}^{\alpha} \qquad (4.1)$$

A zero magnitude value is assumed initially for the other velocity components v and w. The semi-empirical formula of Launder and Spalding (1974) is used for the initial distribution of the kinetic energy, k and its dissipation rate ε. Necessary under-relaxation factors are also fixed during the operation of module 1. The under-relaxation factors always have values less than unity to ensure the stability of the iteration process. The following values are used for the present study, as recommended by Patankar and Spalding (1972) and Patankar (1980) for the calculations involving SIMPLE algorithm:

Variable	u	v	w	p	k	ε
Factors	.5	.5	.5	.3	.7	.7

These factors are found to be satisfactory for various 2D and 3D recirculating flows (Gosman and Pun, 1974). Attempts made by the present study in changing these standard values have not resulted in any improvements of the solution.

4.2.2 Structure of Module 2

Having the grid locations and the initial velocity and turbulence distributions, module 2 performs the iteration process for specified convergence criteria. Module 2 has three main sub modules, namely ASSEMBLER, BOUNDS and SOLVER which are internally called for all six dependent variables (u, v, w, p, k and ε). The structure of this module is shown diagrammatically in Fig. 4.2.

The ASSEMBLER allocates the velocities (u, v, w) in coordinates different from those of the scalars (p, k, ε) in accordance with the staggered grid arrangement. The Hybrid Difference Scheme (HDS) of Spalding (1972) is used to obtain the discretized coefficients for the convective terms of the differential equations. These coefficients are calculated for each grid node in a particular direction- say x direction, by considering all the grid nodes lying on the other two directions y and z and then they are assembled into Tri- Diagonal Matrix (TDM) form. The necessary details of the TDM assembly are given in Appendix 2.

BOUNDS sub-module checks the location of the assembled coefficients and modifies these coefficient values only, if the nodes lie at the boundary of the computational domain or boundaries of the building envelope. As discussed in the previous chapter the standard wall functions are applied, both for the velocity and turbulence variables. The advantageous staggered grid arrangement eliminates the need for pressure boundary conditions. During the application of boundary conditions first the local Reynolds number is calculated and then the source term of each equation is modified. To bridge the boundary cells which are inside the buildings with the outer cells a very large coefficient value is used for the source term during the calculation. The symmetry of

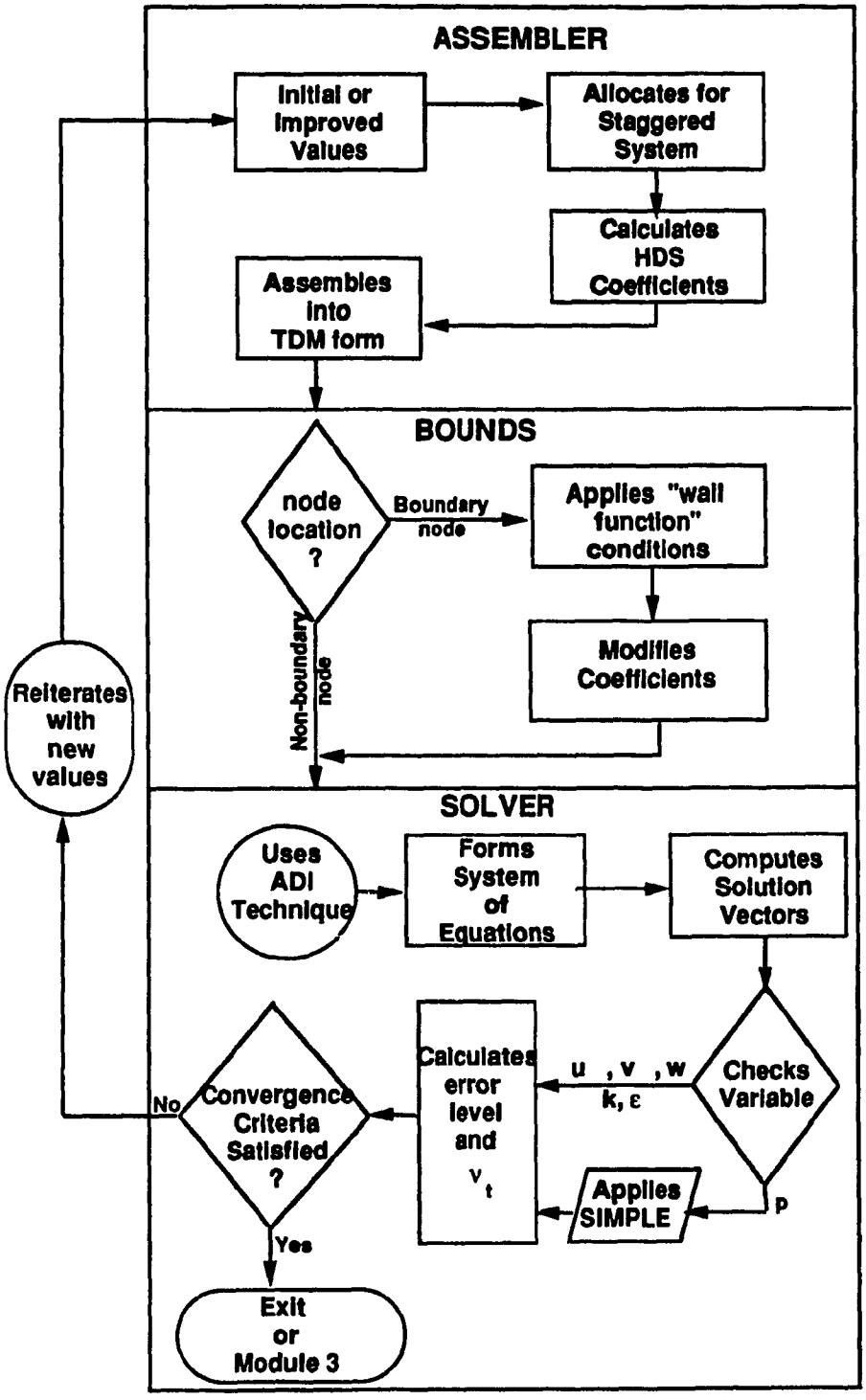

Fig.4.2: Structure of Module 2

the building which is assumed along the lateral direction is also taken into account by BOUNDS. Further description of the boundary conditions and the necessary equations have been provided in section 3.4.

SOLVER uses the Alternative Direction Implicit (ADI) method to solve the arranged system of algebraic equations and the solution vectors are copied into the old values of the respective variables. Each direction is swept once for each iteration. However, when sweeping along one direction for a particular variable all the nodes of the other directions are visited. In the computational domain, the velocity gradients are higher along the vertical (z) than the horizontal (x) and (y) direction. Hence the vertical sweeps are carried out first by using the new values, followed by the longitudinal and then the lateral directions. Thus the property of any particular variable is modified three times during each iteration process.

At the end of each iteration for all variables, except pressure (p), module 2 calculates the error levels immediately. For pressure, the SIMPLE algorithm of Patankar (1980) is utilized to correct the assumed pressure field by using the computed pressure correction value. A residual is calculated for each grid node by equating the difference equation (3.16) to zero. Summation of these residuals for all grid nodes is taken as the total error for the particular variable. This error will indicate how well the discretization equations are satisfied by the current values of the dependent variable. The initial error of the computation is used to normalize the total error and the normalized error factors are monitored based on the specified level of convergence criteria. Decisions are then made for terminating the computation or cycling for another iteration. For the present study a convergence criterion of 0.2 (- ref: section 8.3, Eq.8.1) is used whereas the algorithm is said to be diverged when the normalized error of any particular variable exceeds 20 during an iteration. Moreover, the iteration process is terminated if no convergence is achieved after 200 iterations.

However, this limit has never been reached in the present study for any computational case. In other words, the iteration is always terminated based on the convergence criterion. These values are selected after analyzing the sensitivity of the numerical solution. Steps involved in the sensitivity study and other results are presented in Chapter 8.

After solving the difference equations for all variables, the fluid turbulent viscosity is computed based on the improved kinetic energy and its dissipation rate. Thus module 2 brings a new set of improved values to the computational domain during each iteration process.

4.2.4 Structure of Module 3

MODULE 3 performs post-processing based on user needs and thus it is usually activated after module 2 by using the converged solution values. Various existing options in module 3 are pictured in Fig. 4.3 and they are grouped under three main headings namely analyzing grid system, analyzing velocity field and analyzing pressure field. The processed output can be viewed, printed or plotted based on the selected output device. Comparing with the other modules, module 3 has a more user friendly character which is helpful for the clear understanding and the interpolation of extensive numerical output following the computation. The CPU time consumed by module 3 mainly depends on the selection made by the user. However, for analyzing a particular variable with a set of options, it takes approximately 15 minutes of CPU time in the VAX/1.2 computer system.

Figure 4.4 shows the steps involved in analyzing the grid system. Selecting a 2D view will provide the options of displaying plots under three major co-ordinate planes

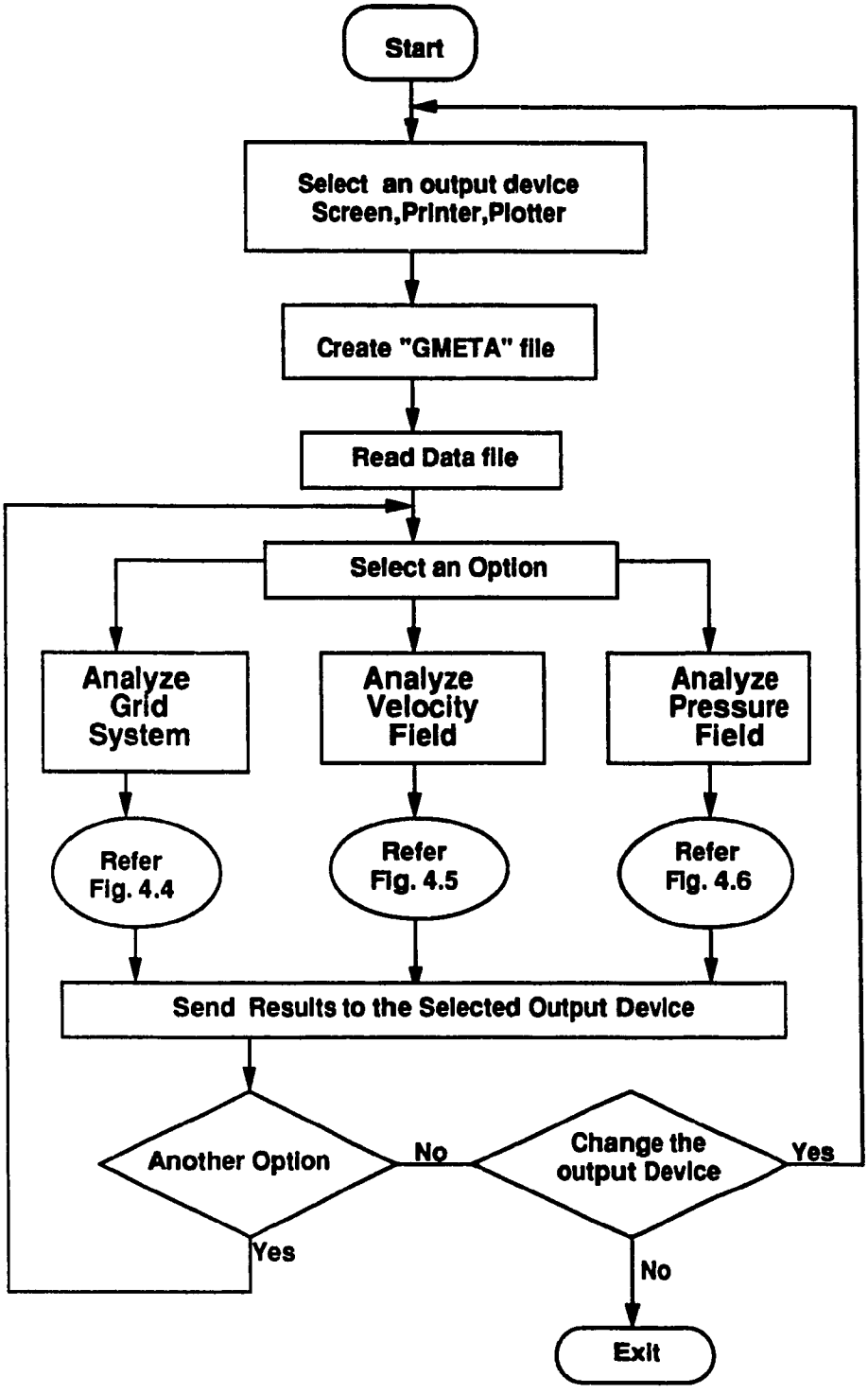

Fig.4.3: Structure of Module 3

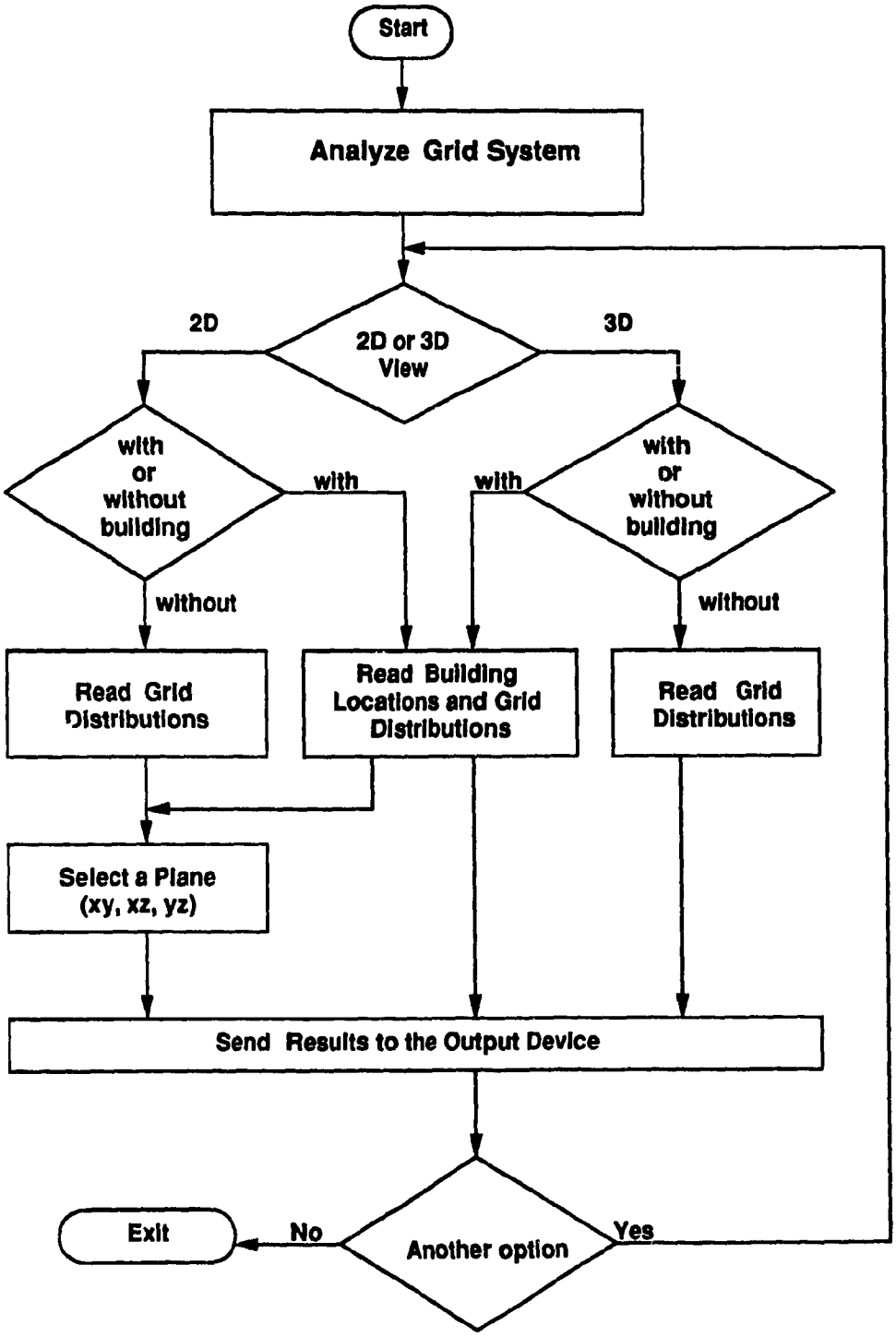

Fig. 4.4: Flow Chart to Analyze the Grid System

sectional view. The clustering of grids around the building and the relative locations of the building with respect to the computational domain are observed by selecting the 3D view option. Both 2D and 3D grid arrangements are obtained with and without including the buildings.

The converged velocity field is analyzed by using the options shown in Fig. 4.5. The data corresponding to a particular plane of computational domain can be extracted and tabulated. Different kinds of plots such as Linear, Log-log or Semi-log can be obtained by using the extracted data. These plots are useful in identifying the variation of a velocity component at different locations. By following the same procedure the changes in the velocities at different locations can be viewed and compared. Finally the dispersion of a variable over a surface can be displayed by means of contour plots. The least square distance method is used to interpolate the extracted data for contouring.

The flow distributions and changes in the flow directions are easily identified by using the option of vector or streamline plots. Only 2D patterns are feasible and the following convention is used for all the vector and streamline plots presented in the thesis:

- to obtain for xy plane (plan view) the components u and v are used.,
- to obtain for xz plane (side view) the components u and w are used.,
- to obtain for yz plane (sectional view) the components v and w are used.

The wind-induced pressure coefficients on the building envelope are also computed and displayed. The options for analyzing the pressure field is shown in Fig. 4.6 which is similar to Fig. 4.4. Conventionally the pressure coefficients on buildings are calculated by normalizing the static pressure with dynamic pressure at the roof height of the building. The post-processed coefficients are used for the evaluation of wind-induced design loads for buildings and structures. The processed values always represent the

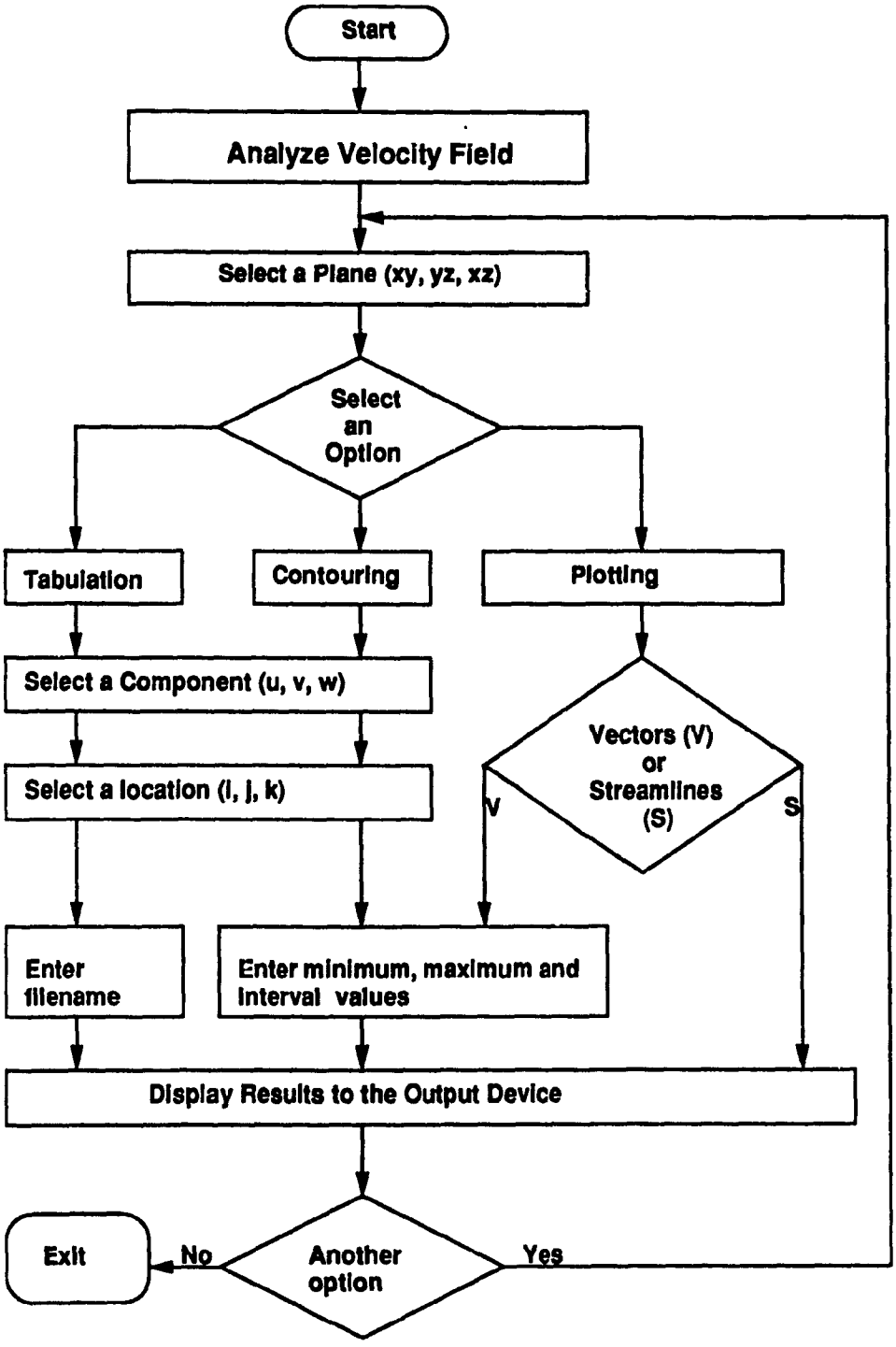

Fig. 4.5: Flow Chart to Analyze the Velocity Field

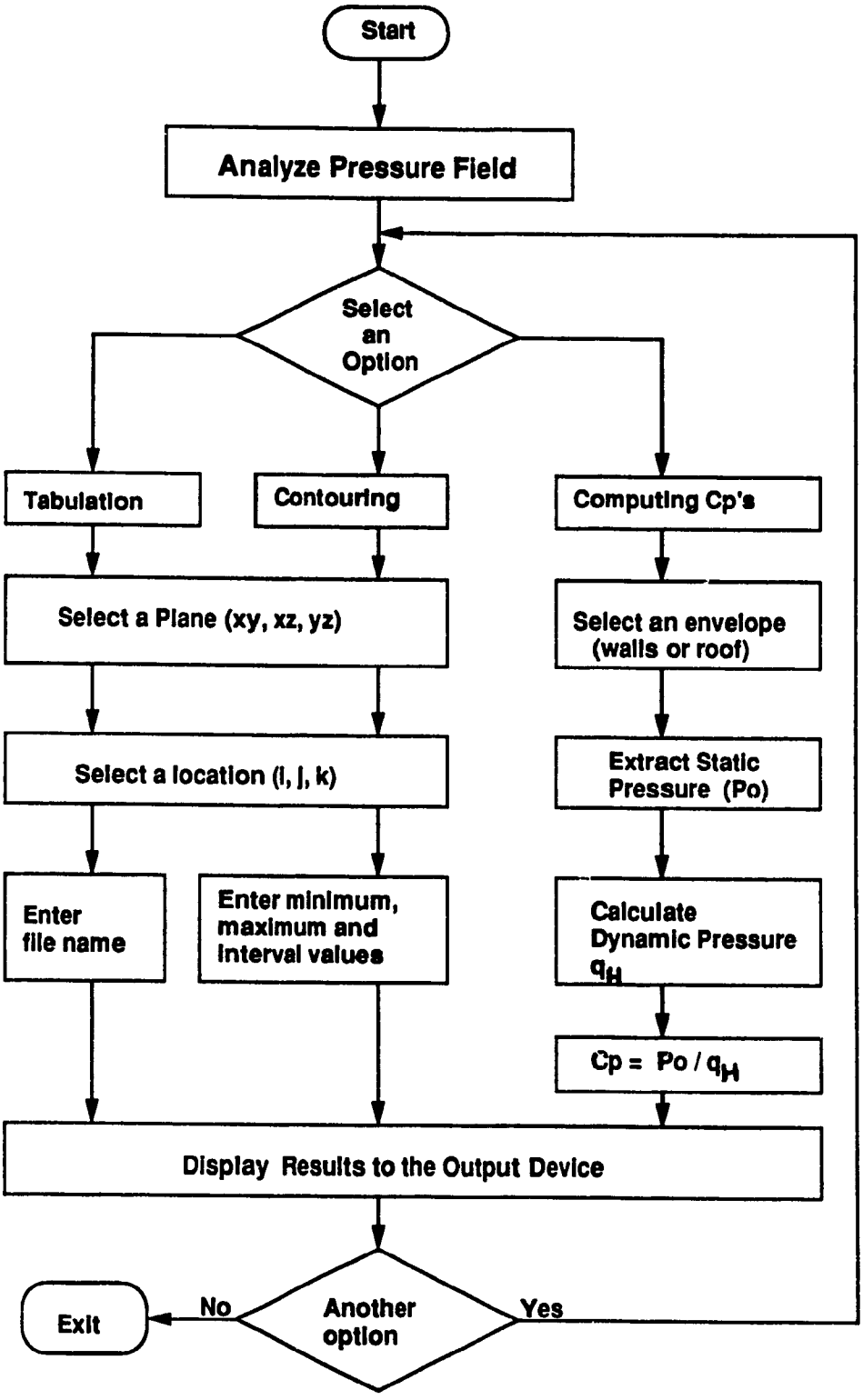

Fig.4.6: Flow Chart to Analyze the Pressure Field

worst case for each horizontal plane, however, options are also available to calculate the coefficients for any desired location on the building envelope.

CHAPTER 5

COMPUTATION OF WIND FLOW CONDITIONS AROUND A BUILDING

" A good turbulence model has extensive universality and it is not too complex to develop or use. Universality implies that a single set of empirical constants inserted into the equations, provides close simulation of a large variety of flow. Complexity is measured by the number of equations which the model contains " - B. LAUNDER

The prediction of three - dimensional turbulent wind flow around a single building is described in this chapter. Based on the direction of the incoming wind both normal flow effects and angled flow conditions have been studied. In the former, the flow bisects the building width and the flow domain can be divided into two symmetrical regions. By taking advantage of symmetry, only half of the domain is included in the calculations. Two parameters, namely wind-induced velocities around the building and wind-generated pressures on the building, are derived from the computed numerical output. The first section presents and discusses these parameters by comparing them with respective measured data from boundary layer wind tunnels. Comparisons have also been made with the results of the previous computational attempts.

Section two considers the oblique flow conditions for numerical modelling. This has been carried out as a feasibility study to examine the flexibility of the developed code, TWIST, for modifications. Moreover, the features of the angled flow conditions are identified and compared with those of the normal flow case. The necessary modifications on the code to account for angled flow conditions, the predicted flow behaviour and the comparison of the computed results with experimental data are also presented in this section. It is worth to mention again that computations have been performed by including the standard $k - \varepsilon$ models for the turbulence in the flow field and the universal wall functions are

used to specify boundary conditions, both for velocity and turbulence variables. Computations are made by using the VAX/1.2 computer system.

5.1 Computing for Normal Wind Flow Conditions

5.1.1 Comparisons of the Velocities with Measured Data

The wind flow field developed around a single rectangular building is quite complex and involves major difficulties in quantification even for the geometrically simple case of wind blowing perpendicular to the building. A graphical display of the computed flow streamlines may provide first hand information about the flow field for the professional engineer. One such side view flow pattern is presented in Fig. 5.1, which also contains the flow visualization photograph obtained from tests of a similar building model placed in a boundary layer wind-tunnel (Lemberg, 1973). Overall, the computed flow pattern compares well with the experimentally determined field. Clearly, separation from the windward edge and recirculations behind the building are similar in both cases. Lemberg observed a recirculation region extending approximately 2.5 to 3.5 building heights and a separated flow region to a height about 1.5 building height above the ground. A recirculation length of 3 H is obtained in the computation by considering the edge of the recirculation zone at a point where the ratio of the longitudinal velocity to free stream velocity takes a value close to zero, i.e. $u/u_g = 0.0$, (Vasilic - Melling,1977). A similar exercise is also performed for the height of the separation region defined as the point where $u/u_g = 0.75$. As a result of the calculation, the height has been found equal to 1.75 H from the ground level. This is an encouraging agreement between measured and computed overall features of the wind field around a building.

Figure 5.2 presents the time averaged longitudinal velocity component, (u). Data are presented as percentages of velocity ratios referenced to free stream values of a particular location and they are compared for a number of points, two locations at the

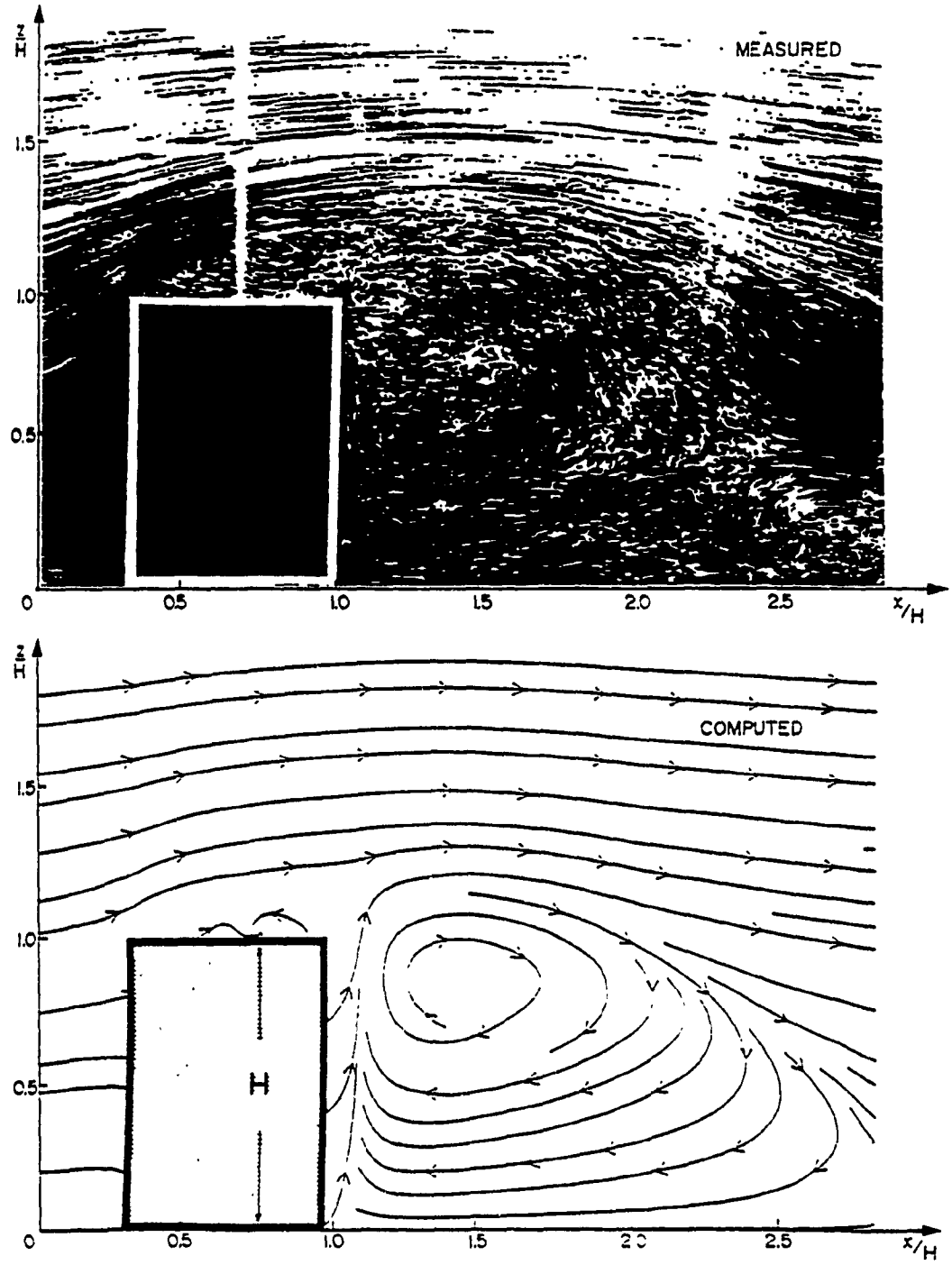

Fig.5.1: Side view of Flow Pattern Around a Building

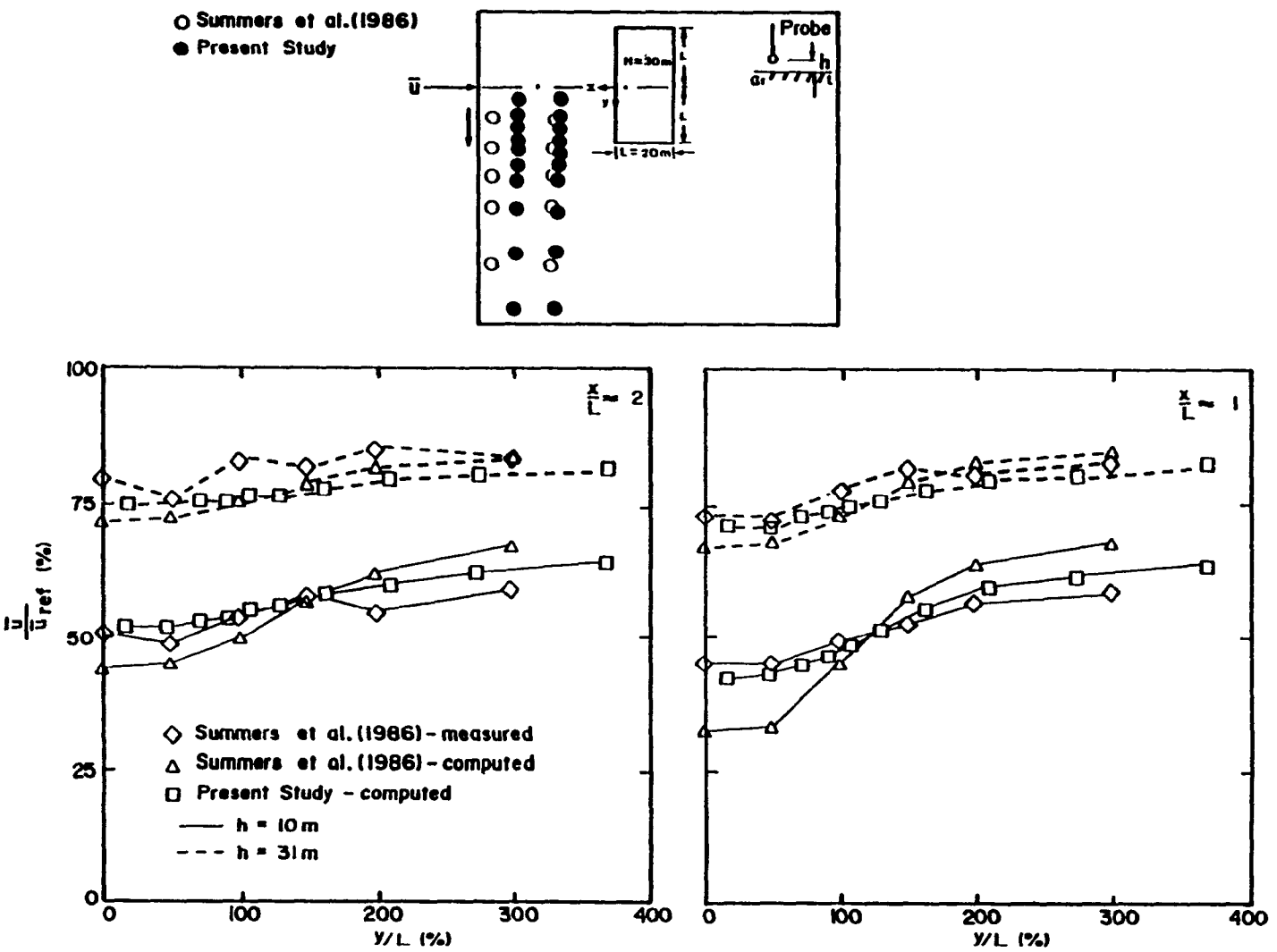

Fig.5.2: Comparison of the Upstream Longitudinal Wind Velocities (u) with and without Turbulence Models

building upstream, for flow normal to the building face. Due to symmetry, both measurements and computations were made only for half of the flow domain at two heights of approximately 5 and 16 cm representing 10 and 31 m respectively in full scale from the ground level. Three curves on each set represent: the computed values of the present study; the computed values of Summers et al, (1986); and the wind tunnel data also reported by them.

Note that the present study includes the standard $k - \varepsilon$ turbulence model during the computation whereas the computed values of Summers et al. (1986) were generated without giving standard treatment for turbulence. The measured data are obtained from a boundary layer wind tunnel. The incident wind was modeled by the power law form with the exponent equal to 0.215 and the reference height equal to 38 cm. The building block had the following dimension ratios: width: length: height = 4 : 2 : 3. Further details of the measurements are provided in Everett and Lawson (1984).

From the comparisons it is clear that the computational tools can predict the overall nature of the flow conditions. However, deviations from the wind tunnel values smaller than those of Summers et al. (1986) are noted in the present study. A similar feature appears in Fig. 5.3. which shows comparisons for two downstream locations, in the same format as in Fig. 5.2. Poor agreement of both sets of computational values is evident near the building. For the downstream side when the measurement height is 10 m from the ground level, the numerical simulations determine negative values (i.e. a reverse flow is calculated), whereas the wind tunnel measurements show at these locations a positive (i.e. streamwise) flow. However, the values obtained in the present study are generally closer to the wind tunnel data. As shown in the figure the solution grids are slightly different and did not exactly correspond in the two studies but this makes little difference in these comparisons. The pertinent question of Summers et al. (1986): " *Where the most obvious deficiency of the simulation - its failure to reproduce the*

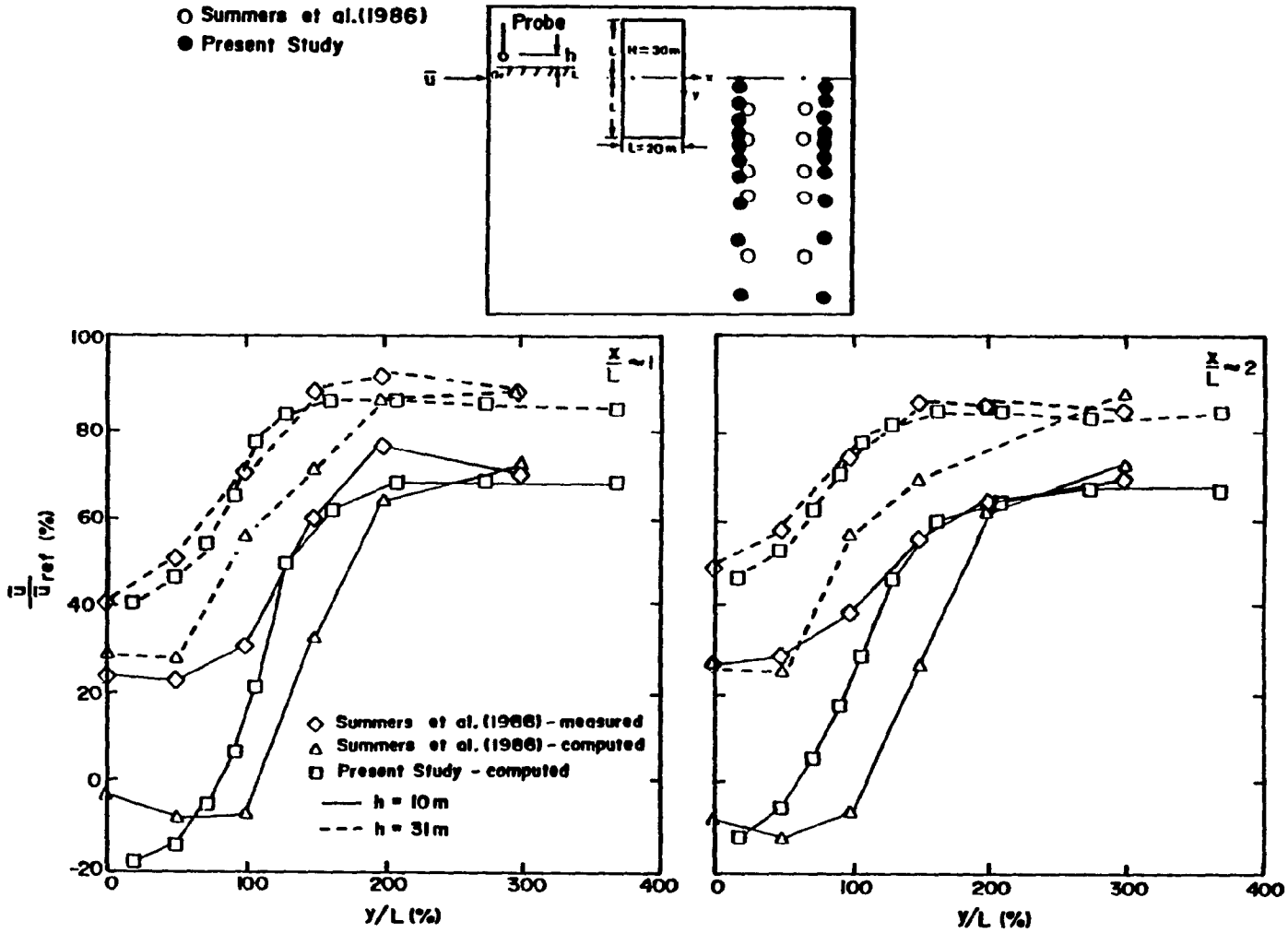

Fig.5.3: Comparison of the Downstream Longitudinal Wind Velocities (u) with and without Turbulence Models

compactness of the wake - could be improved by the introduction of a more detailed treatment of turbulence, " is considered by the present study, in which the turbulent nature of the flow is incorporated in the computation by using the well-known $k - \varepsilon$ models. The better agreement of the present results with the experimental data is attributed to this additional mathematical treatment of the flow.

Figures 5.4 and 5.5 display the results for the cross-stream component, v, in similar fashion as Figs. 5.2 and 5.3 respectively. These velocity ratios have smaller magnitude than the previous values. Again the comparisons are much better in the upstream locations than the downstream ones (Fig. 5.5). For both cases the, computed values of Summers et al. (1986) deviate more than the computed values obtained by including the turbulence models. Similar observations (not shown) are also noticed for the vertical component, w. In any event, from the above comparisons there is no doubt that the additional mathematical equations included in the modelling improve the velocities.

Fig. 5.6 compares the measured with the computed velocity fields around a building. The measured values are taken from experiments carried out in a boundary layer wind tunnel by Stathopoulos (1985). Velocity amplification factors i.e. mean wind speed in the presence of the building divided by the mean wind speed in the absence of the building at 10 m above the ground level are presented in contour form. Since both velocities are measured at the same height, these ratios directly provide the changes in the local flow conditions due to the presence of the building. Low velocity ratios on the windward side, high ratios at the corner of the building and very low ratios on the leeward side are evident from the figure. It is interesting to note that most of the measured high velocity amplification values are also predicted well by the computer modelling. Although the overall trends in both measured and computed ratios are similar, some differences may be explained by the much denser grid used in the computation.

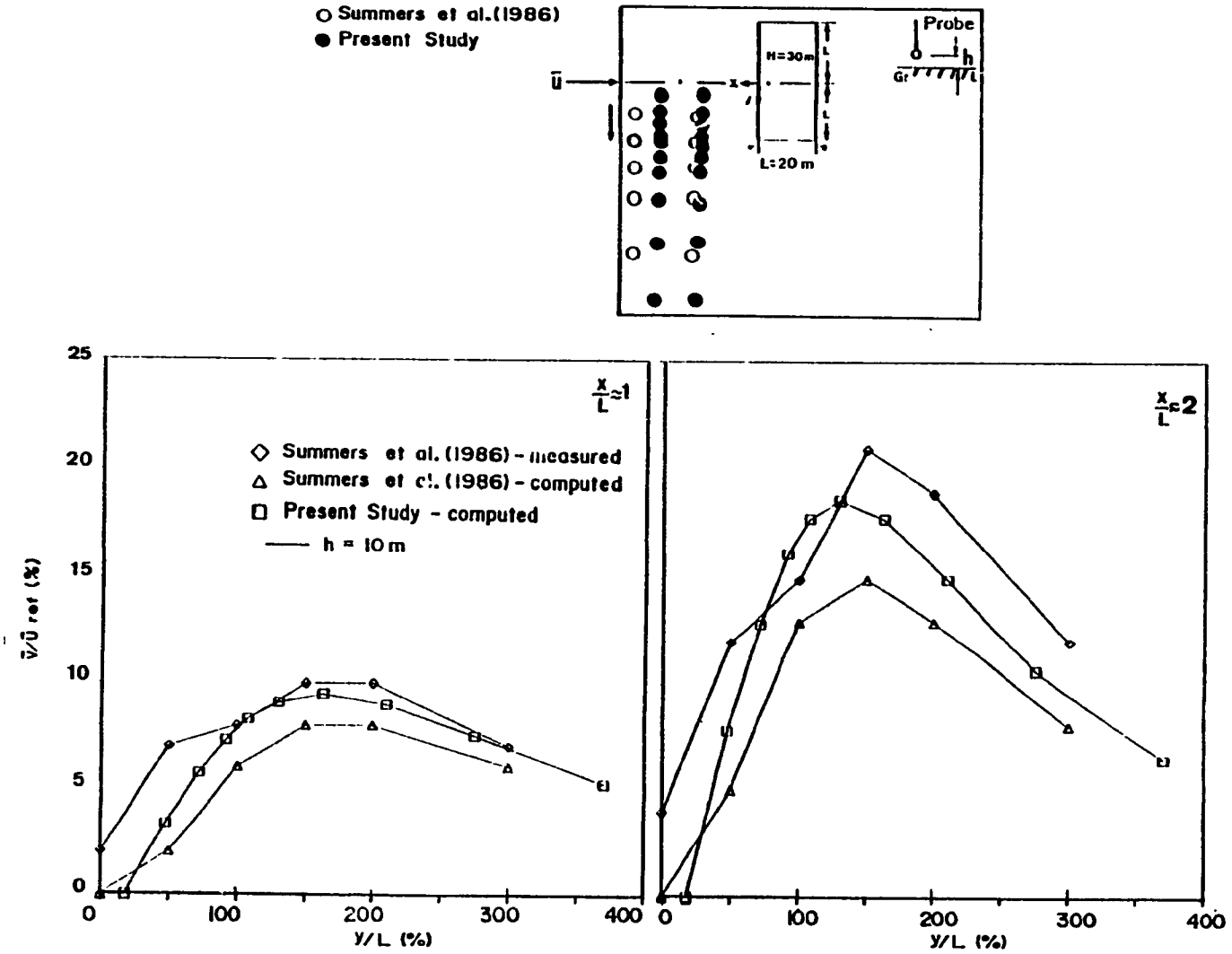

Fig.5.4: Comparison of the Upstream Lateral Wind Velocities (v) with and without Turbulence Models

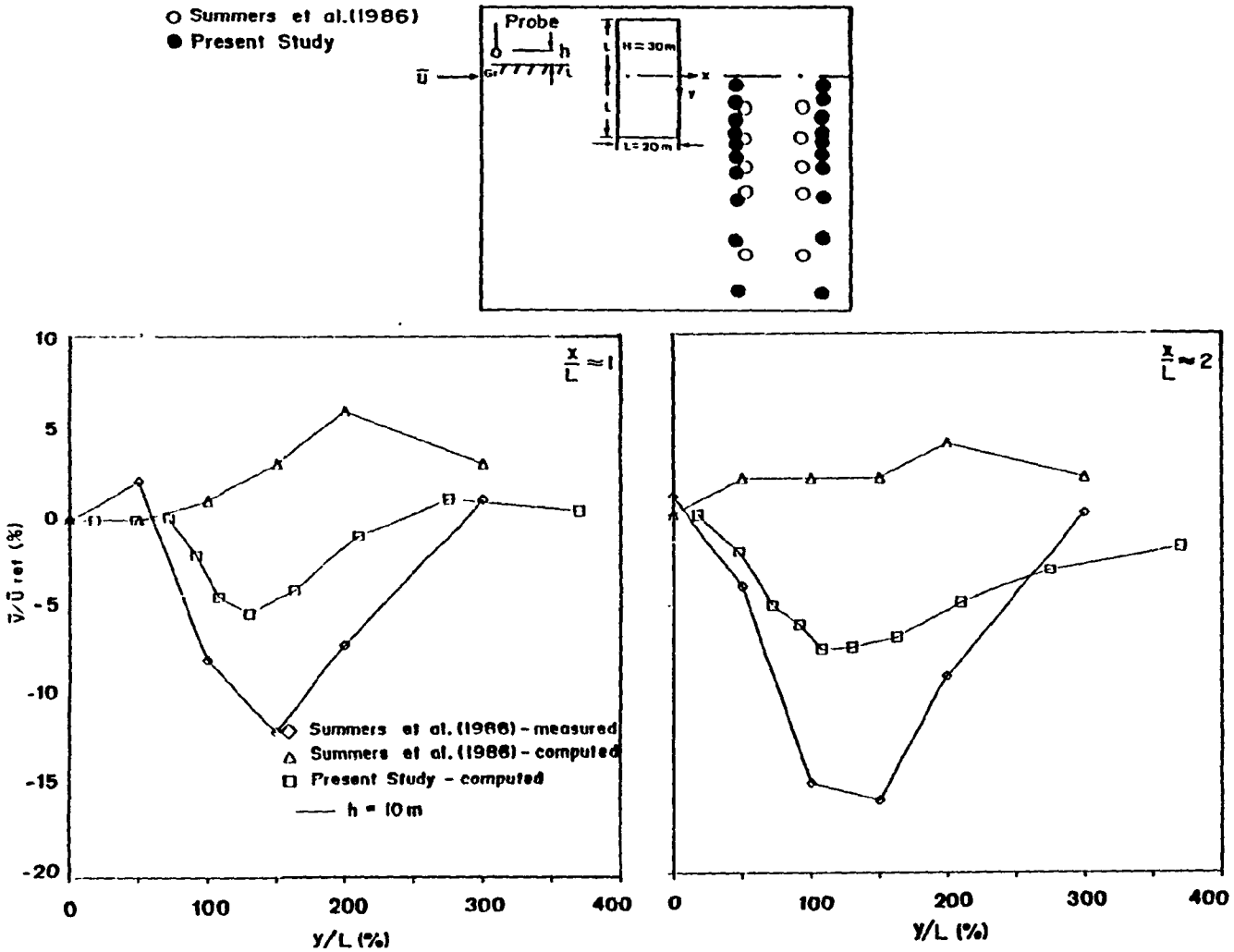

Fig.5.5: Comparison of the Downstream Lateral Wind Velocities (v) with and without Turbulence Models

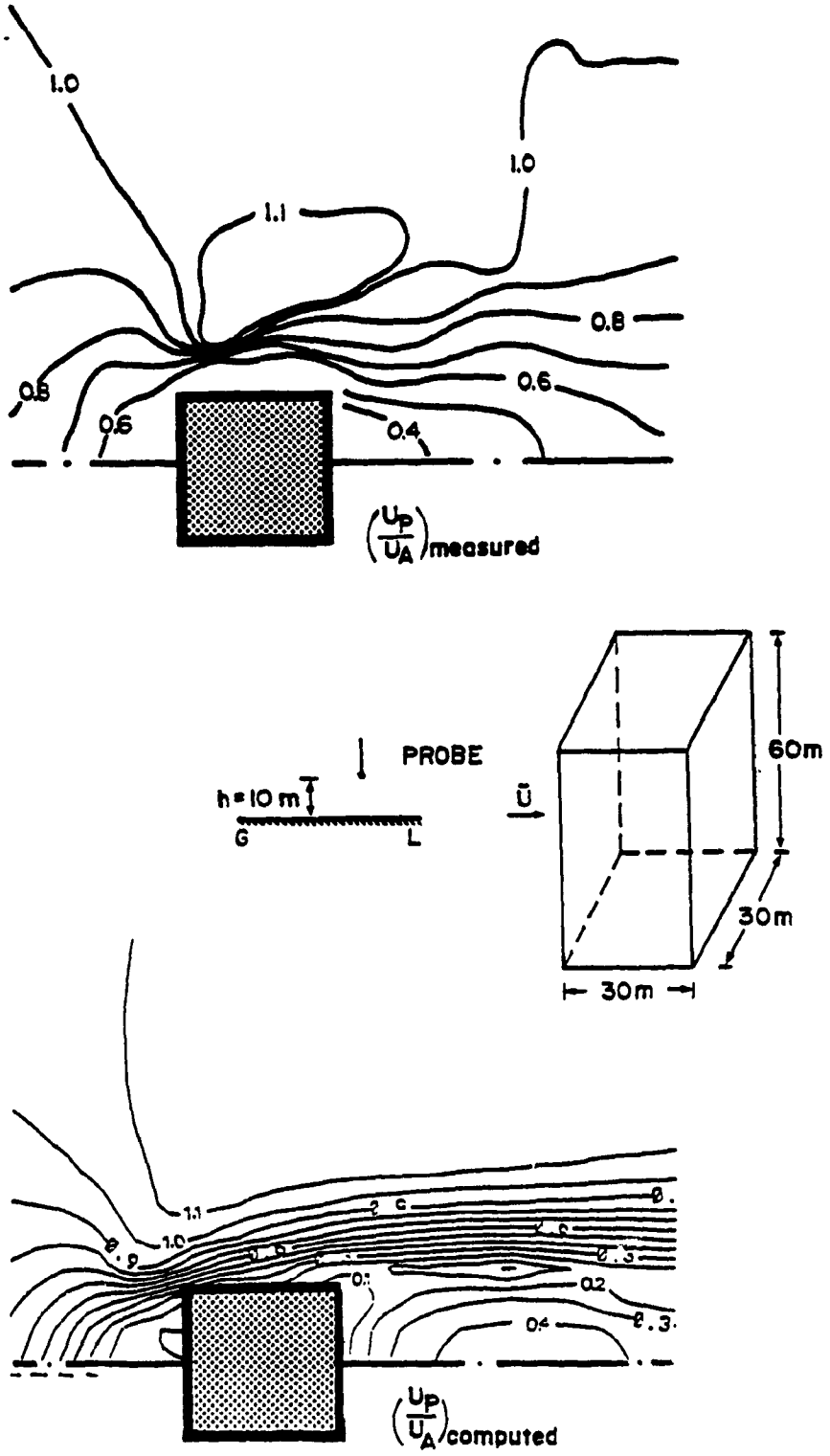

Fig.5.6: Comparisons of the Wind Speed Amplification Factors Measured around a Building and Computed by using the Standard Turbulence Models (H = 60 m)

Fig. 5.7 presents and compares the velocity ratios for a 180 m tall building in the same format as in Fig. 5.6. The effect of the building height on the velocity amplification ratios is evident, i.e. the high velocity ratios at the corner region increase as the building height increases. A similar trend in the velocity ratios has also been found in the experiment of Kamei and Maruta (1979). For the 180m building an increase of 50% in the local velocity was measured. On the other hand, the computed ratios increase from 1.1 to 1.7 as the building height increases from 60 m to 180 m. Note that for both buildings, velocities were measured and computed at the same height of 10 m from the ground level.

5.1.2 Comparisons of Computed Pressures with Measured Data

Comparisons between computed and measured pressure on the building envelope have also been made to establish the adequacy of the computational approach. Pressures are converted into the conventional form of non-dimensional pressure coefficients normalized with the dynamic pressure at the building roof height.

Fig. 5.8 shows typical comparisons for the walls. The coefficients are plotted against the ratios of z/H, where z is the height of the pressure tap or the grid location measured from the ground level and H is the height of the building. Experimental values provided in Stathopoulos and Dumitrescu-Brulotte (1990) are used as the measured wind tunnel data. These data originate from the model of a 55 m high building tested in a turbulent boundary layer wind tunnel. Pressures were measured by using SETRA 237 dynamic pressure transducers (0.1 psid range) placed in a scanivalve. Measurements from normal wind flow conditions are considered for the comparisons. Overall the computed pressure coefficients agree well with the measured values. There is little difference between the measured and computed values for the front and leeward walls. However,

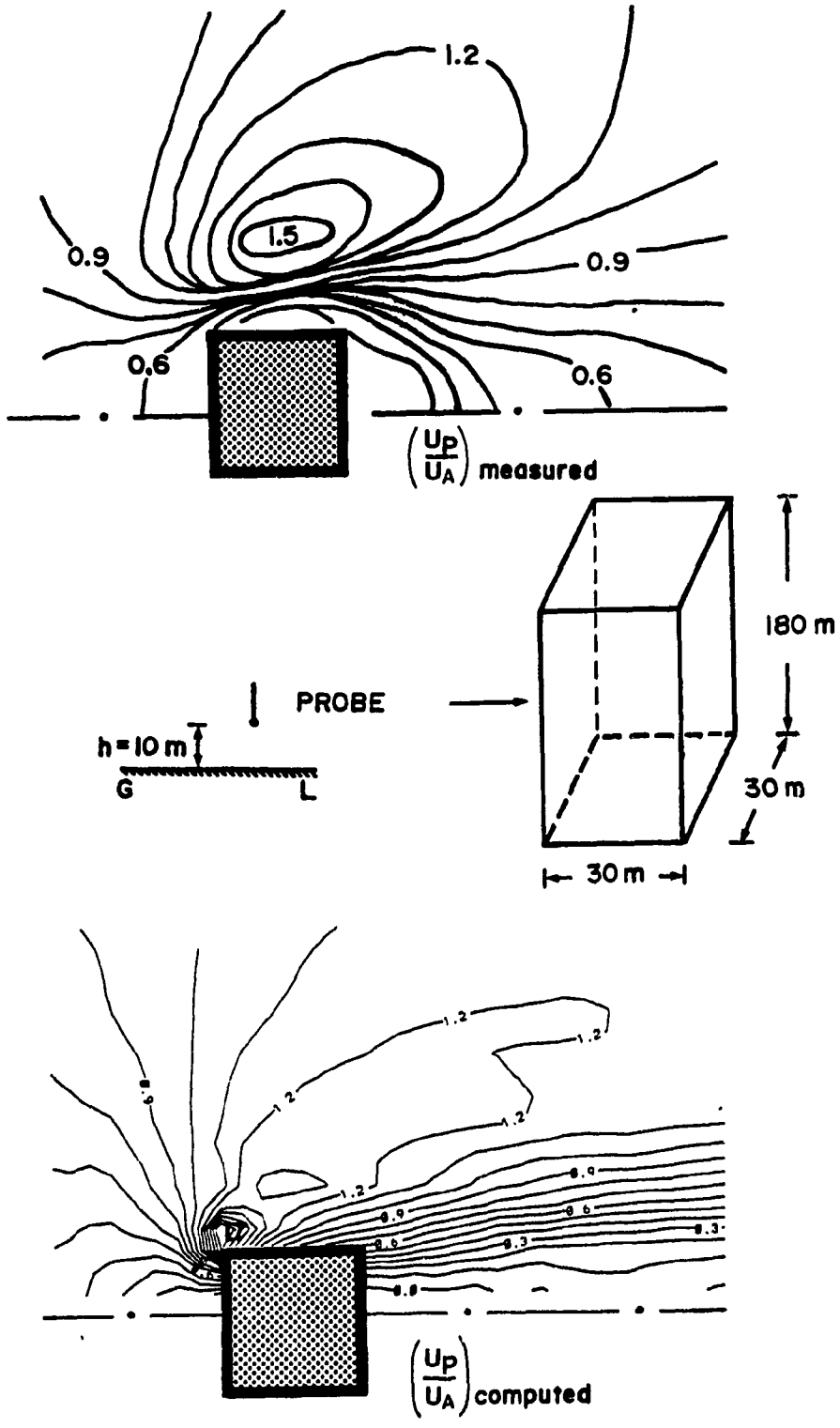

Fig.5.7: Comparisons of the Wind Speed Amplification Factors Measured around a Building and Computed by using the Standard Turbulence Models (H = 180 m)

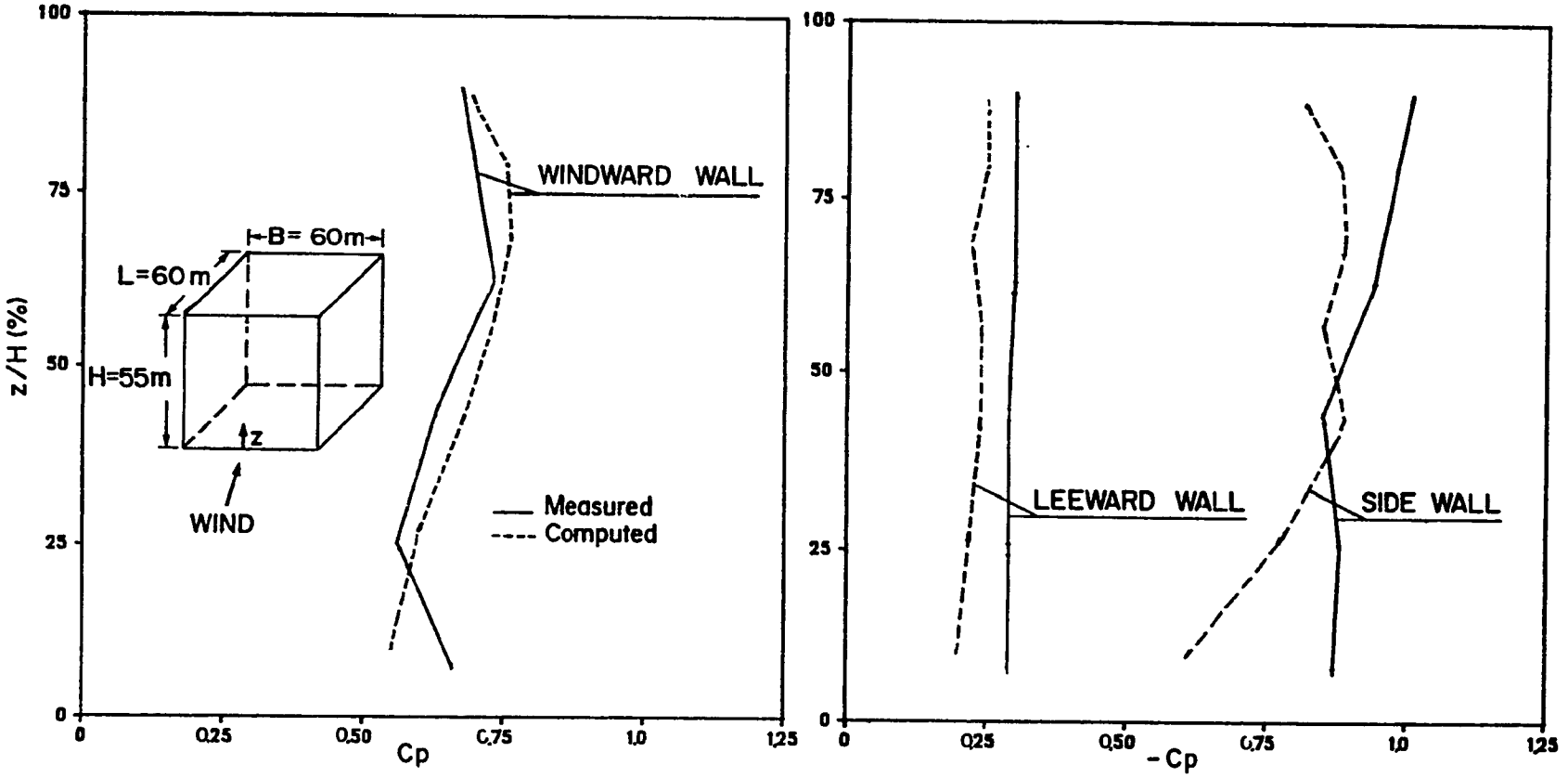

Fig.5.8: Wind-Induced Wall Pressures on a Building Computed by using the Standard Turbulence Models (H = 55 m)

deviations are more significant when computed negative values are compared with suctions measured on the side wall particularly near the bottom and the top of the wall.

Pressure coefficients of a 120 m tall building are shown in Fig. 5.9 in the same format with the previous figure. The variation of positive pressure coefficients on the windward wall and negative values on the leeward and side walls are shown along the centre line of each wall surface. The measured data have been received from boundary layer wind tunnel tests described in Zhu (1987). For this building configuration the agreement between measured and computed values is also encouraging for the windward wall. The pressure coefficient is maximum at about 3/4 of the windward height (stagnation point). However, in the case of side and leeward walls, the induced suctions are significantly underestimated by the computational procedure. The side walls are more affected than the leeward wall. This discrepancy is attributed to the mathematical equations based on the standard $k - \varepsilon$ turbulence model which may be insensitive to the streamline curvature of the flow.

Jansson (1987) computed the wind-generated pressure values on the roof of a square building by using PHOENICS. To validate the computed results, measurements were carried out by Jansson at various locations on the flat roof of a model tested in a wind tunnel which had been operated with a free stream wind speed of 30m/s at the building roof height. The velocity profile measured at the centre of tunnel working section, in the absence of the building, can be derived by using a power law equation with exponent value 0.2. To exclude the errors induced due to difference between the grids of computation and measurement locations, computational grids were placed exactly at the measurement locations. By providing the same input parameters to TWIST, computations have also been performed in the present study and computed roof pressure values are also converted into pressure coefficient form normalized with the dynamic pressure at the roof height.

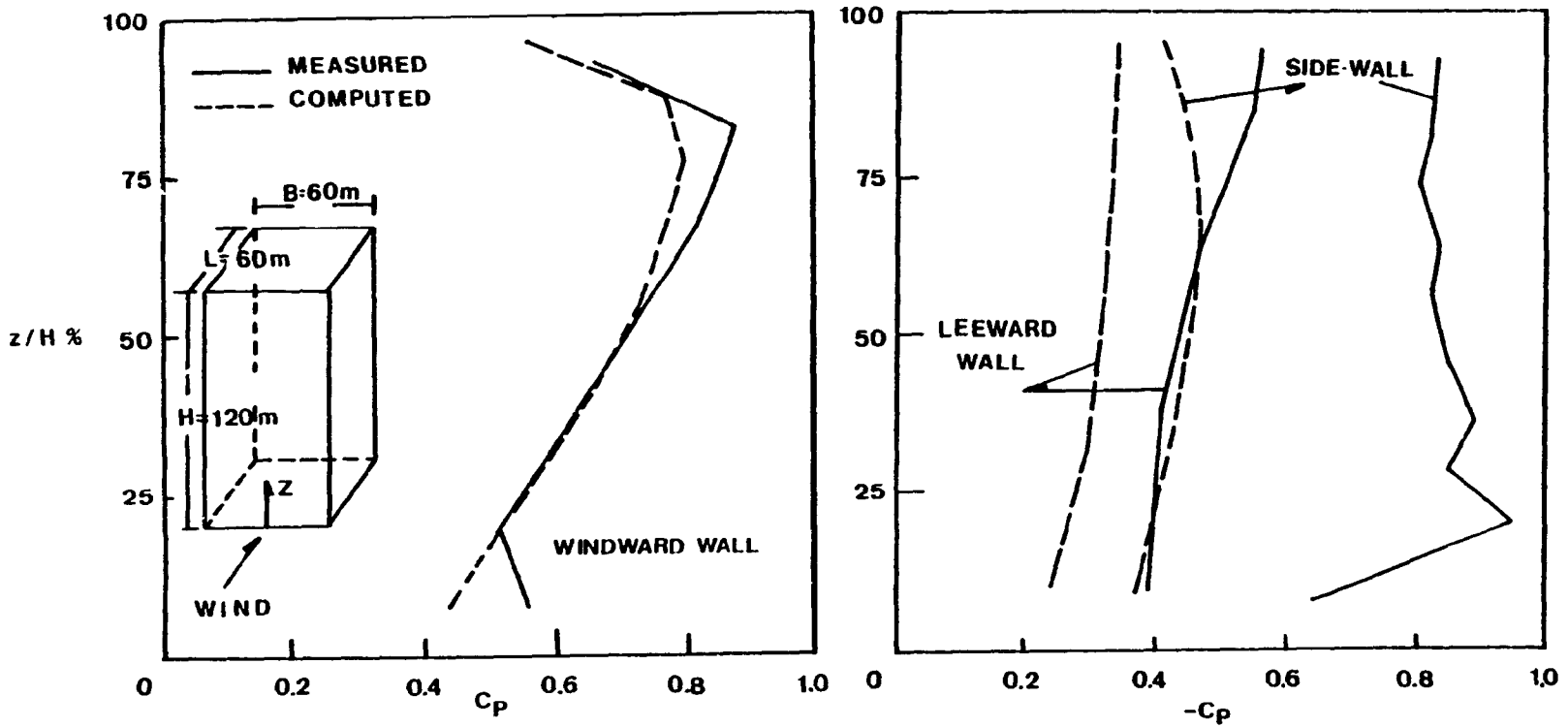

Fig.5.9: Wind-Induced Wall Pressures on a Building Computed by using the Standard Turbulence Models (H = 120 m)

Figs. 5.10 and 5.11 respectively display the results of the comparisons for two buildings of L/H ratios 6 and 3. Due to symmetry, both measurements and computations were made only for half of the roof. Data shown are for two typical locations on the roof, one close to the edge and the other near the centre of the roof. Computed values by using PHOENICS form a steeper gradient from the leading edge in comparison to the measured data for both locations. On the other hand data using TWIST are closer to the measured values on the windward half of the roof, but this agreement breaks down in the leeward part of the roof. However, it is equally clear that the present methodology yields better predictions of wind pressure on building roofs than those obtained by Jannson (1987). The present study computes higher suction values at the downstream side of the roof in comparison to the measured data. As previously mentioned, this may be due to the inadequacy of the $k - \varepsilon$ model in predicting the turbulence generated by smaller eddies near separation and reattachment zones of the roof.

From the above presented comparisons and discussion it is clear that the present computer code TWIST is capable of predicting the overall features of the flow over a single building. Nevertheless, the standard $k - \varepsilon$ model included for the creation of turbulence in the flow fails to capture the details of the recirculation and the involved eddies. Moreover, the computed suction values on the building envelope are significantly underestimated, particularly for the building side wall.

5.2 Computing the Wind Directionality Effect

In the preceding section and in most of the previous studies carried out in this field of research, only wind blowing normal to a single building is considered. Some computations for oblique wind conditions have been performed by Baetke (1986). In

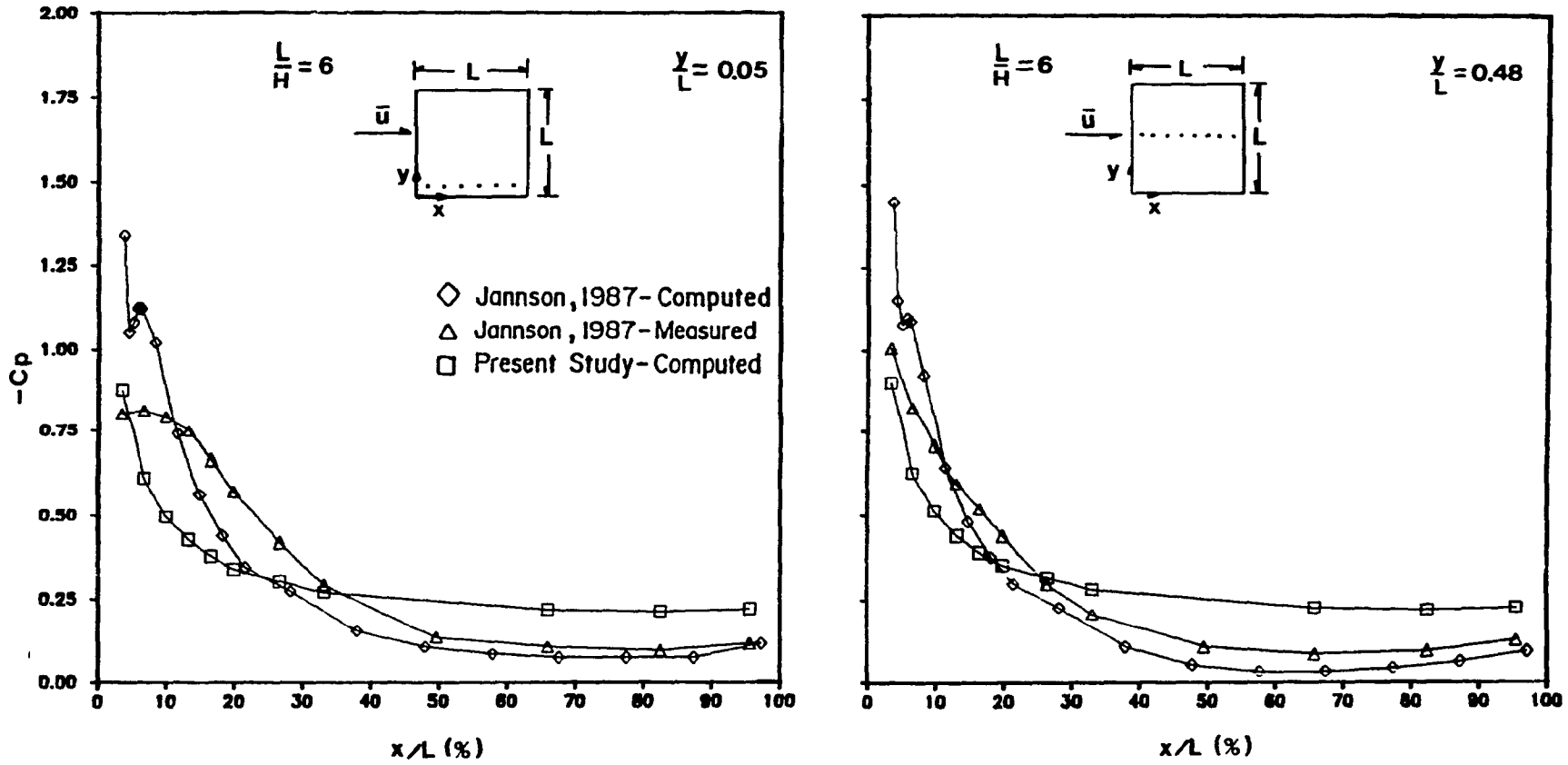

Fig.5.10: Measured and Computed Pressure Coefficients on a Flat Roof (L/H = 6)

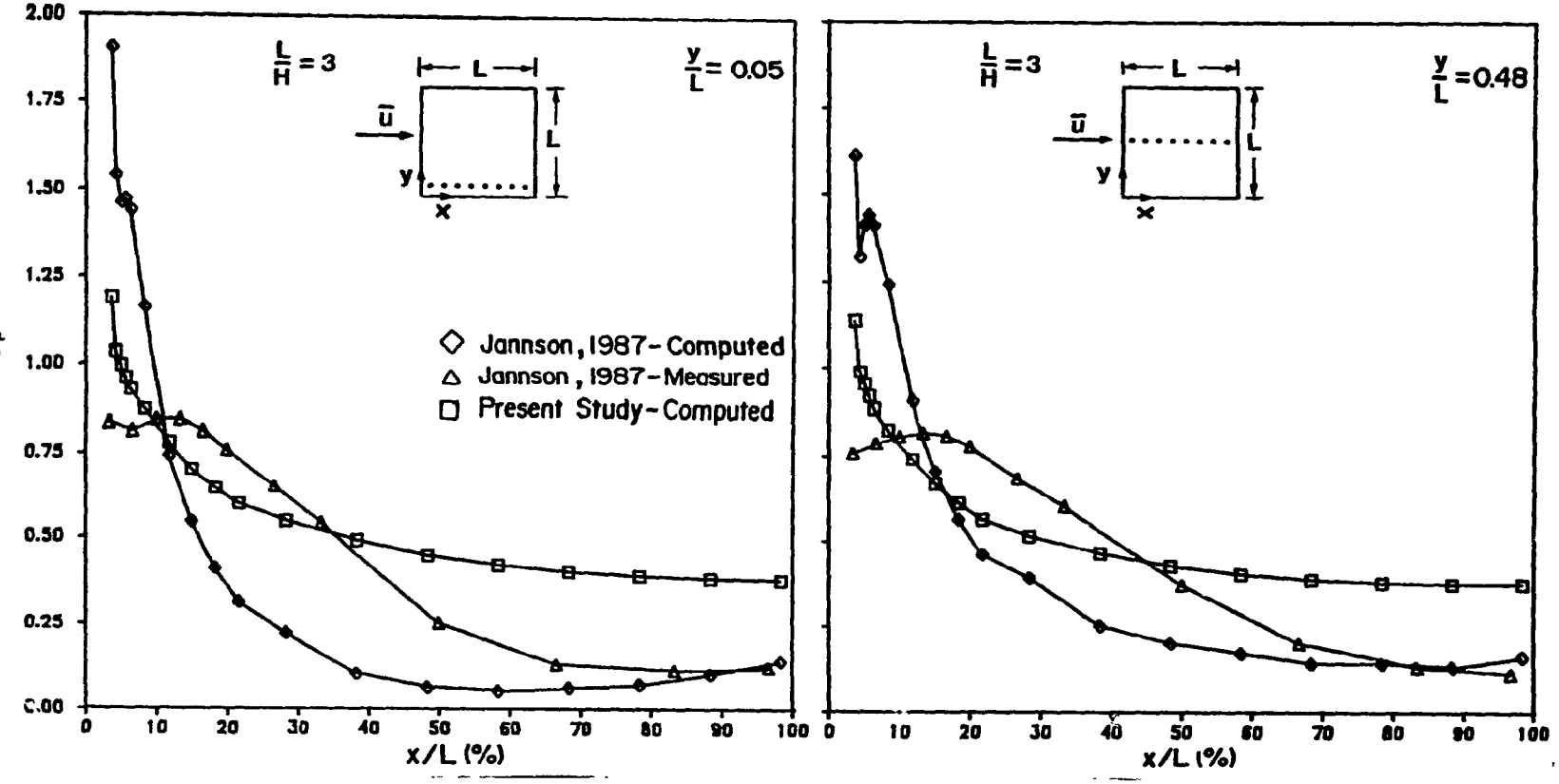

Fig.5.11: Measured and Computed Pressure Coefficients on a Flat Roof (L/H = 3)

fact, his study is the first carrying out computation and comparison of results for an oblique wind direction. However, only uniform inflow conditions have been considered during the modelling. Paterson (1986.b) also computed the wind flow around a group of buildings with a 20^{o} inclined incoming flow but no attempts were made to validate the computed results with the measured data.

It is clear that the normal flow computations are easier and economical in comparison to the angled flow conditions. This is due to the fact that the direction of the flow is parallel to the grid lines of the computational domain and it has the advantage of symmetry along the wind direction for regular shape buildings. Moreover, the well - known false diffusion (Γ_{false}) will be minimum for the case of normal flow condition (Raithby, 1976.b). This can be verified based on the following approximate expression for false diffusion coefficient for 2D situation which has been given by de Vahl Davis and Mallinson (1972); it is

$$\Gamma_{false} = \frac{\rho\sqrt{u^2+v^2}\,\Delta x\Delta y \sin 2\theta}{4\left(\Delta y \sin^3\theta + \Delta x \cos^3\theta\right)} \qquad (5.1)$$

in which u and v are velocity component along x and y directions respectively and θ is the flow angle with the x - axis. It is easy to see from this equation that no false diffusion is present when the flow is along one sets of grid lines; on the other hand the false diffusion is most serious when the flow makes an angle of 45^{0} with the grid lines. Further discussion of this issue can be found in Patel (1982).

Nevertheless, the wind may flow from any direction depending on the geographical location and surroundings of the building. Thus to generalize the present computer code, it is also necessary to compute and validate the results for other directions in addition to the normal flow conditions. To accommodate wind directionality changes, the present

computer code is modified and computations are performed for various wind directions. A building 60 m high having a square cross-section of 30 x 30 m is selected as a test case. A typical example for the above considered case with 45^{o} inclined wind is the Hall building of Concordia University exposed to westerly wind, the principal wind direction for Montreal. Moreover, experimental data for this particular case are available which can be used for the purpose of comparisons. Three different wind directions (0^{o}, 30^{o} and 45^{o}) are considered during the modelling.

5.2.1 Modifications on the Present Code

TWIST has been modified to account for the wind directionality effect. The desired wind direction can be obtained in either of the following ways: The building may rotate from its original position similar to the wind tunnel approach. Provisions are available in the literature for performing computations by rotating the building. This can be achieved by using advanced grid generation techniques such as the Body - Fitted Co-ordinate system (BFC) as explained in Thompson (1986, 1980) or by the adaptive grid generation approach of Anderson (1983). These techniques however, have not been tested for wind flow conditions around buildings.

Another way of changing the wind direction is to do it as it happens actually. In this procedure, the grid lines coincide with the surface of the building envelope and hence it has various advantages such as specification of wind inclination for the calculation and application of boundary condition during the computation. Moreover, no control volumes are excluded from the calculations which ensures the conservation property of the control volumes. In addition, this approach is practically easier to adapt in the existing computer code, which is developed based on a regular rectangular grid.

In fact, two major modifications are necessary to implement in TWIST to test oblique wind directions: the calculation of initial inclined flow distribution and the specification of the boundary conditions. The first is in module 1 and the other is in the BOUND submodule of module 2. The inclined wind conditions can be obtained by recalling Eq. 4.1 as:

$$\frac{u}{u_g} = \left\{\frac{z}{z_g}\right\}^{\alpha} \qquad (4.1)$$

where u is the velocity component along the longitudinal direction, x, at a distance, z, from the ground level. u_g and z_g are the gradient velocity and height respectively of a power law profile with exponent, α.

Let i, j and k represent unit vector in rectangular cartesian co-ordinate system for the directions x, y and z respectively . If U is a vector in space having components u, v and w in x, y and z directions respectively, then:

$$U = iu + jv + kw \qquad (5.2)$$

The magnitude of U is

$$|U| = \sqrt{u^2 + v^2 + w^2} \qquad (5.3)$$

The directional cosines of U are:

$$l = \cos\alpha = \frac{u}{|U|}$$
$$m = \cos\beta = \frac{v}{|U|}$$
$$n = \cos\gamma = \frac{w}{|U|} \qquad (5.4)$$

Only a two-dimensional flow distribution is assumed for the initial condition and by using Eqs 4.1 and 5.4, the following expressions are implemented in the computer code:

$$u = u_g\left\{\frac{z}{z_g}\right\}^{\alpha}\cos\alpha$$
$$v = u_g\left\{\frac{z}{z_g}\right\}^{\alpha}\cos\beta$$
$$w = 0 \qquad (5.5)$$

The initial conditions of the other variables remain as before.

Secondly, BOUNDS in module 2 (ref: section 4.3 and Fig. 4.2) needs modifications for the non - symmetrical nature of the flow. In other words, the symmetrical boundary condition is removed and the whole flow field is solved without setting the normal velocity, v, as zero along the axis of symmetry. For other variables, the cross-stream gradient conditions are also calculated (ref: section 3.4 and Fig. 3.4). Since the whole flow field is considered, one more free boundary is added in the computation, for which the Dirichlet conditions are specified. Eventhough, the flow lines will be inclined to the grid lines, only the Hybrid Difference Scheme (HDS) is used for the sake of simplicity. However, Raithby (1976. a) critically evaluated the false diffusion problem that can arise due to the inclined nature of the flow to grid lines and suggested a new powerful numerical scheme named Skew Hybrid Difference Scheme (SHDS) to minimize the likelihood of occurrence of the false diffusion.

Leonard (1979) also presented the quadratic upstream weighted interpolation scheme (QUICK) to modify the conservation processes. Recently, a set of thirteen numerical schemes (i.e., interpolation techniques that account for the non-symmetrical phenomena of convection processes) have been reviewed by Patel (1982), in order to evaluate the accuracy and the practicality in implementing the various schemes. Nevertheless, the present study used the HDS for the convective term interpolation and extended the existing code for predicting the directionality effect. Implementing the existing powerful schemes or developing a new solution scheme are excluded due to time limitations. Thus no attempts were made to change the structure of ASSEMBLER sub-module of module 2 (ref: section 4.3).

5.2.2 Predicted Flow Behavior

A staggered grid arrangement having 40 x 40 x 32 grid nodes is used and the computed results are analyzed in this section whereas the comparisons with the measured data are presented in the next section. Fig. 5.12 displays the plan view of the grid arrangement. The figure shows the relative location of the building with respect to the computational domain. The extent of computational domain in various directions is decided based on a sensitivity study (-ref. chapter 8) carried out for the normal wind flow conditions. Moreover, the grids are distributed to form better continuity between the control volumes even when there is a steep gradient for a variable. This can be clearly viewed from the dense grid distribution near the windward faces of the building.

As an example, the plan view of the initially assumed velocity field near the ground level for a 45^0 oblique wind direction is shown in Fig. 5.13. These values are given to the computer code by using Eqs. 5.5, as previously explained. A power law profile having exponent 0.16 and a wind speed of 12 m/s at the wind-tunnel gradient height of 60 cm is used. These data are implemented in the computer modelling, since measured

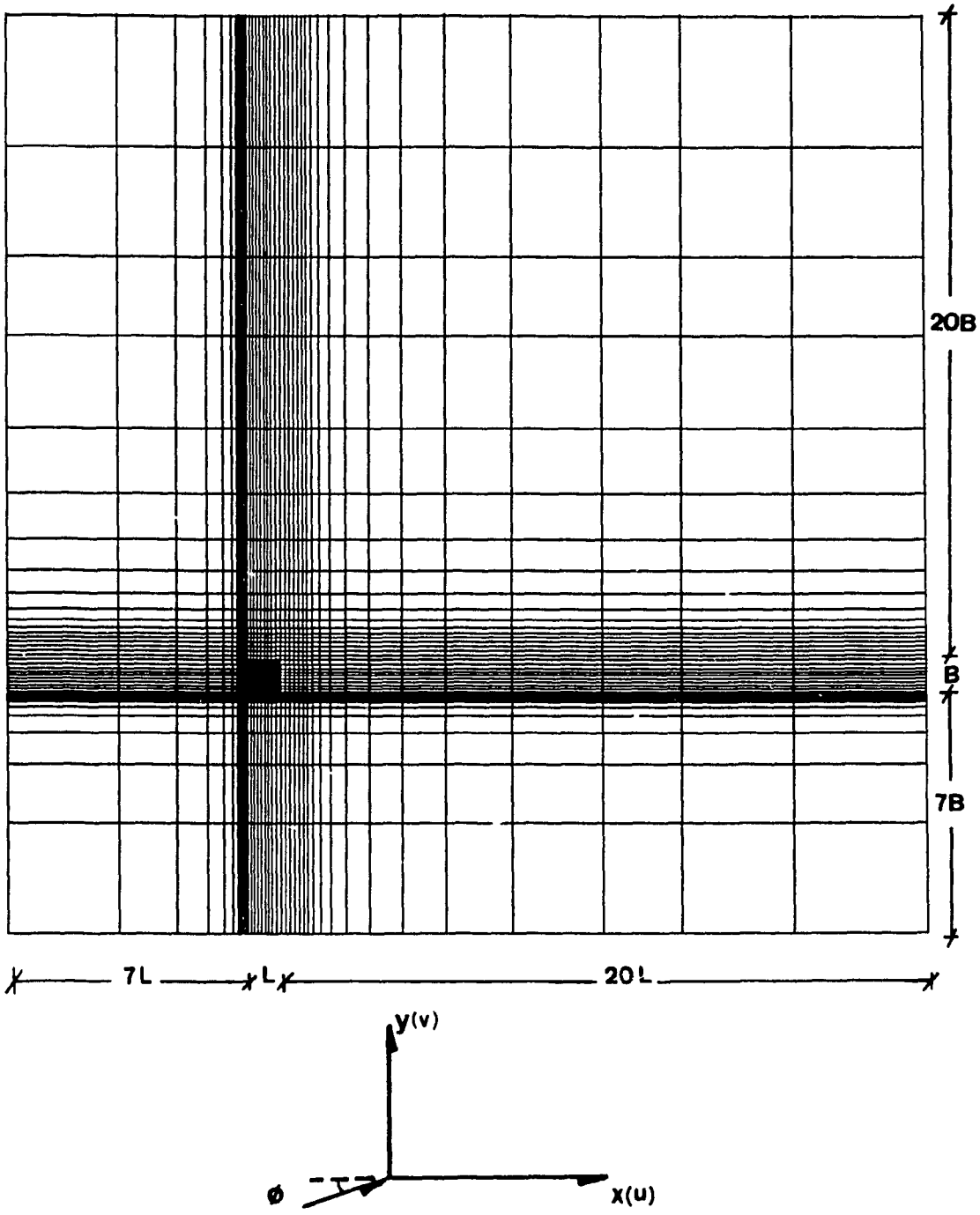

Fig.5.12: Plan View of the Grid Arrangement for Oblique Flow Modelling

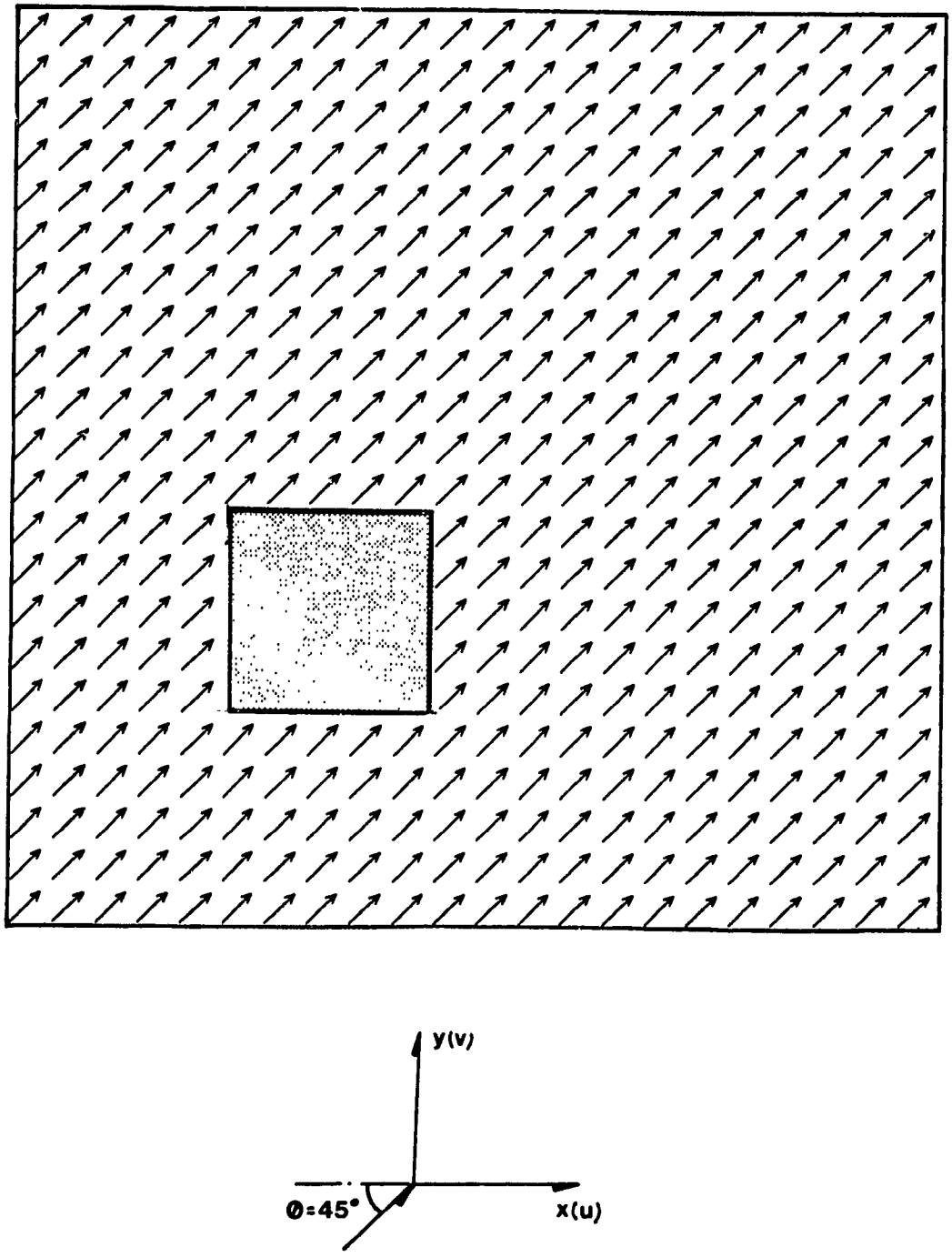

Fig.5.13: Initial Assumed Flow Distribution for Oblique Wind Condition

experimental data are available for this particular velocity profile. No initial attempts are made to identify the presence of the building for the incoming flow. This can be clearly seen from the figure where a uniform distribution of the vectors are shown.

The converged velocity distributions and streamline plots are shown in Figs. 5.14 and 5.15 respectively for three wind directions, namely 0^o, 30^o and 45^o. The flow field at 2 m from the ground level is used to obtain these figures. A clear separation of the flow from the windward face(s), the recirculations and the reverse flow at the leeward side(s) of the building are evident. The wind directionality effect on the building and changes in the flow recirculations are clearly predicted by the present code.

The size of the recirculations and involved eddies are shown in the streamline plots. The recirculation zone is considerably more pronounced for the normal flow as opposed to the oblique flow. Due to symmetrical conditions only half of the flow field is shown for 0^o and 45^o. No concrete rules are available to quantify the extent of the recirculations, however, an exercise has been performed based on the approach of Vasilic-Melling (1977), by fixing the edge of the recirculation at $u/u_g = 0.0$ from the leeward side of the building along the longitudinal direction. As a result, the calculated length of recirculation (l_R) is 2.5 L, 1.6 L and 1.7 L for 0^o, 30^o and 45^o respectively . Also changes in the flow distribution among 0^o , 30^o and 45^o conditions are evident from the figure.

Figure 5.16 and Figure 5.17 show the flow distribution at 10 m height from the ground level. The size of the eddies and recirculations are reduced for all three directions of the flow in comparison to the previous plot. This is not surprising due to the fact that only interaction due to building is affecting the flow at this level, whereas the flow field at lower level will interact both with the ground and the building surfaces. This shows the

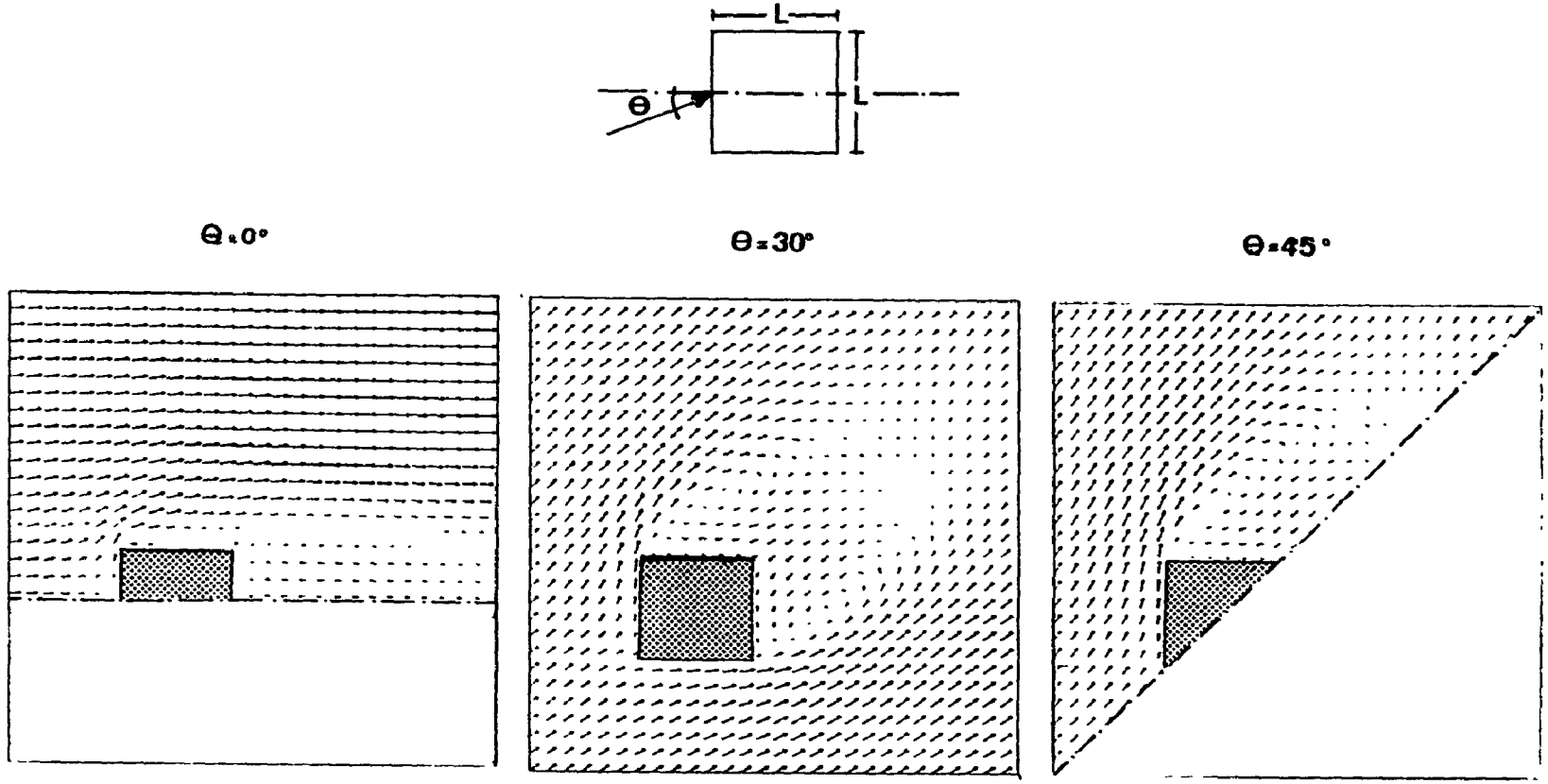

Fig.5.14: Vector plots of the Computed Velocity Field around a Building for Different Wind Directions, (h = 2 m)

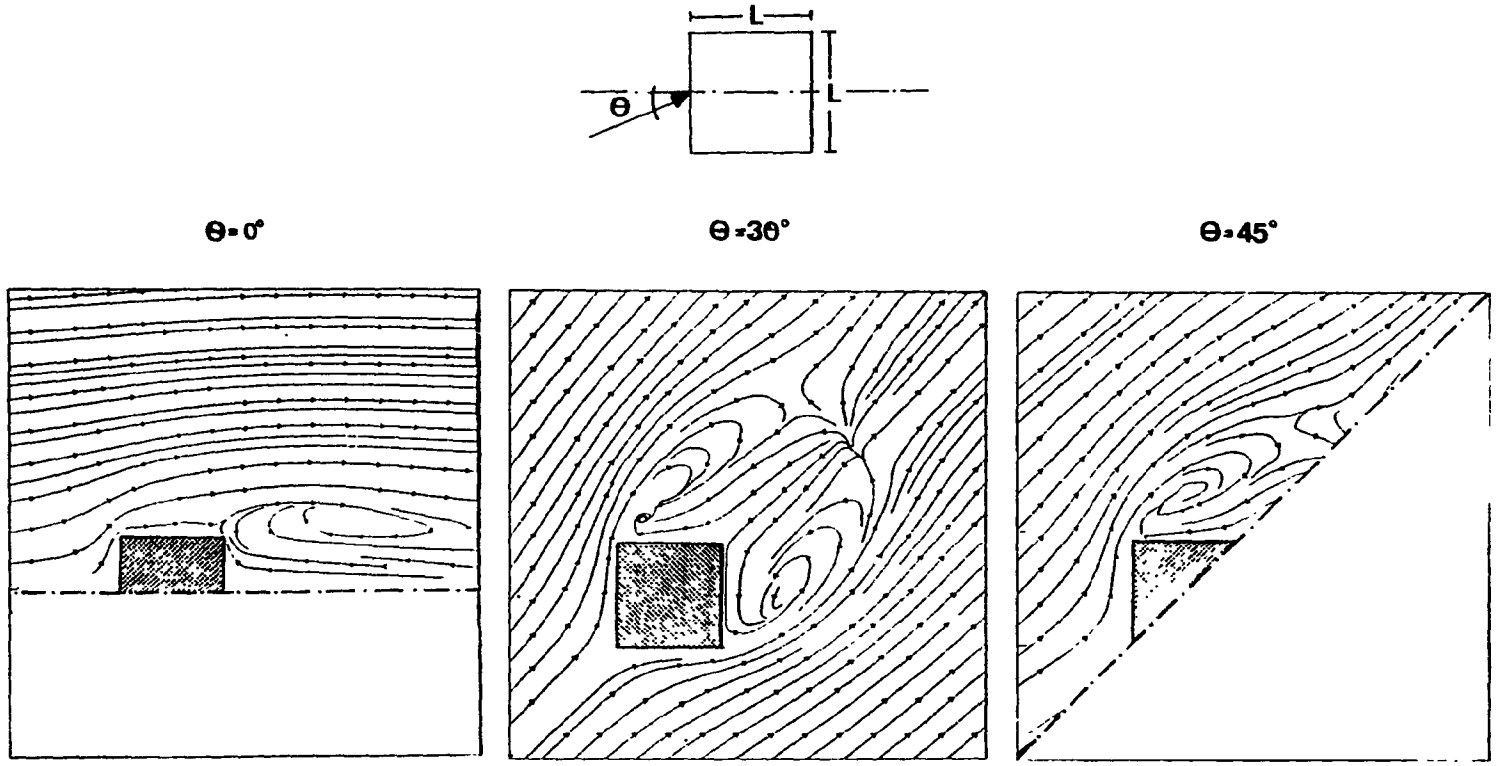

Fig.5.15: Streamline plots of the Computed Velocity Field around a Building for Different Wind Directions, (h = 2 m)

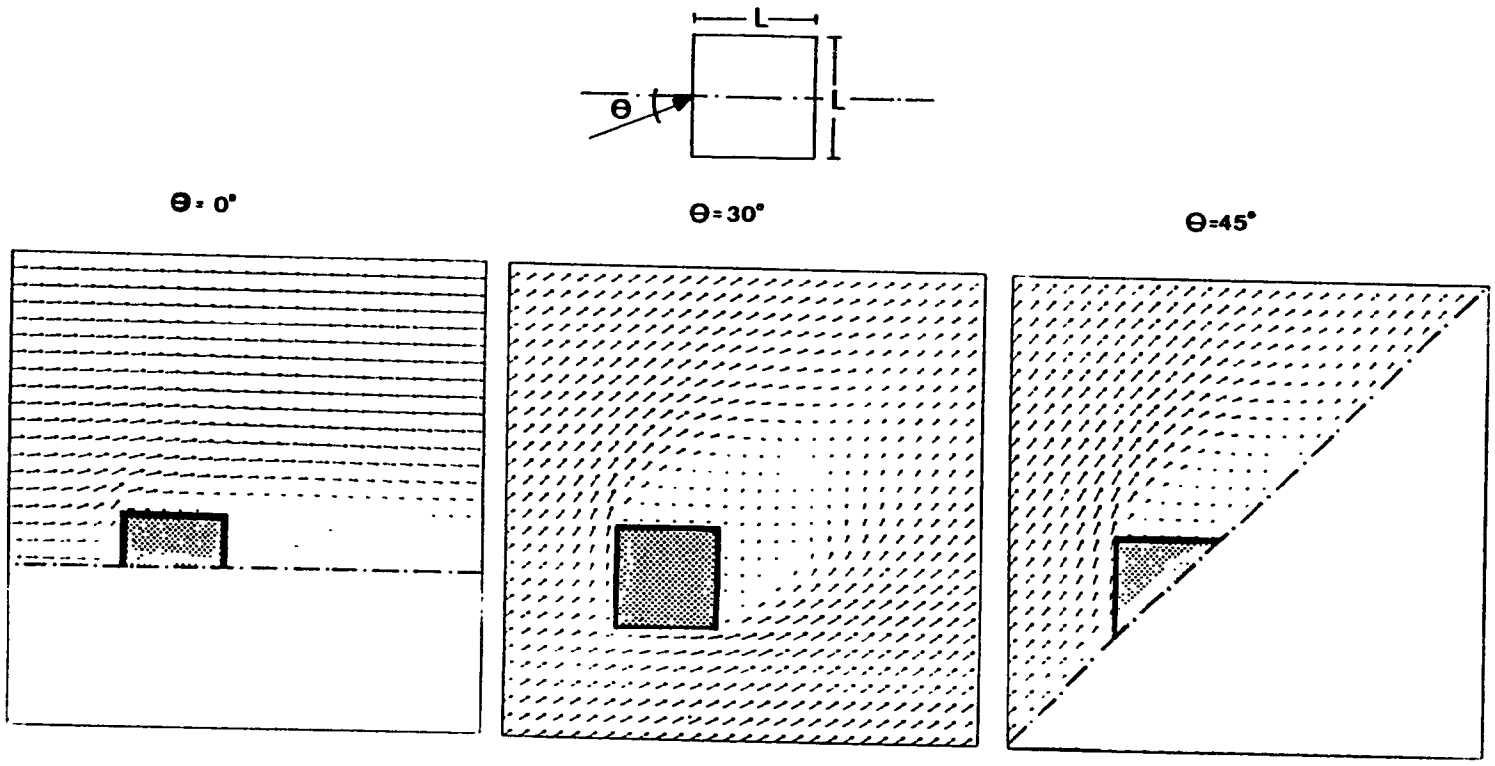

Fig.5.16: Vector plots of the Computed Velocity Field around a Building for Different Wind Directions, (h = 10 m)

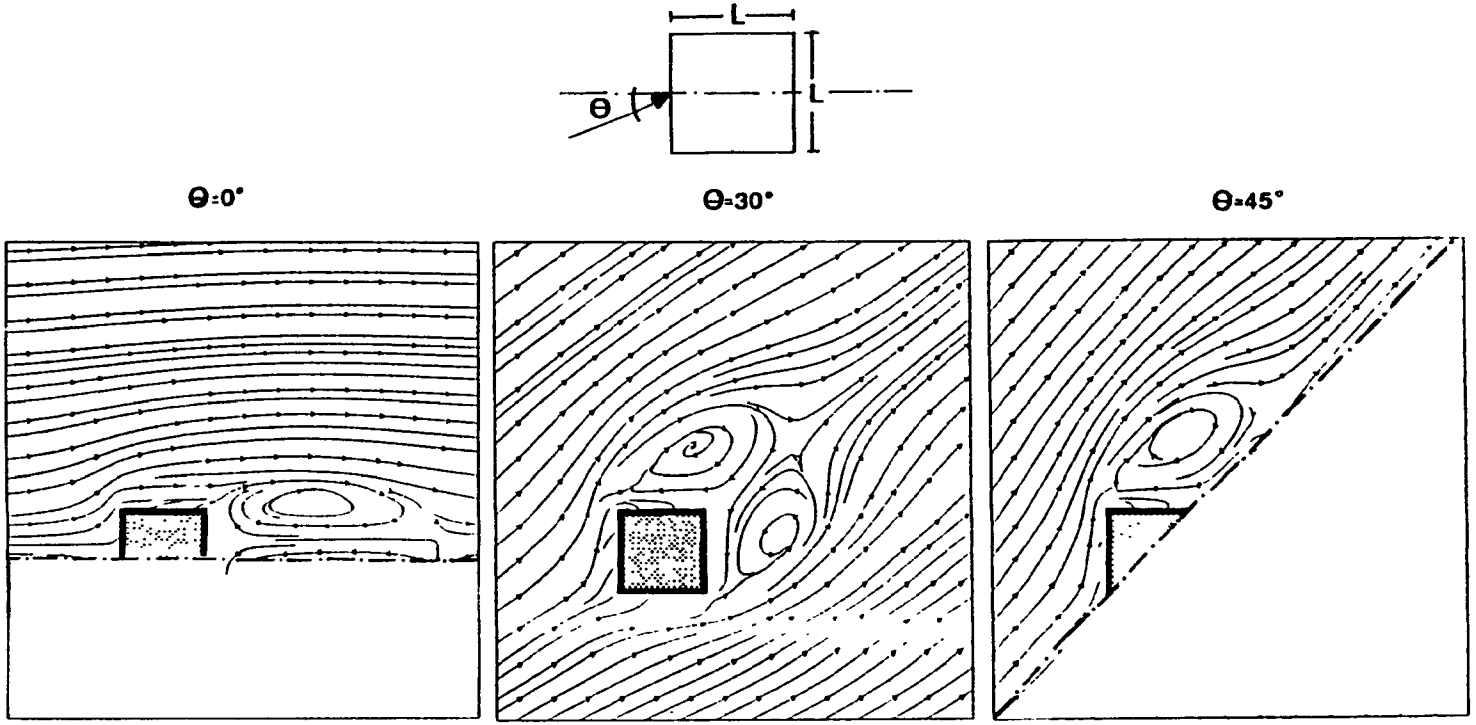

Fig.5.17: Streamline plots of the Computed Velocity Field around a Building for Different Wind Directions, (h = 10 m)

turbulence levels will be reduced as one moves further away from the ground level. The calculated l_R is approximately 2.2 L for the normal flow and 1 L for other directions. Thus the reduction in recirculation length is found to be more pronounced for the case of angle flow as opposed to normal flow conditions. This may be due to the upward diffusion of the wake from the ground level as it proceeds downstream but this qualitative observation needs further examination with data from wind tunnel testing.

5.2.3 Comparison of the Computed Results With Measured data

Comparisons of the computed results with the measured wind-tunnel data are made both for wind velocities around the building and wind-induced pressures on the building envelope. Both for computation and measurements, the conventional velocity ratios are calculated by dividing the velocity at a particular location in the presence of a building to the velocity value at the same location in the absence of the building. Since both velocities are taken at the same height (h =10 m), these ratios directly identify the building influence on the local wind environmental conditions. Figure 5.18 compares such computed ratios with the experimental data. Both sets are presented in the form of contours. The models used for the wind-tunnel study was made by wood and a geometric scale of approximately 1:400 was adapted for its fabrication. All velocity measurements around building models were carried out by using a TSI 1056 linearized hot-film anemometer and a TSI 1076 digital mean and RMS meter. The included experimental values are taken from Stathopoulos (1985) where the details of the experimentation can also be found.

The previous results of normal wind flow are also included in the figure to analyze the wind directionality effect on the velocity ratios. Due to symmetry only half of the flow field is compared as well as measured. Some of the small computed velocity ratios

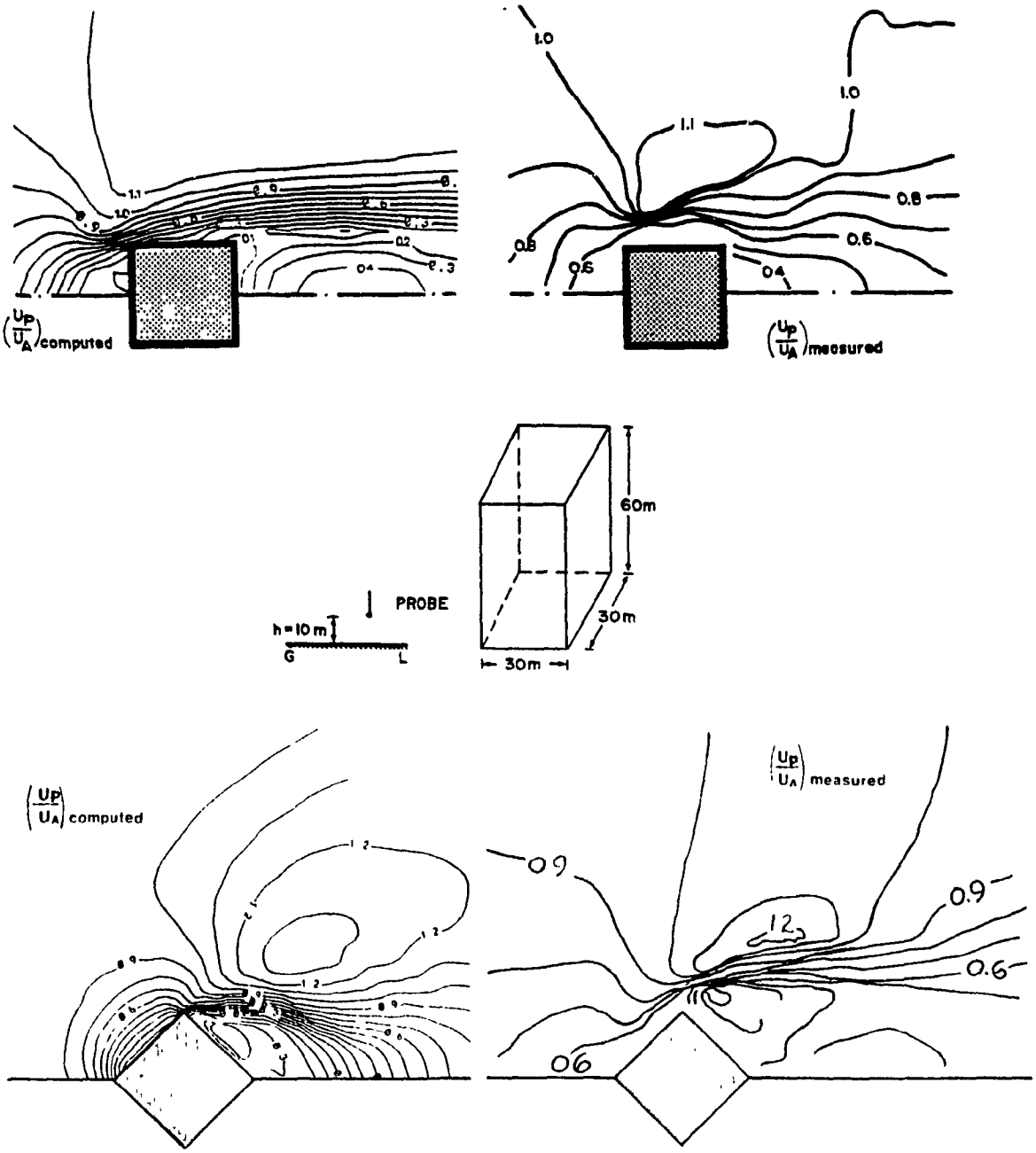

Fig.5.18: Comparison of the Computed Velocity Ratios with Measured Data for Different Wind Directions (h = 10 m)

behind the building are also compared well with the measurements for the skew wind conditions. The maximum ratio increases from 1.1 to 1.2 when the wind direction changes from 0^o to 45^o during the measurements and the corresponding values of the computation are 1.1 to 1.3. In measurement, the building increases the local velocity ($U_P/U_A > 1.0$) up to a distance 1.5 L from the leeward side of the building whereas this trend has been extended up to a distance 3 L in the case of computation. A similar observation has also been made for normal flow conditions. Overall the comparison between the measurement and computation is found to be better for the normal flow condition as opposed to the 45^0 oblique flow and this is due to the difficulties involved in the numerical modelling of the skew flow conditions.

Fig. 5.19 compares the ratios in the same format as that of Fig. 5.18 at 2 m from the ground level. Since experimental data are not available for normal flow, the corresponding set is excluded from the comparisons. Near the ground, the velocity ratios are higher in comparison to the 10 m from the ground level so as the difference between the measured and computed values. The difference near the ground level can be attributed to the assumed power law profile behavior in the numerical modelling for the initial velocity distribution. Assuming a linear variation for the velocity near the ground, may minimize the error due to computation. The uncertainties are also involved in the experiments when a single hot film sensor is used for measurements near the ground level. It has been estimated that this error will be about 13 % for 50 % turbulence intensity and less than 2 % for an intensity at 20 % level (TSI, Inc.). More accurate measurements may be carried out by using a more sophisticated measurement system or a Laser-Doppler anemometer but none of them were available for the present study.

Based on the above discussion, it is clear that the present code can predict the basic wind environmental conditions around a building for different wind directions with the

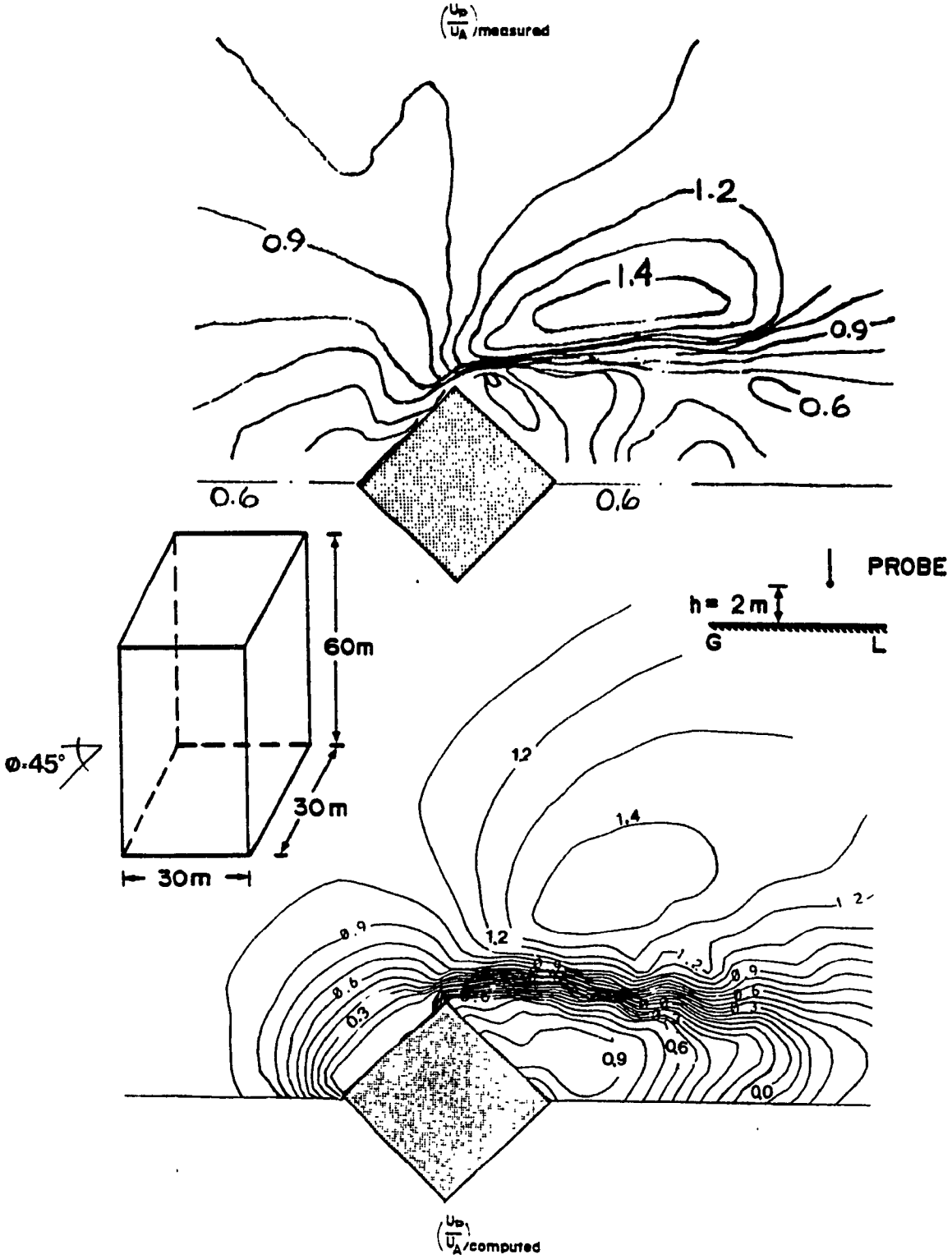

Fig.5.19: Comparison of the Computed Velocity Ratios with Measured Data for Oblique Wind Direction (h = 2 m)

minimum modifications as explained in section 5.2. Despite the differences in the grid arrangement of the computation and measurement locations, the overall agreement of the velocity ratios around the building is satisfactory. The computed results are further analyzed for the wind-induced pressure values and are also compared with the experimental data. The results from the normal wind flow conditions have also been included to identify the wind directionality effect.

Figs. 5.20 and 5.21 compare the pressure coefficient in contour form of 0.1 equal intervals for the windward and leeward wall respectively. The 60 x 60 m building considered is 55 m high. Extensive experiments were performed by Dumitrescu-Brulotte (1987) at the Centre for Building Studies' boundary layer wind tunnel for this geometry. A power-law velocity profile with exponent 0.15 and free-stream or gradient velocity approximately 13 m/s was simulated in the wind-tunnel. The dynamic velocity of the flow at the boundary layer height (60 cm) was monitored for the determination of the pressure coefficients which are referenced at the roof height. Further details of the wind tunnel parameters and other information were well documented in Stathopoulos and Dumitrescu-Brulotte (1990).

Figure 5.20 compares the experimental data with the computed values for windward wall. It consists of results from normal as well as angled flow conditions. When the flow is normal to the building the axis of symmetry can be formed along the center line of the building and hence only half of the pressure field is shown. For the skew wind, symmetrical flow conditions are assumed along the building diagonal and the four walls are grouped into two major areas as windward walls and leeward walls.

Agreement of the pressure coefficients is better for normal flow than for inclined wind condition. Some small negative pressures values near the edge of the wall are also

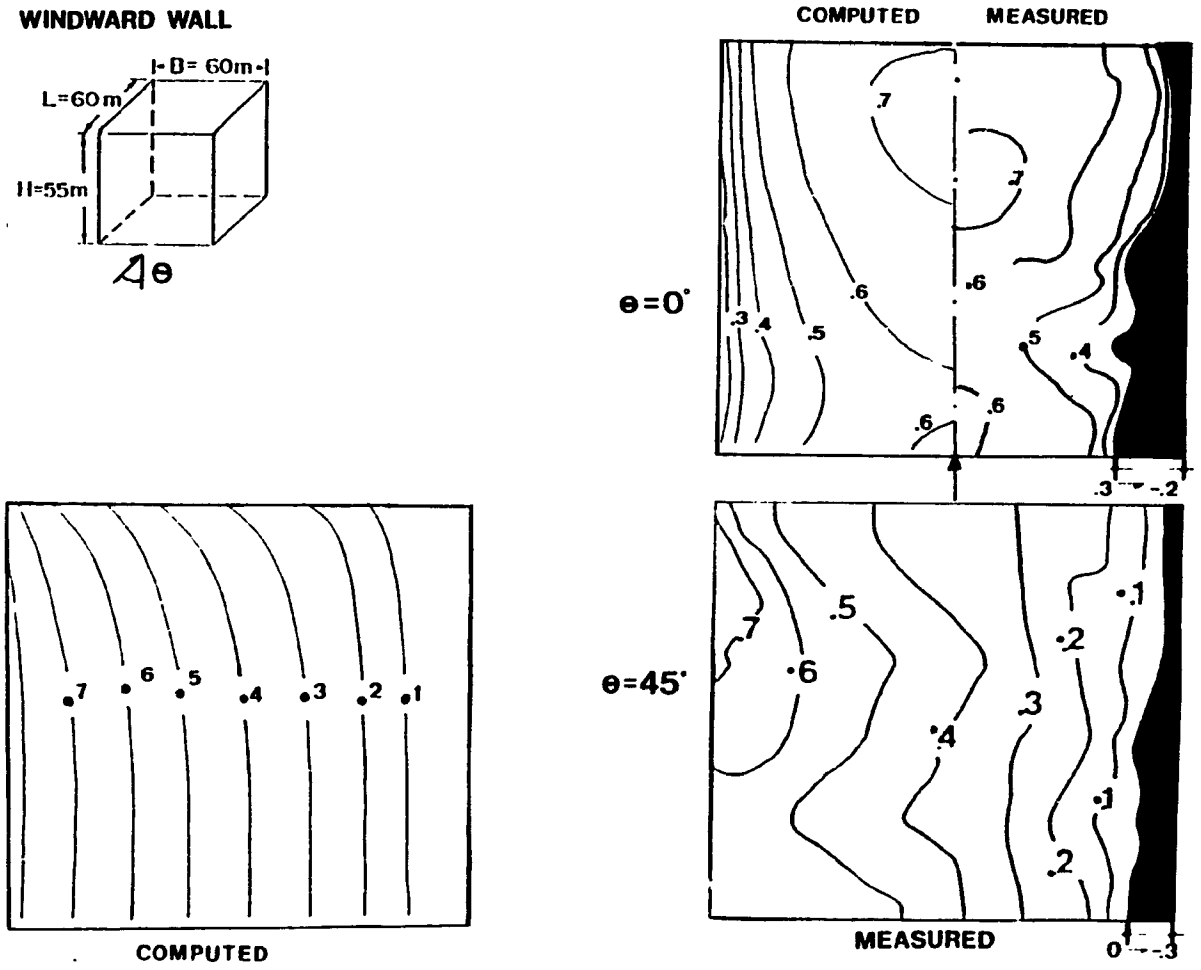

Fig.5.20: Comparisons of the Pressure Coefficients for the Windward Wall of a Building

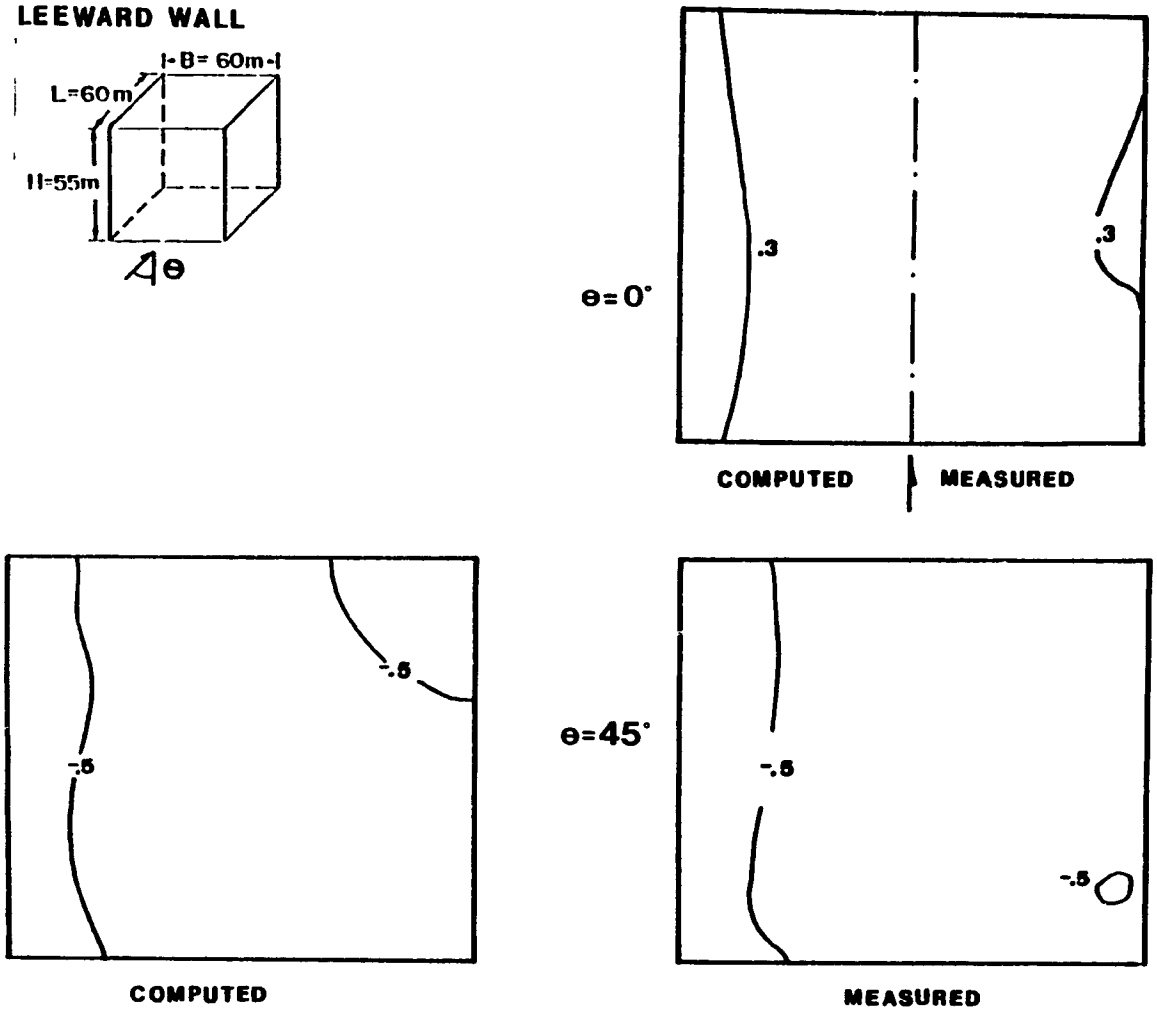

Fig.5.21: Comparisons of the Pressure Coefficients for the Leeward Wall of a Building

measured in the experiments due to the flow separation from the building. The computer model fails to capture this complex flow region and hence no negative values are computed on the front wall. Baetke (1986) also observed similar difficulties when computing 45^0 uniform flow condition around a cube. This may be due to the false diffusion problem which can be conveniently eliminated by using higher order schemes in the numerical modelling. In addition the considered standard turbulence model is well-known for its insensitivity towards flow streamlines and for its low dissipation rate near the solid boundaries. Figure 5.21 displays the comparisons for the leeward wall in the same format as that of Fig. 5.20. For both directions negative pressures are measured and computed. It is interesting to note that this constant suction is also predicted well by the computer modelling.

From the above limited discussion on the pressure and velocity values, the feasibility of the present code in predicting the wind directionality effect is examined and the following features are formulated:

1) the present code with only minor modifications as discussed in section 5.2, can provide encouraging results for various directions of the inflow conditions.
2) overall, the basic characteristics of the flow and changes in its patterns are computed well by the numerical modelling.
3) computed velocities and pressure values agree well qualitatively and quantitatively, at least for some cases, with the measured data.
4) implementing some of the higher order interpolation scheme for the convective part of the differential equations may reduce the differences between the measured and computed values.

CHAPTER 6

COMPUTATION OF WIND EFFECTS FOR MULTIPLE BUILDING CONFIGURATION

" Of course the flow of wind with a prescribed velocity profile, and with an arbitrary direction of incidence over even a single building is a problem of considerable physical complexity: when this problem is extended to an arbitrary configuration of buildings, this complexity is obviously compounded "- T.HANSON, D.M.SUMMERS and C.B.WILSON

A literature survey shows that only very few studies were made on the numerical computation of wind flow conditions around more than one building. Hanson et al. (1986) attempted the prediction of the wind flow field between two parallel buildings without including standard treatment of turbulence conditions. Haggkvist et al. (1989) used the commercially available software PHOENICS developed by Spalding (1981) for the non-quantitative study of wind flow conditions around a house surrounded by a group of similar houses. Significant differences found between the computed pressure values and measured data are attributed to the specification of the boundary conditions when using PHOENICS. Murakami and Mochida (1989. a) also presented the flow field around a group of buildings. However, no attempts were made to validate the computed results by comparison with wind tunnel test data.

The present study examines the feasibility of extending the developed computer code, TWIST, to evaluate wind environmental conditions around multiple building configurations. Therefore, an attempt has been made to simulate the wind environmental conditions around an existing downtown location of Montreal. This chapter has three sections: the first section describes the specifications of the selected multiple building configuration and the surroundings; section two presents and discusses the computed

results whereas section three is dedicated to the experimental measurements and the comparisons of computed results with measured data.

6.1 Specification of the Selected Configuration

A downtown Montreal region, in which the central (Hall) building of Concordia University is located, has been selected. Fig. 6.1 shows the area under consideration as well as the wind direction assumed in the analysis. This direction reflects SW winds. Fig. 6.2 shows probability estimates for the excedance of mean hourly wind speed from different directions at a height equal to 300 m above Montreal. The estimates originate from data measured at Dorval airport at 10 m height for a 10 year period during winter daylight hours. It is apparent from the figure that southwesterly winds are the strongest followed by northeasterly winds. Assuming that the same conditions prevail for downtown locations, the SW winds are likely to be critical for wind environmental studies.

The cluster of buildings A, B, C, D, E and F around the Hall building, X, under consideration is shown in Fig. 6.3. These are the major buildings in the so-called proximity region, which have been modelled for the numerical computation as well as for the experimental measurements. These buildings have been assumed to have rectangular cross-sections. Approximate dimensions of all these buildings and the exact locations of the points of measurements of wind speeds are also shown in the figure. The selected points are at the sidewalks or corners of the building under consideration to monitor the local wind environmental characteristics. Furthermore, the boundaries of computational domain are indicated. The size of the domain are selected based on the previous experience of computing normal wind conditions around a single building (ref:

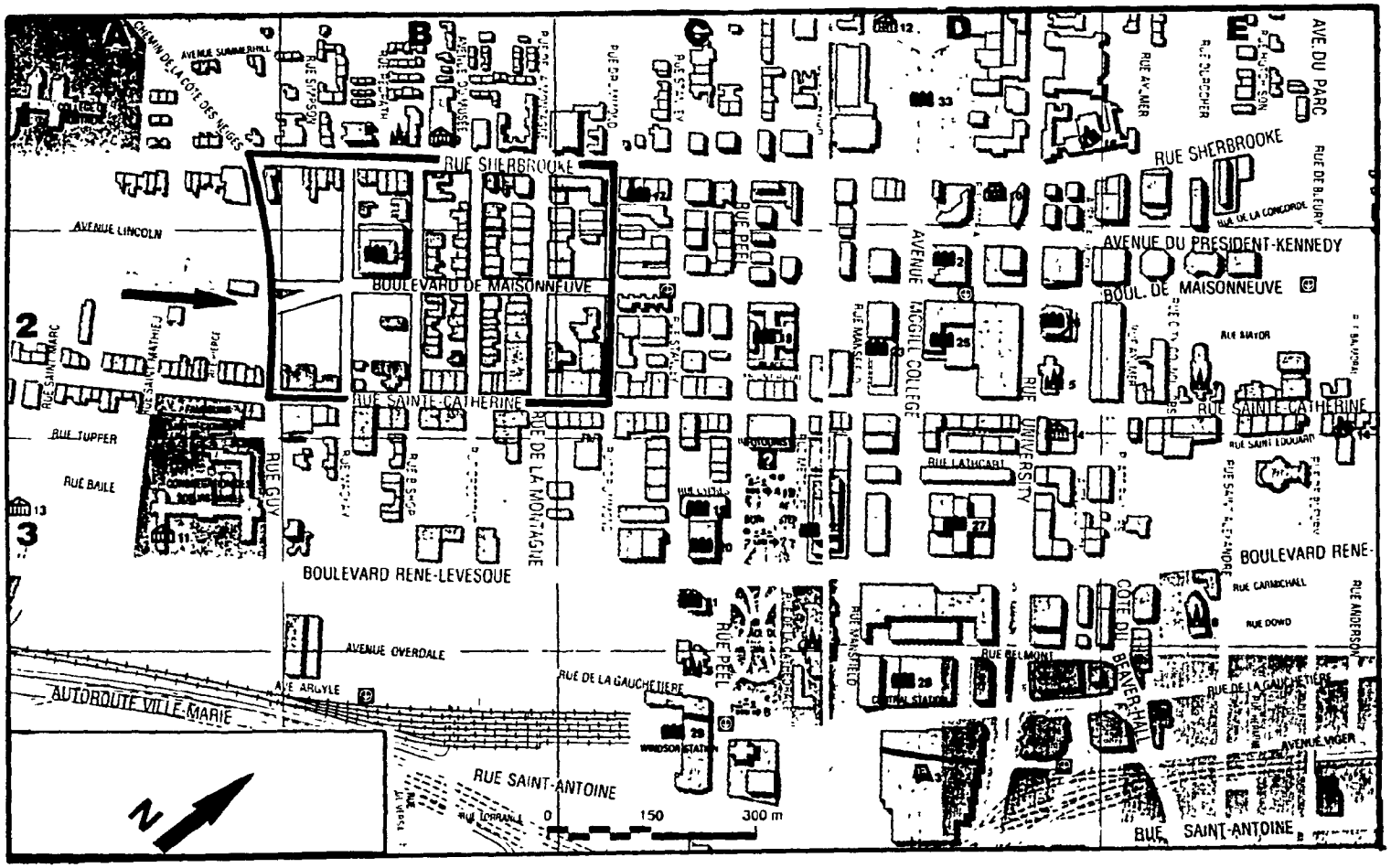

Fig.6.1: Downtown Montreal Highlighting the Region of the Building Under Consideration

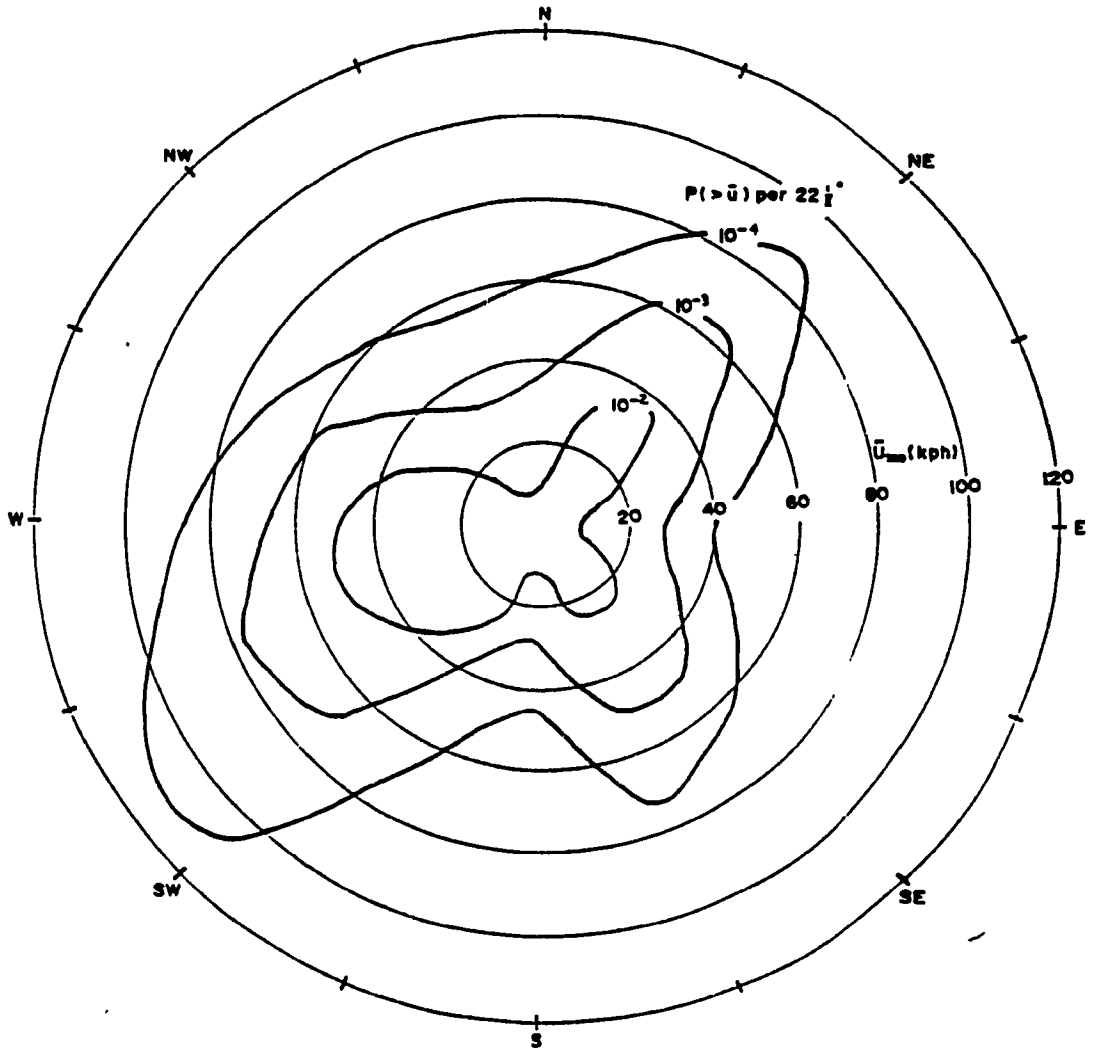

Fig.6.2: Probability Distributions of Hourly Mean Wind Speed at 300 m over Montreal for Daylight Hours (07:00 - 19:00) During the Winter. (Derived from Data Obtained at 10 m Height at Dorval Airport for the Period 1974 - 1983).

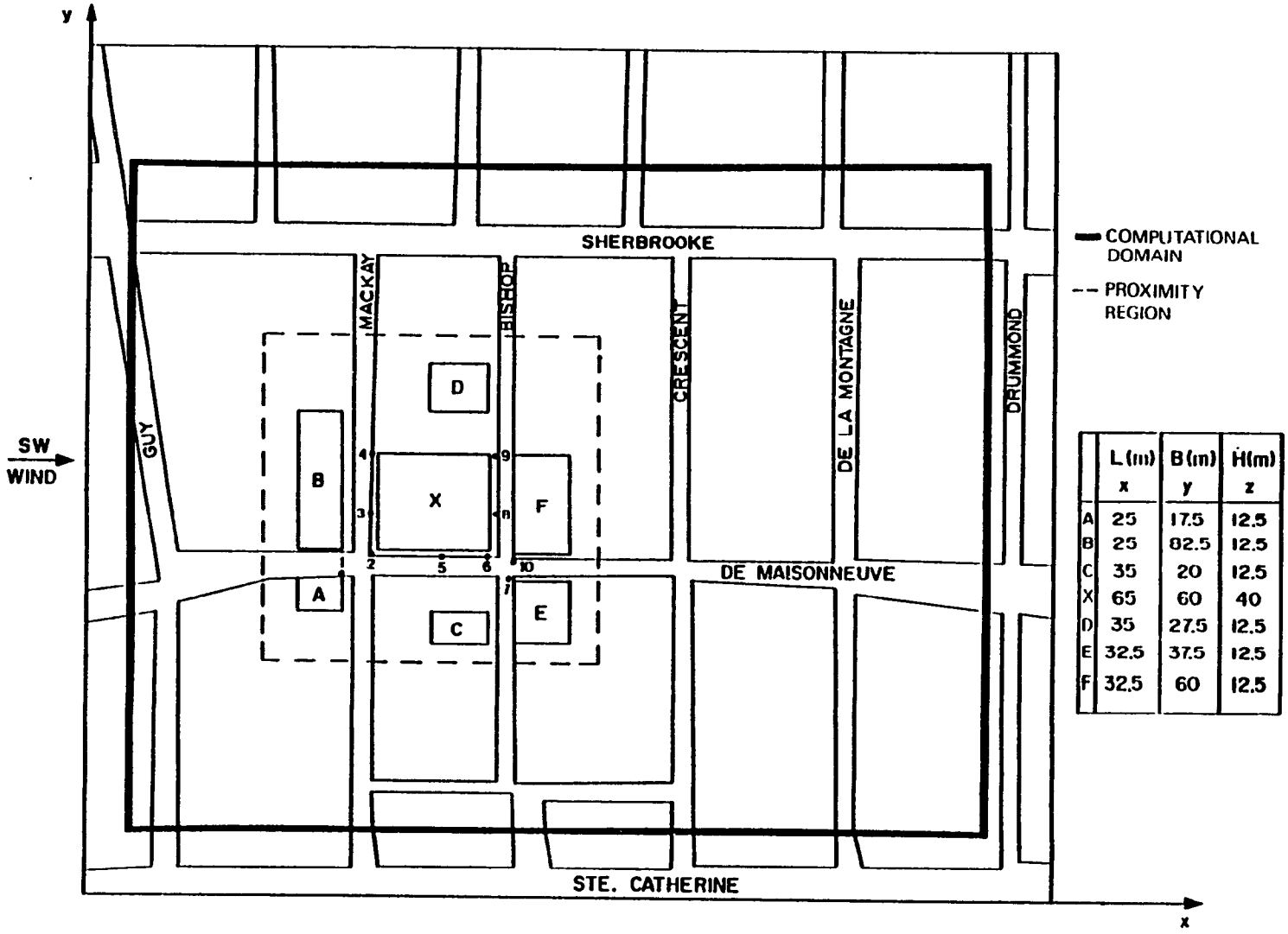

	L(m) x	B(m) y	H(m) z
A	25	17.5	12.5
B	25	82.5	12.5
C	35	20	12.5
X	65	60	40
D	35	27.5	12.5
E	32.5	37.5	12.5
F	32.5	60	12.5

Fig.6.3: Computational Domain, Proximity Region and Buildings Considered

chapter 5). The domain extends from Guy street to Drumond street and for the lateral direction, it goes from north of St.Catherine to Sherbrooke street.

A computational grid mapping of the domain is shown in Fig. 6.4 which displays the relative building location as well. Both the plan view and the side view of the buildings are shown. In the plan view there are 82 nodes along the wind direction and 69 nodes along the lateral direction. Module 1 of TWIST (see: Fig. 4.1) is used to develop this grid system and the non-uniform distribution of the grids point is evident. In the side view it is clear that there are 48 nodes in the vertical direction. The size of the computational domain in each direction is also shown. The grid distribution is denser in the proximity region and the arrangement contains in total 267,648 nodes. From the figure it is also clear that the assumption of symmetrical conditions are not valid, even for the normal (SW) wind flow conditions. This makes the size of the computational domain different from the study of wind flow around a single building. More over available computer resources do not permit any increase in the number of nodes. However, attempts made to reduce the number of nodes to 52 x 55 x 42 led to divergence of the computational algorithm. This is because with the reduction of number of nodes the grid spacing increases and this creates larger discontinuities of the calculated variable which in turn causes divergence in the computation.

TWIST has been modified suitably for the evaluation of wind conditions in the case of multiple building configuration. Major modifications were carried out in the sub-module of BOUNDS which specifies the details of boundary conditions for the computation (see: Fig. 4.2). In fact three new sub-modules were added to BOUNDS to take care of the boundary specification for buildings in the blocks surrounding the Hall building of Concordia University. The implemented algorithm is converged after 61 iterations by

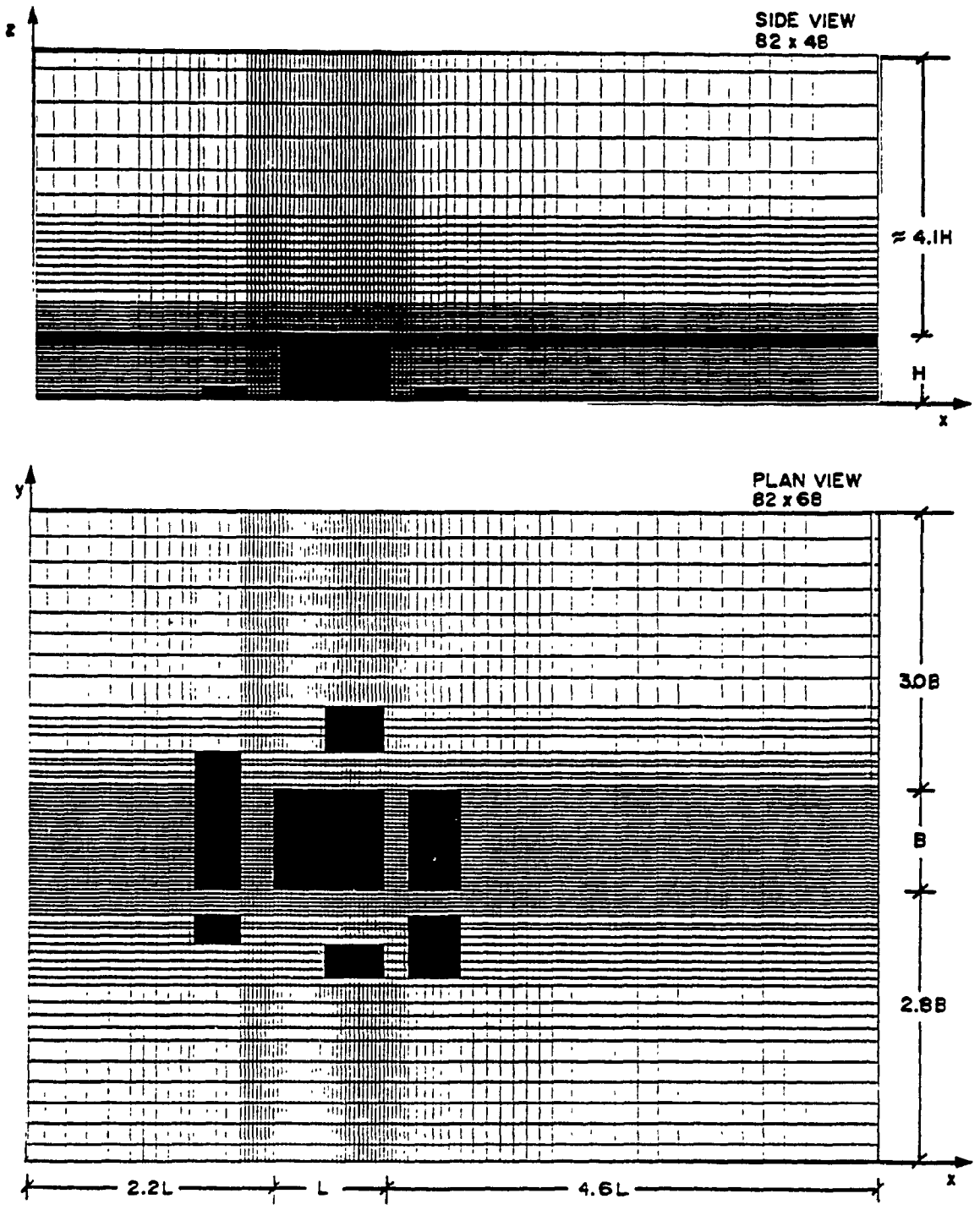

Fig.6.4: Plan and Side view of the Computational Grid

taking around 10 hours of CPU time in VAX /1.2 computer system under batch mode operation.

6.2 Computed Results and Discussion

Figure 6.5 shows the plan view of the computed velocity fields around the buildings at 2 m from the ground level. This 2-D velocity plot was obtained by using the post-processing module of TWIST and considering the longitudinal u and lateral v components of the velocity vectors. The arrows in the figure indicate both the magnitude and direction of the velocity for the respective location of the building surroundings. Flow separation points, changes in wind directions along the two sides of the Hall building, X and wake regions are clearly shown in the figure. The velocity components are smaller in the recirculation area and also at the centre of the building front. The changes in the wind flow direction around the surrounding buildings are also clearly indicated. Vector plots, such as this of Fig. 6.5 are useful as preliminary information for the designer - architect or engineer. Quick derivation by the computer and flexibility in incorporation of changes are features sufficiently impressive to stimulate enthusiasm about computer evaluation of wind effects on buildings as opposed to the traditional physical modelling approach.

To evaluate the changes in the local wind environmental conditions, the calculated velocities are converted into conventional velocity ratios. These velocity ratios are obtained by dividing the magnitude of the velocities around the building under consideration by the velocities in the absence of the building. Since the velocities are taken at the same height for a particular location, these ratios will directly indicate the influence of the building under consideration on the local wind conditions. Values greater than unity indicate an increase in the velocity due to the presence of the buildings. On the

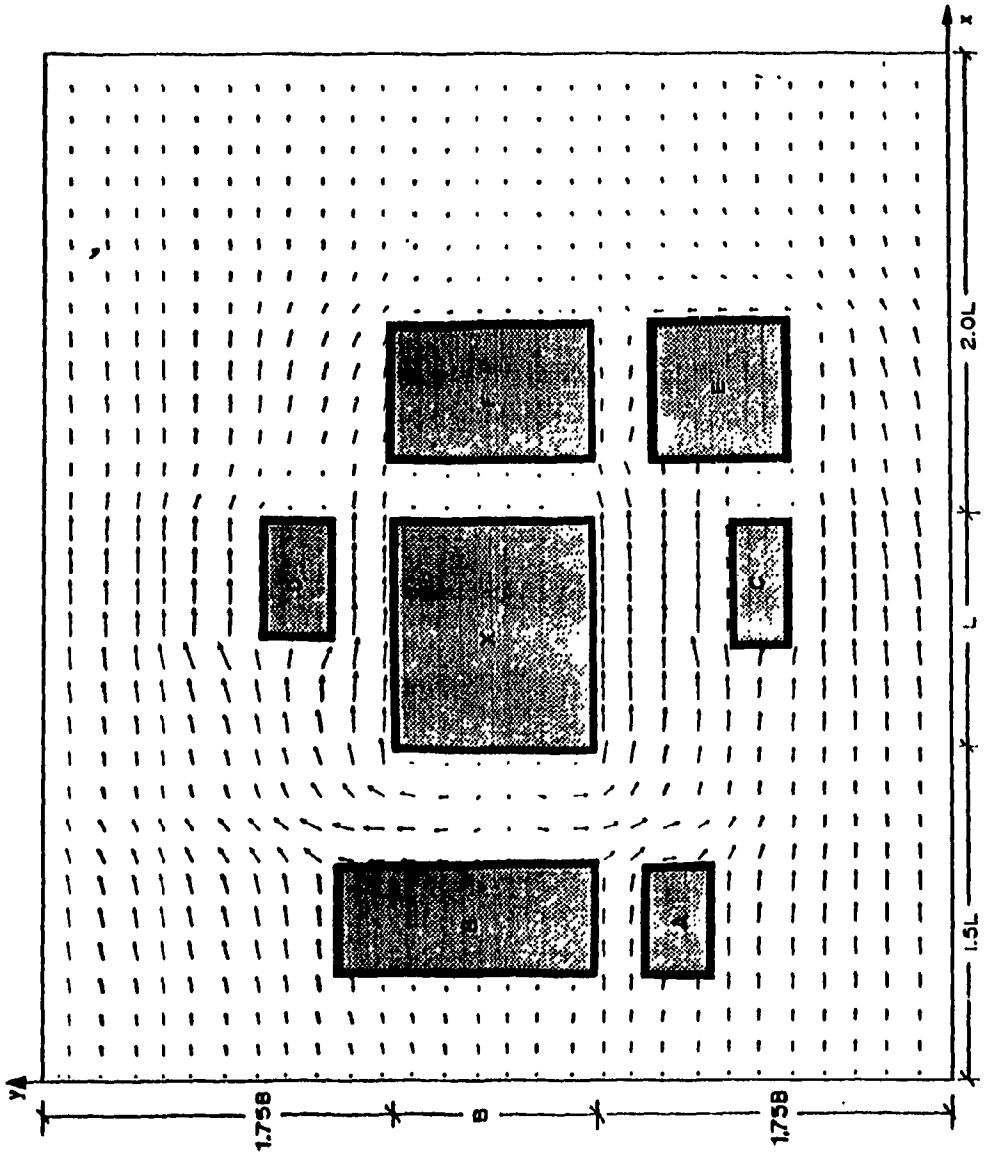

Fig.6.5: Vector Plots of the Computed Velocity Field around the Buildings of the Selected Configuration.

other hand ratios less than one indicate reduction of local velocity when the building is added. Contours of velocity ratios computed at a height of 2 m above the ground, i.e. the normal pedestrian level, are shown in Fig.6.6 which displays high velocity ratio values along the two sides of the Hall building with a maximum of 1.6 at one corner. A 40% increase is also found near building D (top of the figure). These ratios can be further used to evaluate pedestrian comfort around building X and to examine the impact of the construction of building X, if this is a proposed building, on the wind environmental conditions in the area.

6.3 Experimental Measurements and Comparisons

To validate the discussed computed results, experiments were conducted at the boundary layer wind tunnel of the Center for Building Studies, Concordia University. The wind tunnel is of open return circuit type and it is 12 m long with a cross-section of 1.8 x 1.8 m. The roughness of the wind tunnel floor can be changed to simulate open country, sub-urban and urban environments. The diameter of the turntable is 1.21 m and this serves as the working section for the tunnel, where the model buildings are set. Any desired wind direction can be obtained by rotating the turntable either manually or electrically. A speed control system operating manually can produce variable speeds to a minimum of about 4 m/s through outlet volume control. Further details of the wind tunnel parameters and necessary information regarding the simulation criteria can be found in the paper by Stathopoulos (1984.b).

A typical experimental set-up used for velocity measurements is shown in Fig. 6.7 diagrammatically. The temperature of the circulating air is monitored and the tunnel operates only if the fluctuation is within $1^{o}C$. A vertical probe with a hot film sensor connected to the TSI 1034 anemometer is used for the measurements. The location of the

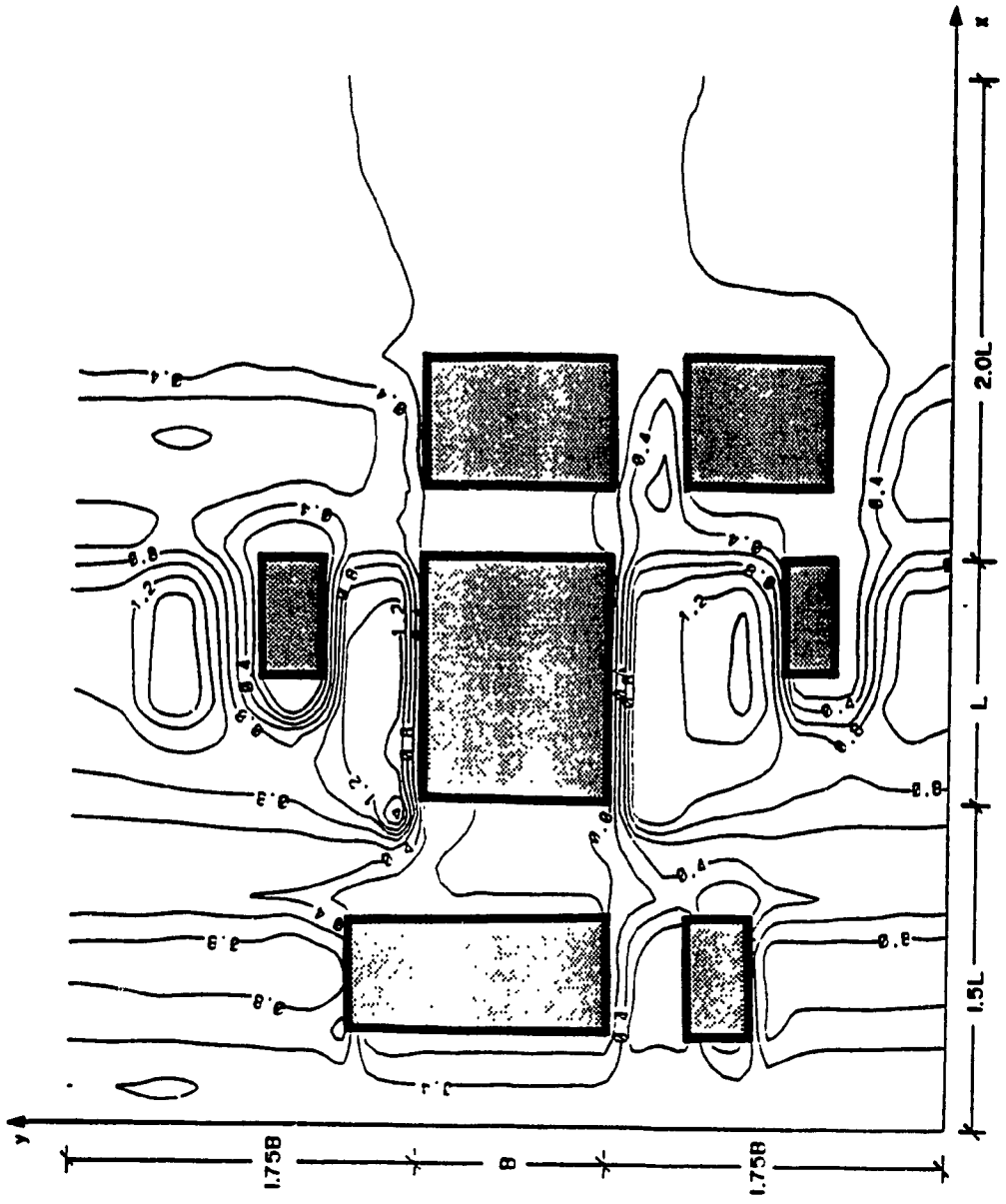

Fig.6.6: Computed Velocity Ratios around the Buildings of the Selected Configurations

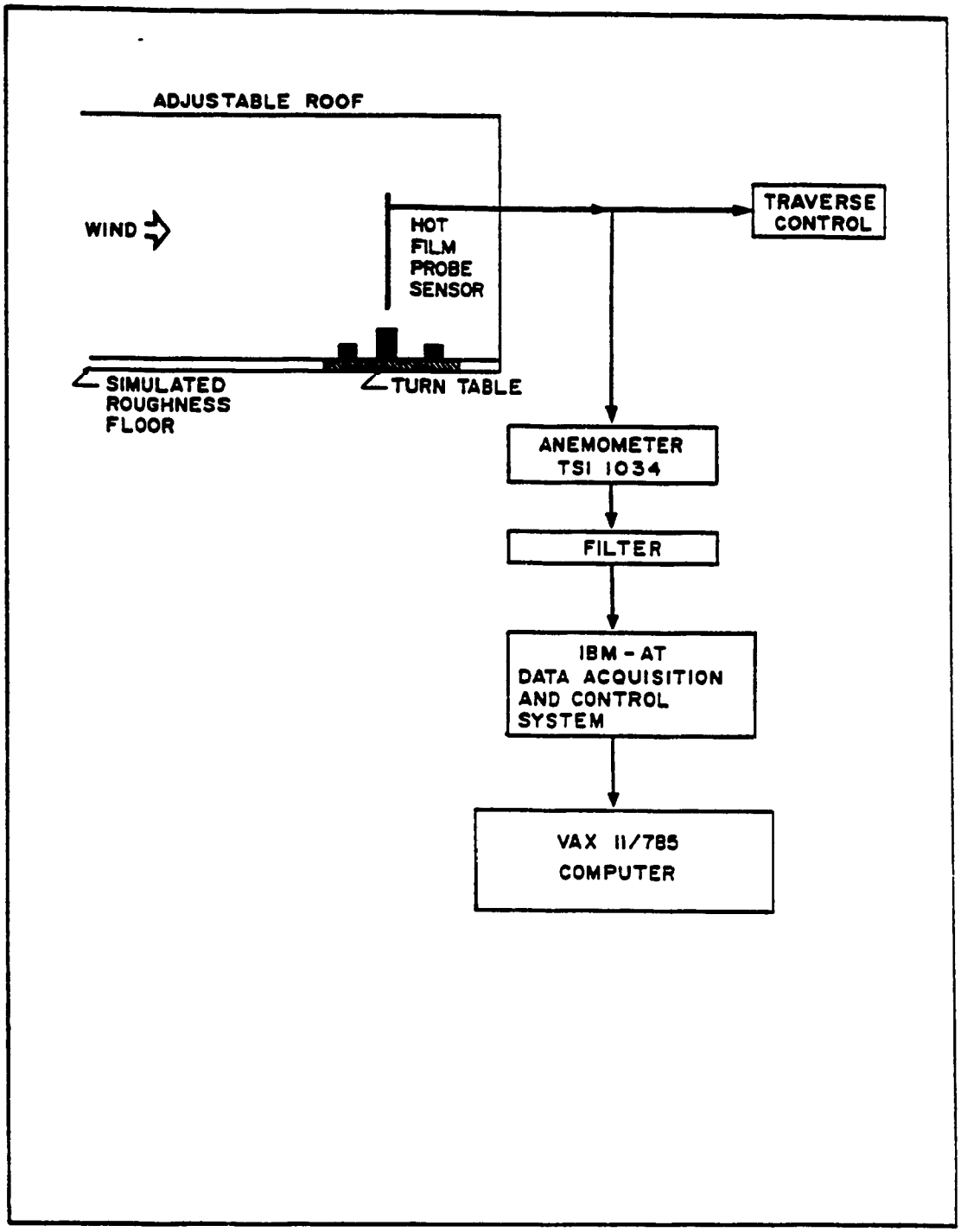

Fig.6.7: Experimental Set - up for Velocity Measurements

probe is controlled by a traverse gear arrangement. Collected velocity signals are passed through a low pass filter and the filtered signal is then analyzed in an IBM 286/12 computer system with data acquisition board. The signal is discretized at the rate of 500 samples/seconds over a sampling period of 30 seconds, during which various statistics such as maximum, minimum, mean and rms velocity values are stored into a file. Collected data files are then transfered to the VAX/1.2 computer for further post-processing by using the kermit network system. This permits a faster analysis of data in comparison to using the IBM-AT system.

In the present study a suburban exposure is considered appropriate with velocity and turbulence intensity profiles shown in Fig. 6.8. The normalized velocity and height from the ground level can be correlated by using the conventional power law profile with exponent 0.25. The turbulence condition is maximum near the ground with a value higher than 20 % and reduces to about 5 % at the gradient height level. The wind tunnel operates using its maximum speed of 13 m/s. Based on the simulation criteria a geometric scale of 1: 500 is used to fabricate the wooden models which are glued on a masonite board in their appropriate location. The set up is placed at the center of the wind tunnel working section such that the Hall building, X, lies at the center of the turntable. Note that only major features are considered for the representation of buildings and details are not included. A variety of low-rise buildings on each side of the Hall building are replaced by a single long low-rise structure and the height of the all surrounding buildings are assumed to be one third of the height of the Hall building for simplicity. This is not exactly representative of the actual buildings but an identical configuration was considered for the numerical modelling.

Wind velocity signals are collected by using the experimental set-up shown in Fig. 6.7. For each location six velocity records are gathered and the arithmetic average of their mean value is calculated as the representative value of the velocity at the location. The

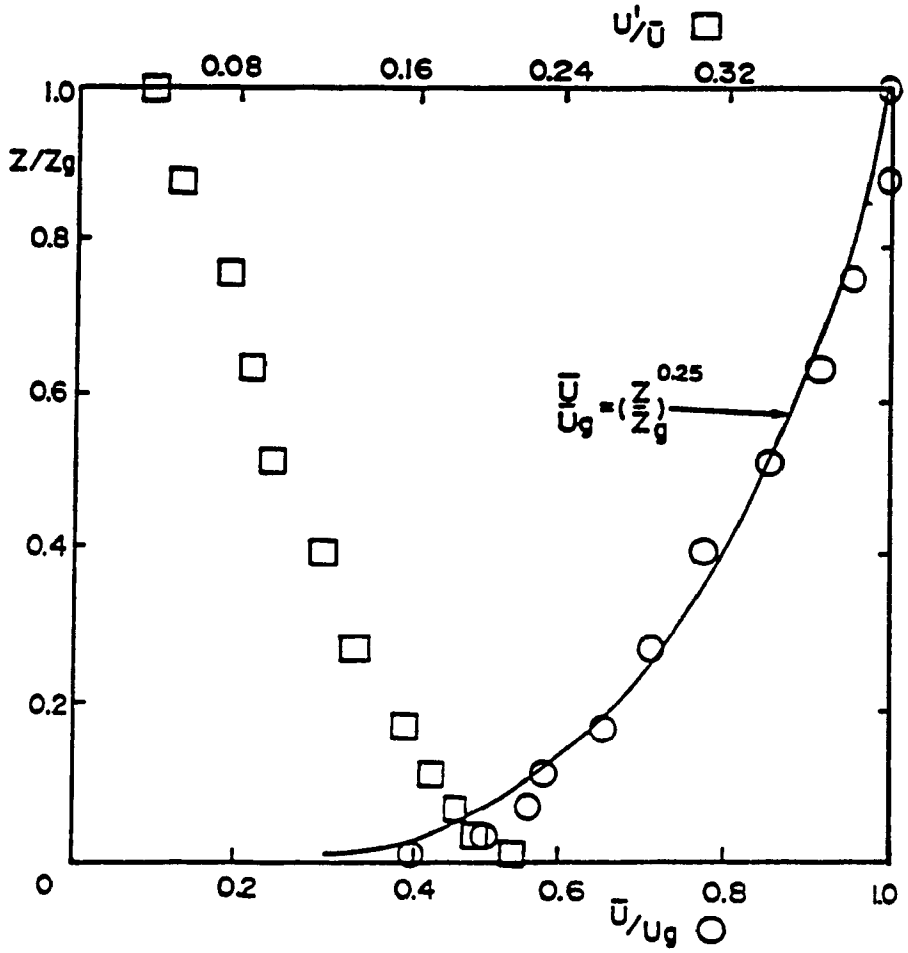

Fig.6.8: Velocity and Turbulence intensity Profiles for a Simulated Suburban Exposure in the Boundary Layer Wind Tunnel

vertical hot film sensor, when placed against the flow will provide a combined effect of the longitudinal u and lateral v components of the velocity at this location. Therefore, the computed velocities are also evaluated as $(u^2 + v^2)^{1/2}$. It should be mentioned however, that the experimental velocities are mainly obtained at points of high turbulence intensity, such as locations very close to the building surfaces. Therefore, the hot film anemometer technique used involves an error in the measured values. As mentioned in the previous chapter, it has been estimated that this error will be about 13 % for 50 % turbulence intensity and less than 2 % for an intensity at 20 % level (TSI, Inc., Lomas,1986). More accurate measurements may be carried out by using a more sophisticated measurement system or a Laser-Doppler anemometer but none of them were available for the present study.

Velocity ratios (amplification or reduction factors) similar to these presented in Fig. 6.6, are shown in Fig. 6.9 for each considered location of the multiple building configuration. Each ratio of the wind velocity in the presence of the building over the velocity in the absence of the building shows directly the effect of the building on the wind environmental conditions. Both measured and computed ratios are included for the comparisons. The magnitude of the ratios are higher at the building corners in comparison to the other locations. The results show generally good agreement within 30 % discrepancy with the exception of points 3 and 8 on which measured and computed values differ more significantly. Note that both these points are in locations of highly complex recirculating flow regions. Consequently, neither measured nor computed values are considered accurate in these locations.

For overall performance evaluation of computation, the same data are plotted in different format as shown in Fig. 6.10. The points above the 45^0 line indicate that the computed ratios are higher than the measured values for that particular location, whereas points below the common line correspond to the lower velocity ratio of the computed values. A

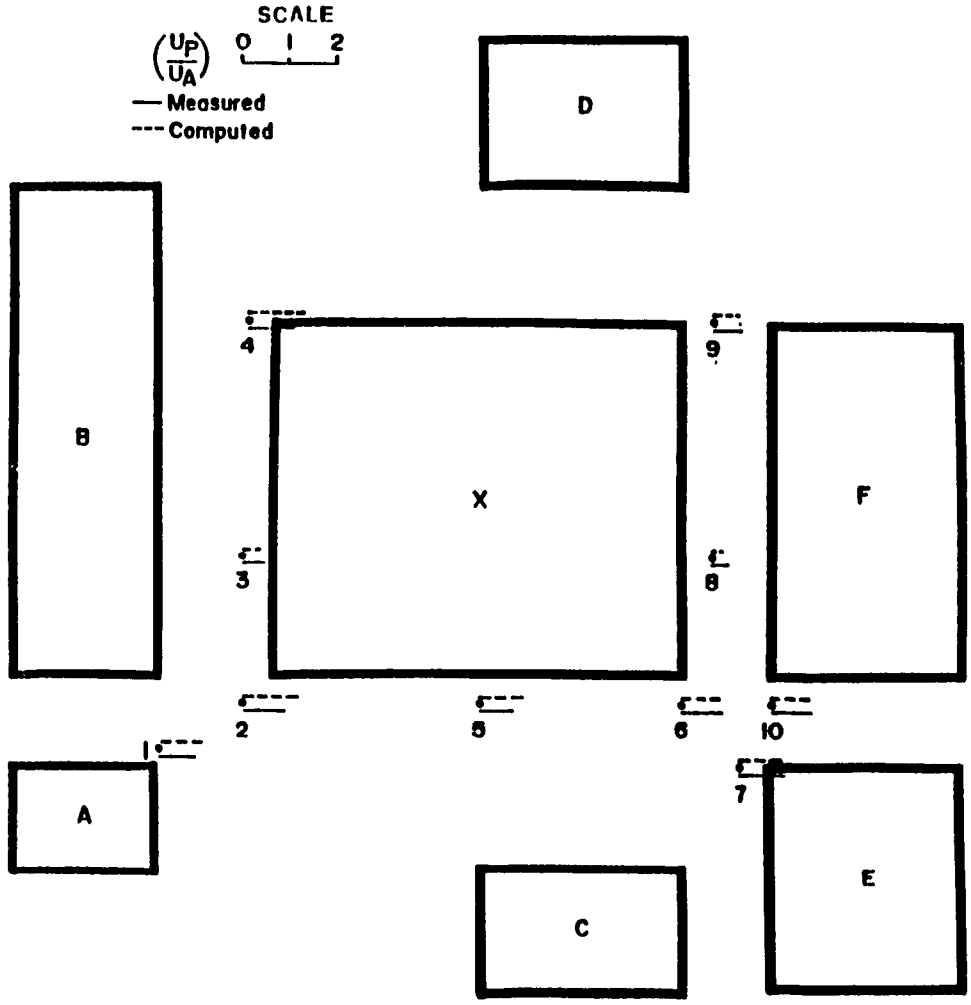

Fig.6.9: Comparisons of the Computed and Measured Velocity Ratios at 2 m from the Ground Level for Various Locations around the Buildings

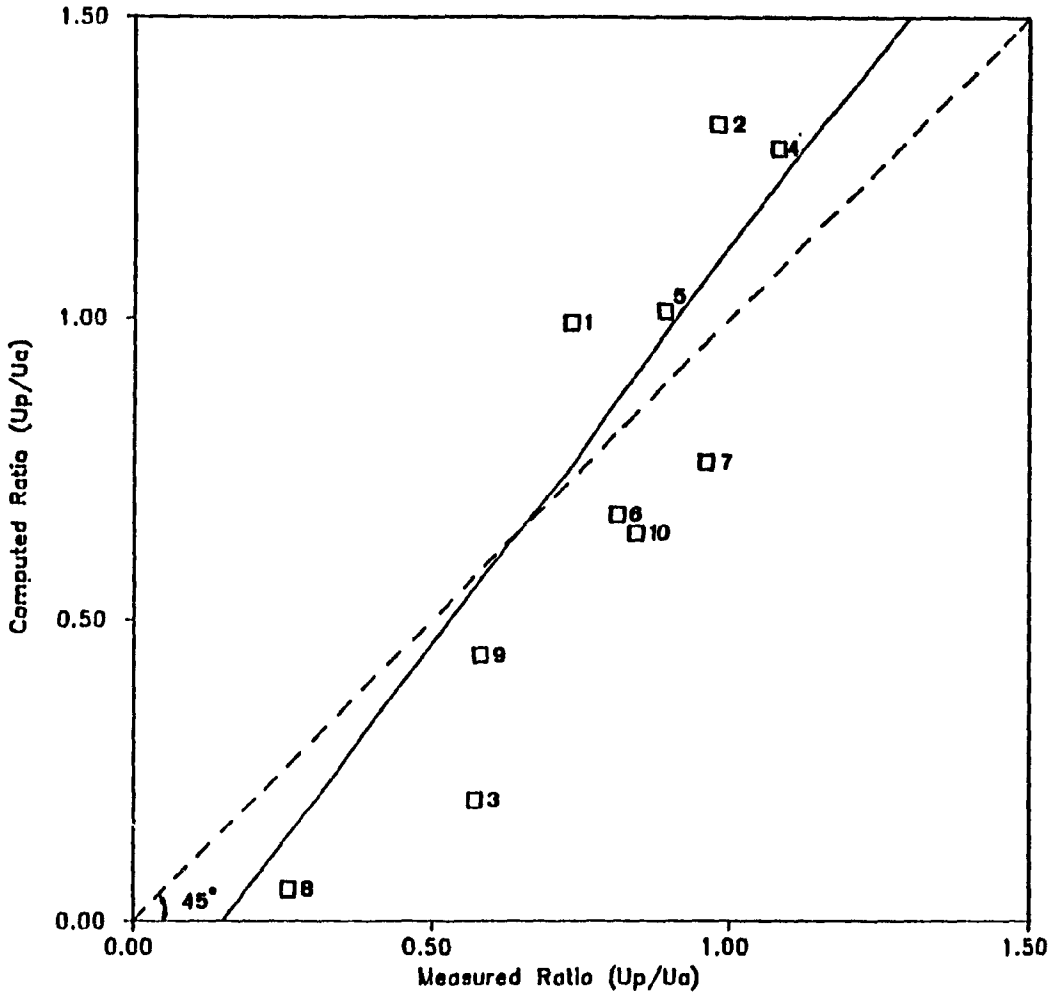

Fig.6.10: Relation Between Measured and Computed Velocity Ratios

point on the line represents no difference between the two sets of data. Most of the points are closer to the 45^{o} line indicating good correlation between the measured and computed velocity ratios. Excluding points 3 and 8, a least square best fit straight line seems to fit the data quite adequately, as Fig. 6.10 shows.

CHAPTER 7

IMPROVEMENTS ON THE TURBULENCE MODELS AND BOUNDARY CONDITIONS

" Should a computer code which provides numerically accurate solutions to the k-ε equations be regarded as validated ? or is it the k-ε model of turbulence that is properly in need of validation ?. In the view of the author, the latter is the case " - D. SPALDING.

Computations for normal as well as angled flow conditions over a single building have been carried out in chapter 5. By making necessary modifications on the computer code, TWIST is further extended for the evaluation of wind environmental conditions around a cluster of buildings. All the computations have been made by using the standard k-ε model to mimic the turbulence in the flow. The conventional wall - functions are used as boundary conditions for all six variables involved in the computation. Comparisons of the computed results with respective wind tunnel data reveal the following:

- mathematical equations and boundary specifications incorporated in TWIST, can predict overall flow features around buildings;
- computed velocity fields at the downstream of the flow and the length of recirculation zones behind the building are significantly underestimated;
- induced suction values on the building envelope have not been computed accurately particularly on building side walls and near the downstream side of the roof where usually the flow is complex in nature.

To improve the predictions, two kinds of refinements have been performed in the numerical modelling process. These are modifications on the standard k-ε model

(section 7.1) and the application of a new zonal treatment method for the boundary specification of the turbulence variables (section 7.2 and 7.3). Section 7.4 compares simulated results based on the new method with the measured data from boundary layer wind tunnels. To generalize the procedure computations and comparisons have also been made for a variety of buildings .

7.1 Modification on the Turbulence Models

7.1.1 Streamline Curvature Correction

For the computation of wind flow conditions around buildings, fluid viscosity is calculated based on the eddy - viscosity concept by using Eq. 3.4,

$$\nu_t = C_\mu \frac{k^2}{\varepsilon} \qquad (3.4)$$

in which k and ε are the kinetic energy and dissipation rate of kinetic energy respectively. The empirically determined proportionality factor, C_μ has a value 0.09, as recommended by Launder and Spalding (1974) along with other universal constants involved in the standard turbulence model, as discussed in section 3.3. However, based on experimental observations, Rodi (1975) has shown that turbulent shear stresses are very sensitive to the streamline curvature of the flow and the viscosity calculated by using the constants of standard k - ε turbulence model does not reflect this sensitivity. He also experimentally found that C_μ will vary from 0.03 to 0.7 depending on the flow region.

An algebraic relation has been derived for the Reynolds stress with a correction that can account for the variation of C_μ. This *adhoc* modification attempts to reflect the variations of the streamline curvature to the turbulent shear stresses and it is named as

streamline curvature correction, Gibson (1978). For the calculation of flow in parallel jets, Leschziner and Rodi (1981) included the streamline curvature and found that the discrepancies between the computed results and measured data are reduced. Influence of the modifications on three numerical schemes namely Upwind Difference Scheme (UDS), Skew Upwind Difference Scheme (SUDS) and Quadratic Upwind Difference Scheme (QUDS) have also been analyzed and the SUDS performed well for the application considered.

The algebraic equation balancing the rate of production γ_{ij} of the Reynolds stress $(\overline{u_i u_j})$, pressure-strain and dissipation can be collectively written, following Leschziner and Rodi (1981), as

$$\frac{\overline{u_i u_j}}{k} = \frac{1-\beta}{\alpha\varepsilon}\gamma_{ij} - \frac{2}{3}\frac{\delta_{ij}}{\alpha}(1-\alpha-\beta) \qquad (7.1)$$

in which δ_{ij} is the well-known Kronecker delta. For local equilibrium of turbulence energy, expressed by $\gamma_k = \varepsilon$, the constants α and β are equal to 1.5 and 0.6 respectively.

Converting (i, j) into streamline coordinates (s, n) the expression for C_μ can be rewritten as:

$$C_\mu = \frac{-K_1 K_2}{1 + 0.57\frac{k^2}{\varepsilon^2}\left(\frac{\partial u_s}{\partial n} + \frac{U_s}{R_c}\right)\frac{U_s}{R_c}} \qquad (7.2)$$

Note that u_s is the velocity along the streamline s with the radius of curvature equal to R_c and K_1 and K_2 are constants equal to 0.27 and - 0.49 respectively. The velocity vector, U_s consists of two components which may be u and v or u and w or v and w. The combination which provides the maximum vector has been considered. This is different from the 2-D approach of Leschziner and Rodi (1981), in which only u and v were used to determine Us.

This expression is evaluated for each grid node during the computation. However the negative velocities at the recirculation zone produce a negative C_μ which is not feasible. To overcome this difficulty, C_μ is not allowed to take a value less than 0.09 (the same as in the case of the standard k- ε model). Similarly, varicus values for - K_1K_2 are also numerically examined by running different computer runs and an empirical value of 0.09 was used in the final computation instead of the actual value which is 0.13 (Durao et al., 1987). Therefore, the equation used in the present study takes the form:

$$C_\mu = \mathrm{Max}\left\{0.09, \frac{0.09}{1 + 0.57\frac{k^2}{\varepsilon^2}\left(\frac{\partial u_s}{\partial n} + \frac{U_s}{R_c}\right)\frac{U_s}{R_c}}\right\} \qquad (7.3)$$

7.1.2 Preferential Dissipation Correction

In addition to the streamline curvature correction, a second modification on the dissipation rate of k, originally proposed by Hanjalic and Launder (1979), has also been implemented. Let us reconsider Eq. 3.13 :

$$U_j \frac{\partial \varepsilon}{\partial x_j} = \frac{\partial}{\partial x_j}\left(\frac{\nu_t}{\sigma_\varepsilon}\frac{\partial \varepsilon}{\partial x_j}\right) + C_1 G\frac{\varepsilon}{k} - C_2\frac{\varepsilon^2}{k} \qquad (3.13)$$

The second term on the RHS of the above equation can be viewed as production or generation and it is defined as:

$$m_\varepsilon = C_1 G\frac{\varepsilon}{k} \qquad (7.4)$$

where a value of 1.44 is used for the constant C_1 in the standard k - ε model. Since m_ε is a positive term in Eq. 3.13, an increase in C_1 may leads to a direct increase in ε. On the other hand, recalling Eq. 3.12 as:

$$U_j \frac{\partial k}{\partial x_j} = \frac{\partial}{\partial x_j}\left(\frac{\nu_t}{\sigma_k}\frac{\partial k}{\partial x_j}\right) + G - \varepsilon \qquad (3.12)$$

in which ε appears as negative source term and thus any increase in ε may indirectly reduces the turbulence level, k. Due to this combined effect, the turbulent viscosity (Eq. 3.4) may be reduced, i.e. the flow will become less viscous. In order to enhance the diffusion process by promoting the formulation of smaller eddies, on which the normal stresses are more effective than the shear stresses, Leschziner and Rodi (1981) suggested the use of

$$m_\varepsilon = \left[C_1' G - C_1'' \nu_t S_{ns}^2\right]\frac{\varepsilon}{k} \qquad (7.5)$$

where C_1' (= 2.24) and C_1'' (= C_1' - C_1) are modified constants to be used instead of C_1. The shear strain in the direction of streamline, S_{ns} is given by:

$$S_{ns} = 0.5\{S_{yy} - S_{xx}\}\sin 2\theta + S_{xy}\cos 2\theta \qquad (7.6)$$

where θ is the angle between the velocity vector and the x-axis, and

$$S_{xx} = 2\frac{\partial u}{\partial x}$$
$$S_{yy} = 2\frac{\partial v}{\partial y}$$
$$S_{xy} = \frac{\partial u}{\partial y} + \frac{\partial v}{\partial x} \qquad (7.7)$$

Eventhough the above modifications are derived by Leschziner and Rodi (1981) so far they have not been tested for the numerical modelling of wind flow conditions around buildings. In addition, the influence of these modifications has not been analyzed when using the Hybrid Difference Scheme (HDS) in the computational procedure. In the present study utilization of these modifications shows significant improvement in the computed pressure values (ref: section 7.1.3). This may be due to the better modelling of the separated flow characteristics. By including these modifications the general equations for wind flow conditions around buildings are regrouped in Table 7.1, it is clear that the modifications not only influence the turbulence properties (k, ε), but they also affects the momentum equation through the proportionality factor, Γ_ϕ. Thus the inter - linkage among the PDE's helps for the improvement of the solution regardless of the difficulties involved in the numerical modelling. Careful examination of the streamline curvature correction reveals that the new C_μ value also affect the boundary specifications and the calculations involved (ref: Eqs. 3.27, 3.29 and 3.33).

Viscosity	$\nu_t = \max\left\{0.09, \frac{0.09}{1+0.57\frac{k^2}{\epsilon^2}\left(\frac{\partial U_s}{\partial n}+\frac{U_s}{R_c}\right)\frac{U_s}{R_c}}\right\}\frac{k^2}{\epsilon}$	7.3
Continuity	$\frac{\partial u}{\partial x}+\frac{\partial v}{\partial y}+\frac{\partial w}{\partial z}=0$	3.5
Compact Form	$U_j\frac{\partial \phi}{\partial x_j}=\frac{\partial}{\partial x_j}\left[\Gamma_\phi\frac{\partial \phi}{\partial x_j}\right]+S$	3.8
x-Momentum	$U_j\frac{\partial u}{\partial x_j}=\frac{\partial}{\partial x_j}\left[\nu_t\frac{\partial u}{\partial x_j}\right]-\frac{\partial p}{\partial x_1}$	3.9
y-Momentum	$U_j\frac{\partial v}{\partial x_j}=\frac{\partial}{\partial x_j}\left[\nu_t\frac{\partial v}{\partial x_j}\right]-\frac{\partial p}{\partial x_1}$	3.10
z-Momentum	$U_j\frac{\partial w}{\partial x_j}=\frac{\partial}{\partial x_j}\left[\nu_t\frac{\partial w}{\partial x_j}\right]-\frac{\partial p}{\partial x_1}$	3.11
Kinetic Energy	$U_j\frac{\partial k}{\partial x_j}=\frac{\partial}{\partial x_j}\left[\frac{\nu_t}{\sigma_k}\frac{\partial k}{\partial x_j}\right]+G-\epsilon$	3.12
Dissipation Rate	$U_j\frac{\partial \epsilon}{\partial x_j}=\frac{\partial}{\partial x_j}\left[\frac{\nu_t}{\sigma_\epsilon}\frac{\partial \epsilon}{\partial x_j}\right]+\frac{\epsilon}{k}\left(C_1'G-C_1''\nu_t S_{ns}^2\right)-C_2\frac{\epsilon^2}{k}$	7.8

Table.7.1: Modified PDE's Representing Wind Flow Conditions Around Buildings

7.1.3 Results and Discussion

Both modifications discussed in the previous subsection have been utilized in the present study in an attempt to better represent the separated flow characteristics. Computations were repeated by keeping all the other parameters such as inlet velocity profile, number of grids on the computational domain and its size as constant. The new results were then compared with those obtained by using the standard k-ε model. This subsection presents two such comparisons for pressure coefficients. More comparisons, to demonstrate the combined influence of these modifications and the newly developed boundary treatment method are given to the following section.

Figures 7.1 and 7.2 present the newly computed pressure coefficients along with the old values and the measured data respectively for buildings of 55 m and 120 m high. These pressure coefficients are normalized with respect to the dynamic velocity pressure at the building roof height. The modifications implemented in the k-ε model reduce the differences between the experimental data and the computed values for all walls. Although pressure coefficients are marginally affected on the windward wall, there is significant improvement in computed suctions on the side wall. Remarkable reductions in the differences between the methods, particularly for nodes that are near the ground and at the top of the building (H = 55 m) are obtained. This can be related to the improved mathematical representation of recirculation zones and involved eddies. Improvements in the separation of the flow on the side of the building and the modified curvature of the shear - layer also increase suctions on the leeward wall. The inclusion of two additional equations { equations (7.3) and (7.5) } in the computer coding naturally demands more computer resources. Nevertheless, the improvements in the predicted pressure would justify these additional resources.

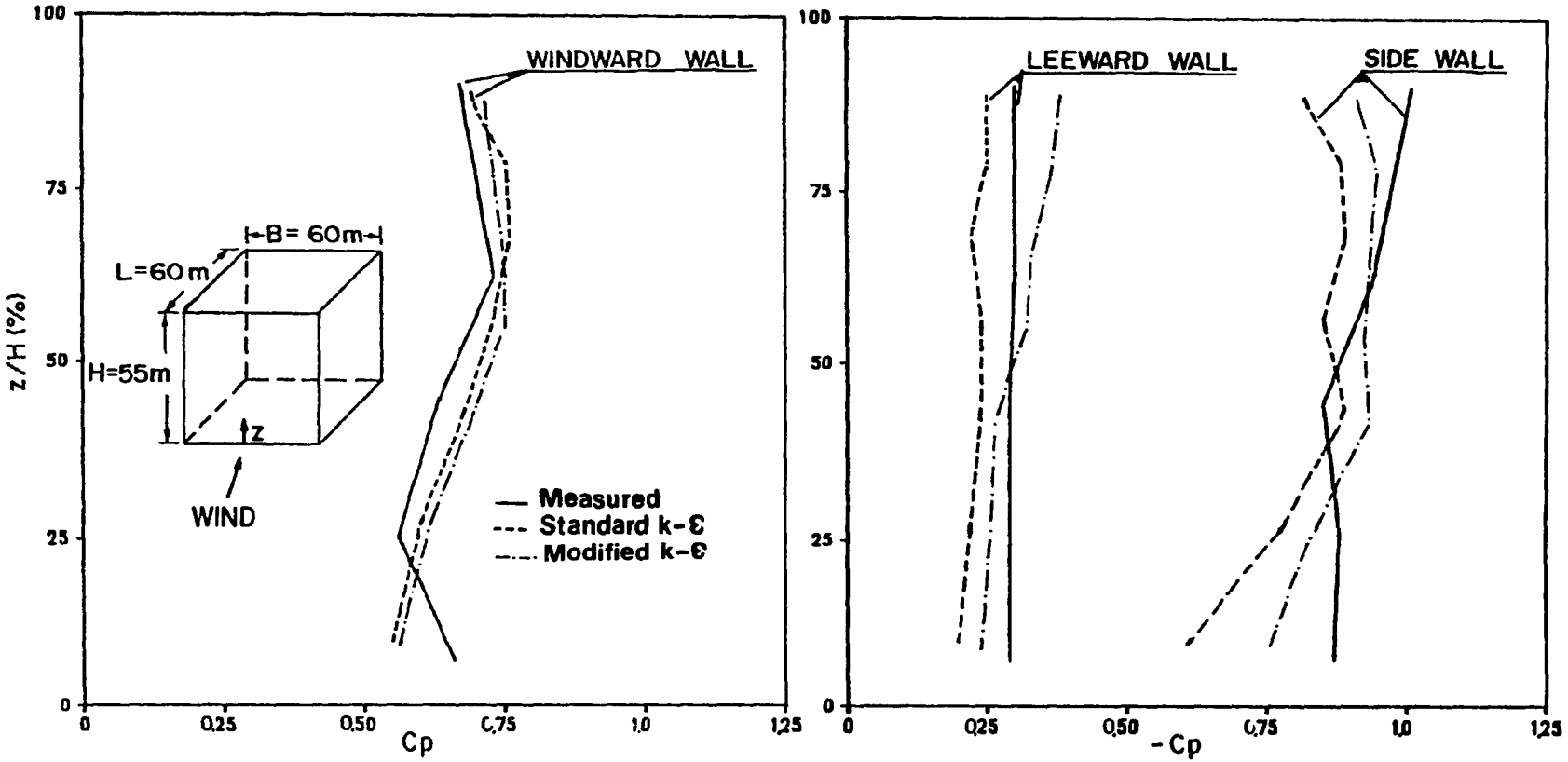

Fig.7.1: Wind - Induced Wall Pressures on a Building Computed by using the Modified Turbulence Models (H = 55 m)

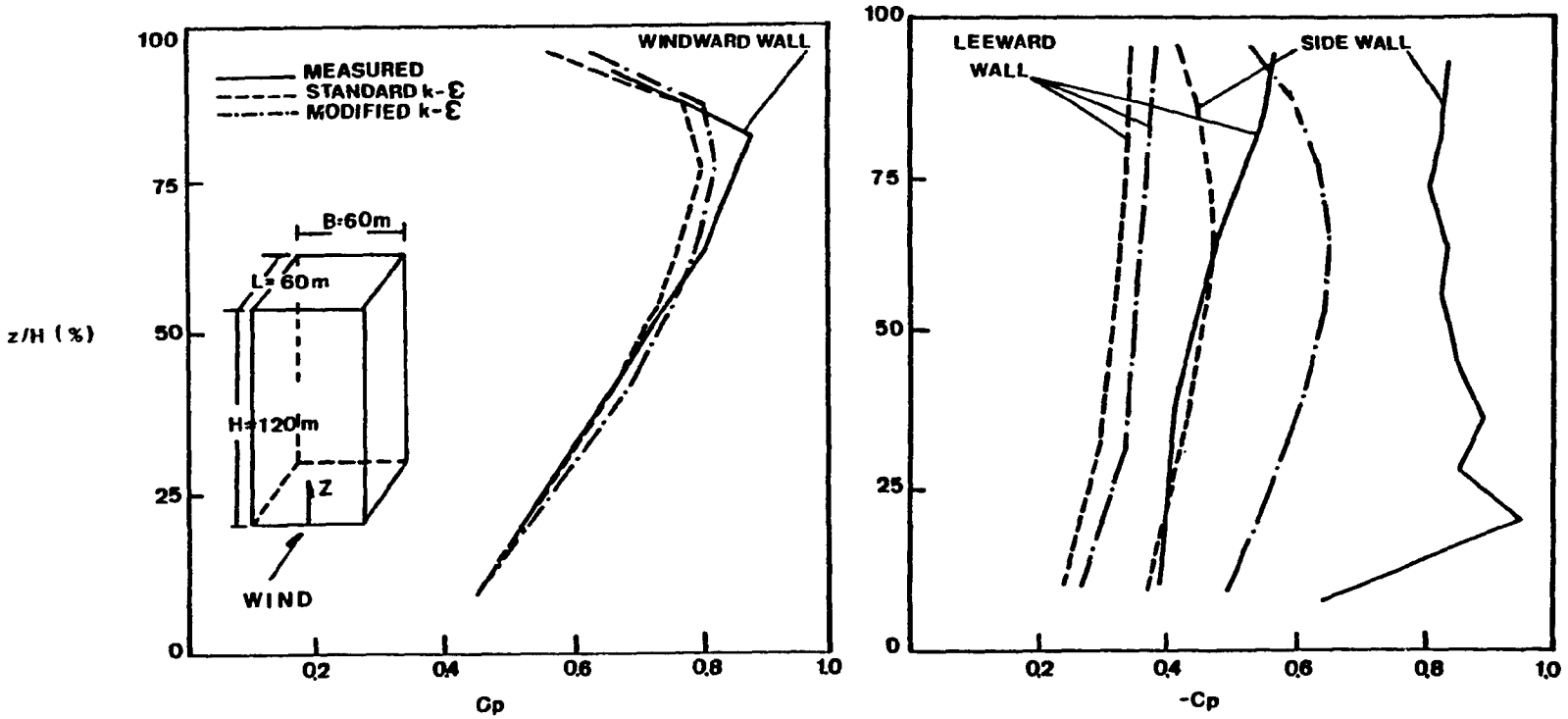

Fig.7.2: Wind - Induced Wall Pressures on a Building Computed by using the Modified Turbulence Models (H = 120 m)

When comparing the results of Figs. 7.1 and 7.2, it is clear that the agreements between the measurement and computation are better for the 55 m high building in comparison to the 120 m high building, in particular for side wall, eventhough L/B = 1.0 for both cases. It is interesting to note that the implemented streamline curvature is developed based on 2-D flow (u,v) assumption whereas only 1-D flow field is considered for the derivation of preferential dissipation correction. For tall buildings the contribution from the vertical velocity component (w) may be significantly important near the building envelope. It is also difficult to separate and identify the reasons due to the strong non-linear nature of the problem.

To evaluate the building height effect, additional computational runs are performed by keeping L/B =1 for two other building (H = 24 m and 145 m) with slightly different grid arrangements. Comparisons of the computed pressure coefficients with measured data have not shown consistent changes with respect to the building height. In conclusion, an overall assessment of tests indicated that modifications alone cannot improve the numerical results as whole; therefore the attention was turned to the influence of boundary conditions.

7.2 Zonal Treatment Method for Solid Boundaries

In numerical modelling processes boundary specifications for the involved variables play a major role in the computed results. This section introduces a new boundary treatment method for two variables involved in the computation of 3-D wind flow conditions around buildings. Comparisons of the computed results made with the measured wind tunnel data indicate that wind velocities, turbulence properties and wind generated pressures are significantly improved when the new method is applied.

In the previous section Eqs. 3.12 and 7.8 are used to compute the turbulence properties of the flow. The conventional wall functions are incorporated to account for the presence of the building in the fluid. This fails to reproduce the details of the local viscous effect and also creates numerical stiffness problems - see Spalding, (1982). Numerical stiffness occurs when the source term is forced to take full burden of transforming the presence of building to computational domain. Moreover when the grids near the solid boundaries are not fine enough the computed wall shear stress is not realistic and this can induce numerical divergence during the computational procedure. Naturally, this unwanted situation demands a very dense grid layout near each solid surface which is practically not feasible.

In addition, Eqs. 3.12 and 7.8 have been developed, basically for high Reynolds number fluids and they are referenced as High Reynolds number Turbulent Models, hereafter abbreviated as HRTM. These are used as engineering tools to simulate only the gross features of turbulence and they do not pay much attention in identifying the interactions between the various scales of motion {Spalding, 1982 and Bernard, 1986 }. Moreover, for the laminar flow validity of these equations is questionable. For numerical computation of flow with low Reynolds number and to reproduce the local laminarization phenomenon the so-called Low Reynolds number Turbulent Models, hereafter abbreviated as LRTM, have been developed by Jones and Launder (1972), Ng and Spalding (1972) and subsequently modified by Hoffman (1975) and Chien (1982). An excellent review of the LRTM used for near wall fluids is presented by Patel et al. (1985). Thus two sets of equations, one for the fully turbulent zones and the other for near wall fluids appears as an ideal solution when the wind flow conditions around buildings are considered. However, this approach increases the number of variables to handle and it also demands more computer resources.

To overcome the numerical stiffness problems and to reduce the computational cost, a new zonal treatment method is presented for the solid boundary treatment of k and ε. In the present approach the HRTM are used only (in discretized form) for fully turbulent regions where they are valid. In order to account for the thin VSL the following procedure is developed and incorporated into the computer code.

7.2.1 Treatment for Kinetic Energy

The kinetic energy, k, for isotropic turbulent motion can be expressed as:

$$k = \frac{1}{2}\left(\overline{u'}^2 + \overline{v'}^2 + \overline{w'}^2\right) \qquad (7.9)$$

where u', v' and w' are the fluctuating velocity components along x, y and z directions respectively as shown below:

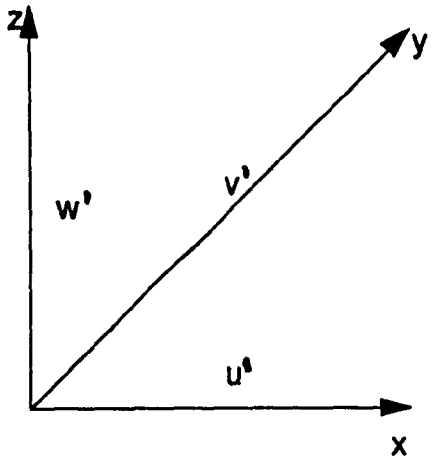

By using the Taylor series expansion for fluctuating velocity components near the wall it can be shown - see Jones and Launder (1972) and Chien (1982) - that the kinetic energy of the fluid varies with the square of the distance from the solid boundary.

$$k \approx d_P^2 \qquad (7.10)$$

where dP is the distance of the considered grid node from solid boundary as shown below:

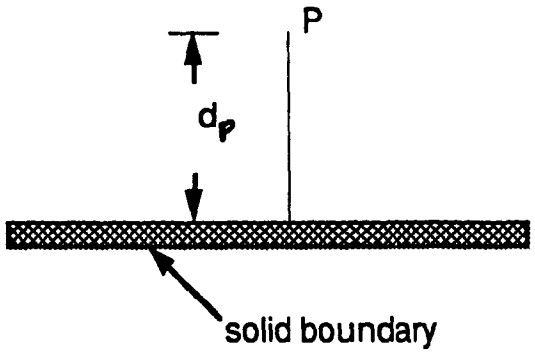

One can then obtain the following expression for k within the VSL:

$$k_s = k_e \frac{d_s^2}{d_e^2} \qquad (7.11)$$

in which k_e and k_S are the kinetic energy at the edge and within the VSL respectively. It is worth mentioning that k_e is evaluated as previously and k_S can be calculated for all grid nodes in the VSL.

7.2.2 Treatment for Dissipation Rate of Kinetic Energy

As previously explained the HRTM is not valid to calculate ε within VSL and hence attempts have also been made to formulate algebraic equations for the computation of ε. The total dissipation rate is not zero near the wall due to isotropic part of the energy dissipation, as explained by Jones and Launder (1972) and Markatos (1986). The wall dissipation, D is given by the equation:

$$D = \nu\left[\left(\frac{\partial \bar{u}'}{\partial y}\right)^2 + \left(\frac{\partial \bar{w}'}{\partial y}\right)^2\right]_{y=0} \qquad (7.12)$$

Near the solid boundaries the fluctuating vertical component is presumed negligible. For instance along the lateral direction at y = 0, the fluctuating component v' can be assumed as zero and therefore the kinetic energy can be deduced from equation 7.9 as:

$$k_{y=0} = \frac{\overline{u'}^2 + \overline{w'}^2}{2} \qquad (7.13)$$

Assuming a linear variation of the velocity with distance from the wall and combining Eqs. 7.12 and 7.13, the following relationship is obtained:

$$D = \frac{2\nu k}{y^2} \qquad (7.14)$$

Within the VSL, the wall dissipation (D) is equal to the flow dissipation rate of kinetic energy (ε) and thus the dissipation rate of kinetic energy can be expressed by:

$$\varepsilon_s = \frac{2\nu_e k_e}{d_e^2} \qquad (7.15)$$

where ν_e is the fluid viscosity at the edge of the VSL.

The algebraic equations 7.11 and 7.15 are used to calculate k and ε within the VSL. Equations 3.12 and 7.8 (ref: Table 7.1) are used only for zones outside the VSL. The problem of fixing the edge of VSL is effectively handled by using the conditions from Eqs. 3.29 and 3.30 (ref: section 3.4).

Eventhough considerable difficulty exists for application of the zonal treatment methodology in the computation, its utilization has been found advantageous over the current approach. The new procedure is physically valid and it also alleviates the source term burden in transforming all the information about the presence of solid boundaries into the computational domain. Thus the new approach is not numerically stiff. Most importantly, improvements are made in the computed values so that better agreement with the experimental data is achieved.

7.2.3 Predicted Flow Behaviour

Before comparing numerical results by using the new approach with experimental data, it will be informative to examine the computational evaluations obtained with two boundary treatment methods (wall functions, zonal treatment). Compared parameters include the kinetic energy (in terms of turbulence intensity of the flow), its rate of dissipation, pressure and the improved velocity field around the building. They are presented in Figures 7.3 to 7.13 where the flow distribution represents a side view passing through the middle of the building.

Figures 7.3 and 7.4 present the distribution of turbulence intensity around buildings 55 m and 120 m high respectively. The square-root of the computed k values normalized with streamwise velocity at the gradient height is used to represent turbulence intensity. Results are plotted in contour form. Values obtained by using the conventional wall function approach and those computed with the new boundary treatment method are compared. It is useful to recall that for the wall function method the source term of equation (3.14) is modified for all the five variables (u, v, w, k, ε) when solid boundaries are identified during the computational procedure. However, in the new zonal treatment approach only velocity variables are modified based on the local Reynolds number. In contrast, the kinetic energy k and its dissipation rate ε are calculated using

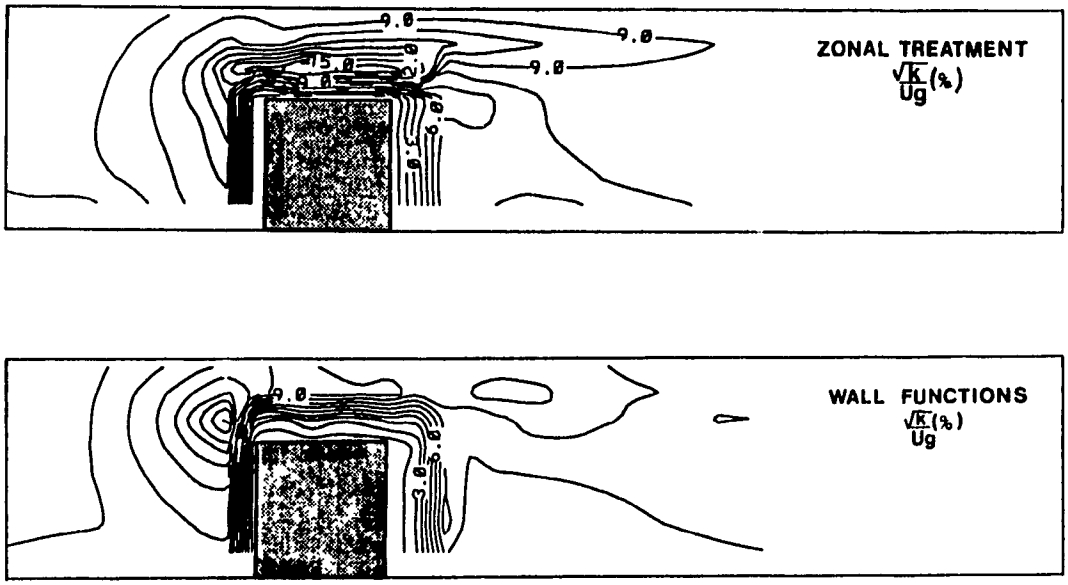

Fig.7.3: Computed Turbulence Intensity around a Building
(Side view, H = 55 m)

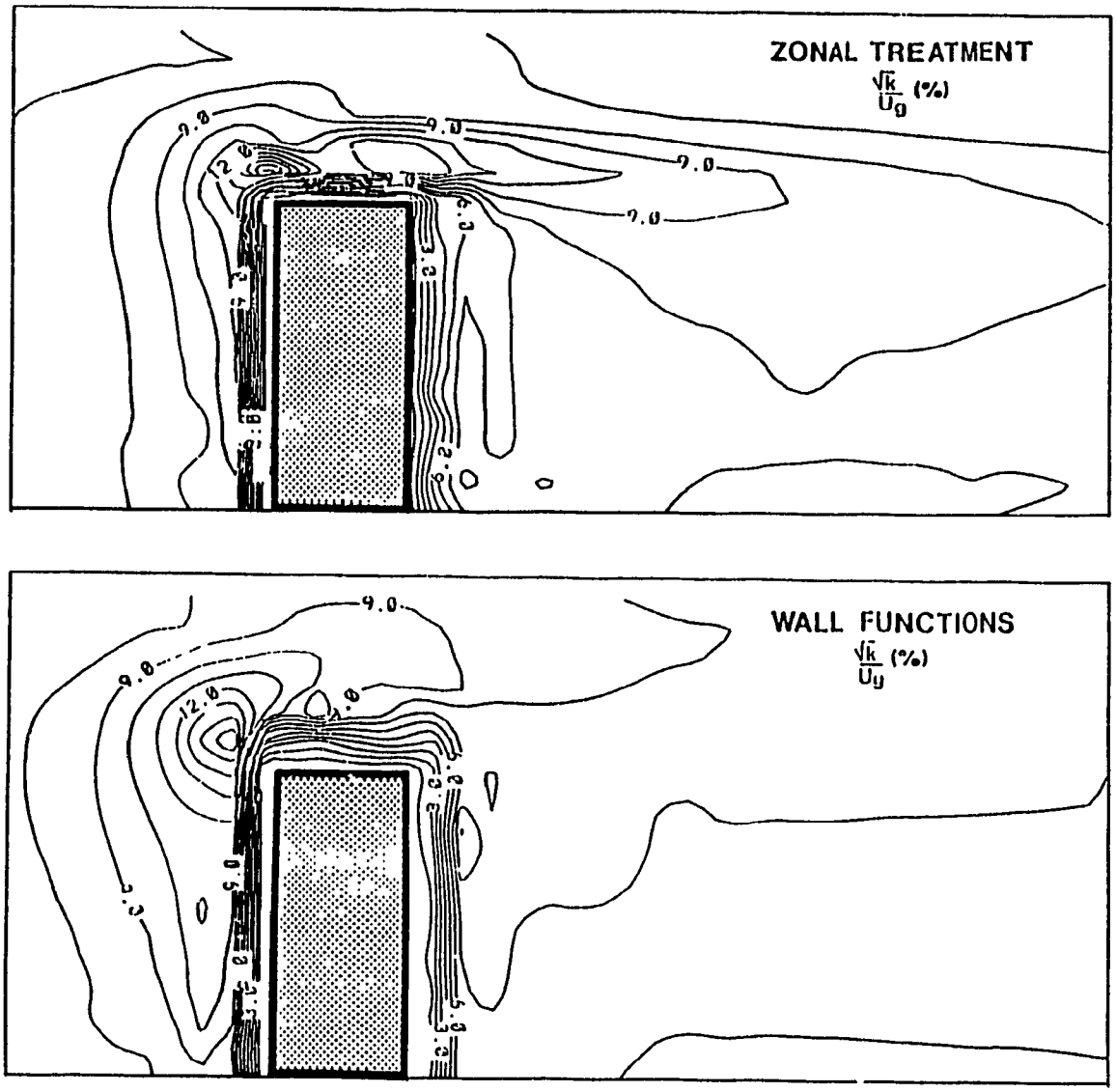

Fig.7.4: Computed Turbulence Intensity around a Building
(Side view, H = 120 m)

the algebraic equations (7.11) and (7.15) within the VSL whereas for the turbulent zone, discretized equations are modified using the wall function approach .

In comparing the turbulence intensity obtained by using the two approaches, it can be observed that the zonal treatment method provides higher k values near the flow separation region and above the roof surface. In addition, the intensity is also higher in the wake region in comparison to the data obtained by the wall function approach. The peak value of the intensity dies down more slowly in the case of zonal treatment and this is consistent with previous experimental observations discussed in Vasilic-Melling (1977). Figure 7.5 and 7.6, show the distribution of dissipation rate of k of the same buildings. Increased k near the boundary provides higher ε values in the zonal treatment method - see Equation (7.15)- and these are found to be more representative of the fluid interaction with the solid surface, as explained by Patel et al. (1985) and Rodi and Scheuerer (1986).

Figures 7.7 and 7.8 show the pressure distribution around the buildings for normal wind conditions and in dimensionless form. Increasing positive pressure in the upstream and constant negative pressure at the downstream of the building with a zone of zero pressure near separation are clearly shown. Only marginal differences are found between the two methods for the upstream pressure field. However, differences in the generated negative pressures both on the leeward wall and on the roof of the building are evident. The zonal treatment method yields results showing higher suctions on the windward portion of the roof and constant suctions maintained further downstream in the wake. This will be further discussed in the comparisons of computed pressure coefficients with respective experimental data.

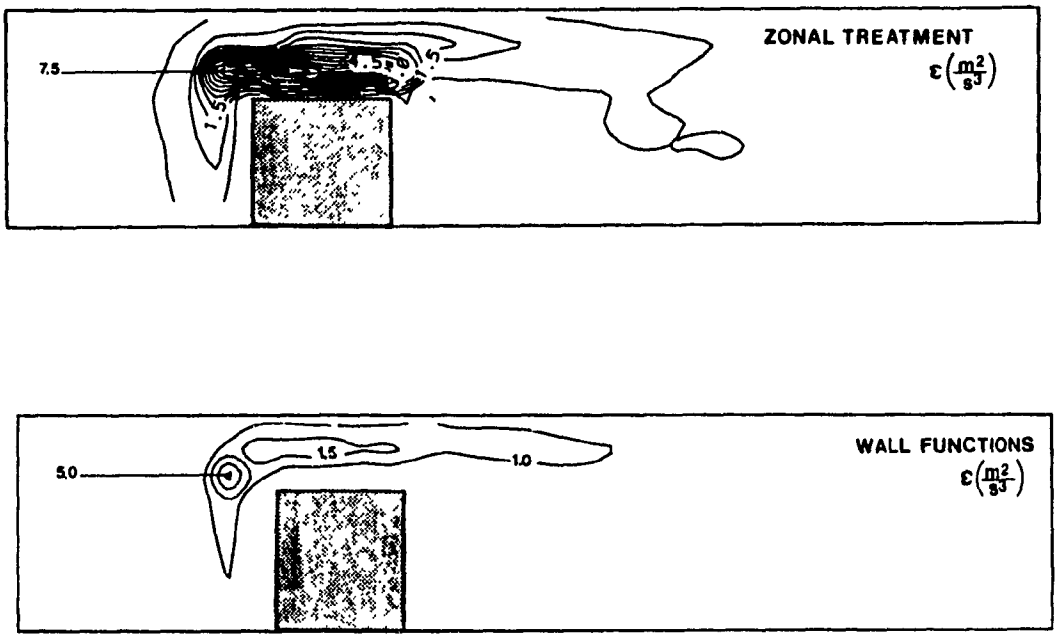

Fig.7.5: Computed Dissipation Rate of kinetic Energy around a Building (Side view, H = 55 m)

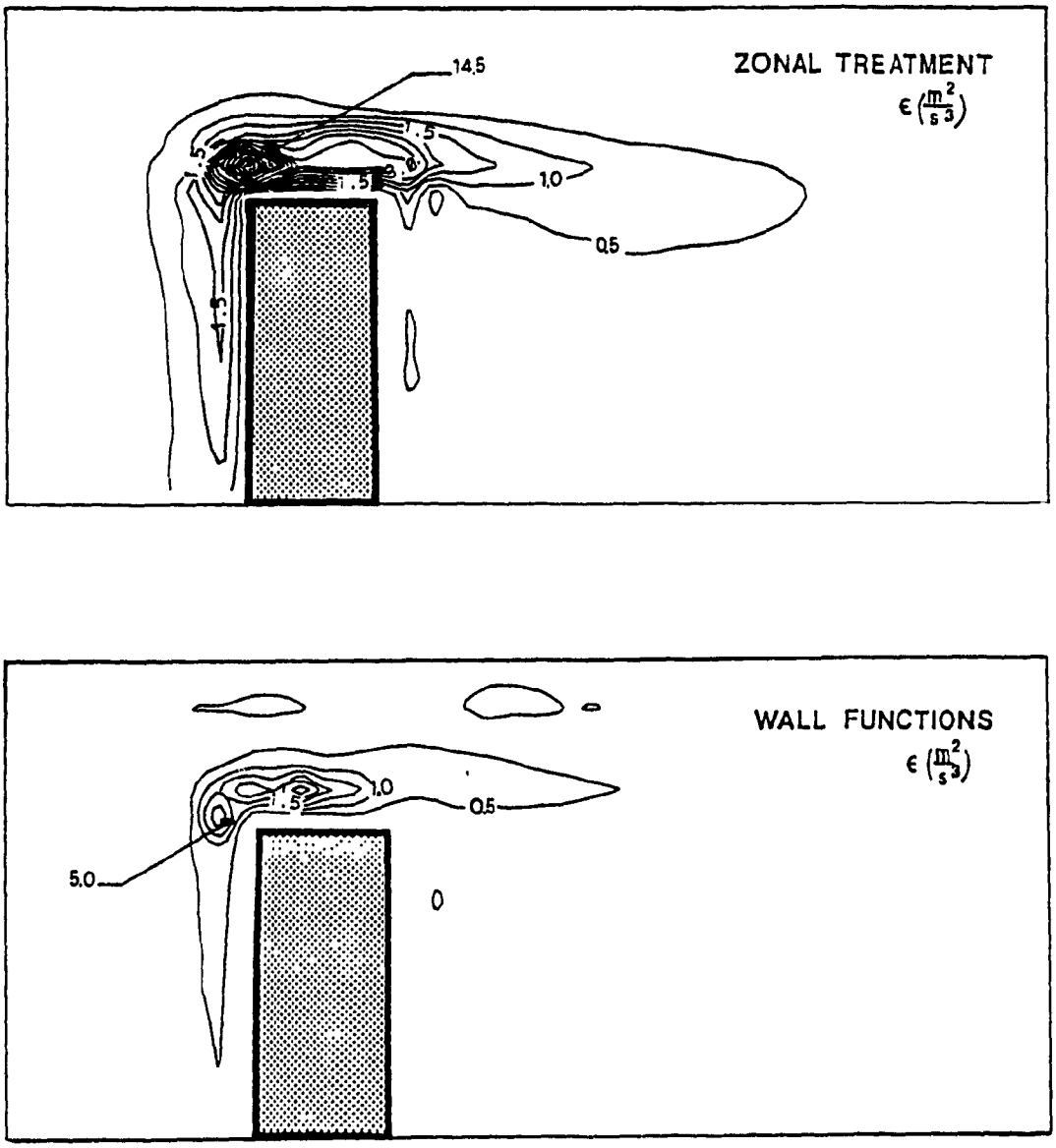

Fig.7.6: Computed Dissipation Rate of Kinetic Energy around a Building (Side view, H = 120 m)

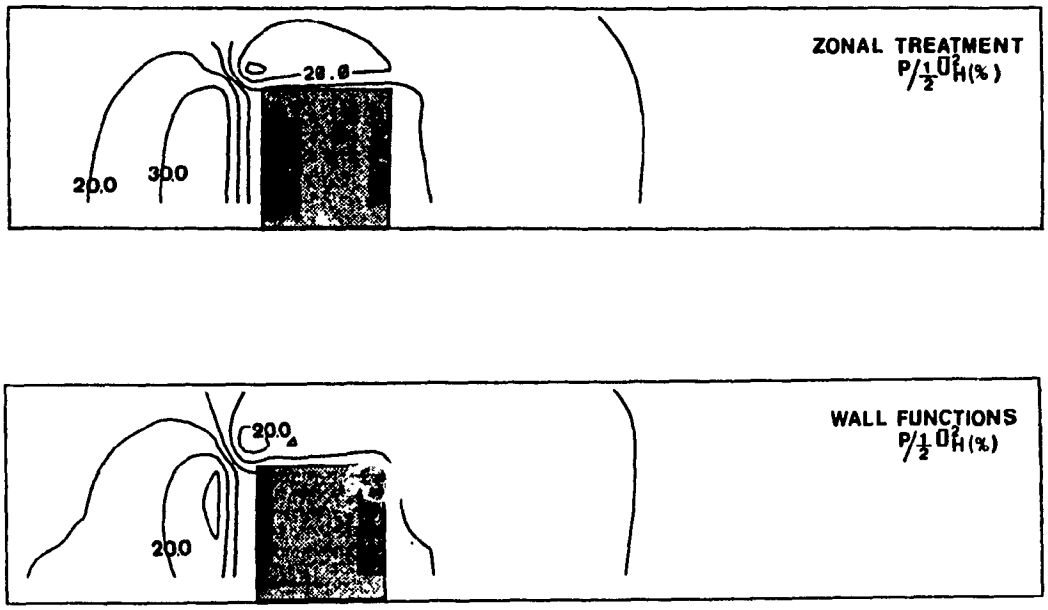

Fig.7.7: Computed Pressure Field around a Building
(Side view, H = 55 m)

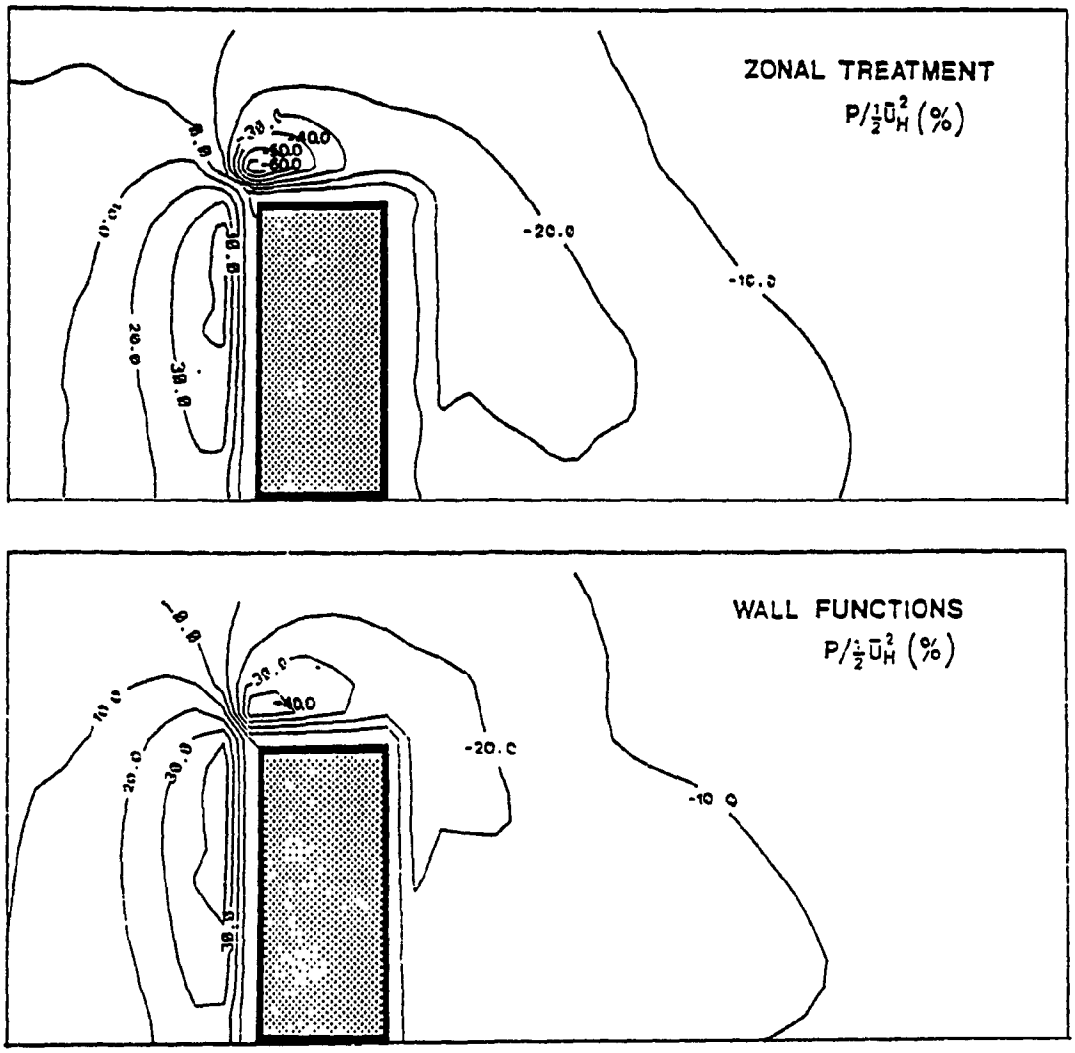

Fig.7.8: Computed Pressure Field around a Building
(Side view, H = 120 m)

Velocity vectors representing the combined influence of the streamwise and vertical velocities are displayed in Figures 7.9 and 7.10 again for H = 55 m and 120 m respectively. The values are taken for a vertical section passing through the centre of the building. The direction of the fluid and its speed locally are clearly shown by the vector plots. Comparing the vectors obtained using the wall function approach and the zonal treatment method, more clear separation from the leading edge and uniform mixing in the recirculation regions are evident when the latter method is used. The vectors plots (H = 120 m) based on the wall function approach provide a steep vertical flow behind the building and a strong reverse flow on the roof which do not appear realistic.

The streamline plots around the buildings are obtained by using the velocity values of the previous figures and they are shown in Figs. 7.11 and 7.12 for the 55 m and 120 m high building respectively. The changes in the fluid path relative to the computational domain are clearly shown in the figures. Comparing the computed streamline patterns, the length of the recirculation zone behind the building is larger and the eddies are more uniformly distributed in the case of new method. However, the modifications encountered for streamline curvature correction and dissipation correction on the standard k- ε HRTM are also contributing for these improvements.

From the above discussion two features become clear: The first is that the turbulence properties seem to improve when the new boundary treatment is used. The second feature, which is based on the vector and streamline plots, is that without proper modelling of the local flow conditions, unrealistic numerical predictions may be obtained. A more instructive picture emerges when the computed pressure coefficients and turbulence properties are compared with the respective measured wind-tunnel data.

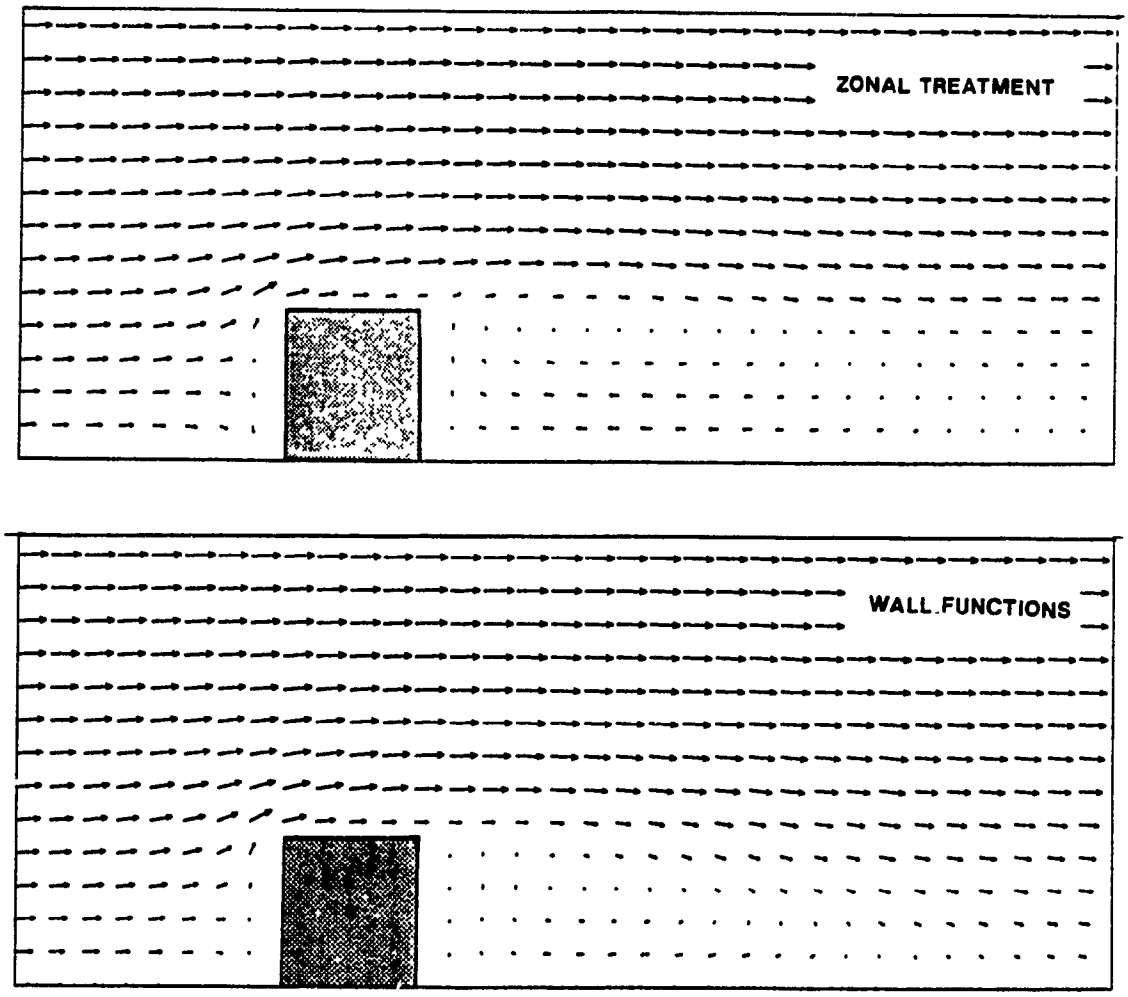

Fig.7.9: Comparison of the Velocity Vectors around a Building
(Side view, H = 55 m)

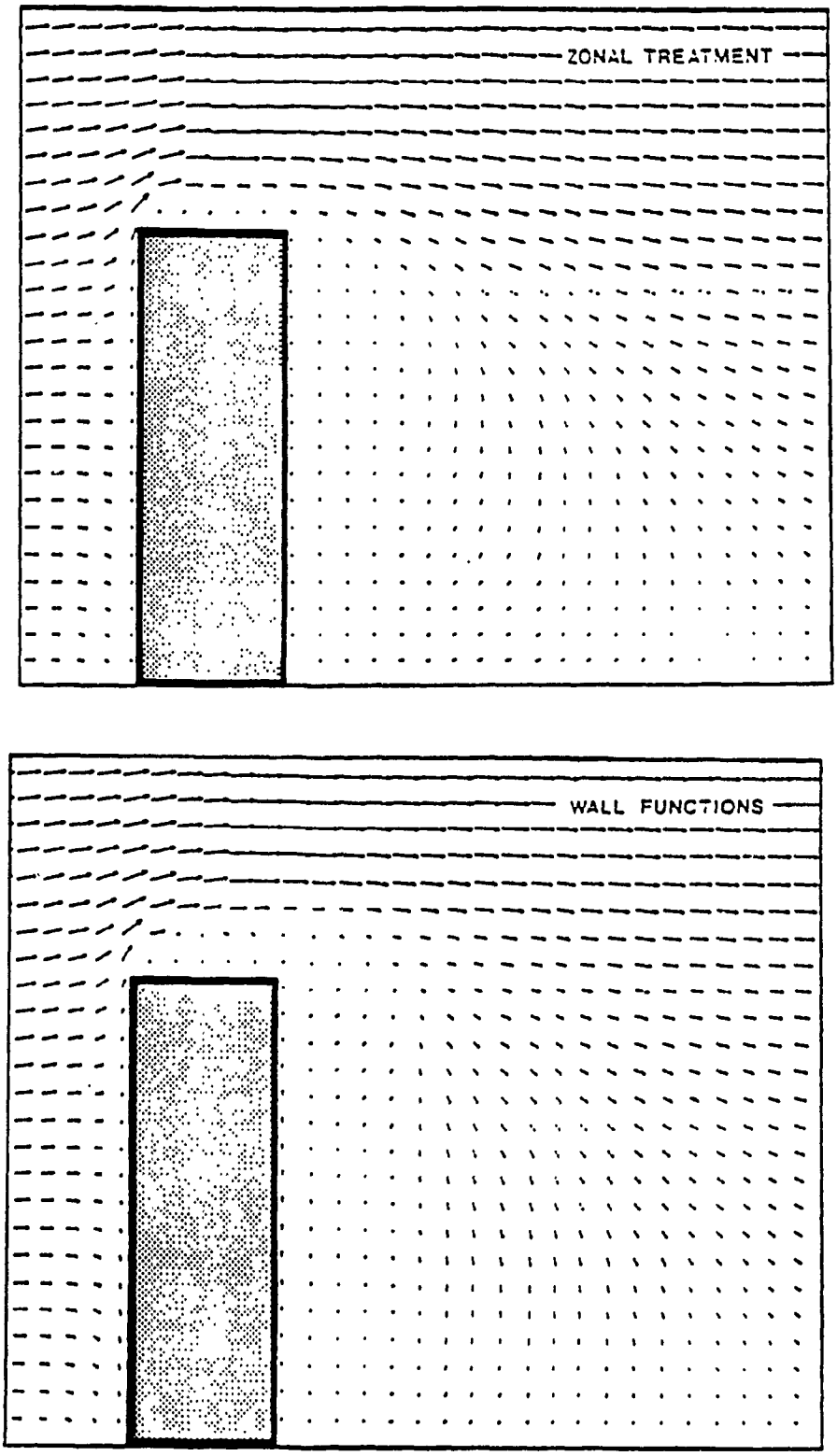

Fig.7.10: Comparison of the Velocity Vectors around a Building
(Side view, H = 120 m)

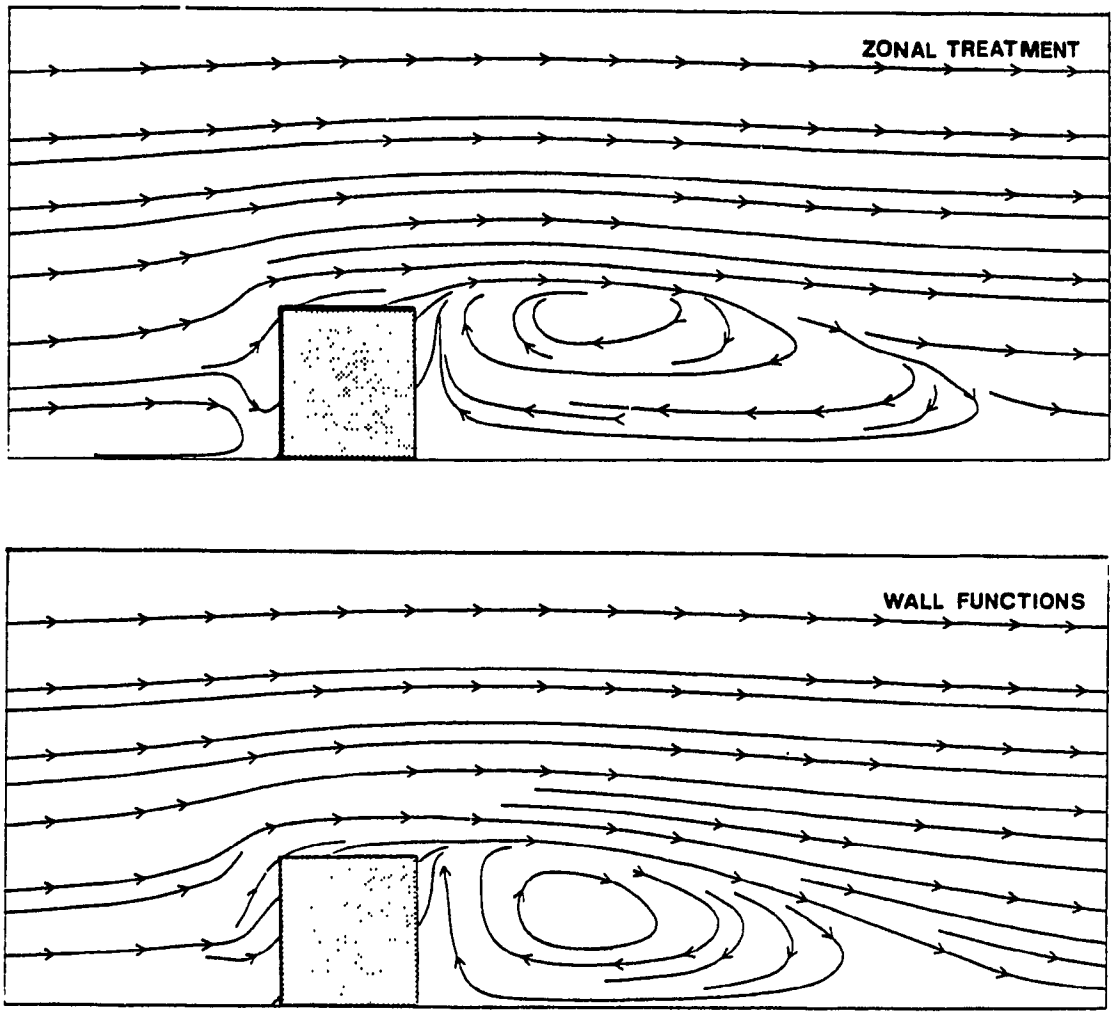

Fig.7.11: Comparison of the Streamline Plots around a Building
(Side view, H = 55 m)

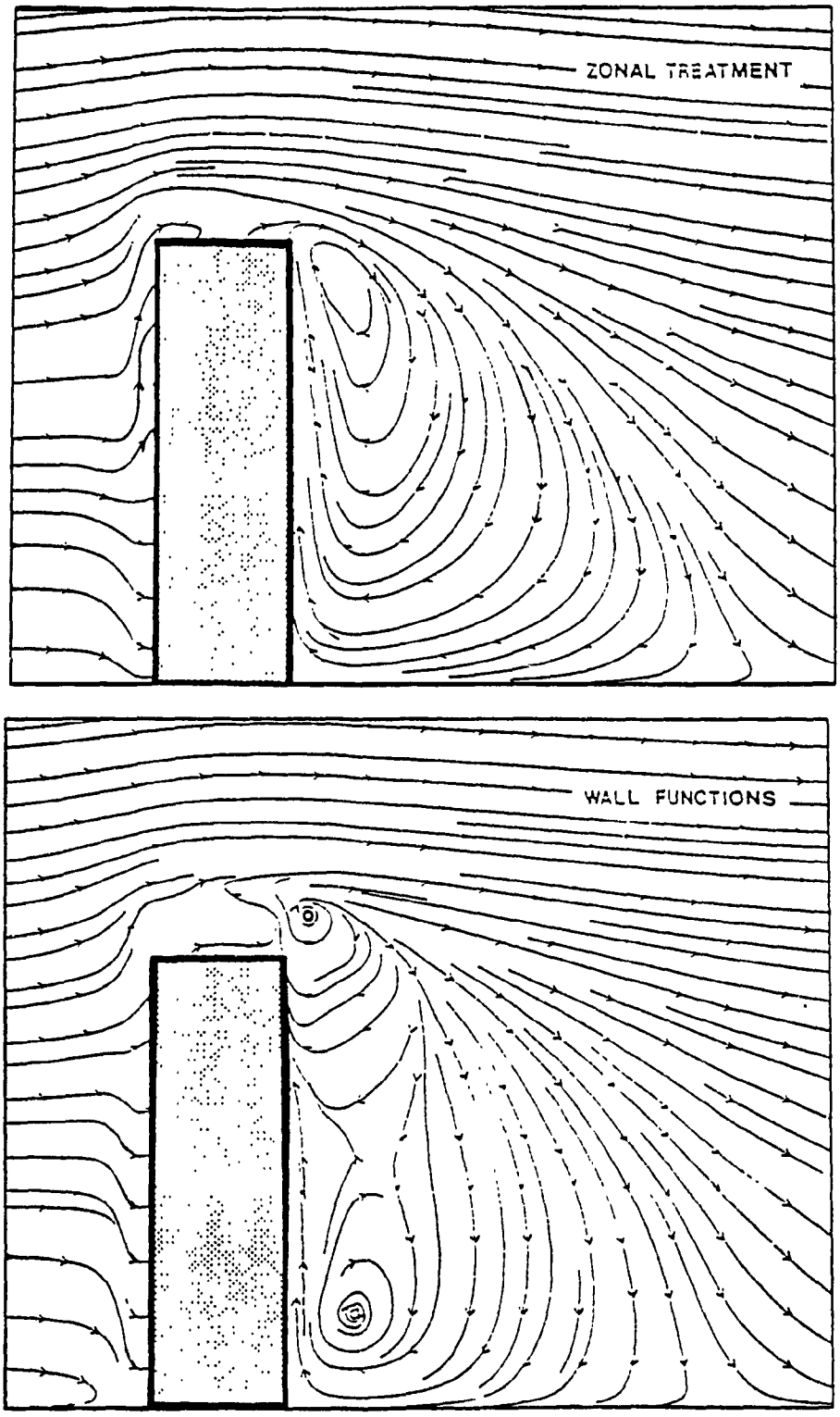

Fig.7.12: Comparison of the Streamline Plots around a Building
(Side view, H = 120 m)

7.3 Comparisons of the Computed Results with Measured Data

This section presents and compares the computed velocities, turbulence intensities and pressure coefficients with the respective data obtained from the various boundary layer wind - tunnels. Figure 7.13 presents one such comparison for the streamwise velocity profile. The measured data have been taken from the experimental study of flow over surface- mounted cubes by Castro and Robins (1977). Both uniform and turbulent flow conditions were considered in the experiments. However, computations and comparisons are made for a turbulent boundary layer profile described by a power law exponent equal to 0.25. The vertical velocity profile normalized by the gradient velocity is shown for three different locations. The location x/L = 0.5, corresponds to the centre of the roof and the other two locations are in the wake of the building. For all three locations the computed results agree well with the measured wind-tunnel data. The new boundary treatment provides better results in the near wake region (x/L = 1.5), whereas both approaches show similar results in other areas.

Figure 7.14 compares the computed and measured turbulence intensities in the same format with Figure 7.13. All curves are normalized by the free stream velocity. There are significant differences between the measured and computed results in most locations. On the other hand differences also exist between experimental results as well. In order to stress this experimental uncertainty, additional measured data taken from Hunt and Smith (1969) and Hunt (1970) are also included. Note that they correspond to building models of similar dimensions with some variation in the exposure conditions. The range of these experimental data is highlighted in the figure (cross-hatched area). Nevertheless, it is quite clear that the data computed by using the new zonal treatment approach follow the measured results much closer than those computed by the wall function methodology. This is particularly true for areas near the solid boundary such as

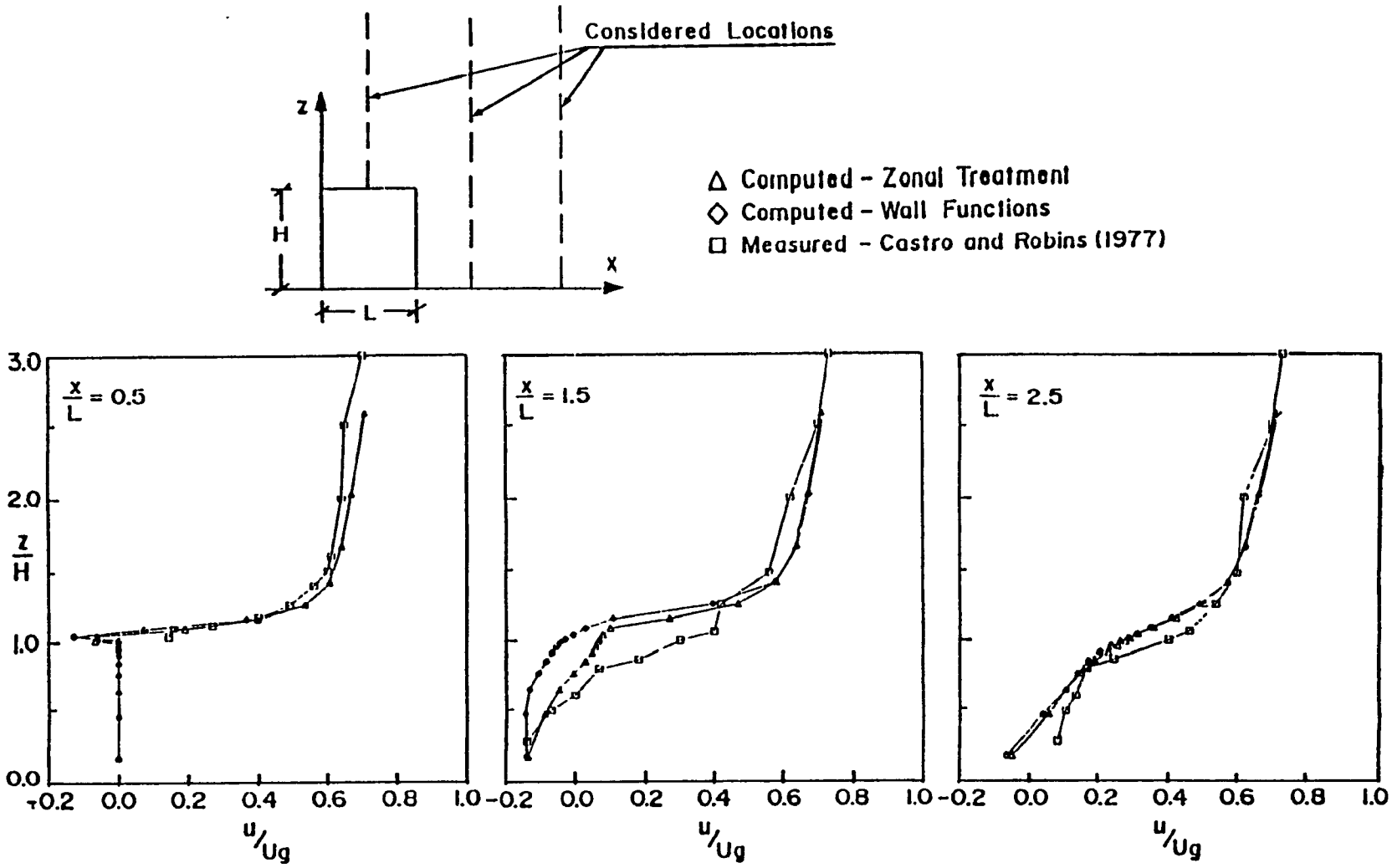

Fig.7.13: Comparisons of the Computed Velocity Profiles with Measured data

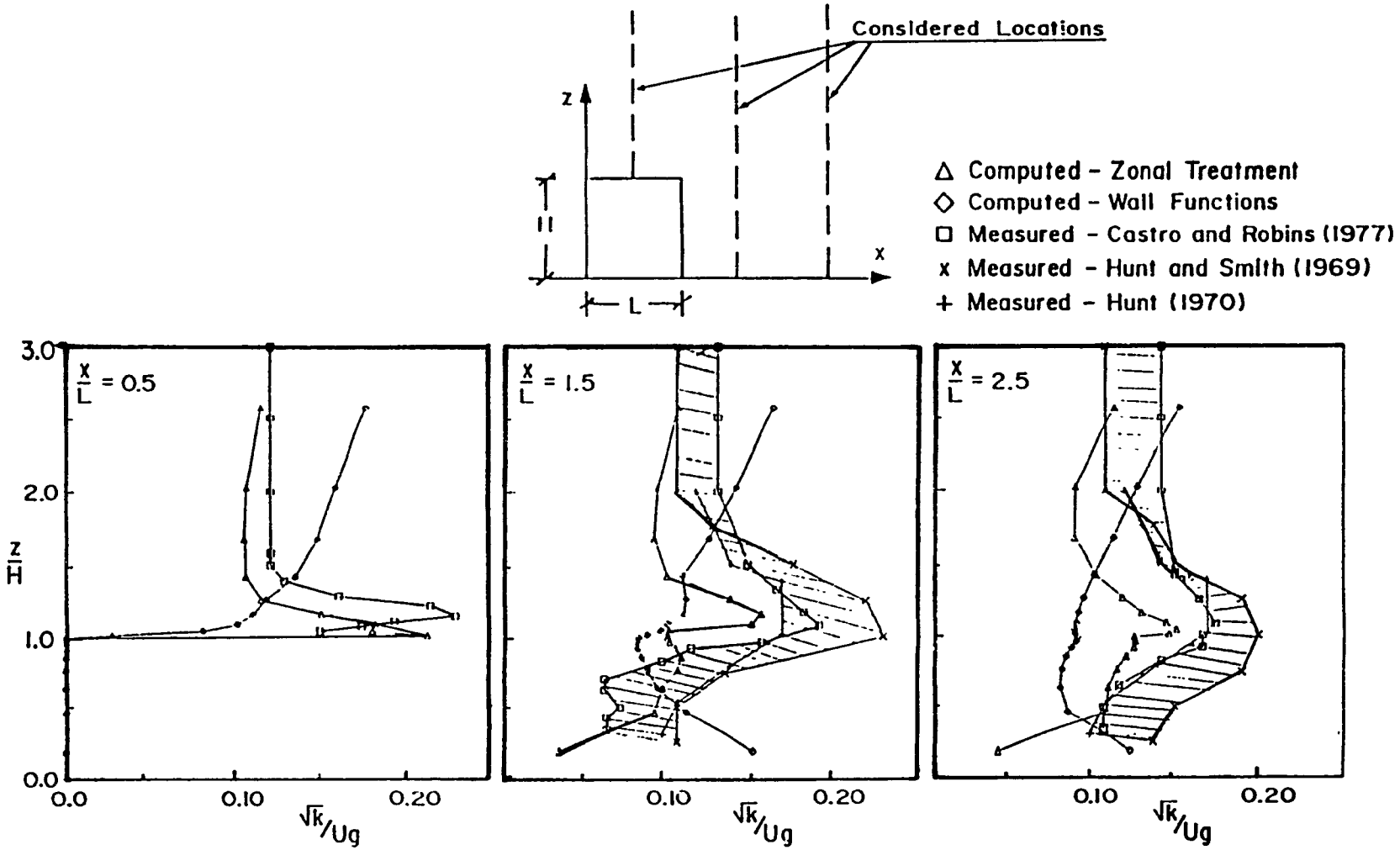

Fig.7.14: Comparisons of the Computed Turbulence Intensities with Measured Data

right above the roof of the building. Clearly these are areas in which the considered characteristics of VSL have more influence on the computation.

Comparison of the pressures for the building walls are shown in Fig. 7.15 and 7.16 which contain three sets of curves taken from buildings 24 m, 55 m and 120 m high. These building heights may typically represent the features of wind effects on a low, intermediate and high-rise building respectively. For each set, three curves representing the measured data, the computed values based on the zonal treatment method and those derived by the conventional wall function approach are depicted. The experimental values are taken from Stathopoulos and Dumitrescu-Brulotte (1990). All the values are presented in the non-dimensional pressure coefficient form i.e. pressures normalized by the dynamic velocity pressure measured or computed at the building roof height. Each point in the curves provides the maximum value that has been recorded during the measurements or calculated in the computation at the considered height level of the relevant building. Note that these pressure coefficients are different from those shown in Fig. 5.9, which have been measured and computed along the centre line of the each wall. These values can be directly used for evaluation of external wind generated pressure loads on the building envelope. These loads are necessary for design purposes. Windward wall positive pressure coefficients and suction coefficients on the side and leeward walls are presented in the x - axis whereas the vertical axis indicates height normalized by the building height.

Small differences are found for the front wall in the cases of 55 m and 120 m building. However, irrespective of building height, significant improvement in the leeward wall and better agreements between the computed and measured data for side wall are evident when the new boundary treatment is applied. It is also equally clear that improvements on the leeward walls are better than side walls. It appears that the side wall of the low building is more benefited in comparison to the other building walls. This will be further discussed when the new zonal treatment is validated for various H/B values.

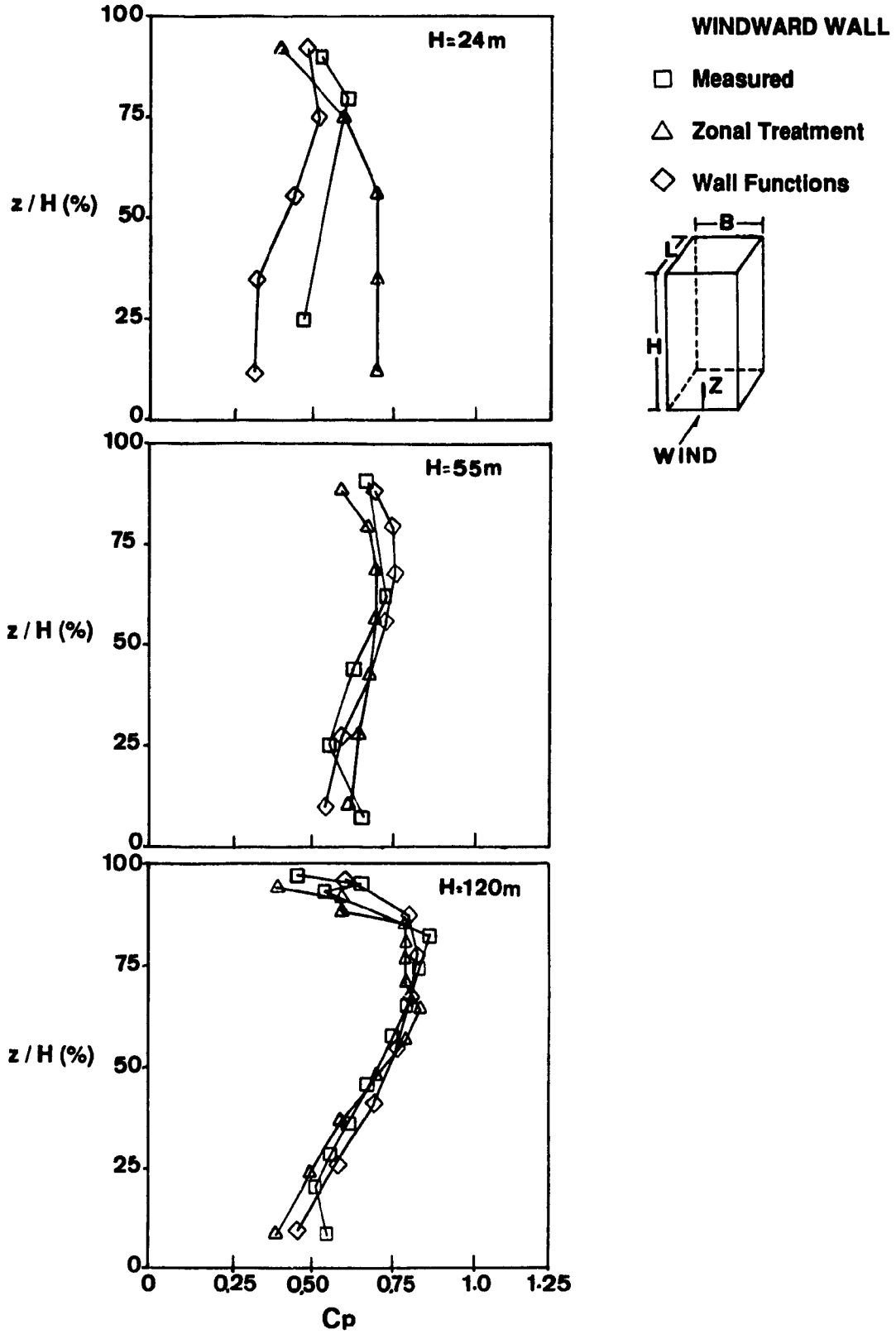

Fig.7.15: Computed and Measured Pressure Coefficients on the Windward Wall of Different Buildings

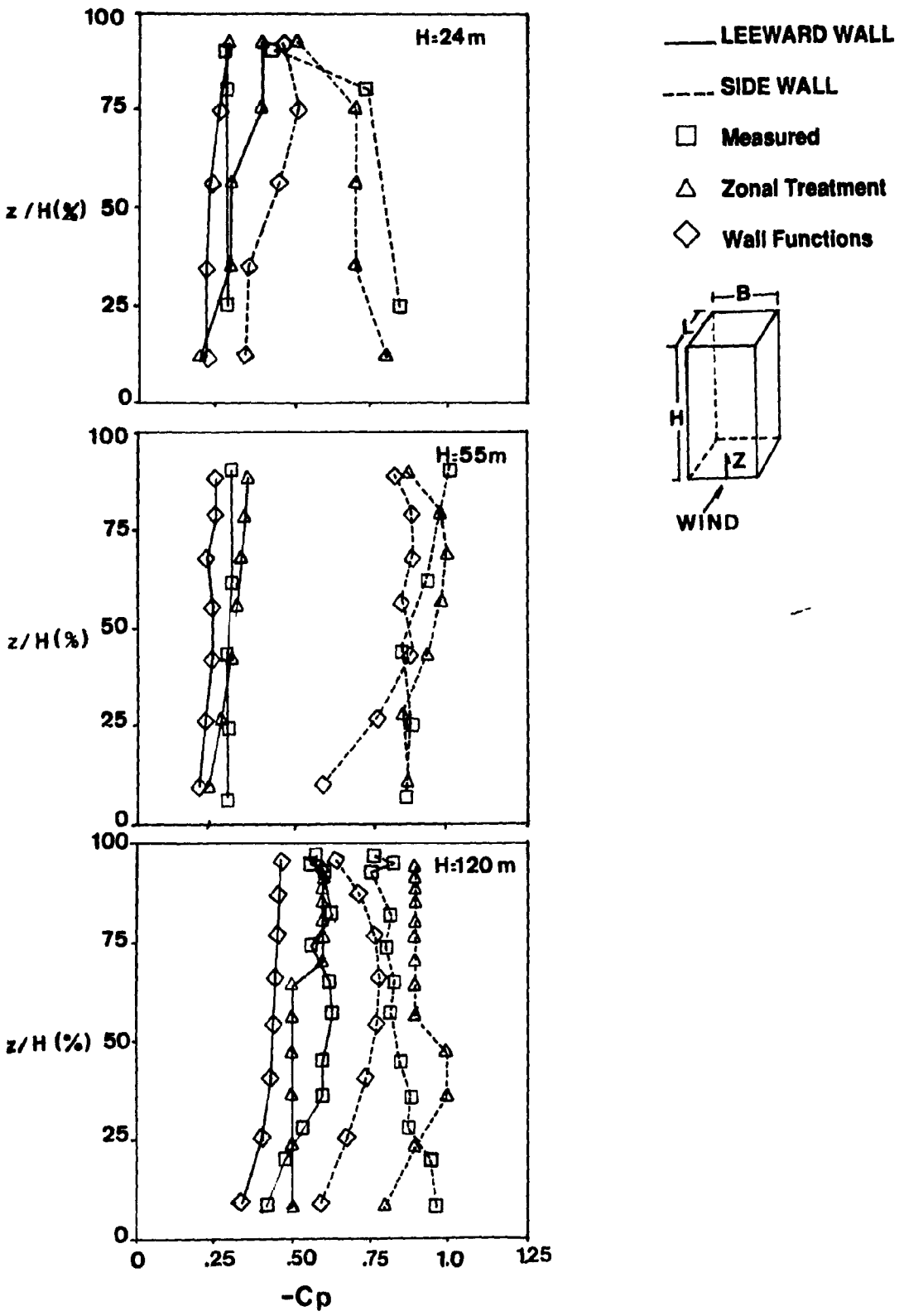

Fig.7.16: Computed and Measured Pressure Coefficients on the Leeward and Side Walls of Different Buildings

Figure 7.17 compares the computed roof pressure coefficient values with the available measured data. For the 55 m building height, the measured values originate from two boundary layer wind-tunnel studies, namely Stathopoulos et al. (1981) at the University of Western Ontario and Stathopoulos and Luchian (1989.b) at the Centre for Building Studies of Concordia University. Close similarities exist between geometrical and exposure characteristics in both studies. For the comparison of 24 m building the experimental data are taken from Baskaran (1986). In the case of 120 m high building, note that the experimental values are available only for a building of 96 m high and those values used for the comparison. All building models have a square cross-section and the exposure simulates open country terrain conditions. The x - axis is normalized by the building length and the mean pressure coefficients are presented in the vertical axis. Since the building is exposed to normal wind, only half of the roof is considered for the computation. The values used in the comparisons are taken from the central roof location of the respective buildings.

For all buildings the results obtained via the boundary treatment method are found to be more satisfactory in comparison to the results of the wall function procedure, so as the agreements with the measured data. This is justified by the improved turbulence conditions above the roof (ref: Figs 7.3 and 7.4). The analysis based on the common wall function approach yields to significant underestimation of the pressure coefficients on the roof. On the other hand some overestimation of pressure coefficients produced by the zonal treatment method near the windward edge of the roof may not be problematic due to the variability of the measured data in this region.

In order to validate the zonal treatment method in a general way, a more systematic parametric study has been carried out and the results are compared with the measured data. The wealthy of experimental results available from Stathopoulos and Dumitrescu-

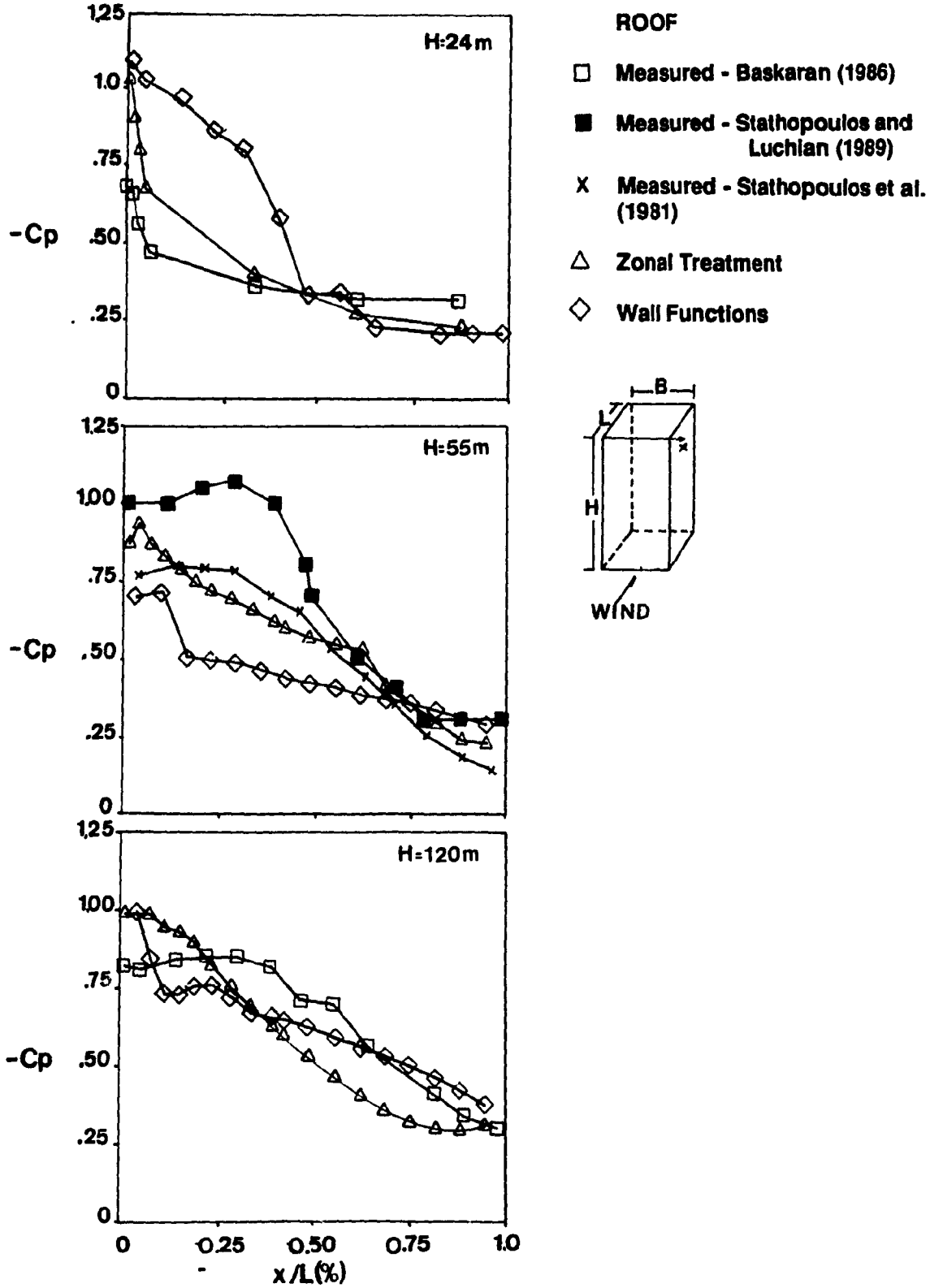

Fig.7.17: Computed and Measured Pressure Coefficients on the Roof of Different Buildings

Brulotte (1990) are used for the comparisons. Computations have also been performed both by using the wall function approach and zonal treatment method, for each building configuration and exposure condition. Computed and measured pressures are transformed into non-dimensional pressure coefficient forms referenced to the respective building roof height. From the pressure coefficients computed or measured the maximum value that has been found on each horizontal wall section is retained. The arithmetical mean of all these values provides an average critical pressure coefficient for each wall. Thus a single parameter i.e. average pressure coefficient for each wall is obtained by post - processing large amounts of available data in order to judge the general accuracy of the numerical predictions.

Figure 7.18 shows comparisons of such average pressure coefficients for all three walls of a square planform building with different H/B ratios. Computed results by using the new zonal treatment method are mostly in good agreement with the measured data. Clearly encouraging improvements are obtained for the building side wall irrespective of the building heights. The measured suction values of the leeward wall increase as H/B increases. In the computational approaches this trend breaks down for H/B > 2 and at H/B = 2.4 a significant difference can be noticed between the computed and measured values. This discrepancy may be also due to experimental uncertainties involved in the measurements including differences between the location of pressure taps and computational grid points. Overall the zonal treatment method is preferable in comparison to the wall function approach.

A similar exercise has also been performed for the roofs of the different buildings by taking the maximum value for each section along the flow direction and Fig. 7.19 compares the computed results with the measured data. Experimental data have been taken from Baskaran (1986) who measured the wind loads on flat roofs with and without parapets. Experimental results are also available for different wind directions and

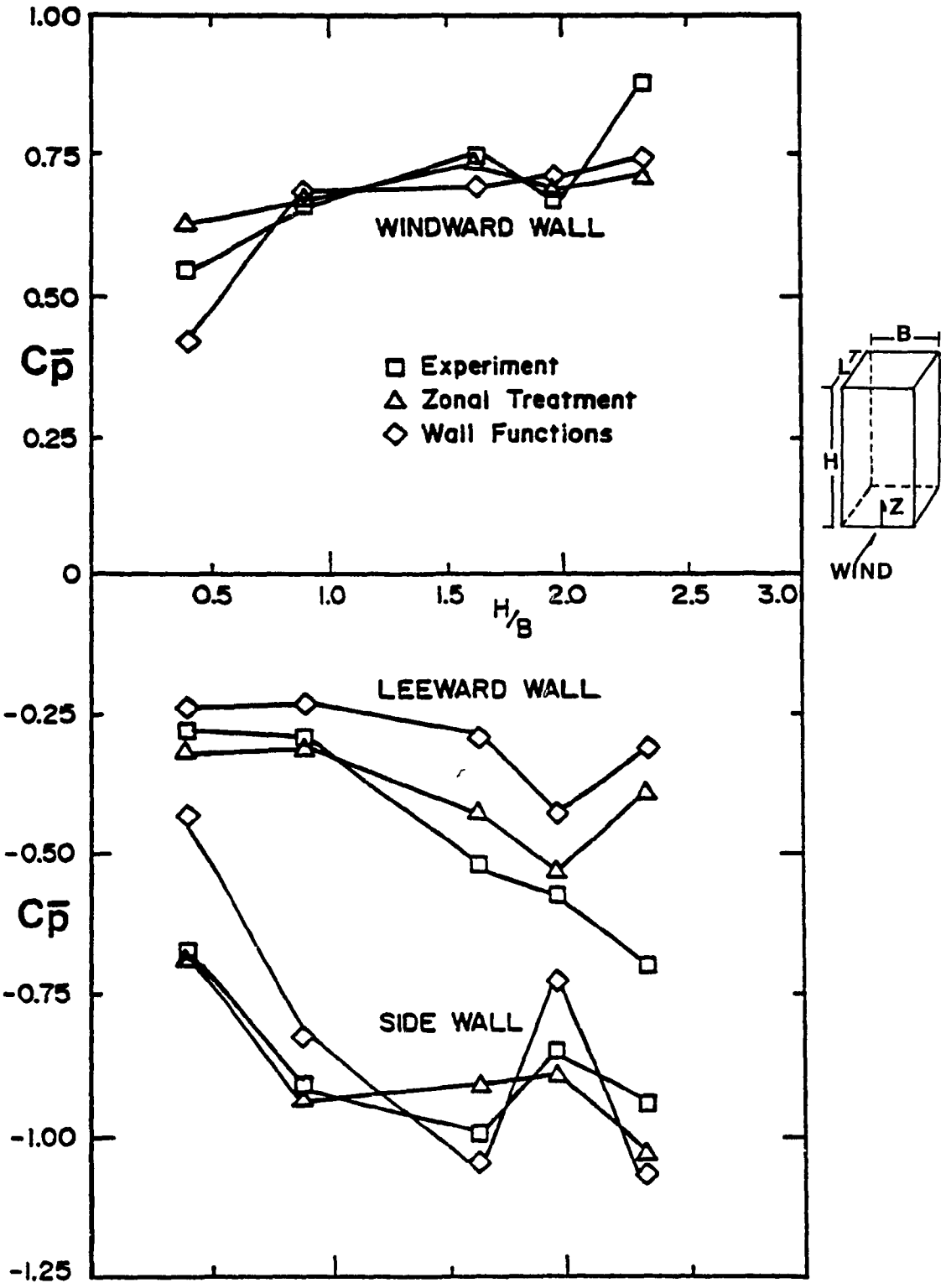

Fig.7.18: Computed and Measured Average Pressure Coefficients on the Walls of Buildings with Different Aspect Ratios

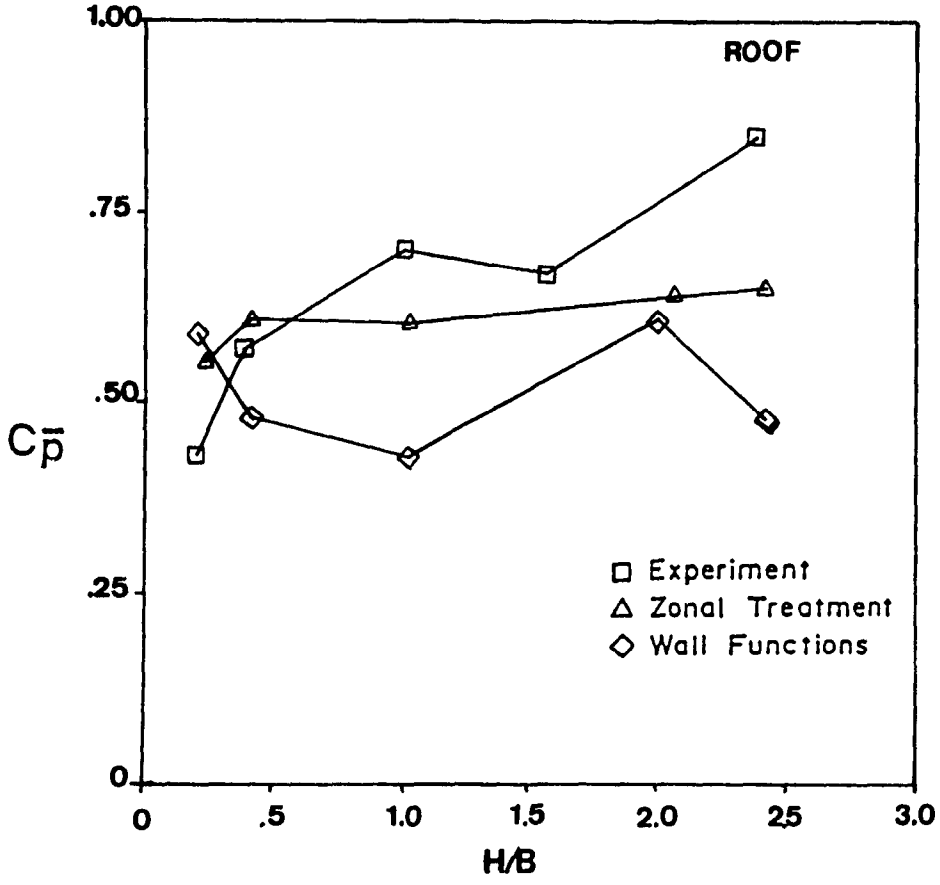

Fig.7.19: Computed and Measured Average Pressure Coefficients on the Roofs of Buildings with Different Aspect Ratios

exposure conditions. However, the present comparison is limited to normal flow conditions under open country exposure. Measured values generally increase when H/B increases, whereas the averaged pressure coefficient derived based on the new zonal treatment is approximately constant for all aspect ratios. Nevertheless, the difference between the results of computation and measurements are small when the zonal treatment method is included in the computer code.

CHAPTER 8

SENSITIVITY STUDY FOR THE NUMERICAL SOLUTION

" Numerical Simulation can not be entirely free from various numerical errors and its reliability must be confirmed by means of experiments. The diagnostic system for assessing the results of numerical simulation should be developed from the viewpoint of engineering application " - S. MURAKAMI

Any iterative procedure is said to be converged when the difference between the exact solution and the successive approximation tends to approach zero as the number of iterations increases. The performance of the iterative procedure can be characterized by using two key elements namely stability and sensitivity. A stable numerical solution means that errors made at one stage, say roundoff errors of the calculation, do not cause increasingly large errors as the computation continues, but rather they will eventually damp out. This concept is mostly applicable for time marching problems (Smith, 1984). Since the present focus is on the steady-state behaviour of wind flow conditions around buildings, the stability criterion is excluded from the analysis. The second factor namely , sensitivity is defined from the behaviour of the system output for variations in the system input. Thus this chapter is dedicated to the sensitivity of the numerical solution under steady - state conditions.

The sensitivity issue is addressed by considering mainly three factors - extent of the computational domain, number of nodes and criteria of terminating the iteration process. Eventhough the first two aspects can be grouped based on the grid spacing, for the sake of clear understanding these are analyzed separately. Sensitivity of the numerical solution due to the changes in the computational boundaries is presented in the

first section whereas the second section discusses the influence of the number of nodes on the computed results. The third section addresses the issue of convergence criteria. In all cases, variations in velocities, turbulence and pressures have been considered. The required CPU time has also been monitored in order to quantify the computational economy of the considered problem. The recorded CPU time corresponds to the computational time required for module 2 operations only, as explained in section 4.2. A trade-off between the computational cost and the changes in the numerical solution has also been established at the end of the discussion.

A single building of about 14 cm high and 15 x 15 cm cross-section (56 x 60 x 60 m in full-scale) is considered as the test case. Computations are performed for a power law inlet velocity profile having exponent 0.16 with a free stream wind speed of 12 m/s at a wind-tunnel gradient height of 60 cm. All computations have been made by using the modified turbulence models along with standard wall functions for the boundary specifications of the velocity variables. For the case of turbulence variables the newly formulated zonal treatment method is applied to bridge the boundary nodes with the computational domain. Necessary details of the numerical methodology have been presented in Chapter 3. The developed computer code - TWIST is used for the computation and its description has been given in Chapter 4.

Figure 8.1 shows the grid cluster for the considered test case both in plan (xy) and sectional (xz) views and the distances $\delta x, \delta y, \text{and } \delta z$ are not equal. Indeed the use of non-uniform grid is often desirable. The misconception that non-uniform grids lead to less accuracy than uniform grids has no sound basis and, in general, an accurate solution can be obtained only when the grid distribution is sufficiently fine. But there is no need to emphasize a fine grid in regions where the dependent variable changes rather slowly such as the velocity above the gradient height. On the other hand a fine grid is required

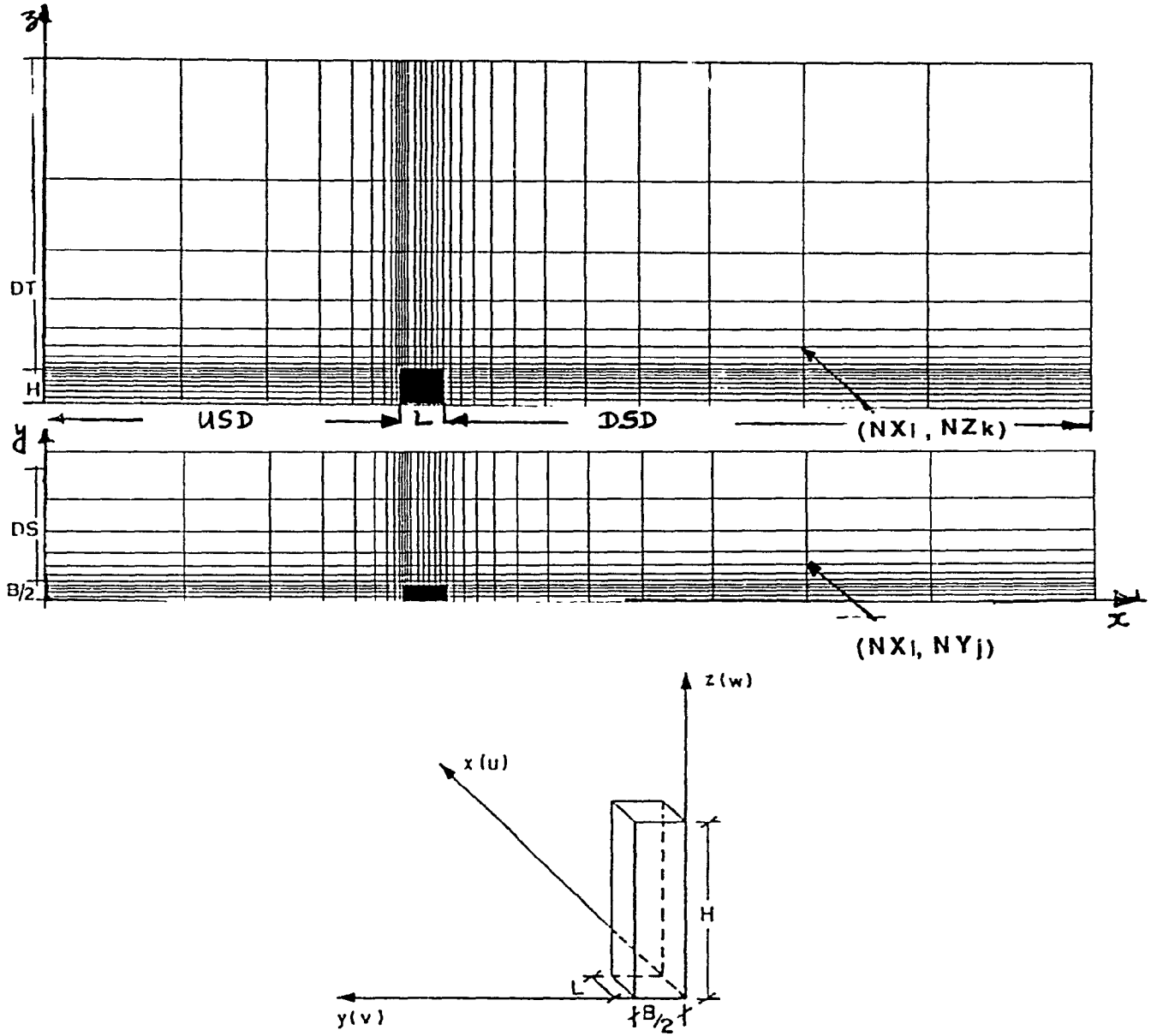

Fig.8.1: Computational Mesh Distributions and Co-ordinate System used

near the (windward) wall or the roof of a building for numerical approximation of the high gradients. These basic ideas are well taken into consideration during the grid generation as it can be clearly identified from the figure. Moreover, by using less grid spacing near the solid boundaries and arranging for non-uniform spacing in other regions, the efficiency of the present computation increases.

An Up-Stream Distance (USD) from the windward wall and a Down-Stream Distance (DSD) from the leeward wall define the boundaries of computational domain along the x direction. For other directions distances DS and DT are used as shown in the figure. Note that (NX_i, NY_j) is a node in the plan view (xy direction) which has (NX*NY) total nodes. Similar explanations also apply for the side and sectional views. The co-ordinate system used in the computational procedure is also indicated in Fig. 8.1. The x - axis carries the streamwise velocity whereas the lateral and vertical velocities are directed in the y and z directions respectively. All the computations have been performed in the Computer Aided Building Design (CABD) laboratory of the Centre for Building Studies by using the VAX/1.2 computer system. A typical run takes approximately 150 minutes of CPU time for about 40 iterations.

8.1 Influence of the Domain Size on the Computed Results

The influence of the domain distances are analyzed first because experimental data are available which can be used as preliminary information for the numerical solution. The other two factors will be scrutinized only subsequently. Systematic studies { Hunt (1969), Hunt and Smith (1970) } had been initiated during early 70's for the understanding of the wind generated wakes around the building and continued by Lemberg (1973), Gandemer (1975), and Woo, Peterka and Cermak (1977). Research efforts have also been made by Beranek and Koten (1978) and Corke et al. (1979) for wind

flow conditions around buildings. Beranek (1979) grouped some of those results for the determination of the influence area for wind flow around tall slender buildings, tall buildings of transition type (building which has significantly smaller dimension along the flow direction than the other two directions) and long buildings. These general guidelines are well taken into account by the present study for the calculation of the computational boundaries.

As listed in Table 8.1 four domain sets are considered in the present analysis. The extent of the computational domain along the x, y and z directions is shown for each domain. During this exercise the other parameters namely the total number of nodes (81,600) and the convergence criterion (0.2) are kept constant. The DD2 set is selected based on the 2-D experimental study by Antoniou and Bergeles (1984) and Bergeles and Athanassiadis (1983) and it is consistent with the previous computational work of Paterson (1986.b) and Murakami and Mochida (1988, 1989.a). Having DD2 as the base, the effects on the computed results by increasing as well as decreasing the domain size are analyzed. Detailed examinations could have been performed even by changing individual distances - say DSD -, however, due to time limitations it has been decided to analyze the overall changes of the computational domain.

Figure 8.2 shows the streamline plots for the four considered cases. These plots show the side view pattern of the flow distribution for a plane that is passing along the center of the building which is exposed to normal wind flow conditions. The plots are obtained using the converged velocity components u and w. In all four figures the incoming flow separates from the leading edges and then forms recirculations behind the building. Overall no significant differences are noted among the four figures. However, the recirculation zone of DD4 is found to be smaller in comparison to the others. To quantify these changes, the length of recirculation is calculated as explained in Vasilic - Melling (1977), by specifying the distance from the leeward wall, where $u/u_g = 0.0$. These

Number of Nodes : 81,600
Convergence Criterion : 0.2

SET	x		y	z
	USD	DSD	DS	DT
DD1	3L	6L	3B	3H
DD2	6L	12L	5B	4H
DD3	10L	20L	8B	6H
DD4	13L	26L	10B	9H

Table.8.1 Specification of the Different Computational Domain Considered in the Present Study

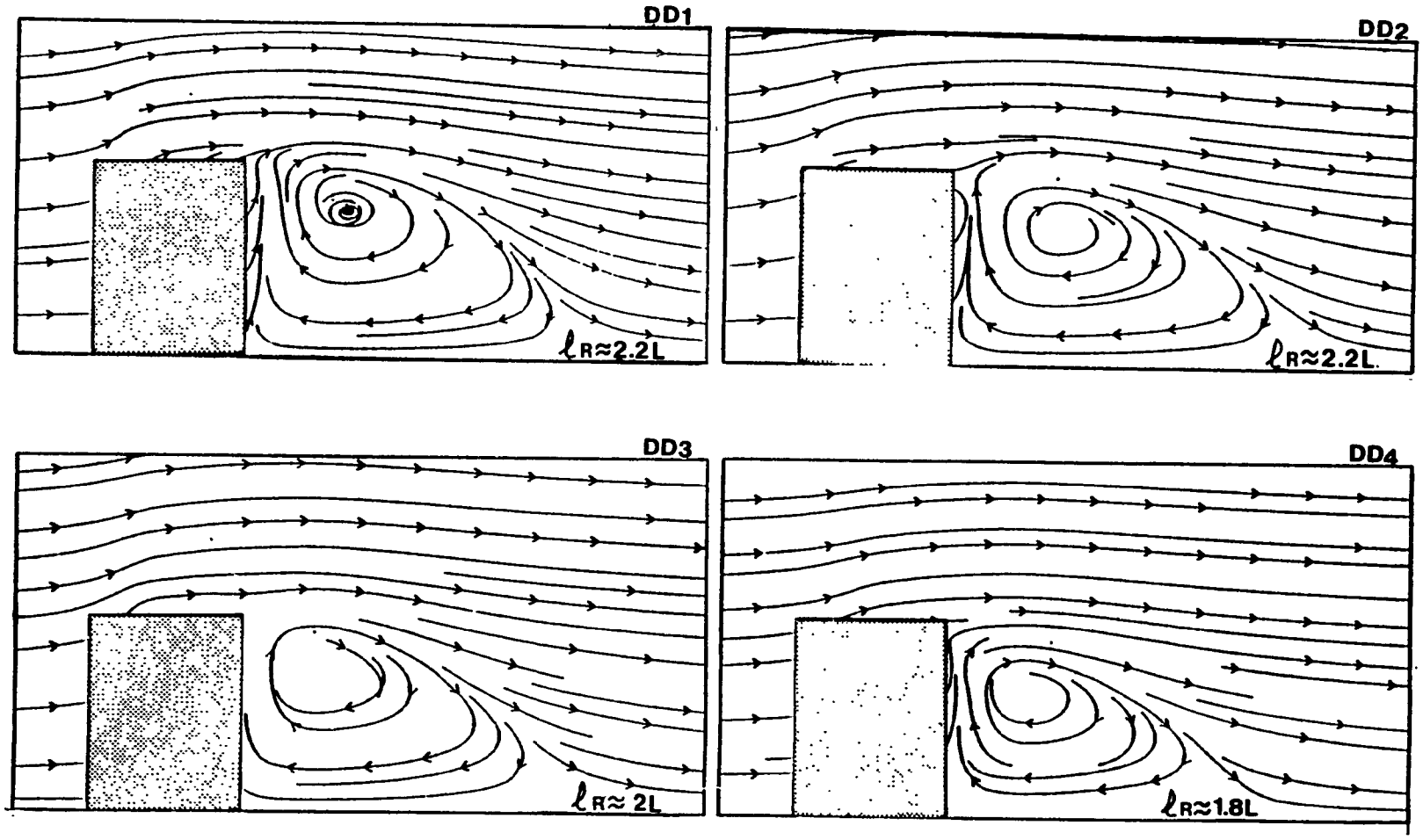

Fig.8.2: Side view of Streamline Plots for Different Computational Domains

locations can also be easily identified from the streamline plots and the respective recirculation lengths have been found equal to 2.2 L, 2.2 L, 2 L and 1.8 L for DD1, DD2, DD3 and DD4. Increasing the domain from DD2 decreases the length of recirculation, whereas the value of DD1 is found to be the same as DD2. This is not surprising and can be explained as follows.

Increasing the size of the domain by keeping the number of grid points constant, increases the grid spacing. Refer to the two exploded views that are qualitatively sketched in Fig. 8.3 representing part of DD2 and DD4 from the previous figure. In DD2 there are 8 nodes for the longitudinal and 4 in the vertical directions and the nodes reduced as 4 and 3 respectively in DD4. This reduction occurs when the domain distances are increased by keeping the total nodes constant as 81,600. The reduced node set of DD4 fails to capture the reverse flow that occurs on the node 7 of the DD2 set due to the large discontinuity between the nodes and this may be one of the reasons for the reduction in the recirculation length. On the contrary for DD1 set the domain distances are reduced by keeping the same number of nodes. Thus the details are predicted as in DD2. From this discussion it is evident that an increase in the quantity (size) of the domain without increasing the number of nodes will reduce the quality of the computed results.

The induced pressure values are also analyzed for the variation in the domain distances as shown in Fig. 8.4. The windward wall positive pressures and suctions induced both on the leeward and side walls are shown in the figure. All the results are presented in the form of pressure coefficients, normalized by using the dynamic pressure at the building roof height. Maximum difference among the four sets is found for the pressure nodes which are near the ground level of the front wall. Nevertheless, the DD1 curve is always away from the others irrespective of the building wall and the pressure coefficient values are not significantly affected when the domain distances are increased to DD2 and

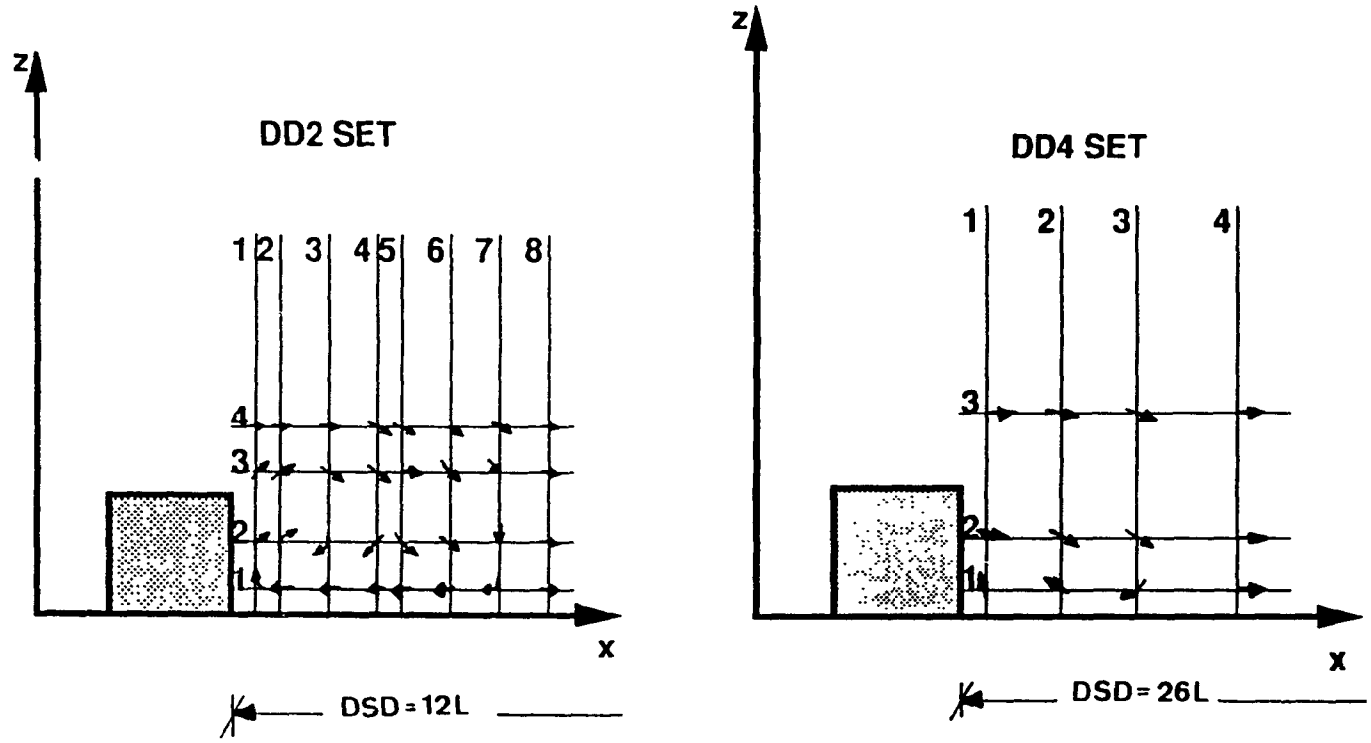

Fig.8.3: Exploded View of the Flow Distribution for DD2 and DD4

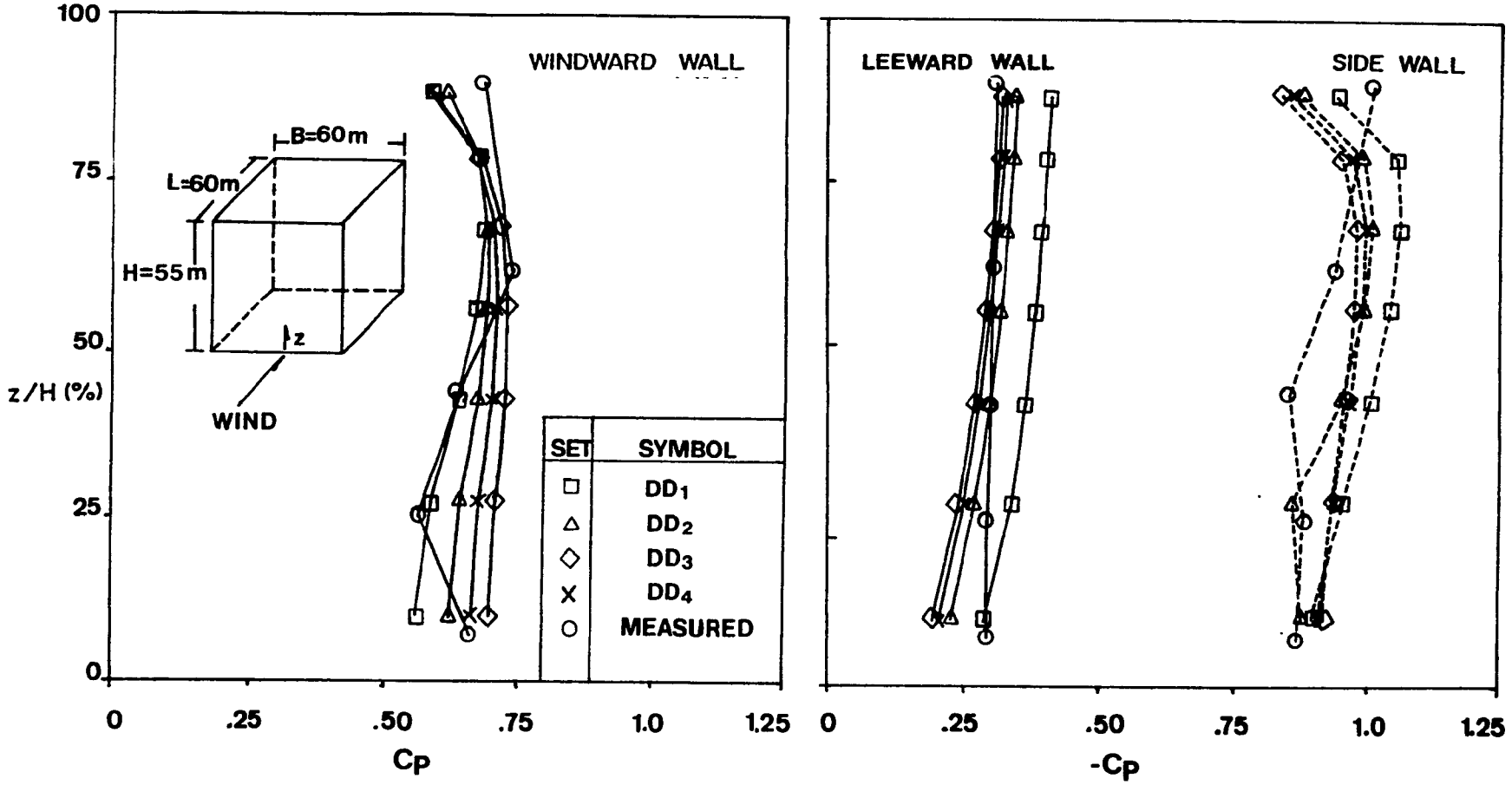

Fig.8.4: Computed Pressure Coefficients on the Building Walls with Different Computational Domains

beyond. When comparing the observations of this figure including the experimental results, selecting DD2 domain specifications for further examination of the problem appears as a good choice. In addition to the changes in the numerical solution, the economical aspects of the computation are analyzed and discussed below.

Figure 8.5 compares the CPU time requirements which are obtained under batch mode operation of VAX /1.2 computer system. The figure also contains the number of performed iterations for a specified convergence criterion of 0.2 (this will be discussed in detail at the end of the chapter). Basically two features are evident from the figure. The first is that an increase in the domain distances increases the necessary CPU time requirements and the second is that the number of iterations are also increased as the boundaries of computational domain are moved further away from the building. By keeping the total number of grid nodes constant, increasing the domain size will increase the grid spacing which in turn may cause large discontinuity between the nodes. So, the numerical procedure needs additional time (CPU) and effort (Iterations) to obtain a converged solution. Thus increase in the domain not only increases the number of iterations for convergence but also increases the CPU time.

8.2 Influence of the Number of Nodes on the Numerical Solution

In the previous section the effect of computational domain is studied by analyzing the computed velocities and pressures. From the discussion it is clear that the numerical solutions are rather insensitive for the domains beyond DD2. The CPU time requirement also favours the DD2 domain selection. Thus by keeping the domain constant as DD2, this section presents the influence of the number of grid nodes on the numerical solution. Four sets of grid systems are generated as shown in Table 8.2 by increasing as well as decreasing the grid set NN4 that is used in the previous section (ref: Fig.8.1). Table 8.2

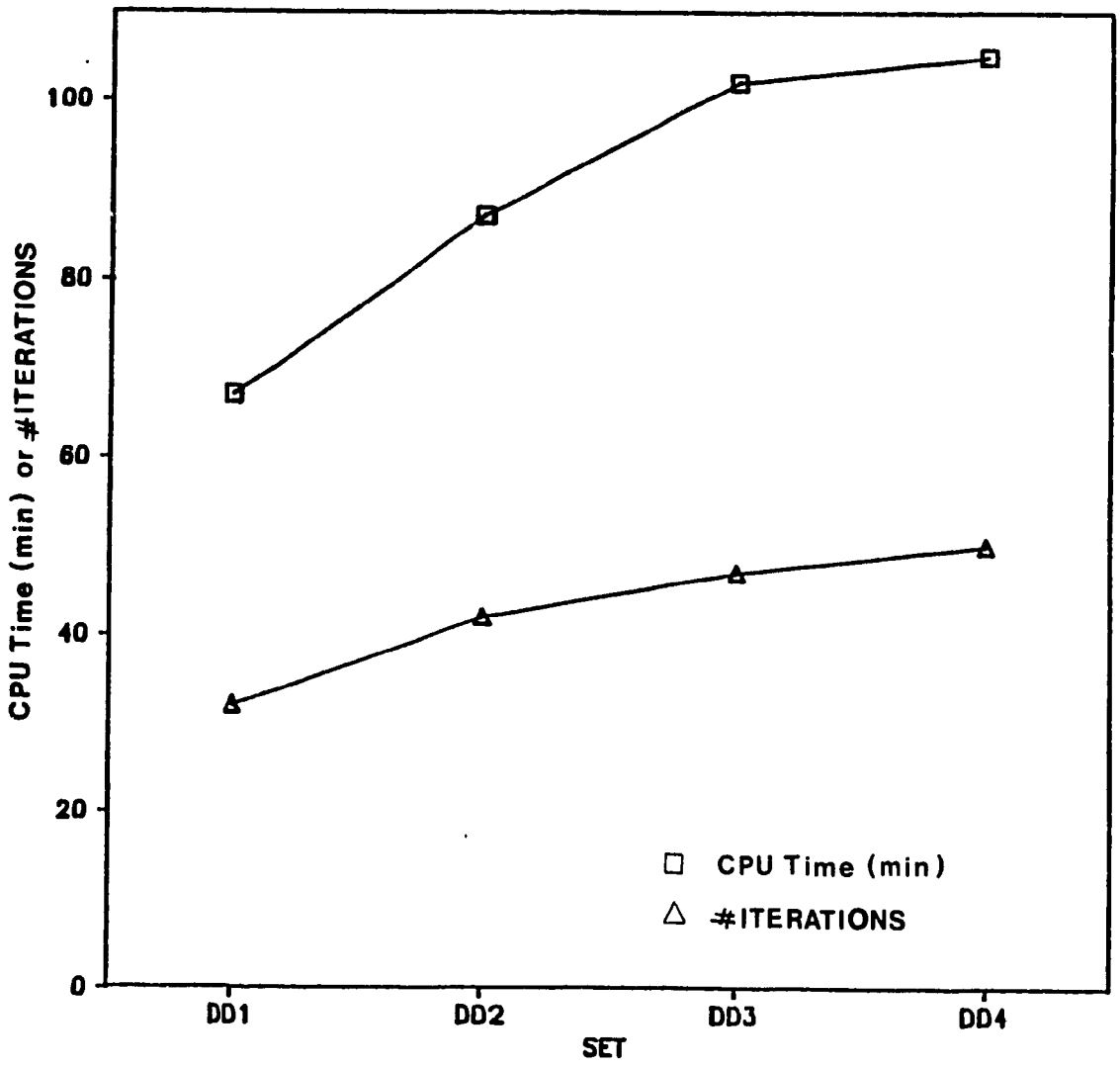

Fig.8.5: CPU Time or Iteration Requirements for Different Computational Domains

Domain Specification : DD2
Convergence Criterion : 0.2

SET	NX	NY	NZ	TOTAL
NN1	38	20	28	21,280
NN2	48	22	32	33,792
NN3	58	26	36	54,288
NN4	68	30	40	81,600
NN5	78	36	40	112,320

Table.8.2 Specification of the Different Computational Grid Distribution Considered in the Present Study

also provides the number of nodes for each direction. As the total number of nodes of the computation increases, the number of nodes on the each direction also increases. However, the number of nodes along the longitudinal direction (x) are increased more than on the other two directions.

A side view of the converged velocity fields for various grid sets is shown in Fig. 8.6. This view represents a plane passing through the building center and the components u and w are used for plotting. Since only minimum differences are noticed between the vector plots of NN2 and NN3, the former is not included in the figure. However, other results of NN2 will be further considered and discussed. The small number of vectors displayed for set NN1 is due to the small number of grid nodes in comparison to the others. The respective values of the recirculation length are calculated as explained before, and marked on the figure. The length of recirculation zone increases when the nodes increase from NN1 to NN3 and shows approximately a constant value for sets beyond NN3. On the other hand, a very small recirculation zone is calculated for the NN1 set and this may be explained as discussed in Fig. 8.3. Nevertheless, to support this description of the expected flow behaviour, experimental evidence of flows over building, such as flow visualization techniques will be necessary.

A typical location near the windward wall of the building is selected to analyze the local effect of nodes on the velocity and turbulence and the results are shown in Figs. 8.7 and 8.8. respectively . The vertical axis of figures shows the node distance from the ground level normalized by the building height. Longitudinal velocity and square root of the kinetic energy are normalized by the gradient velocity. Such non-dimensional values are shown in the horizontal axis. In both cases the differences due to grid are diminishing as one moves away from the ground. Maximum turbulence values occur at z/H =1.0, where the flow has high gradients due to its separation from the leading edge. The effect of the number of nodes on the velocities is clearly shown in Fig. 8.7 and this effect has direct

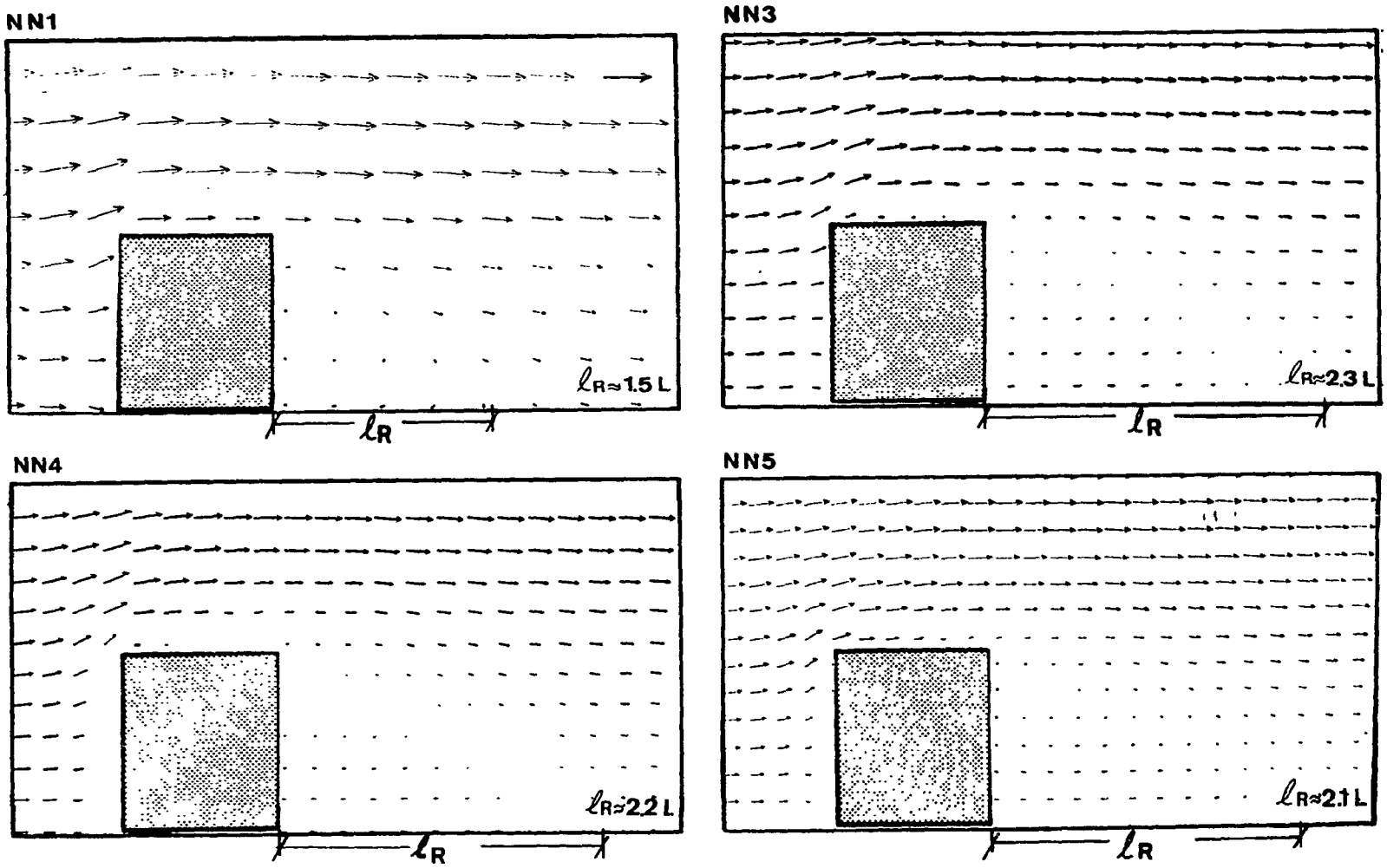

Fig.8.6: Computed Vector Plots with Different Number of Computational Nodes

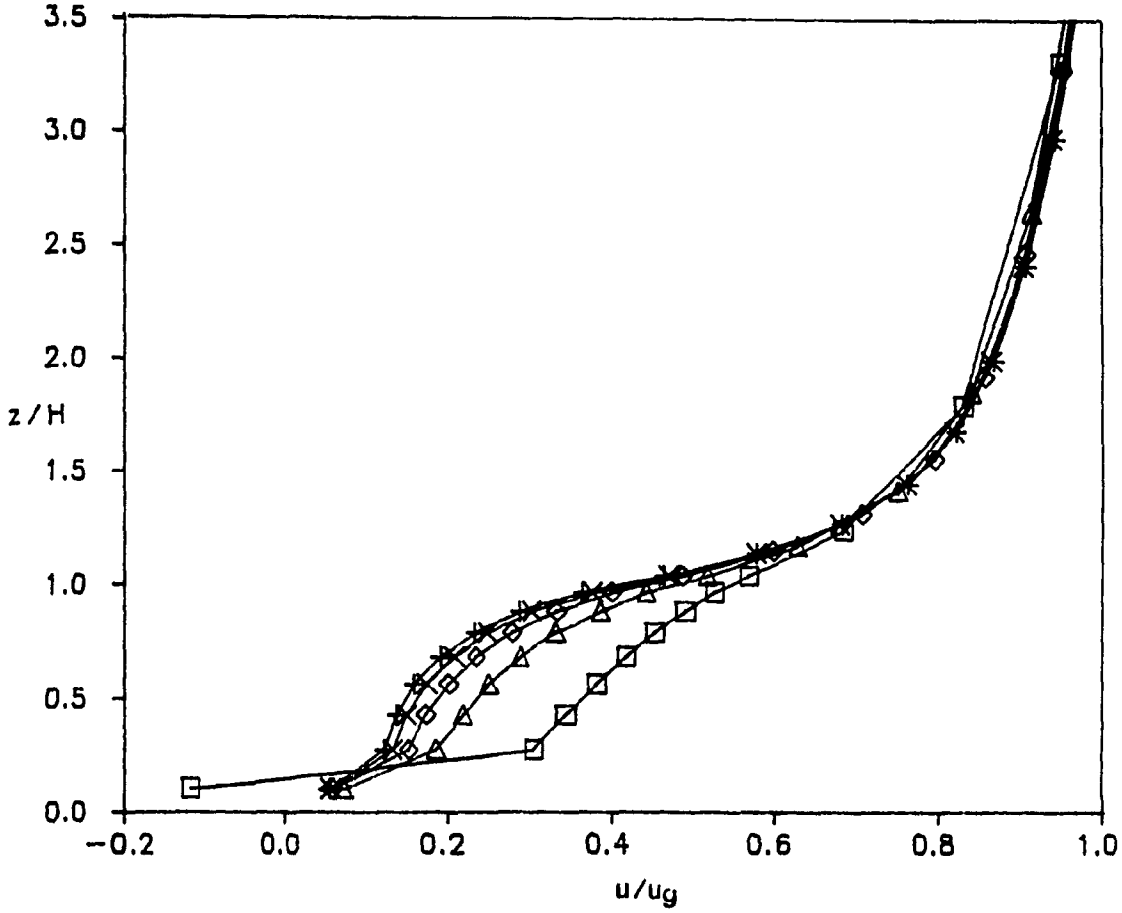

Symbol	Nodes
□	21,280
△	33,792
◇	54,288
x	81,600
+	112,320

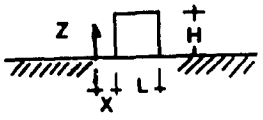

$\frac{X}{L}$=0.05

Fig.8.7: Computed Longitudinal Velocity on the Building Upstream for Different Number of Computational Nodes

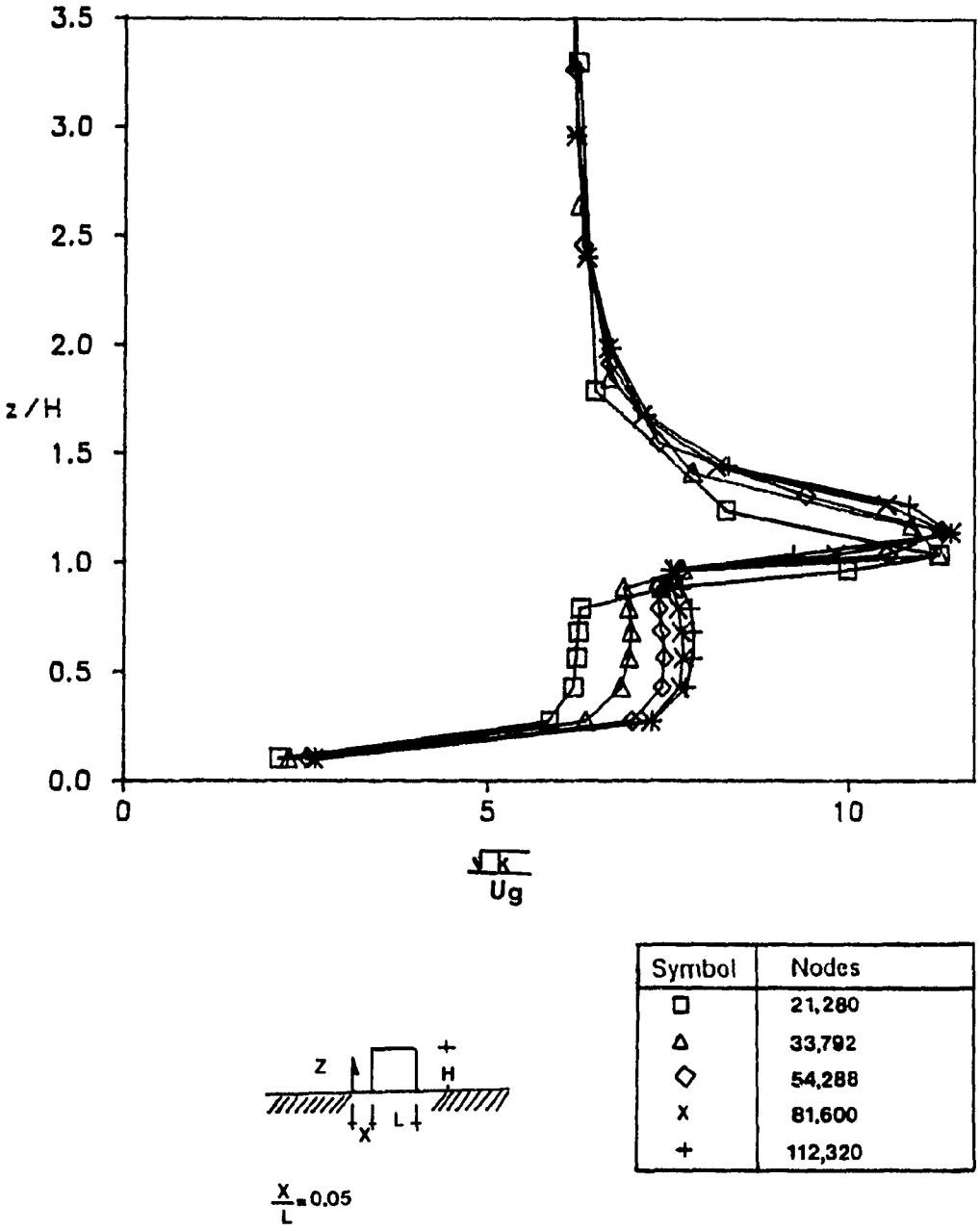

Fig.8.8: Computed Turbulence Intensity on the Building Upstream for Different Number of Computational Nodes

influence on the computed turbulence values (see: Fig. 8.8) which are increased when an increase in the nodes are made. On the other hand, for both variables only minimum changes are observed when the grids increase beyond NN4. Similar observations have also been made for the other locations of the flow domain.

Pressure values in coefficient form have also been computed for different grid systems and presented in Fig. 8.9 in the same format as that of Fig. 8.4. Among the three walls, the influence of the nodes is pronounced significantly for the side wall where flow is complex in nature. As noted for the velocities and turbulence, here also the set NN4 is found to be numerically optimum if one considers all the walls. When comparing various grid set values with experimental data, even the NN3 grid set may be considered sufficient for the computations. However, further investigations and repetitive runs are necessary to generalize these above observations.

Figure 8.10 displays the CPU time requirement of the above discussed case. The plotted CPU times are obtained based on the batch mode operation of the VAX/1.2 computer. The number of iterations required to yield a converged solution for different grid sets is also shown in the figure. The iterations are increased with an increase in the nodes since the process needs additional iterations to settle down. A similar increase is readily observed for the CPU time and this can easily be explained by considering the increased number of arithmetical operations required. Moreover, the required CPU time is also influenced by the number of performed iterations, which itself increases with the number of nodes.

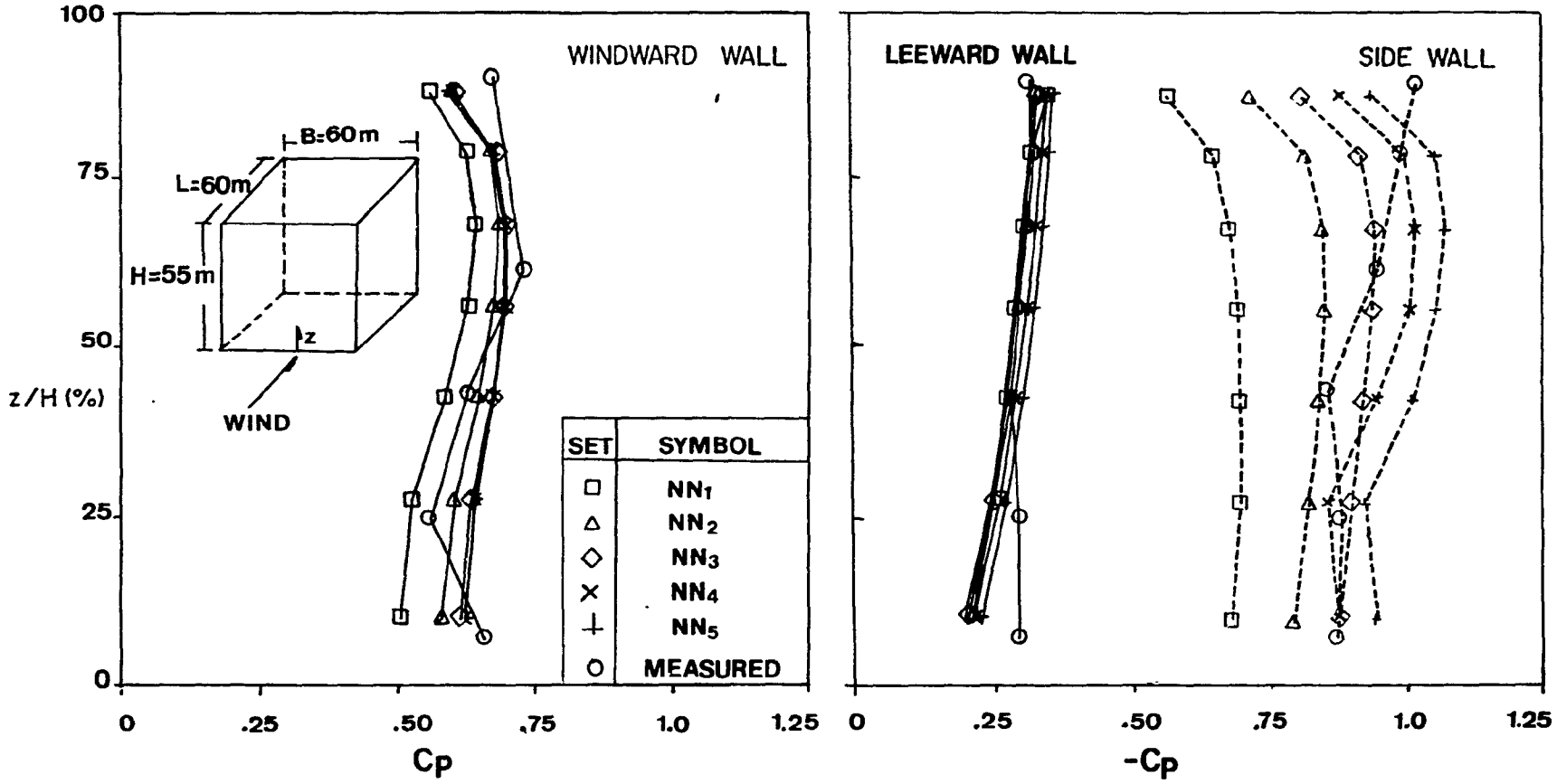

Fig.8.9: Computed Pressure Coefficients on the Building Walls with Different Number of Computational Nodes

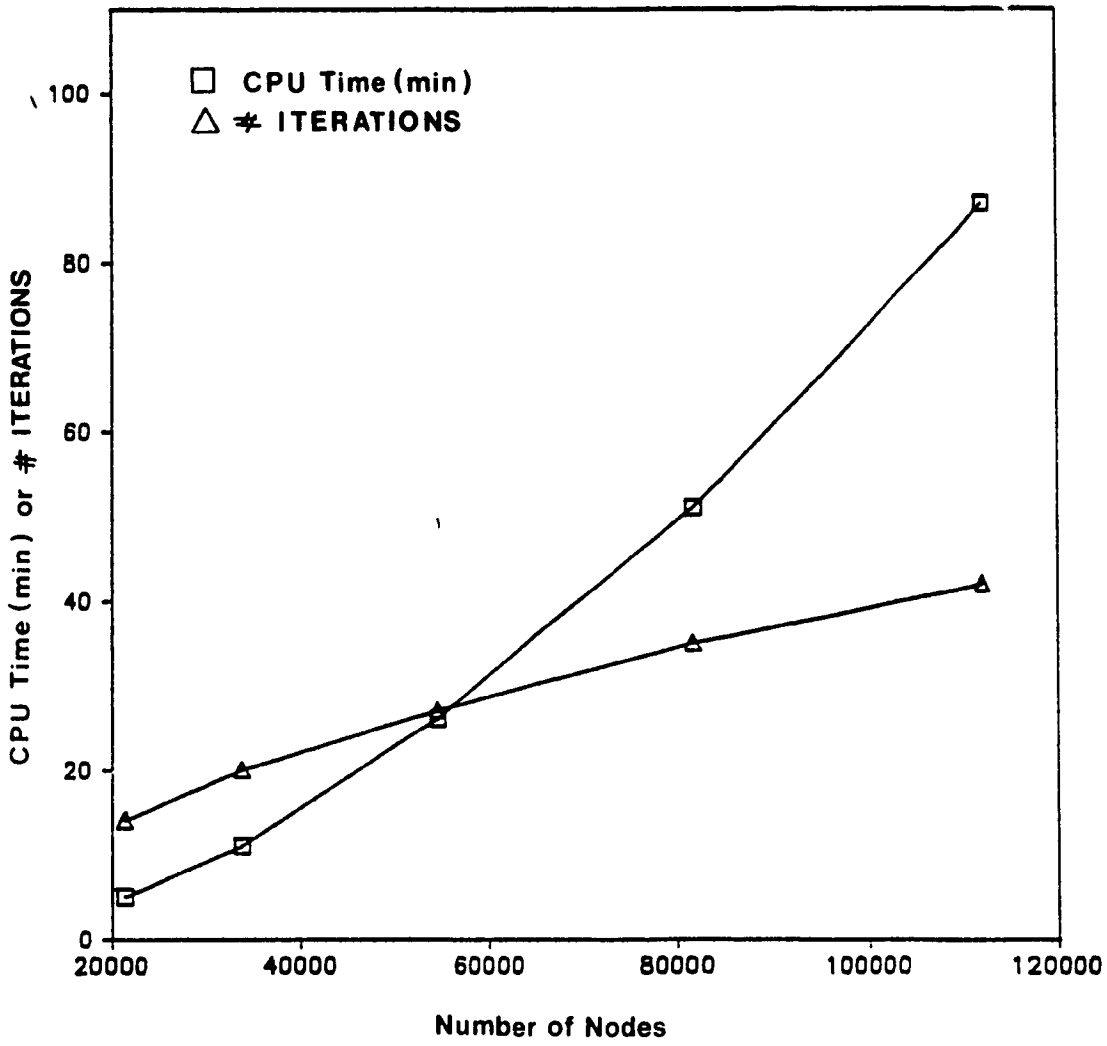

Fig.8.10: CPU Time or Iteration Requirements with Different Number of Computational Nodes

8.3 Effect of Error Level on the Computed Solution

For pressure - coupling schemes such as SIMPLE, the convergence of the numerical solution mainly depends on the under-relaxation factors or acceptable error level of the solution. As discussed in section 3.2, the former group will be excluded from the discussion since the used values are optimum. Before presenting an acceptable error level for the numerical solution, it is useful to explain the inter - relation of the term with the iterative procedure.

Conventionally, an iterative process is said to have converged when further iterations will not produce any changes in the values of the dependent variables. Such a criterion may sometimes be misleading (Patankar,1980 and Habashi,1988). When a heavy under-relaxation factor is used, intentionally, the change in the dependent variable between successive iterations is slowed down. This may create a false image, eventhough the current working solution is far away from convergence. One way to overcome this numerical illusion is by monitoring how well the discretized equations are satisfied by the current value of the dependent variable and this can be conveniently performed as follows:

Recalling the discretized equation

$$a_P\phi_P = \sum_{m=1}^{n_p} a_m\phi_m + S_L \qquad (3.16)$$

where ϕ_P is the dependent variable, which takes values of u, v, w, p, k and ε for the node under consideration, P, a's are the HDS coefficients of the respective nodes and S_L

is the lineralized source term, the residual of a particular iteration for node P can be obtained by

$$R_\phi = \sum_{m=1}^{n_p} a_m \phi_m + S_L - a_P \phi_P \qquad (8.1)$$

For a fully satisfied discretized equation the L.H.S of Eq. 8.1 has zero or near zero value. When ϕ_P takes the velocity variable (u, v and w) the calculated R_ϕ represents an imbalance in conservation of momentum. Since for the present study the continuity condition is solved by using the SIMPLE algorithm, R_p will represent an imbalance in the conservation of mass. Similarly with the turbulence variable (k or ε), R_ϕ, represents an imbalance in turbulence quantities.

For the present study the convergence criterion is obtained, based on the normalized error. Using Eq. 8.1, R_ϕ for each node is calculated and at the end of each iteration the summation of R_ϕ for all nodes is obtained. This is the total error of the iteration for the respective variable. The total error obtained for the first iteration is called the initial error of the computation. Then the normalized error is obtained by dividing the total error of each iteration by the initial error. For example a normalized error of 0.7 reveals that the iteration process reached a stage where the initial error is reduced by 30%.

Such error levels are displayed in the vertical axis of Fig 8.11 which has three curves representing the maximum value among the velocity variables (imbalance in the momentum), the error in pressure (imbalance in the conservation of mass) and the maximum value between the turbulence quantities. For the considered building

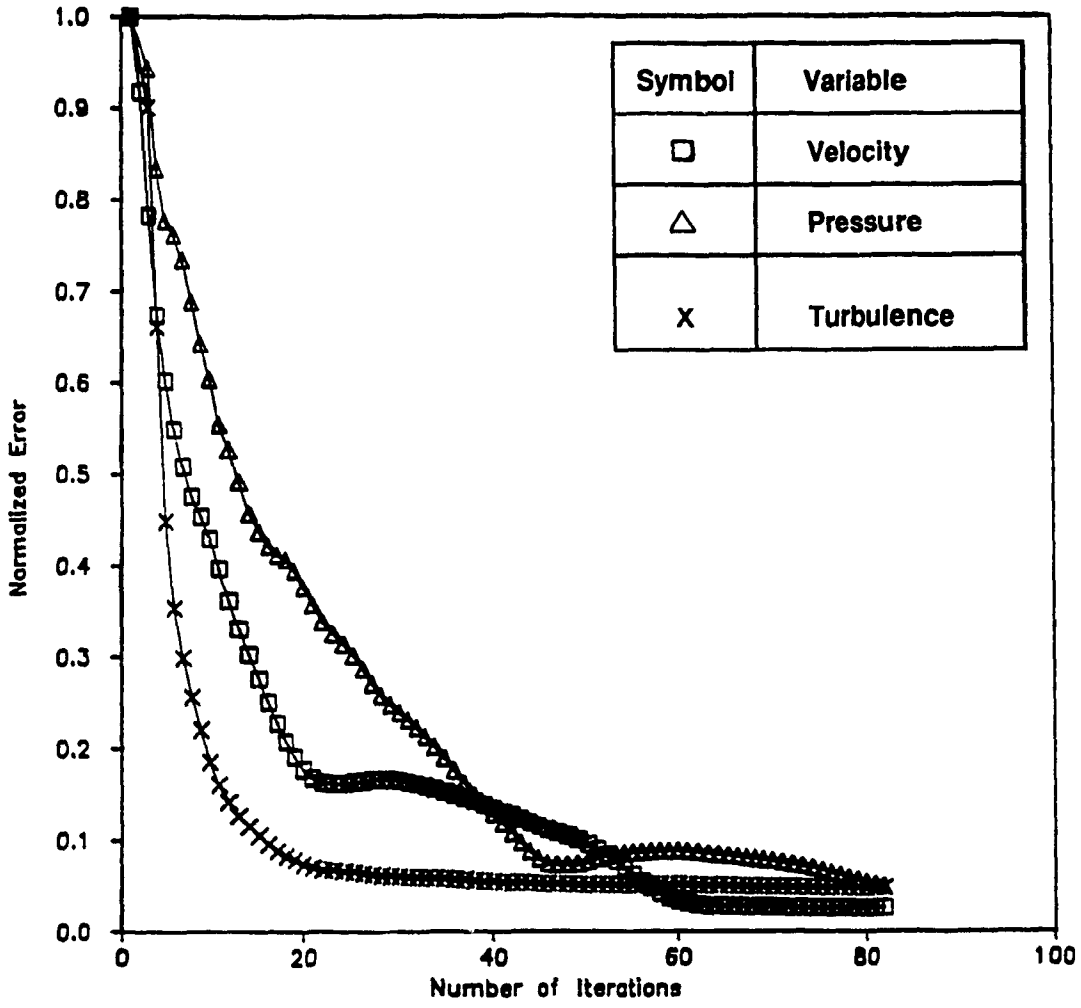

Fig.8.11: Reduction in the Normalized Error Level for Different Variables of Computation

eometry, the error in pressure is always higher than the other variables. The same trend has also been found for other buildings that are tested and this is probably due to the fact that a zero value is initially assumed for the unknown pressure field (ref: section 3.3.3). This is why most of the studies using the SIMPLE algorithm follow a convergence criterion based only on the imbalance of conservation of mass.

Another interesting feature also observed in Fig.8.11 is the reduction in error factor during the initial stage of the iteration process. A significant reduction of about 60% is found within the first 20 iterations and this steep gradient in reduction tends to slow down for further iterations. Additional increase of about 30 iterations (from 50 to 80) reduces only about 0.05 the normalized error. Therefore, a decision of terminating the process after 50 iterations is found to be reasonable. However, its consequences on the changes in the numerical solution as well as on the computational cost must be discussed.

Computations were performed based on four convergence criteria namely 0.4, 0.2, 0.1 and 0.05 without specifying any upper limit on the number of iterations. The DD2 computational domain and the NN4 grid set have been used. The computed pressure and velocity values are analyzed as previously and found insensitive for the factor 0.1 and beyond. Differences are noted between the results of 0.4 and 0.1 and only marginal changes are found in the computed results for 0.2 and 0.1 sets.

On the other hand the convergence criteria are more pronounced on the computational cost as shown in Fig. 8.12. Both the iterations and the CPU time increase when the normalized error levels are reduced. Based on the available limited data points the curve can be divided into two segments at a point 0.1 on the x - axis. The curve is steeper for the x axis region up to 0.1 in comparison to the other part. This reveals that the computational cost will increase significantly if one requires an error level less than

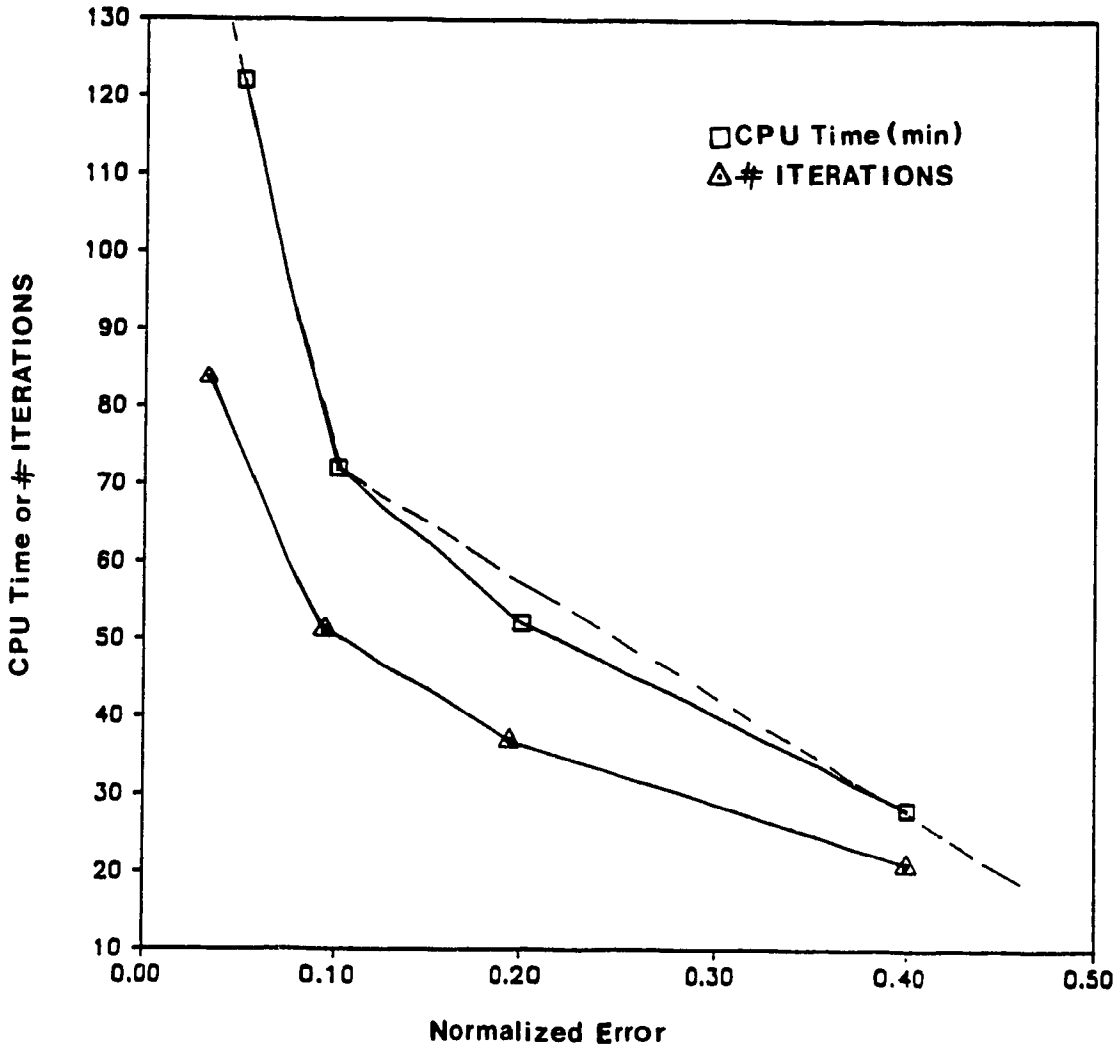

Fig.8.12: Effect of Normalized Error on the CPU Time or on the Number of Iterations

0.1. On the other hand no changes are observed in the computed results beyond this point. Thus it can be concluded that selecting 0.1 as the normalized error factor is acceptable by considering both the computed results and the cost. However, further research efforts are necessary to validate this observation by changing the other parameters such as building height and inlet velocity profile.

CHAPTER 9

APPLICATION OF THE PRESENT COMPUTER CODE

" A survey of 1250 practicing engineers indicates that 87 % of respondents are using microcomputers whereas only 9 % have access to a mainframe " - ASCE, (1989).

9.1 Evaluation of Wind-Effects on Microcomputers

Advancements in microcomputer hardware technology provides not only large storage space but also high computational speeds at a moderate cost (see: Table 9.1). Research efforts have thus been undertaken to modify current mainframe codes or to develop new computer codes for the solution of various engineering problems in microcomputers. One recent study by Filiatrault and Cherry (1989) has produced a Friction Damped Braced Frame Analysis Program (FDBFAP) which is adaptable to microcomputer environment. This structural analysis program compares well with DRAIN-2D (Kannan and Powell, 1973) which runs exclusively on mainframes. Table 9.2 shows the CPU time required to run the new program, FDBFAP, in different computer systems. Along the same lines, microcomputer program versions (Herron et al., 1981) are now available for the well-known building energy analysis program BLAST (Hittle, 1977). Figure 9.1 compares the CPU time requirements by different computer systems for annual heat calculation of a particular dental clinic.

Year	Word Length (bit)	Clock Speed (mHz)*	Hard Disk (MB)	RAM (KB)*	Hard Disk Access Time (ms) #	Model
1981	8	4.77	N/A	128	N/A	IBM PC
1983	16	12	32	640	40	IBM XT or IBM AT
1987	32	33	340	36000	16	AST 386
1990	32	60	N/A	N/A	8	IBM 486

* - Maximum Value
# - Minimum Value

Table.9.1 Performance Improvements in Microcomputers

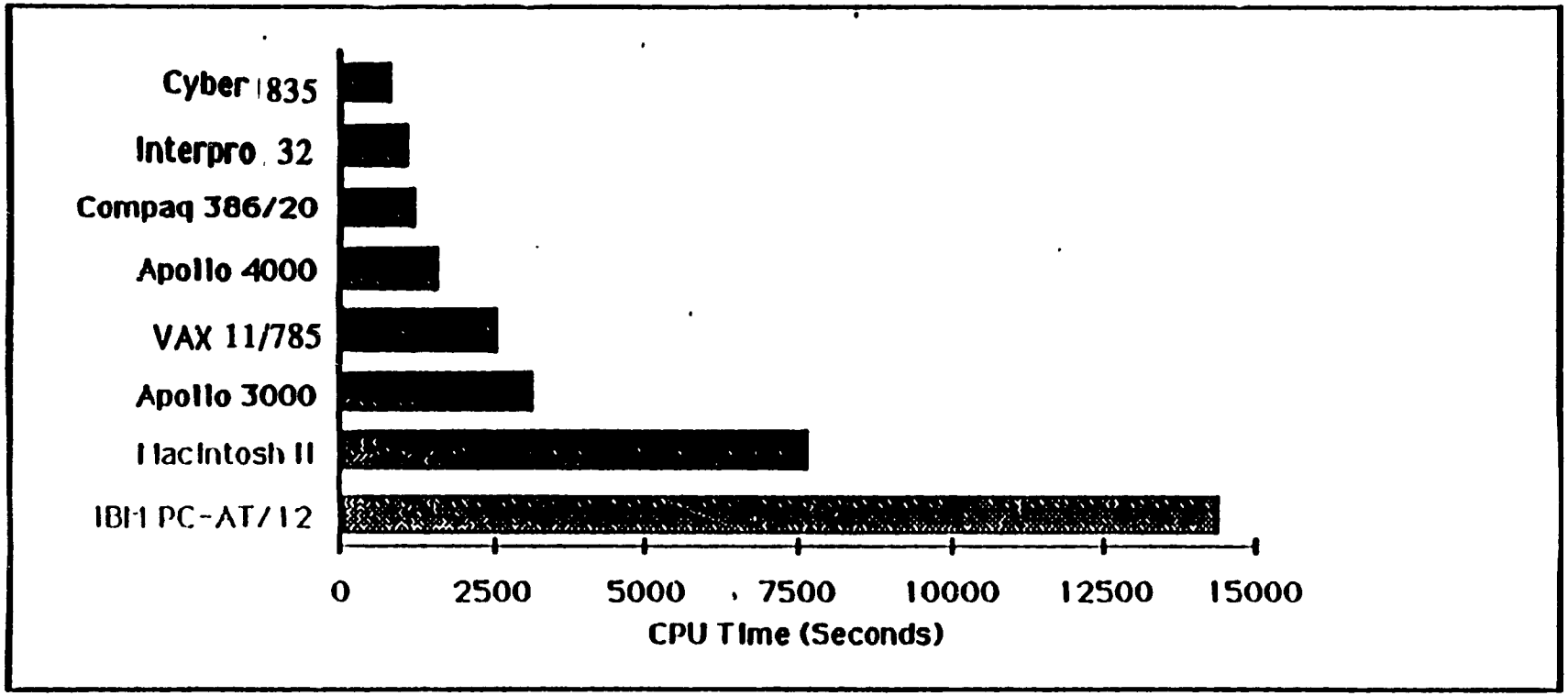

Fig.9.1: CPU Time Requirements for BLAST in Various Computer System (BLAST, 1988)

COMPUTER	CPU time (sec.)	Relative Performance
Micro,4.77 mHz PC (with 8087)	1254.6	1.00
Micro, 10 mHz AT (with 80287)	418.5	3.00
Mini, Sun 3/260	50.9	24.65
Main frame, Amdahl V8	11.9	105.43

Table.9.2 Comparison of CPU Time for FDBFAP (Filiatrault and Cherry,1989)

Software evaluating wind effects on buildings would be an attractive tool for the design process particularly if appropriate for microcomputer environments. This will be a useful tool for the practicing engineer to carry out design. Nevertheless, it appears from the literature review that no studies have been made along this line of research. As an application of the present study a version of TWIST for the evaluation of wind effects on buildings has been developed and implemented in various microcomputers. This chapter analyzes the influential parameters of the computation for wind velocities around buildings and wind - induced pressures on buildings.

A 120 m high building having a square cross-section of 60 m X 60 m has been used as a test case for the comparisons. A power law profile with gradient wind speed of 12 m/s and an exponent equal to 0.16 (corresponding to open country terrain conditions) have been considered for the modelling. Due to memory restrictions only the standard turbulence models along with the conventional wall functions are used in the numerical modelling and computational runs have been carried out in three different microcomputers, namely AST Premium 386/20, DELL 286/20 and IPC 286/12. The computed results have been compared both with measured data obtained from boundary layer wind tunnel experiments as well as with computed results from VAX/1.2 and VAX/6.3 computers. The specification details of the different computer systems used in the present study are given in Table 9.3.

9.2 Computed Results and Discussion

The number of computer grid nodes plays a major role in the CPU time required for the numerical evaluation of wind effects on buildings. Keeping the extent of computational domain constant, the number of control volumes inside the domain has been varied to establish the parameters for economical computation. Runs were made on the different computer systems based on feasibility, i.e. capacity limits. Figure 9.2 presents the results in which the CPU time needed only for module 2 is plotted as function of the

Model	Word Length (Bits)	Clock Speed (Mhz)	Hard Disk Access Time (ms)	Accessories
IPC AT 286 (1986)	16	12	24	MS-Dos Operating System V3.3 MS-Fortran Compiler V4.0 Linker V5.1 287 Math Co-processor
DELL AT 286 (1988)	16	20	29	"
AST Premium 386 (1988)	32	20	15	MS-Dos Operating System V3.3 MS-Fortran Compiler V4.0 Linker V5.1 387 Math Co-processor
VAX 11/785	32	1.2 MIPS	N/A	VMS- Operating System V5.01 VMS-Fortran Compiler V4.8 Linker V5.1 Single Procession
VAX 8550	32	6.3 MIPS	N/A	"

Table.9.3 Specification Details for the Computer System Used in the Present Study

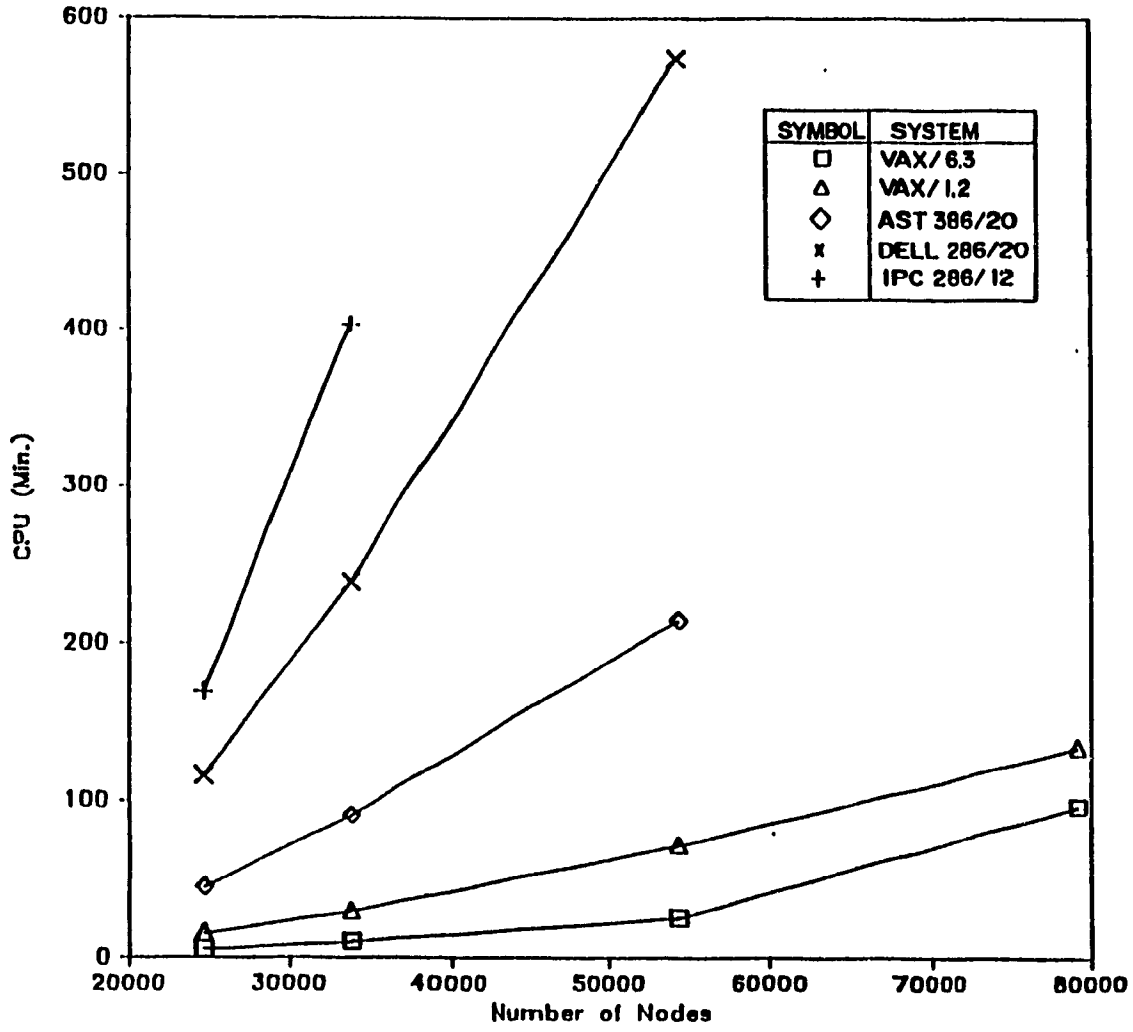

Fig.9.2: CPU Time taken by TWIST for Test Runs with Different Grids

number of grid nodes. The CPU time corresponding to microcomputers represents the direct, continuous access time whereas the CPU time for VAX machines is taken under batch mode operation. Microcomputers with longer word length and higher clock speed consume less CPU time, as expected. On the other hand, the hard disk access time does not affect the CPU time due to the iterative nature of the problem. Both IPC/12 and DELL 286/20 have the same Intel 286 microprocessor but the high clock speed DELL takes less CPU time. It is also interesting to note that both DELL and AST have the same clock speed but the AST with longer word length consumes less CPU time.

The VAX machines operate with the unique page faulting and virtual memory address technology. However, the difference in MIPS (Millions of Instructions Per Second) is not directly affecting the CPU time. The following relationships have been formulated for the CPU times required to run the considered test case:

$$t\,[VAX/1.2] \approx 3 * t\,[VAX/6.3]$$
$$t\,[386/20] \approx 9 * t\,[VAX/6.3]$$
$$t\,[286/20] \approx 24 * t\,[VAX/6.3]$$
$$t\,[286/12] \approx 36 * t\,[VAX/6.3]$$

Note that the test case takes about 20 minutes (CPU time) to run in the VAX / 6.3 with 54,288 grid nodes.

Another significant parameter of the computation is the error level of convergence. Conventionally, a normalized error level is used for terminating the iteration process. As discussed in section 8.3, this error level shows the deviation of the approximated difference equation from the exact differential equation. Fig. 9.3 displays the largest normalized error level value among the six variables (u, v, w, p, k, ε) for the respective iterations. From the figure it is clear that the required CPU time for

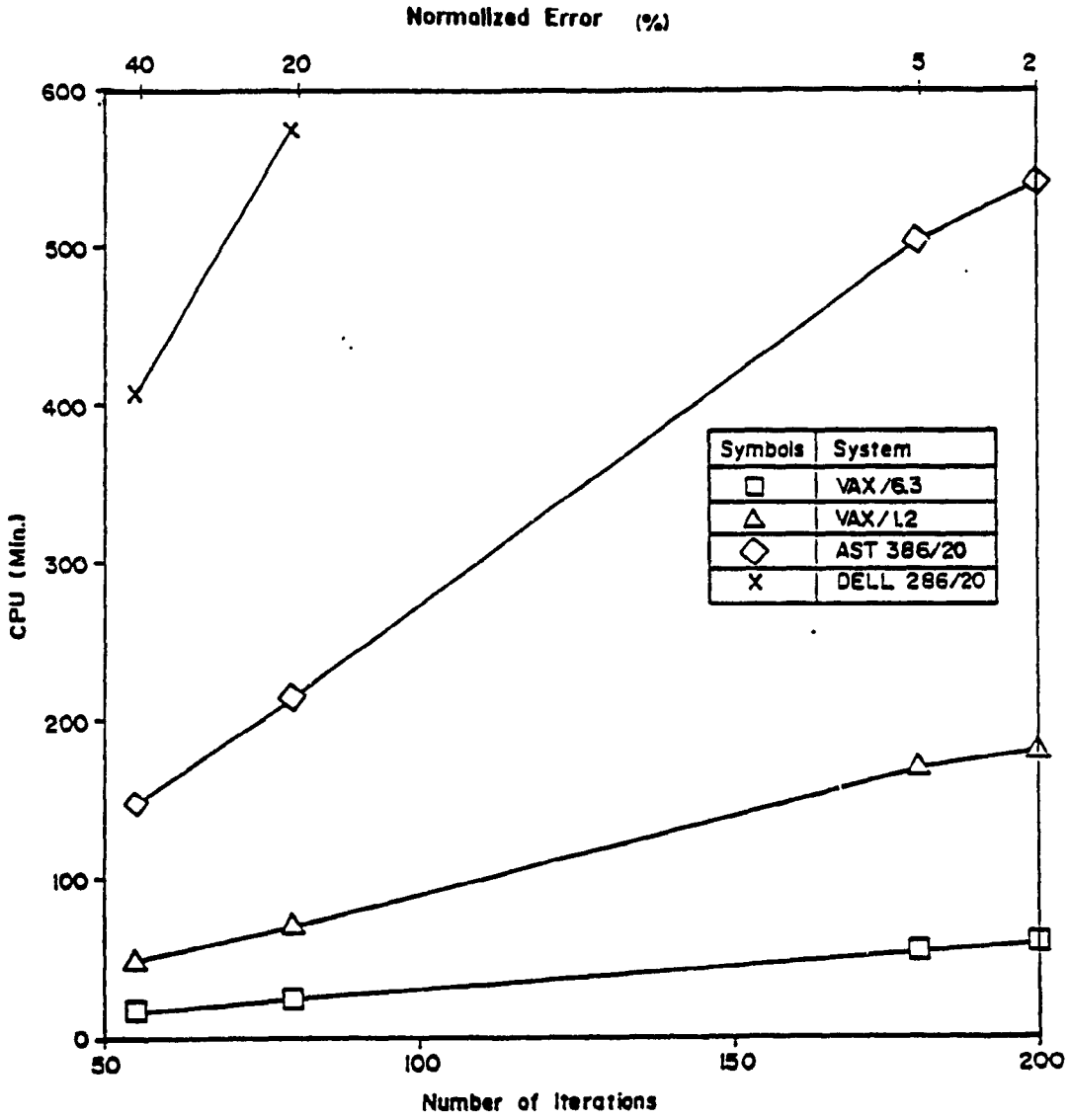

Fig.9.3: CPU Time taken by TWIST for Test Runs with Different Number of Iterations

different computers increases when the error levels are reduced. Furthermore, it is clear that the smaller the computer system the more drastic this increase appears to be. Comparing with Fig. 8.11, it can be concluded that the error levels have direct influence on the number of iterations required and hence the CPU time.

Based on the previous observations about the computation of wind effects on buildings in different computer systems the following can be noted:

1. Microcomputers require a CPU time which is 9 to 36 times higher than the respective time necessary for the same run in the VAX machines.

2. Among the various computational parameters, the CPU time required for computation increases quasi-linearly with the number of grid nodes.

3. Since the considered problem is iterative in nature, the disk access time has only marginal influence on the total CPU time required for the solution. This has been found true of all three microcomputer runs examined.

4. Economical computations can be achieved by using 32 bit machines with high clock speed.

Grid density naturally affects the computed wind velocities and pressures. Differences in the computed results have been analyzed for various grid arrangements. Figures 9.4 and 9.5 show typical data for the computed longitudinal velocity and turbulence intensity, both normalized by the free stream velocity on the upstream of the building in the location indicated. Four different grid sets in the same computational domain have been examined. These have 24,640; 33,792; 54,288 and 79,200 nodes respectively. In section 8.3, only marginal changes are noticed in the computed results when the convergence criteria is reduced from 20 % to 10 %. On the other hand the CPU time

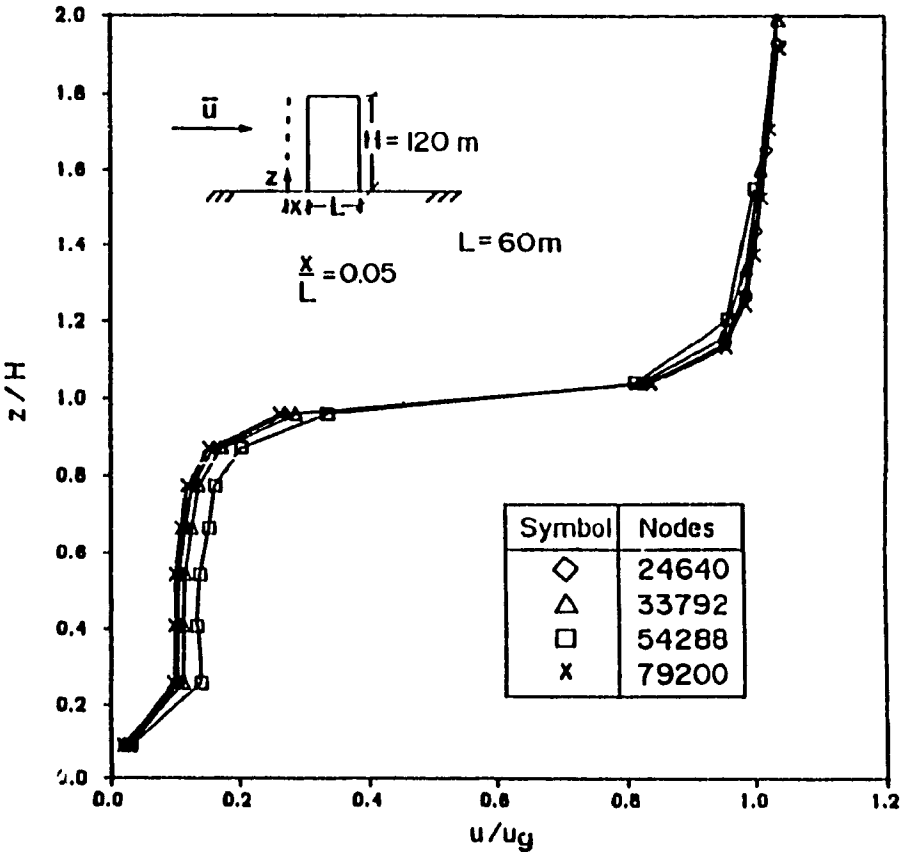

Fig.9.5: Variation of Turbulence Intensity for Test Runs with Different Grids in Micros

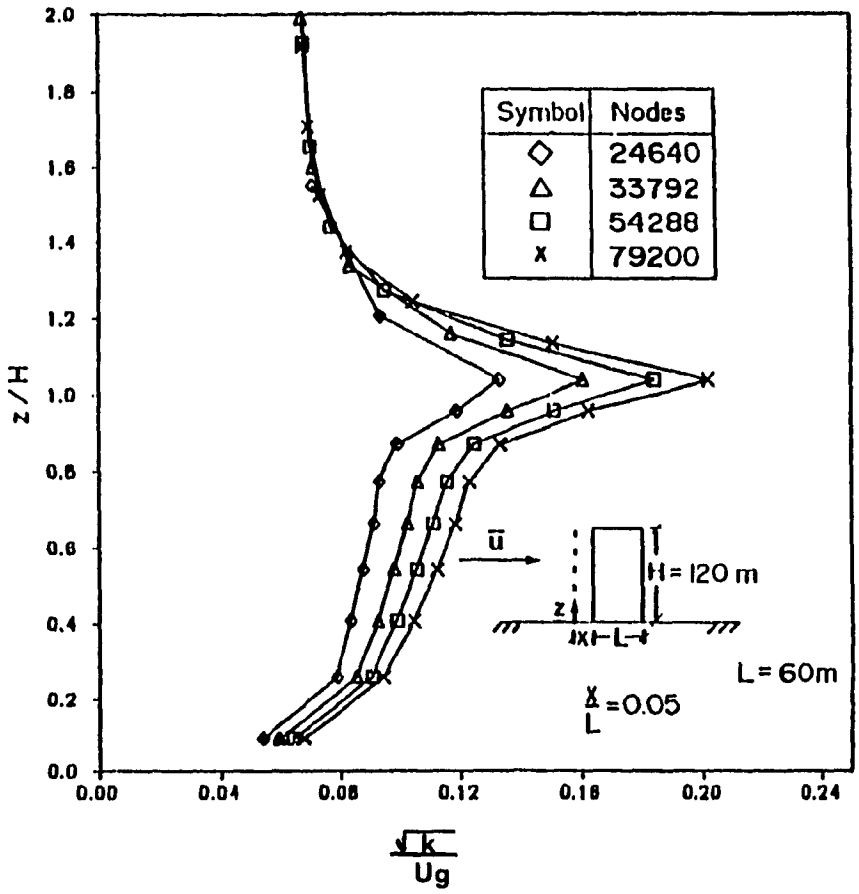

Fig.9.4: Variation of Longitudinal Velocity for Test Runs with Different Grids in Micros

increases significantly. So for the present exercise the iterations are terminated with a convergence criterion of 20 %. As evidenced by the variation of the velocity shown for this particular location, there is little difference in the results obtained from the various grids. Some discrepancy however, is apparent with the lowest density grid. Grid density affects the turbulence values more than the velocities, particularly near the building top. This may be expected because of the high velocity gradients formed when the flow separates from the leading edge. These gradients increase the turbulence intensity values and a very dense grid is necessary to capture the changes. For example at z/H = 1.0, the computed turbulence intensity increases approximately from 0.13 to 0.20 when the grid nodes change from 24,640 to 79,200.

The accuracy of the computed results is also examined based on comparisons with measured experimental data and Fig. 9.6 shows one such comparison. Experimental values are taken from Zhu (1987), in which the details of experimentation and the properties of the boundary layer wind tunnel are provided. For each wall there are five curves representing the measured data and the computed values obtained by using the four different sets of grids, as previously explained. The curves represent the maximum value that has been measured or computed at the different levels of each wall. For the windward wall this occurs at the stagnation point which is about at a height equal to 3/4 H. Differences with the experimental data are more significant for the leeward and particularly for the side walls for which the computed suction values are smaller than the measured data even when the grid with 79,200 nodes is utilized. This implies again that the separation of the flow and the involved eddies demand better mathematical treatment in the computation. Implementing the newly developed zonal treatment along with modifications on the standard turbulence model may enhance the agreements. However, for the other walls the comparison of the computed values with the experimental data is encouraging. It appears that the computed results are reasonable even for the grid with 33,792 nodes.

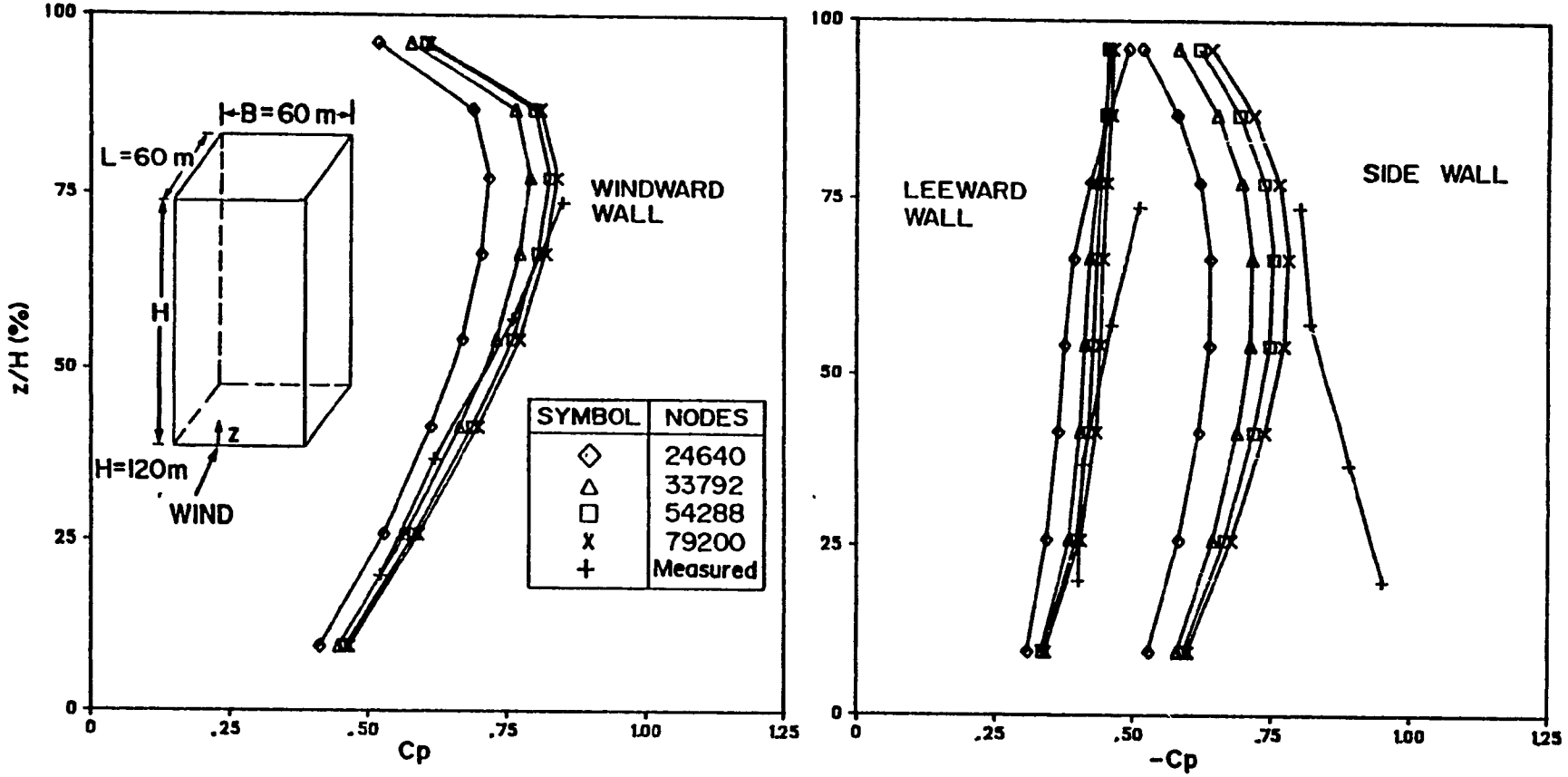

Fig.9.6: Wall Pressure Coefficients Measured and Computed (with Different Grids) in Micros

TWIST runs under MS_DOS operating system for different microcomputers as specified in Table 9.3. The MS_DOS operating system has the disadvantage of 640 K limited base memory size. This permits only runs which have grids with less than 60,000 nodes. However, the same computer code can be implemented under OS/2 operating system as explained by Kogan and Rawson (1988). The OS/2 operating system by-pass the 640 K base memory restriction and allows the user to use the hard disk memory up to 16 MB or perform simulations even with 100,000 nodes. Thus the micro computer version of TWIST can be extended for other cases such as computation for multiple building configurations and modelling of angled flow conditions.

CHAPTER 10

CONCLUSIONS AND RECOMMENDATIONS

" At the bachelor's level our knowledge is broadened, deepened and refined. But it is usually only at the graduate level that we are, in a sense, left alone to explore, experiment and make a personal contribution to the advancement of knowledge " - M. E. SZABO

10.1 Summary of the Present Contributions

A systematic approach for the numerical evaluation of wind effects on buildings has been attempted in the present study. The time - averaged NSE and the $k - \varepsilon$ turbulence models are grouped in a compact form. The control volume technique is used to discretize the differential equations into difference form. For simulations, fluid viscosity is calculated by applying the eddy - viscosity concept.

A computer code named **TWIST** - **T**urbulent **W**ind **S**imulation **T**echnique - has been developed as part of this research. As the new code is modular in fashion, it has several advantages: stand alone tests for debugging are easier and modifications for different problems of interest can be performed without making extensive changes in the basic code. To validate the newly developed code, initial computations were made for a geometrically simple case of a single building exposed to normal wind conditions. Comparisons of the computed results were not only made with measured data from boundary layer wind tunnels but also with the results from other computational studies.

Systematic attempts are also necessary for the evaluation of turbulent wind effects on buildings for different wind directions. As a first step towards this approach, a feasibility study is presented in the thesis for the simulation of wind directionality effect. This has been achieved by suitably modifying the developed computer code. Comparisons of the computed velocities and pressures with the measured data reveals that TWIST can predict overall flow characteristic for different wind directions.

Successful attempts are also reported in predicting the wind environmental conditions around a cluster of buildings in the computer. A typical downtown location of Montreal is selected for the exercise and simplified conditions are used in the numerical modelling. To validate the computed results, experimental work has also been carried out in the boundary layer wind tunnel at the Centre for Building Studies of Concordia University. Computed as well as measured data are converted into conventional velocity ratios. Comparisons of these ratios indicate generally good agreement with the exception of points which are very close to the buildings.

The standard $k - \varepsilon$ model was used in all previous studies to create turbulence in the flow field. However, it was found to be insensitive to the streamline curvature of the flow and it computed a low rate of dissipation of kinetic energy. Moreover, to transfer the boundary information, the conventional wall functions are used during the computation for all six variables. Since wall functions were suitable only for velocity variables, the computed turbulence properties are found to be underestimated. To improve the predictions, two kinds of refinements are made in the present numerical modelling process: modifying the standard $k - \varepsilon$ turbulence models and applying a new zonal treatment method for turbulence variables.

Identified modifications are the streamline curvature correction and the preferential dissipation correction. These modifications are included in the code to predict the condition on flow curvature regions more accurately. In the new zonal treatment method, based on the calculated local Reynolds number, the edge of the Viscous Sub Layer (VSL) is determined. For inner zones of VSL, new algebraic equations are derived and used for calculating the kinetic energy and the dissipation rate of kinetic energy , whereas for outside zones, modified $k - \varepsilon$ equations are applied in discretized form. A variety of computations have been made after implementing these modifications and the new zonal treatment method. Computed results of the new approach are significantly improved and they also agree remarkably well with the measured data from various boundary layer wind tunnels.

Input parameters may affect the numerical solution. In the present study, changes in the system output have been studied systematically by varying three major input parameters, namely the size of computational domain, the number of nodes in the domain and the criteria of convergence. From the computed results it has been shown that the number of nodes affects the accuracy of numerical solution more than the other two parameters. The computational cost is also analyzed by recording the CPU time of the different cases.

To make a wider use of the present research a version of TWIST is developed for microcomputer environments. Computations have been performed in various micros for a building exposed to normal wind conditions. It has been noted that the micros require a CPU time which is 9 to 36 times higher that the respective time necessary for the same run in the VAX machines. Moreover, the CPU time required for computation increases quasi-linearly with the number of grid nodes used.

10.2 Recommendations for Future Research

As the Computational Wind Engineering state of the art is not wealthy, many interesting and innovative topics are readily available for further research. This section recommends some of these works under two main categories. Studies related to the first group can be attempted by extending the present code TWIST, without performing major changes in its basic structure. The second category of recommendations may need different solution algorithms or numerical schemes.

For a single building exposed to normal wind conditions, TWIST needs validation for buildings with predominant geometrical dimensions such as low long buildings, tall slender buildings and buildings of very low height. In order to do this, one may have to perform experiments and/or collect relevant measured data for velocities and pressures. Keeping the flow direction normal to the building, extensive research can be performed for more than one building configurations. Achievements are made by the present study in predicting the wind environmental conditions around a typical multiple building configuration. A useful next step is validating TWIST, for wind-induced pressure loads on the different buildings. Application of the modified turbulence models and the inclusion of the newly developed zonal treatment method are worth considering for these multiple building configurations. Efforts are also needed to gather error free velocity measurement data by using some sophisticated measurement systems or Laser - Dopler anemometry. It is also worth extending the present code such that it will be flexible to accommodate different building clusters. The implementation of these recommendations requires changes only in Module 1 and BOUNDS submodule of Module 2 whereas the other structure of TWIST may remain as is.

In the case of second category, further research is also required in computing the wind directionality effect, in predicting wind-induced instantaneous parameters and in modelling the wind effects for buildings of different shapes. For the wind directionality effect, a feasibility study has been made by the present study in Chapter 5 and it has been found that the inclusion of a powerful numerical scheme such as the Skew Hybrid Difference Scheme (SHDS) or the Bound Skew Hybrid Difference Scheme (BSHDS) is necessary for the interpolation of the convective term. This can be included in the ASSEMBLER submodule of Module 2. Another way of addressing this issue without making changes in Module 2 is by introducing advanced grid generation techniques. Body Fitted Coordinate systems (BFC) or Adaptive grid systems are worth considering along with suitable boundary treatment procedures.

To compute wind-induced peak pressure coefficients on buildings and to calculate instantaneous velocities around buildings, the time dependent form of differential equations needs to be solved. The standard or modified turbulence models and the SIMPLE iterative algorithm are suitable for steady state conditions. One could consider " direct solvers " for the solution of NSE by introducing either the Large eddy simulation technique or by using the Algebraic stress models. Obviously, time dependent simulations need more computer resources (speed and storage) and faster post - processors than those used in the present study.

Studies have not been attempted, even with powerful numerical codes such as PHOENICS to evaluate the wind effects on different building shapes such as circular chimneys and buildings with multilevel roofs. No doubt, this type computer simulation is an ambitious and useful undertaking. One way to approach this problem is by developing a suitable grid generation technique. Significant amount of research effort is also needed in developing a flexible computer code to account for variety of building shapes.

REFERENCES

1. AKINS. R. E. , PETERKA. J. A. and CERMAK. J. E. , (1979), "Average Pressure Coefficients for Rectangular Buildings", Proceedings of the 5th Int. Conf. on Wind Engineering, Fort Collins, Colorado, U.S.A, 1, 369-380.
2. AMSDEN. A. A. and HARLOW. F. H. , (1970), "The SMAC Method : A Numerical Technique for Calculating Incompressible Fluid Flow", Los-Alamos Scientific Laboratory Report, LA-4370.
3. ANDERSON. D.A , TANNEHILL. J. C. and PLETCHER. R. H. , (1984), "Computational Fluid Mechanics and Heat Transfer", Mc - Graw Hill, London.
4. ANDERSON.D.A, (1983), " Adaptive Grid Methods for Partial Differential Equations", Eds. K.Ghia and I.Ghia, Advances in Grid Generation, 1-15.
5. ANDERSON. C. and GREENGARA. C. , (1985), "On Vortex Methods", SIAM, J. Numer. Anal. , 22, 3, 413-439.
6. ANDERSON. C. R. , (1985), "A Vortex Method for Flows with Slight Density Variations", J. Comput. Phys. , 61, 417-444.
7. ANTONIOU. J. and BERGELES. G. , (1984), "Development of the Reattached Flow Behind Surface-Mounted Two-Dimensional Prisms", Transactions of ASME, J. Fluids Engng. , 110, 127-133.
8. AREF. H. and KAMBE. T. , (1988), "Report on the IUTAM Symposium: Fundamental Aspects of Vortex Motion", J. Fluid Mech. , 190, 571-595.
9. ARENS,E.A and WILLAIAMS, P.B., (1977), " The Effect of Wind on Energy Consumption in Buildings ", Energy and Buildings, 1, 77 - 94.
10. "ASCE News", (1989). American Society of Civil Engineering, New York, NY,14,8.
11. AWBI.H.B, (1989), " Application of Computational Fluid Dynamics in Room Ventilation", J. Bldg. Envir., 24, 1, 73 - 84.
12. BACK. L. H. and ROSCHKE. E. J. , (1972), "Shear-Layer Flow Regimes and Wave Instabilities and Reattachment Lengths Downstream of an Abrupt Circular Channel Expansion", Transactions of ASME, J. Appl. Mech. , 72, 677-681.
13. BAETKE. F. , WERNER. H. and WENGLE. H. , (1987), "Computation of Turbulent Flow around a Cube on a Vector Computer", 6th Symposium on Turbulence and Shear Flows, 9, France, 20-2-1-20-2-6.

14. BAETKE. F. , (1986), "Numerische Berechnung der Turbulenten Umstromung eines kubischen Korpers", Ph.D. Thesis, Technische Universitat Munchen, Germany.

15. BAKER. C. J. , (1980), "The Theory of Flow between Two Buildings - Experimental Verification of the Assumptions of Britter and Hunt's Theory", J. Wind Engng. and Ind. Aerodyn. , 6, 169-174.

16. BASKARAN. A. and STATHOPOULOS. T. , (1990.a), " Numerical Evaluation of Wind Effects on Buildings", Proceedings of ASME Computers in Engineering Conf. , Boston, U.S.A, Aug. 5-9.

17. BASKARAN. A. and STATHOPOULOS. T. , (1990.b), " Computer Simulation of 3D Turbulent Wind Effects on Buildings", Annual Conference, Canadian Society of Civil Engineering, Hamilton, Canada.

18. BASKARAN. A. and STATHOPOULOS. T. , (1989.a), " Evaluation of Wind Effects on Buildings through Microcomputers ", Proceedings of the 4th Int. Conf. on Engineering Software, New Delhi, India, Dec 8-12.

19. BASKARAN. A. and STATHOPOULOS. T. , (1989.b), "Computational Evaluation of Wind Effects on Buildings", J. Bldg. Envir. , 24, 4, 325 - 333.

20. BASKARAN. A. and STATHOPOULOS. T. , (1989.c), "Computer Simulation of Wind Effects on Buildings", Proceedings of the 12th CANCAM Conf. , Ottawa, Ontario, Canada, June 2 - 6.

21. BASKARAN. A. and STATHOPOULOS. T. , (1988), "Computational Techniques for the Evaluation of Wind Effects on Buildings", Proceedings of 7th ASCE/EMD Specialty Conference, Blacksburg, VA, USA.

22. BASKARAN. A. and STATHOPOULOS. T. , (1987), "Computer Simulation of Wind Flow around Buildings - An Introduction", Annual Conference, Canadian Society of Civil Engineering, Montreal, Canada.

23. BASKARAN. A. , (1986), "Wind Loads on Flat Roofs with Parapets", M.Engng. (Building) Thesis, Concordia University, Montreal, Canada.

24. BATCHELOR. G. K. , (1967), "An Introduction to Fluid Mechanics", Cambridge University Press, London.

25. BENODEKAR. R. W. , GODDARD. A. J. H. , GOSMAN. A. D. and ISSA. R. I. , (1985), "Numerical Prediction of Turbulent Flow over Surface-Mounted Ribs", AIAA Journal, 23, 3, 359-366.

26. BERANEK. W. J. , (1979), "General Rules for the Determination of Wind Environment", Proceedings of the 5th Int. Conf. on Wind Engineering, Fort Collins, Colorado, U.S.A, 1, 225-235.

27. BERANEK, W.J and KOTEN, H.Van, (1978), " Wind Environment Around Buildings ", Proceedings of 3rd U.S. National Wind Engng Conference, Gainesville, U.S.A, 193 - 197.

28. BERGELES. G. and ATHANASSIADIS. N. , (1983), "The Flow Past a Surface-Mounted Obstacle", Transactions of ASME, J. Fluids Engng. , 105, 461- 463.

29. BERNARD. S. P. , (1986), "Limitations of the Near Wall k-ε Turbulence Model", AIAA Journal, 24, 4, 619 - 622.

30. BIENKIEWICZ. B. and KUTZ. F. R. , (1989), "Applying the Discrete Vortex Method to Flow about Bluff Bodies", Proceedings of the 6th U.S. National Wind Engng. Conf. , Houston, Texas, U.S.A, A-7-11 : A-7-20.

31. BLAST News Letter (1988), BLAST Support Office, Department of Mechanical Engng, University of Illinois at Urbana - Champaign, Urbana, IL, U.S.A, 6, 12, 3.

32. BLESSMANN, J. and RIERA, J . D., (1979), " Interaction Effects in Neighboring Tall Buildings", Proceedings of the 5th Int. Conf. on Wind Engineering, Fort Collins, Colorado, U.S.A, 1, 381-395.

33. BORGES. A. R. J. and SARAIVA. J. A. G. , (1979), "An Erosion Technique for Assessing Ground Level Winds", Proceedings of the 5th Int. Conf. on Wind Engineering, Fort Collins, Colorado, U.S.A, 1, 235-242.

34. BORIS. J. P. , (1989), "New Directions in Computational Fluid Dynamics", Ann. Rev. Fluid Mech. , 21, 345-385.

35. BRADSHAW. P. , (1973), "Effects of Streamline Curvature on Turbulent Flow", AGARD No. 169.

36. BRERETON. G. J. and REYNOLDS. W. C. , (1987), "Kinetic-Energy Transfer in an Unsteady Turbulent Boundary Layer", Proceedings of the 6th Symposium on Turbulence and Shear Flows, 9, France, 4-4-1 - 4-4-6.

37. BRITTER. R. E. , (1989), "Atmospheric Dispersion of Dense Gases", Ann. Rev. Fluid Mech. , 21, 317-344.

38. BUDKOWSKA. B. B. and FU. Q. , (1987), "Analysis of Stability Criteria of Finite Difference Method in Viscoelastic Granular Media", Proceedings of the 12th CANCAM Conference, Ottawa, Ontario, Canada.

39. BUI. T. D. and OPPENHEIM. A. K. , (1987), "Evaluation of Wind Effects on Model Buildings by the Random Vortex Method", J. Appl. Num. Math. , 3, 195-207.

40. CARETTO. L. S. , CURR. R. M. and SPALDING. D. B. , (1972), "Two Numerical Methods for Three-Dimensional Boundary Layers", Computer Meth. Appl. Mech. and Engng. , 1, 39-57.

41. CASTRO. I. P. and DIANAT. M. , (1983), "Surface Flow Patterns on Rectangular Bodies in Thick Boundary Layers", J. Wind Engng. Ind. Aerodyn. , 11, 107-119.

42. CASTRO. I.P and ROBINS. A. G. , (1977), "The Flow around a Surface-Mounted Cube in Uniform and Turbulent Streams", J. Fluid Mech. , 79, 2, 307-335.

43. CERMAK. J. E. , (1987), "Advances in Physical Modelling for Wind Engineering", ASCE, J. Engineering Mechanics, 113, 5, 737-757.

44. CERMAK. J. E. , (1984), "Wind-Simulation Criteria for Wind-Effect Tests", ASCE, J. Structural Division , 110, 2, 328-339.

45. CERMAK. J. E. , (1976), "Aerodynamics of Buildings", Annual Review of Fluid Mech. , 8, 75-106.

46. CERMAK. J. E. , (1975), "Applications of Fluid Mechanics to Wind Engineering - A Freeman Scholar Lecture", Transactions of ASME, J. Fluids Engng. , 9-38.

47. CERMAK. J. E. , (1971), "Laboratory Simulation of the Atmospheric Boundary Layer", AIAA Journal, 9, 9, 1746-1754.

48. CHAPMAN. D. R. , (1979), "Computational Aerodynamics Development and Outlook", AIAA Journal, 17, 12, 1293-1313.

49. CHAPMAN. D. R. , MARK. H. and PIRTLE. M. W. , (1975), "Computers vs. Wind Tunnels for Aerodynamic Flow Simulations", Astronautics and Aeronautics, 13, 25-35.

50. CHEER. A. Y. , (1978), "BOUNDL: A Program for Calculating Flow Past a Semi-Infinite Flat Plate Using the Vortex Sheet Method", Report No. LBL-6443, Laurence Berkeley Laboratory, University of California, U.S.A.

51. CHIEN. K. Y. , (1982), "Predictions of Channel and Boundary-Layer Flows with a Low-Reynolds-Number Turbulence Model", AIAA Journal, 20, 1, 33-38.

52. CHIO.H.L et al., (1988), " An Application of the $k-\varepsilon$ Turbulence Model to Predict Air Distribution in a Slot-Ventilated Enclosure ", Transactions of the ASAE, 31, 6, 1804 -1814.

53. CHORIN. A. J. , (1986), "Vortex Methods and Turbulence Theory", Report No. PAM-32ℓ, Center for Pure and Applied Mathematics, University of California, Berkely, U.S.A.

54. CHORIN. A. J. , (1980), "Vortex Models and Boundary Layer Instability", SIAM J. Sci. Stat. Comput. , 1, 1, 1-21.

55. CHORIN. A. J. , (1979), "A Mathematical Introduction to Fluid Mechanics", Spriger-Verlag, New York, NY.

56. CHORIN. A. J. , (1978), "Vortex Sheet Application of Boundary Layers", J. Comput. Phys. , 27, 428-442.

57. CHORIN. A. J. , (1973), "Numerical Study of Slightly Viscous Flow", J. Fluid Mech. , 57, 4, 785-796.

58. CHORIN. A. J. , (1968), "Numerical Solution of NSE", J. Math. Comp. , 745-762.

59. Clare. F, Kennison.D and Lackman. B, (1987), "NCAR Graphics User's Guide", Version-2.

60. COOK. N. J. and REDFEARN. D. , (1976), "Calibration and Use of a Hot-wire Probe for Highly Turbulent and Reversing Flows", J. Ind. Aerodyn. , 1, 221-231.

61. CORKE. T. C. , NAGIB. H. M. and TAN-ATICHAT. J. , (1979), "Flow Near a Building Model in a Family of Surface Layers", J. Ind. Aerodyn. , 5, 139-158.

62. CORKE. T. C. and NAGIB. H. M. , (1979), "Wind Loads on a Building Model in a Family Surface Layers", J. Ind. Aerodyn. , 5, 159-177.

63. CORKE. T. C. , NAGIB. H. M. and TAN-ATICHAT. J. , (1977), "Flow near a Model of a Building in Simulated Atmosphere Surface Layers Generated by the Counter-Jet Technique", Eds. Eaton et. al, Wind Effects on Buildings and Structures, Cambridge, University Press, 515-527.

64. COTTON. M. A. and JACKSON. J. D. , (1987), "Calculation of Turbulent Mixed Convection in a Vertical Tube Testing a Low Reynolds Number $k-\varepsilon$ Turbulence Model", 6th Symposium on Turbulence and Shear Flow, 9, France, 9-6-1 - 9-6-6.

65. COUNIHAN. J. and HUNT. J. C. R. , (1974), "Wakes Behind Two-Dimensional Surface Obstacles in Turbulent Boundary Layer", J. Fluid Mech. , 64, 3, 529-563.

66. CROSS. M. , RICHARDS. C. W. , KNIGHT. B. and MARKATOS. N. C. , (1988), "Engineering CFD Software for the Next Decade", Eds. Davis et al. , Computational Fluid Dynamics, 31-41.

67. CULLEN. M. J. P. , (1986), "Numerical Modelling of Discontinuous Atmospheric Flows", Eds. Morton. K. W. and Baines. M. J. , Num. Meth. for Fluid Dyn. II, Clarendon Press, Oxford.

68. DALGLIESH.W.A., TEMPLIN.J.T and COOPER.K.R, (1980), " Comparison of Wind-Tunnel and Full-Scale Building Surface Pressure with emphasis on Peaks, Proceedings of the 5th Int. Conf. on Wind Engng, Fort Collins, Colorado, U.S.A, 1, 553 - 560.

69. DALGLIESH. W.A. (1975)," Comparison of Model/Full-Scale Wind Pressures on a high-rise Building", J. Ind. Aerodyn., 1, 55 -61.

70. DAVENPORT et al., (1985), " BLWT II: The Design and Performance of a New Boundary Layer Wind Tunnel ", Proceedings of 5th U.S. National Conference on Wind Engineering, Lubbock, Texas, U.S.A , 2A-35 - 2A-40.

71. DAVIES. M. E. , QUINCEY. V. G. and TINDALL. S. J. , (1979), "The Near-Wake of a Tall Building Block in Uniform and Turbulent Flows", Proceedings of the 5th Int. Conf. on Wind Engng, Fort Collins, Colorado, U.S.A, 1, 289-298.

72. DEARDORFF. J. W. , (1970), "A Numerical Study of Three-Dimensional Turbulent Channel Flow at Large Reynolds Numbers", J. Fluid Mech. , 41, 2, 453-480.

73. de Vahl Davis. G and Mallinon. G .D (1972), " False Diffusion in Numerical Fluid Mechanics, University of New South Wales, School of Mech and Ind. Eng, Report. 1972/FMT/1.

74. DJILALI. N. , (1987.a), "An Investigation of Two-Dimensional Flow Separation with Reattachment", Ph.D. Thesis , Department of Mechanical Engineering, University of British Columbia, Vancouver, Canada.

75. DJILALI. N. , GARTSHORE. I. S. and SALCUDEAN. M. , (1987.b), "Computational Study of the Separated Reattaching Flow on a Blunt Rectangular Section", Proceedings of 11th CANCAM, University of Alberta, Edmonton, B-42-43.

76. DJILALI. N. , GARTSHORE. I. S. and SALCUDEAN. M. , (1987.c), "An Experimental and Numerical Study of the Flow around a Blunt Rectangular Section: A Test Case for Computational Methods ?", Proceedings of 6th Symposium on Turbulent Shear Flows, France, 19-3-1 - 19-3-6.

77. DOUGLAS. J. and RACHFORD. H. H. , (1956), "On the Numerical Solution of Heat Conduction problems in Two and Three Space Variables", Trans. Amer. Math. Soc. 82, 421-439.

78. DUMITRESCU-BRULOTTE. M. L. , (1987), "Wind Pressures on Buildings of Intermediate Height", M. Engng. (Building) Thesis, Concordia University, Montreal, Canada.

79. DURAO. D. F. G. , HEITOR. M. V. and PEREIRA. J. C. F. , (1988. a), "Measurements of Turbulent and Periodic Flows around a Square Cross-section Cylinder", Experiments in Fluids, 6, 298-304.

80. DURAO. D. F. G. , GOUVEIA. P. S. T. and PEREIRA. J. C. F. , (1988. b), "An Experimental Study of the Flow around a Square Prism", Eds. Hirata. M. and Kasagi. N. , Transport Phenomena in Turbulent Flows, 391-400.

81. DURAO. D. F. G. , HEITOR. M. V. and PEREIRA. J. C. F. , (1987), "The Turbulent Flow in the Near-Wake of a Squared Obstacle", Proceedings of 1987 ASME Applied Mechanics, Bio-Engineering and Fluids Engineering Conference, Cincinnati, Ohio, 45-50.

82. ELDRED. L. B. , KAPANIA. R. K. and BOSCH. H. R. , (1989), "Preliminary Investigations on the Use of Spectral Methods for Flow Calculations", Proceedings of the 6th U.S. National Conference on Wind Engineering, Houston, Texas, U.S.A.

83. EVERETT. T. W. and LAWSON. T. V. , (1984), "Wind-Tunnel Measurements of Pressure and Velocity around a Simple Building in a Turbulent Shear Flow to Allow Validation of Values derived from a Computer Solution of the Navier-Stokes Equations", Department of Aeronautical Engineering, Rep. No. TVL/8401, Bristol University.

84. FERZIGER. J. H. , (1983), "Higher Level Simulations of Turbulent Flows", Ed. Essers. J. A. , Computational Methods for Turbulent, Transonic and Viscous Flows, 93-181.

85. FERZIGER. J. H., (1979), " Large Eddy Numerical Simulation of Turbulent Flows" , AIAA Journal, 15, 9, 1261-1267.

86. FILIATRAULT. A. and CHERRY. S. , (1989), "Efficient Numerical Modelling for the Design of Friction Damped Braced Steel Plane Frames", Can. J. Civ. Engng. , 16, 211-218.

87. FODEMSKI. P. R. , (1988), "The Simulation of Wind Flow and Heat Transfer in Channels with Ribbed Surface", Eds. Hirata. M. and Kasagi. N. , Transport Phenomena in Turbulent Flows Theory, Experimental and Numerical Simulation, 605-618.

88. FORSYTH G. E. and WASOW.W. , (1967), "Finite Difference Methods for PDE's", John Wiley and Sons Inc. , New York, NY.

89. FRANK. W. , (1988), "Experimental and Numerical Studies of Propagation Phenomena in Turbulent Flows Around Buildings. ", Eds. Hirata. M. and Kasagi. N. , Transport Phenomena in Turbulent Flows Theory, Experimental and Numerical Simulation, 630-640.

90. FU. S. , LAUNDER. B. E. and LESCHZINER. M. A. , (1987), "Modelling Strongly Swirling Recirculating Jet Flow with Reynolds Stress Transport Closures", Special Course on Modern, Theoretical and Experimental Approaches in Turbulence Flow Structure and its Modelling, Belgium, AGARD 755, 17-6-1 - 17-6-6.

91. GALPIN. P. F. and RAITHBY. G. D. , (1986. a), "Treatment of Non-Linearities in the Numerical Solution of the Incompressible Navier-Stokes Equations", Int. J. Num. Meth. Fluids, 6, 409-426.

92. GALPIN. P. F. and RAITHBY. G. D. , (1986. b), "Numerical Solution of Problems in Incompressible Fluid Flow: Treatment of the Temperarure-Velocity Coupling", Numerical Heat Transfer, 10, 105-129.

93. GALPIN. P. F. , VAN DOORMAAL. J. P. and RAITHBY. G. D. , (1985), "Solution of the Incompressible Mass and Momentum Equations by Application of a Coupled Equation Line Solver", Int. J. Num. Meth. Fluids, 5, 615-625.

94. GANDEMER. J. , (1975), "Wind Environment around Buildings: Aerodynamic Concepts", Proceedings of the 4th Int. Conf. on Wind Engng. , Heathrow, London, 423-432.

95. GENTZSCH. W. , (1987), "Vectorialization of Computer Programs Applied to CFD", Notes on Numerical Mechanics, 8, Fredr, Viewg and Sohn, Brawschweigh.

96. GIBSON. M. M. , (1978), "An Algebraic Stress and Heat-Flux Model for Turbulent Shear Flow with Streamline Curvature", Int. J. Heat Mass Transfer, 21, 1609-1617.

97. GOLDBERG. U. C. and CHAKRAVARTHY. S. R. , (1987), "Prediction of separated Flows with a New Turbulence Model", Eds. Habashi. W. G. et. al. , Proceedings of the 5th Int. Conf. on Laminar and Turbulent Flows, Montreal, Canada, part 1, 561-571.

98. GOLDBERG. U. C. , (1986), "Separated Flow Treatment with a New Turbulence Model", AIAA Journal, 24, 10, 1711-1713.

99. GORSKI. J. J. , (1986), "A New Near-Wall Formulation for the $k-\varepsilon$ Equations of Turbulence", AIAA Paper No. 86-0556.

100. GOSMAN. A. D. and LAI. K. Y. M. , (1982), "Finite-Difference and Other Approximations for the Transport and Navier Stokes Equations", Proceedings of IAHR Symposium on Refined Modelling of Flows, Paris.

101. GOSMAN.A.D. et al. (1980), " The Flow Properties of Rooms with Small Ventilated Openings", Transactions of ASME, J. Fluids Engng., 102, 316 - 323.

102. GOSMAN. A. D. and PUN. W. M. , (1974), "KASE Problems for the TEACH Computer Programs", Report No. HTS/74/3, Department of Mech. Engng. , Imperial College of Science and Tech. , London, England.

103. GOSMAN. A. D. and IDERIAH. F. J. K. , (1969), "Heat and Mass Transfer in Recirculating Flows", Academic Press, New York.

104. GUSTAFSON. K. , (1987), "Vortex Separation and Fine Structure Dynamics", J. Appl. Num. Math. , 3, 167-182.

105. HABASHI.W.G, (1988), The Finite Difference Methods in Fluid Mechanics, Student Hand Book, Department of Mechanical Engng, Concordia University, Montreal, Canada.

106. HABASHI. W. G. and PEETERS. M. F. , (1987), "Finite Element Solution of the Compressible NSE", AIAA Journal, 25, 7, 944-948.

107. HAGGKVIST. K. , SVENSSON. U. and TAESLER. R. , (1989), "Numerical Simulation of Pressure Fields Around Buildings", J. Bldg. Envir. , 24, 1, 65-72.

108. HAGGKVIST. K. and TAESLER. R. , (1987), "Distribution of Wind Pressure around Freestanding Private dwelling Houses", Report 2945, National Swedish Institute for Bldg. Res. , Sweden.

109. HAGGVIST. K. , ANDERSON. C. and TAESLER. R. , (1986), "PHOENICS - Application in Building Climatology", Numerical Simulation of Fluid Flow and Heat/Mass Transfer Process, Lecture Notes in Engineering, 18, Spring-Verlag.

110. HANJALIC. K. and LAUNDER. B. E. , (1980), "Sensitizing the Dissipation Equation to Irrotational Strains", Transactions of ASME, J. Fluids Engng. , 102, 34-40.

111. HANJALIC. K. and LAUNDER. B. E. , (1979), "Preferential Spectral Transport by Irrotational Straining", ASME, Turbulent Boundary Layer, 101-109.

112. HANSEN. R. J. , HANDLER. R. A. and LEIGHTON. R. I. , (1987)", Prediction of Turbulence-Induced Forces on Structures from Full Numerical Solutions of the Navier-Stokes Equations", J. Fluids and Structures, 1, 431-443.

113. HANSON. T. , SUMMERS. D. M. and WILSON. C. B. , (1986), "A Three-Dimensional Simulation of Wind Flow around Buildings", Int. J. Num. Meth. Fluids, 6, 113-127.

114. HANSON. T. , SUMMERS. D. M. and WILSON. C. B. , (1984), "Numerical Modelling of Wind Flow over Buildings in Two Dimensions", Int. J. Num. Meth. Fluids, 4, 25-41.

115. HANSON. T. , SMITH. F. , SUMMERS. D. and WILSON. C. B. , (1982), "Computer Simulation of Wind Flow around Buildings", CAD, 14, 27-31.

116. HARLOW. F. H. and WELCH. J. E. , (1965), "Numerical Calculation of Time-Dependent Viscous Incompressible Flow of Fluid with Free Surface", The Physics of Fluids, 8, 12, 2182-2187.

117. HERRERO. J. , GRAU. F. X. , GRIFOLL. J. and GIRALT. F. , (1989), "A Near-Wall $k-\varepsilon$ Model for the Numerical Simulation of Heat Transfer at High Prandtl Numbers", Proceedings of the 12th CANCAM Conference, Ottawa, Ontario, Canada.

118. HERRON. D. , WALTON. G. and LAURIE. L. , (1981), "BLAST Program User's Manual, Version 3.0, U.S. Army Construction Engineering Research Laboratory, Champaign, Illinois, U.S.A.

119. HINZE. O. , (1975), "Turbulence", Mc - Graw Hill, New York, N.Y.

120. HIRT. C. W. , RAMSHAW. J. D. and STEIN. L. R. , (1978), "Numerical Simulation of Three-Dimensional Flow Past Bluff Bodies", Computer Meth. App. Mech. & Engng. , 14, 93-124.

121. HIRT. C. W. , NICHOLS. B. D. and ROMERO. N. C. , (1976), "SOLA -A Numerical Solution Algorithm for Transient Fluid Flows", Report No. LA-5852, Los Alamos Scientific Laboratory, Los Alamos, New Mexico.

122. HIRT. C. W. and COOK. J. L. , (1972), "Calculating Three-Dimensional Flows around Structures and over Rough Terrain", J. Comp. Phys. , 10, 324-340.

123. HIRT. C. W. , (1969), "Computer Studies of Time-Dependent Turbulent Flows", High-Speed Computing in Fluid Dynamics, The Physics of Fluids Supplement II, 219 - 227.

124. HITTLE. D. C. , (1977), "BLAST, the Building Load Analysis and System Thermodynamics Program, 1, User Manual, U.S. Army Construction Engineering Research Laboratory, Champaign, Duinois.

125. HOFFMAN. G. H. , (1975), "Improved Form of the Low Reynolds Number $k-\varepsilon$ Turbulence Model", The Physics of Fluids, 18, 3, 309-312.

126. HUNT. A. , (1982), "Wind-Tunnel Measurements of Surface Pressures on Cubic Building Models at Several Scales", J. Wind Engng. Ind. Aerodyn. , 10, 137-163.

127. HUNT. J. C. R. , LALAS. D. P. and ASIMAKOPOULOS. D. N. , (1984), "Air Flow and Dispersion in Rough Terrain: A Report on Euromech 173", J. Fluid Mech. , 142, 201-216.

128. HUNT. J. C. R. , (1988), "Studying Turbulence Using Direct Numerical Simulation: 1987 Center for Turbulence, NASA Ames/Stanford Summer Programme", J. Fluid Mech. , 190, 375-392.

129. HUNT. J. C. R. , (1970), "Further Aspects of the Theory of Wakes behind Buildings and a Comparison of the Theory with Experimental Results", C.E.G.B. Lab. Note, RD/L/R1665, Central Electricity Research Laboratories, Leatherhead.

130. HUNT. J. C. R. and SMITH. G. P. , (1969), "A Theory of Wakes behind Buildings and some Provisional Experimental Results", C.E.G.B. Lab. Note, RD/L/N3169, Central Electricity Research Laboratories, Leatherhead.

131. HUTCHINSON. B. R. and RAITHBY. G. D. , (1986), "A Multigrid Method Based on the Additive Correction Strategy", Numerical Heat Transfer, 9, 511-537.

132. INAMERRO. T. and SAITO. T. (1985), " A Numerical Analysis of Unsteady Separated Flow by Discrete Vortex Method", Proceedings of 5th U.S. National Conference on Wind Engineering, Lubbock, Texas, U.S.A, 5.B-17 - 5.B.24.

133. ISHIZAKI. H. and SUNG. I. W. , (1971), "Influence of Adjacent Buildings to Wind", Proceedings of the 3rd Int. Conf. on Wind Engng. , Tokyo, Japan, I.15-1-I.15-8.

134. ISSA. R. I. , (1986.a), "Solution of the Implicitly Discretised Fluid Flow Equations by Operator-Splitting", J. Comp. Phys. , 62, 40-64.

135. ISSA. R. I. , (1986.b), "The Computation of Compressible and Incompressible Recirculating Flows by a Non-iterative Implicit Scheme", J. Comp. Phys. , 62, 66-82.

136. ISSA. R. I. , (1983), "Numerical Methods for Two- and Three-Dimensional Recirculating Flows", Eds. Visser, Computational Methods for Turbulent and Viscous Flows, 183-211.

137. ISYUMOV. N. , (1978), "Studies of the Pedestrian Level and Environment at the Boundary Layer and Tunnel Laboratory of the University of Western Ontario", J. Ind. Aerodyn. , 3, 187-200.

138. JANG. D. S. , JETLI. R. and ACHARAYA. S. , (1986), "Comparison of the PISO, SIMPLER, and SIMPLEC Algorithms for the Treatment of the Pressure - Velocity Coupling in Steady Flow Problems", Numerical Heat Transfer, 10, 209-228.

139. JANSSON. B. O. , (1987), "Tryckberakning Kring Smaklossar", Report No. Ser. Anr. 149, Water Resources Engineering, Lulea, Sweden.

140. JONES. W. P. and LAUNDER. B. E. , (1972), "The Prediction of Laminarization with a Two-Equation Model of Turbulence", Int. J. Heat Mass Transfer, 15, 301-314.

141. JOUBERT. P. N. , STEVENS. L. K. , GOOD. M. C. , HOFMANN. E. R. and PERRY. A. E. , (1967), "The Drag of Bluff Bodies Immersed in a Turbulent Boundary Layer", Proceedings of Int. Research Seminar, Wind Effects on Buildings, Ottawa, Canada, 1, 297-330.

142. KAMEI. I. and MARUTA. E. , (1979), "Study on Wind Environmental Problems Caused around Buildings in Japan", J. Ind. Aerodyn. , 1, 201-212.

143. KANNAN. A. E. and POWELL. G. M. , (1973), "DRAIN-2D, A General Purpose Computer Program for Dynamic Analysis of Inelastic Plane Structures, Report EERC 73-6, Earthquake Engineering Research Center, University of California, Berkaley, CA, U.S.A.

144. KELNHOFER. Wm. J. , (1971), "Influence of a Neighboring Building on Flat Roof Wind Loading", Proceedings of the 3rd Int. Conf. on Wind Engng. , Tokyo, Japan, II.5-1-II.5-10.

145. KIYA. M. and ARIE. M. , (1972), "A Free Streamline Theory for Bluff Bodies Attached to a Plane Wall", J. Fluid Mech. , 56, 2, 201-219.

146. KOGAN. M. S. and RAWSON. F. L. , (1988), "The Design of Operation System/2", IBM Systems Journal, 27, 2, 90-104.

147. KOT. S. C. and YEUNG. P. K. , (1988), "Computation of Turbulent Flow Normal to Two Rows of Buildings", Proceedings of the 3rd Int. Conf. on High Rise Structure, Beijing, China, 247-251.

148. KUTLER. P. , (1985), "A Perspective of Theoretical and Applied Computational Fluid Dynamics", AIAA Journal, 23, 3, 328-343.

149. LAM. C. K. G. and BREMHORST. K. , (1981), "A Modified Form of the k- ε Model for Predicting Wall Turbulence", Transactions of ASME, J. Fluids Engng. , 103, 456-460.

150. LAUNDER.B.E and SHIMA.N., (1989), "Second-Moment Closure for the Near-Wall Sublayer: Development and Application", AIAA Journal, 27, 10, 1319 - 1325.

151. LAUNDER. B. E. and SPALDING. D. B. , (1974), "The Numerical Computation of Turbulent Flows", Computer Methods in App. Mech. and Engng. , 3, 269-289.

152. LAUNDER. B. E. and SPALDING. D. B. , (1972), "Lectures in Mathematical Model of Turbulence", Academic Press, London.

153. LAURENCE. D. , (1987), "Turbulence Modelling through One Point Closures - Applications- Enlighting by Large Eddy Simulation", Special Course on Modern, Theoretical and Experimental Approaches to Turbulence Flow Structure and its Modelling, Belgium, AGARD 755, 2-1 - 2-22.

154. LAWSON. T. V. , (1980), "Wind Effects on Buildings", 1, Applied Science Publishers, London.

155. LEE. B. K. , CHO. N. H. and CHOI. Y. D. , (1988), "Analysis of Periodically Fully Developed Turbulent Flow and Heat Transfer by $k-\varepsilon$ Equation Model in Artificially Roughened Annulus", Int. J. Heat Mass Transfer, 31, 9, 1797-1806.

156. LEE. B. K. et. al. , (1980), "Predicting Natural Ventilation Forces upon Low Rise Buildings", J. ASHRAE, 35-39.

157. LEMBERG. R. , (1973), "On the Wakes behind Bluff Bodies in a Turbulent Boundary Layer", Ph.D. Thesis, University of Western Ontario, Canada.

158. LEONARD. A. , (1980), "A Review - Vortex Methods for Flow Simulation", J. Comp. Phys. , 37, 289-335.

159. LEONARD. B. P. , (1979), "A Stable and Accurate Convective Modelling Procedure Based on Quadratic Upstream Interpolation", Computer Meth. Appl. Mech. and Engng. , 19, 59-98.

160. LESZCHZINER. M. A. and RODI. W. , (1981), "Calculation of Annular and Twin Parallel Jets Using Various Discretization Schemes and Turbulence-Model Variations", Transactions of ASME, J. Fluids Engng. , 103, 352-360.

161. LESCHZINER. M. A. , (1980), "Practical Evaluation of Three Finite Differences Schemes for the Computation of Steady-State Recirculating Flows", Computer Meth. Appl. Mech. and Engng. , 23, 293 - 312.

162. LIAKAPOULOS. A. , (1985), "Computation of High-Speed Turbulent Boundary-Layer Flows Using the $k-\varepsilon$ Turbulence Model", Int. J. Numer. Meth. Fluids, 5, 81-97.

163. LILLEY. D. G. and RHODE. D. L. , (1982), "A Computer Code for Swirling Turbulent Axisymmetric Recirculating Flows in Practical Isothermal Combustor Geometries", Report 3442, NASA, Scientific and Technical Information Branch, U.S.A.

164. LOMAS . C. G, (1986), " Fundamentals of Hot Wire Anemometry ", Cambridge University Press, Cambridge, London.

165. LOVGREN. R. , (1986), "Numerical 2D Air Flow Simulation over a Backward-Facing Step and a Block", Numerical Simulation of Fluid Flow and Heat/Mass Transfer Processes, Lecture Notes in Engineering, 18, Spring-Verlag.

166. MAJUMDAR. S. and RODI. W. , (1989), "Three-Dimensional Computation of Flow past Cylinder Structures and Model Cooling Towers", J. Bldg. Envir. , 24, 1, 1-22.

167. MANSOUR. N. M. , KIM. J. and MOIN. P. , (1989), "Near-Wall $k-\varepsilon$ Turbulence Modelling", AIAA Journal, 27, 8, 1068-1073.

168. MANSOUR. N. M. , KIM. J. and MOIN. P. , (1987), "Near-Wall $k-\varepsilon$ Turbulence Modelling", Special Course on Modern, Theoretical and Experimental Approaches in Turbulence Flow Structure and its Modelling, Belgium, AGARD 755, 17-4-1 - 17-4-5.

169. MANSON. P.J. and SYKES .R.I., (1979)," Three-Dimensional Numerical Investigation of the Navier-Stokes Equations for Flow Over Surface Mounted Obstacles", J. Fluid Engng, 91, 3, 433 - 450.

170. MARKATOS. N. C. , (1986), "The Mathematical Modelling of Turbulent Flows", J. Appl. Math. Modelling, 10, 190-217.

171. MARKATOS. N. C. and SHAH. P. , (1985), "Turbulence Modelling in Internal Combustion Engines", Proceedings of the Int. Conf. Numerical Methods in Laminar and Turbulent Flow, Swansea.

172. MATHEWS. E. H. CROSBY. C. P. , VISSER. J. A. and MEYER. J. P. , (1988), "Numerical Prediction of Wind loads on Buildings", J. Wind Engng Ind. Aerodyn. , 31, 241-250.

173. MATHEWS. E. H. , (1987.a), "Prediction of the Wind Generated Pressure Distribution on Buildings", J. Wind Engng Ind. Aerodyn. , 25, 2, 219-221.

174. MATHEWS. E. H. and MEYER. J. P. , (1987.b), "Computation of the Wind Loads on a Semicircular Greenhouse", Proceedings of the 7th Int. Conf. on Wind Engng , Aachen, Germany.

175. MATHEWS. E. H. and MEYER. J. P. , (1987.c), "Numerical Modelling of Wind Loading on a Film Clad Greenhouse", J. Bldg Envir. , 22, 2, 129-134.

176. MATHEWS. E. H. , (1985), "The Prediction of Natural Ventilation in Buildings", D.Eng. Dissertation, University of Potchefstroom, RSA.

177. MELBOURNE. W. H. , and JOUBERT. P. N. , (1971), "Problems of Wind Flow at the Base of Tall Buildings", Wind Effects on Buildings and Structures, Proceedings of the 3rd Int. Conf. on Wind Effects on Buildings, Tokyo, Japan, I.11-1 - I.11-10.

178. MOIN. P. and KIM. J. , (1982), "Numerical Investigation of Turbulent Channel Flow", J. Fluid Mech. , 118, 342-377.

179. MURAKAMI. S. and MOCHIDA. A. , (1989.a), "Three-Dimensional Numerical Simulation of Turbulent Flow Around Buildings Using $k-\varepsilon$ Turbulence Model", J. Bldg. Envir. , 24, 1, 51-64.

180. MURAKAMI. S. , (1989.b), "Current Status of Computation Wind Engineering", Proceedings of the 6th U.S. National Wind Engng. Conf. , Houston, Texas, U.S.A.

181. MURAKAMI. S. and MOCHIDA. A. , (1988), "3-D Numerical Simulation of Air Flow around a Cubic Model by Means of the $k-\varepsilon$ Model", J. Wind Engng. Ind. Aerodyn. , 31, 283-303.

182. MURAKAMI. S. MOCHIDA. A. and HIBI. K. , (1987.a), "Numerical Prediction of Velocity and Pressure Field around Building Models", Proceedings of the 7th Int. Conf. on Wind Engng , Aachen, Germany, 31-39.

183. MURAKAMI. S. , MOCHIDA. A. and HIBI. K. , (1987.b), "Three Dimensional Numerical Simulation of Air Flow around a Cubic Model by Means of Large Eddy Simulation", J. Wind Engng. Ind. Aerodyn. , 25, 291-305.

184. MURAKAMI. S. , UEHARA. K. and KOMINE. H. , (1979), "Amplification of Wind Speed at Ground Level due to Construction of High-Rise Building in Urban Area", J. Ind. Aerodyn. , 4, 343-370.

185. NAGIB. H. M. and CORKE. T. C. , (1984), "Wind Microclimate around Buildings: Characteristics and Control", J. Wind Engng. Ind. Aerodyn. , 16, 1-15.

186. NG. K. H. and SPALDING. D. B. ,(1972), "Turbulence Model for Boundary Layers Near Walls", The Physics of Fluids, 15, 1, 20-30.

187. NOYE. J. , (1976), "Numerical Simulation of Fluid Motion ", Proceedings of the 1st Int. Conf. on the Numerical Simulation of Fluid Dynamic Systems, Monash University, Melbourne, Australia.

188. OBI. S., PERIC. M. and SCHEUERER. G. , (1988), "Finite Volume Calculations of a High Reynolds Number Backward Facing Step Flow Employing a Colocated Variable Arrangement", Eds. Hirata. M. and Kasagi. N. , Transport Phenomena in Turbulent Flows Theory, Experimental and Numerical Simulation, 620-636.

189. OLOVSSON. S. , LOFDAHL. L. and CLSSON. E. , (1986), "Flow Calculation in a Turbine Cascade using PHOENICS-BFC", Numerical Simulation of Fluid Flow and Heat/Mass Transfer Processes, Lecture Notes in Engineering, 18, Spring-Verlag.

190. PANNEER SELVAM. R. , (1989), "Computer Simulation of Wind Load on a House", Proceedings of the 6th U.S. National Wind Engng. Conf. , Houston, Texas, U.S.A , A-7-21 - A-7-28.

191. PARSHIONIKAR. W. , (1983), "Experiments on Wind Environment Around Isolated Tall Buildings", M.Eng. (Building), Thesis, Concordia University, Montreal, Canada.

192. PARK. S. W. and CHUNG. M. K. , (1989), "Curvature-Dependent Two-Equation Model for Prediction of Turbulent Recirculating Flows", AIAA Journal, 27, 3, 340-344.

193. PATANKAR. S. V. , (1980), "Numerical Heat Transfer and Fluid Flow", Mc - Graw Hill, London.

194. PATANKAR. S. V. and SPALDING. D. B. , (1972), "A Calculation procedure for Heat, Mass and Momentum Transfer in Three-Dimensional Parabolic Flows", Int. J. Heat Mass Transfer, 15, 1787-1806.

195. PATEL. M. K. , (1982), "On the False Diffusion Problem in the Numerical Modelling of Convection-Diffusion Processes", Ph.D. Thesis, Thames Polytechnic, London.

196. PATEL. V. C. , RODI. W. and SCHEUERER. G. , (1985), "Turbulence Models for Near-Wall and Low Reynolds Number Flows: A Review", AIAA Journal, 23, 9, 1308-1319.

197. PATERSON. D. A. and APELT. C. J. , (1989), "Simulation of Wind Flow Around Three-Dimensional Buildings", J. Bldg. Envir. , 24, 1, 39-50.

198. PATERSON. D. A. and APELT. C. J. , (1988), "Wind Flows around Three-Dimensional Buildings", Eds. Davis. V. G. et. al, Computational Fluid Dynamics, 589-590.

199. PATERSON. D. A. and , APELT. C. J. , (1986.a), "Computation of Wind Flows over Three-Dimensional Buildings", J. Wind Engng. Ind. Aerodyn. , 24, 193-213.

200. PATERSON. D. A. , (1986.b), "Computation of Wind Flows over Three-Dimensional Buildings", Ph.D. Thesis, Department of Civil Engineering, University of Queensland, Australia.

201. PEACEMAN. D. W. and RACHFORD. H. H. , (1955), "The Numerical Solution of Parabolic and Elliptic Differential Equations", Soc. Indust. Appl. Math. , 3, 1, 28-41.

202. PEARSON. R. A. , (1976), "Comparison between Methods - A Review", Ed. John Noye, Numerical Simulation of Fluid Motion, 261-284.

203. PEETERS. M. F. , HABASHI. W. G. and DUECK. E. G. , (1987), "Finite Element Stream Function - Vorticity Solutions of the Incompressible Navier-Stokes Equations", Int. J. Numer. Meth. Fluids, 7, 17-27.

204. PENWARDEN. A. P. and WISE. A. F. W. , (1973), "Wind Environment Around Buildings", BRE Report, HMSO, U.K.

205. PETERKA. J. A. , MERONEY. R. N. and KOTHARI. K. M. , (1985), "Wind Flow Patterns About Buildings", J. Wind Engng. Ind. Aerodyn. , 21, 21-38.

206. PETERKA. J. A. and CERMAK. J. E. , (1976), "Adverse Wind Loading Induced by Adjacent Buildings", ASCE , J. Structural Division, 102,, 533-548.

207. PLETCHER. R. H. and PATANKAR. S. V. , (1983), "Computer in Analysis and Design", Heat Transfer, 105, 73-79.

208. POPE. S. B. and WHITELAW. J. H. , (1976), "The Calculation of the Near-Wake Flows", J. Fluid Mech. , 73, 1, 9-32.

209. PRANDTL. L (1925), " Report on investigation into Developed Turbulence", Zeitschrift fur Angewandten Mathematic und Mechanik, 5, 2, 136- 139, also translated by D.B. SPALDING from German, Imperial College, Heat Transfer Section, Report HTS/TN/80/1.

210. RAITHBY. G. D. , GALPIN. P. F. and VAN DOORMAAL. J. P. , (1986), "Prediction of Heat and Fluid Flow in Complex Geometries Using General Orthogonal Coordinates", Numerical Heat Transfer, 9, 125-142.

211. RAITHBY. G. D. , (1976.a), "A Critical Evaluation of Upstream Differencing Applied to Problems Involving Fluid Flow", Comp. Meth. Appl. Mech. Engng. , 9, 75-103.

212. RAITHBY. G. D. , (1976.b), "Skew Upstream Differencing Schemes for Problems Involving Fluid Flow", Comp. Meth. Appl. Mech. Engng. , 9, 153-164.

213. RICHARDS. P. J. , (1989), "Computational Modelling of Wind Flow around Low-Rise Buildings Using PHOENICS", Report No. DN1508, AFRC Institute of Engineering Research, Wrest-Park, Silsoe, Bedford, U.K.

214. ROACH. P. , (1979), "Computational Fluid Dynamics", Academic Press, London.

215. RODI. W. and SCHEUERER. G. , (1986), "Scrutinizing the $k-\varepsilon$ Turbulence Model Under Adverse Pressure Gradient Conditions", Transactions of ASME, J. Fluids Engng. , 108, 174-179.

216. RODI. W. , (1984), "Turbulence Models and their Applications in Hydraulics - A State of Art Review", Int. Association for Hydraulic Research, Delft, Netherlands.

217. RODI. W. , (1982), "Examples of Turbulence Models for Incompressible Flows", AIAA Journal, 20, 7, 872-879.

218. RODI. W. , (1975), "A Note on the Empirical Constant in the Kolmogorov-Prandtl Eddy-Viscosity Expression", Transactions of ASME, J. Fluids Engng. , 386-389.

219. RODI. W. and SPALDING. D. B. , (1970), "A Two-Parameter Model of Turbulence, and Its Application to Free Jets", Warme-Und Stoffubertragung Bd. , 3 S. 85-95.

220. ROSTEN. H. I. and SPALDING. D. B. , (1986), "PHOENICS 84 and Beyond", Flow and Heat/Mass Transfer Processes, Lecture Notes in Engineering, 18, Spring-Verlag.

221. SCHLICHTING . H., (1968), " Boundary Layer Theory ", Mc - Graw Hill, London.

222. SHIEH. C. F. and FROST. W. , (1979), "Application of a Numerical Model to WECS Siting Relative to Two-Dimensional Terrain Features", J. Wind Engng. Ind. Aerodyn. , 2, 1163-1171.

223. SILL. B. L. , (1988), "Turbulent Boundary Layer Profiles over Uniform Rough Surfaces", J. Wind Engng. Ind. Aerodyn. , 31, 147-163.

224. SIMIU. E. and SCANLAN. R. H. , (1978), "Wind Effects on Structures", John Willey & Sons, New York.

225. SIMPSON. R. L. , (1989), "Turbulent Boundary-Layer Separation", Ann. Rev. Fluid Mech. , 21, 205-234.

226. SINGHAL. A. K. , (1986), "The Importance of the Problem Formulation Process and an Overview of PHOENICS use in the U.S.A", Numerical Simulation of Fluid Flow and Heat/Mass Transfer Processes, Lecture Notes in Engineering, 18, Spring-Verlag.

227. SMITH. G. D., (1984), " Numerical Solution of Partial Differential Equations ", Oxford University Press, London.

228. SOLCHENBACH. K. and TROTTENBERG. U. , (1987), "On the Multigrid Acceleration Approach in Computational Fluid Dynamics", Lecture Notes on Computer Science, Eds. G. Gass and J. Hartinanis, Parallel Computing in Science and Engineering, 4th Int. DFVLR Seminar on Foundations of Engineering Sciences, Bonn, FRG.

229. SPALDING. D. B. , (1982), "Turbulence Models, A Lecture Course", Report No. CFD/82/4, Computational Fluid Dynamics Unit, Imperial College of Science and Tech. , London, England.

230. SPALDING. D. B. , (1981), "A General Purpose Computer Program for Multi-Dimensional One and Two-phase Flow", Math. and Comp. Simulation, XXIII, 267-276.

231. SPALDING. D. B. , (1972), "A Novel Finite Difference Formulation for Differential Expressions Involving Both First and Second Derivatives", Int. J. Numer. Meth. Engng. , 4, 551-559.

232. SPALDING. D.B., (1967), " Heat Transfer from Turbulent Separated Flows", J. Fluid Mech. , 27, 1, 97 -109.

233. STANSBY. P. K. and WOOTON. L. R. , (1977), "The Value of Wind Research to Civil Engineering", Proceedings of the 4th Int. Conf. on Wind Engng. , Heathrow, London, 669-685.

234. STATHOPOULOS. T. and BASKARAN. A. , (1990), " Computer Simulation of Wind Environmental Conditions around Buildings ", Annual Conference, Canadian Society of Civil Engineering, Hamilton, Canada.

235. STATHOPOULOS. T. and DUMITRESCU-BRULOTTE. M. L. , (1990), "Design Recommendations for Wind Loading on Buildings of Intermediate Height", Can. J. Civ. Engng. , 16, 910 - 916.

236. STATHOPOULOS. T. and BASKARAN. A. , (1989.a), "Numerical Modelling of Wind Effects on Buildings", CMEM-Conference, Capri, Italy.

237. STATHOPOULOS. T. and LUCHIAN. H. D. , (1989.b), "Wind Pressure on Buildings with Multi-Level Roofs", Proceedings of the 6th U.S. National Conference on Wind Engineering, Houston, Texas, U.S.A.

238. STATHOPOULOS. T. , (1985), "Wind Environmental Conditions Around Tall Buildings with Chamfered Corners", J. Wind Engng. Ind. Aerodyn. , 21, 71-87.

239. STATHOPOULOS. T. , (1984. a), "Adverse Wind Loads on Low Buildings due to Buffeting", ASCE, J. Structural Division, 110, 10, 2374-2392.

240. STATHOPOULOS. T. , (1984. b), "Design and Fabrication of a Wind Tunnel for Building Aerodynamics", J. Wind Engng. Ind. Aerodyn. , 16, 361-376.

241. STATHOPOULOS. T. , SURRY. D. and DAVENPORT. A. G. , (1981), "Effective Wind Loads on Flat Roofs", ASCE, J. Structural Division, 107, ST2, 281-297.

242. STEPHANI. L. M. and BUTLER. T. D. , (1975), "A Numerical Method for Studying the Circulation Patterns of a Fluid in a Cavity", LA601A, Los Alamos Scientific Laboratory, Los Alamos, New Mexico.

243. STONE. H. L. , (1968), "Iterating Solution of Implicit Approximations of Multidimensional Partial Differential Equations", SIAM, J. Numer. Anal. , 5, 3, 530-558.

244. SUMMERS. D. M. , HANSON. T. and WILSON. C. B. , (1986), "Validation of a Computer Simulation of Wind Flow over a Building Model", J. Bldg. and Envir. , 21, 2, 97-111.

245. SUMMERS. D. M. , HANSON. T. and WILSON. C. B. , (1985), "A Random Vortex Simulation of Wind-Flow over a Building", Int. J. Numer. Meth. Fluids, 5, 849-871.

246. TAMURA. T. , KUWAHARA. K. and SUZUKI. M. , (1989), "Numerical Study of Wind Pressure on a Damed Roof and Near-Wake", Proceedings of the 6th U.S. National Wind Engng. Conf. , Houston, Texas, U.S.A, A-7-1 - A-7-10.

247. TAMURA. T. , KUWAHARA. K. and SHIRAYAMA. S. , (1987), "Numerical Study of Unsteady Flow Patterns and Pressure Distributions on a Rectangular Cylinder", Proceedings of the 7th Int. Conf. on Wind Engng , Aachen, Germany, 41-50.

248. TAYLOR. C. and HUGHES. T. G. , (1981), "Finite-Element Programs for the NSE", Pinerdge Press Ltd, Swansea, U.K.

249. THOMPSON.J.F. (1986)," Composite Grid Generation Code for General 3D regions- the EAGLE Codes", Journal AIAA, 26, 3, 271-272.

250. THOMPOSON.J.F., (1980)," Numerical Solution of Flow Problems using Body fitted Coordiante System", Eds. Kollmann.W, Computational Fluid Dynamics, Hemisphere, Washington, D.C.

251. TSI Inc., "Application of the Heat Flux System in a Low Temperature Gases and Liquids", Technical Bulletin 4, Thermo-System Inc., 2500 Cleveland Ave., N.St.PAwl, Minnesota, U.S.A

252. USUI. N. , (1986), "Wind Tests a Breeze for Supercomputer", ENR, Nov. issue, 24.

253. VAN DER BERG. B. , (1975), "A Three-Dimensional Law of the Wall for Turbulent Shear Flows", J. Fluid Mech. , 70, 1, 139 -160.

254. VAN DOORMAAL. J. P. , TURAN. A. and RAITHBY. G. D. , (1987), "Evaluation of New Techniques for the Calculation of International Recirculating Flows", AIAA, 25th Aerospace Science Meeting, Reno, Nevada.

255. VAN DOORMAAL. J. P. and RAITHBY. G. D. , (1984), "Enhancements of the SIMPLE Method for Predicting Incompressible Fluid Flows", Numerical Heat Transfer, 7, 147-163.

256. VASILIC-MELLING. D. , (1977), "Three Dimensional Turbulent Flow Past Rectangular Bluff Bodies", Ph.D. Thesis, Imperial College of Science and Tech. , University London, England.

257. VEMURI. V. , (1981), "Digital Computer Treatment on PDE", Prentice Hall, London.

258. WACKER. H.M. , (1987), "Introduction to the Seminar", Lecture Notes on Computer Science, Eds. G. Gass and J. Hartinanis, Parallel Computing in Science and Engineering, 4th Int. DFVLR Seminar on Foundations of Engineering Sciences, Bonn, FRG.

259. WEI. S.S. and GUCERI. S. I. , (1987), "The Numerical Study of Separated Laminar and Turbulent Flows Past Bluff Bodies of Arbitrary Shape", Eds. Habashi. W. G. et. al. , Proceedings of the 5th Int. Conf. on Laminar and Turbulent Flows, Montreal, Canada, Part1, 693-702.

260. WILKES. N. S. et al., (1986), "On The Numerical Solution of 3-D Incompressible Flow Problems", Num. Meth. for Fluid Dyn. II, Eds. Morton. K. and Baines. M. J. , Clarendon Press, Oxford.

261. WILSON. D. J. , (1985), "Numerical Studies of Flow through a Wind Breack", J. Wind Engng Ind. Aerodyn. , 21,119-154.

262. WIREN. B. G., (1975)," A Wind-tunnel Study of Wind Velocities in Passages between and through Buildings", Proceedings of 4th Int. Conf. on Wind Engng. , Heathrow, London, 465 - 475.

263. WOO. H. G. C. , PETERKA. J. A. and CERMAK. J. C. , (1977), "Wind Tunnel Measurements in the Wakes of Structures", Report No. JE40, Department of Civil Engineering, Colorado State University, Colorado, Fort Collins, U.S.A

264. WOOD. P. E. and CHEN. C. P. , (1985), "Turbulence Model Predictions of the Radial Jet - A Comparison of $k-\varepsilon$ Models", The Canadian Journal of Chemical Engineering, 63, 177-181.

265. YEUNG. P. K. and KOT. S. C. , (1985), "Computation of Turbulent Flows Past Arbitrary Two-Dimensional Surfaces Mounted Obstructions", J. Wind Engng. Ind. Aerodyn. , 18, 2, 177-190.

266. YOUNIS. B. A. , (1988), "On Modeling the Vortex Shedding from Bluff Bodies in Laminar and Turbulent Streams", Proceedings of the 7th Int. Conf. on OMAE, Houston, Texas, 223-228.

267. YU. X. and HE. G. , (1985), "An Efficient Method for the Computation of Wind Effects on Tall Buildings", Proceedings of the 3rd Int. Conf. on High Rise Structure, 718-722.

268. YUAN. S. W. , (1967), Foundations of Fluid Mechanics", Prentice Hall, London.

269. ZHU. X. , (1987), "Wind Pressures on Buildings with Appurtenances", M. Engng. (Building), Thesis, Concordia University, Montreal, Canada.

270. ZIENKIEWICZ. O. C. , (1972), "Why Finite Elements", Proceedings the of 3rd Int. Conf. on the Application of Finite Element in Fluid Mechanics.

APPENDIX 1

DERIVATION OF DIFFERENCE EQUATION FROM DIFFERENTIAL EQUATION

This appendix provides the details for the discretization of a differential equation into difference form. The differential equation has been considered with a general variable, ϕ, which may be either velocity (vector) or turbulence property (scalar). Thus the following procedure is equally applicable for the momentum equation (ϕ = u, v and w) as well as for the turbulence models (ϕ = k and ε). During the derivation only essential features are given, however, further details are well documented by Vasilic-Melling (1977) and Patankar (1980).

Let us consider the one dimensional version of Eq. 3.8:

$$U\frac{\partial\phi}{\partial x} = \frac{\partial}{\partial x}\left(\Gamma_{\phi}\frac{\partial\phi}{\partial x}\right) + S \qquad \text{(A.1.1)}$$

where:

U is the velocity vector

ϕ is the dependent variable

Γ_{ϕ} is the diffusion proportionality factor of ϕ and

S is the source term.

A control volume has been employed to derive the discretization equation - see Fig. A.1.1. Consider a grid point P which has the grid point E and W as its neighbors (E denotes East side i.e., positive x - direction while W denotes West or the negative side of the x - direction). The dashed lines shown in the figure are the faces of the control volume. The exact locations are unimportant, however, the interface is assumed midway

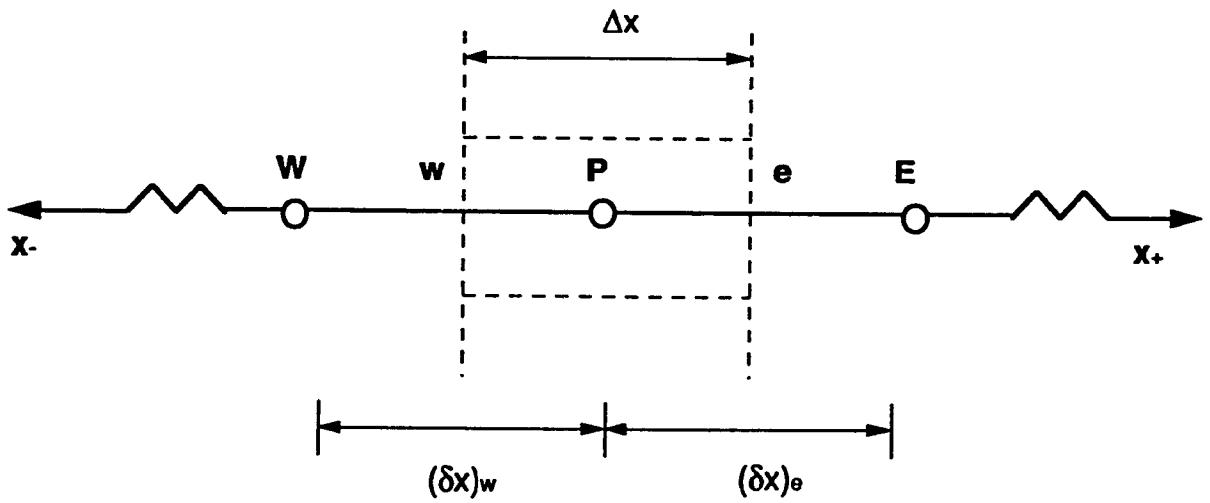

Fig.A.1.1: Typical Grid Point Cluster for a One-Dimensional Problem

between the nodes. Some other interpolation factors would have appeared for the differently located interfaces. For this one - dimensional case, the thickness in y and z direction is unity and the volume is $\Delta x \times 1 \times 1$.

Integrating Eq. A.1.1 over the control volume:

$$(U\phi)_e - (U\phi)_w = \left(\Gamma_\phi \frac{\partial \phi}{\partial x}\right)_e - \left(\Gamma_\phi \frac{\partial \phi}{\partial x}\right)_w + \int_e^w S dx \qquad \text{(A.1.2)}$$

To proceed further, a profile assumption or interpolation formula is needed. Let us consider a piece-wise linear profile as shown in Fig. A.1.2. Here linear interpolation function is used between the grid points. With this in mind the discretization equation can be re-written as follows:

$$(U\phi)_e - (U\phi)_w = \Gamma_e \frac{(\phi_E - \phi_P)}{(\delta x)_e} - \Gamma_w \frac{(\phi_P - \phi_W)}{(\delta x)_w} + \bar{S}\,\Delta x \qquad \text{(A.1.3)}$$

where:

$$(U\phi)_e = U_e \frac{(\phi_E + \phi_P)}{2} \qquad \text{(A.1.4)}$$

$$(U\phi)_w = U_w \frac{(\phi_P + \phi_W)}{2} \qquad \text{(A.1.5)}$$

In Eq A.1.3, $\bar{S}$ is the average value of S over the control volume. To arrange the equation in a more compact form, two new symbols F and D are defined as follows:

$$F = U * \text{Area} \; ; \quad D = (\Gamma / \text{distance}) \text{ Area}$$

$$\text{i.e., } F = U * 1 \; ; \quad D = (\Gamma / \delta x) * 1 \qquad \text{(A.1.6)}$$

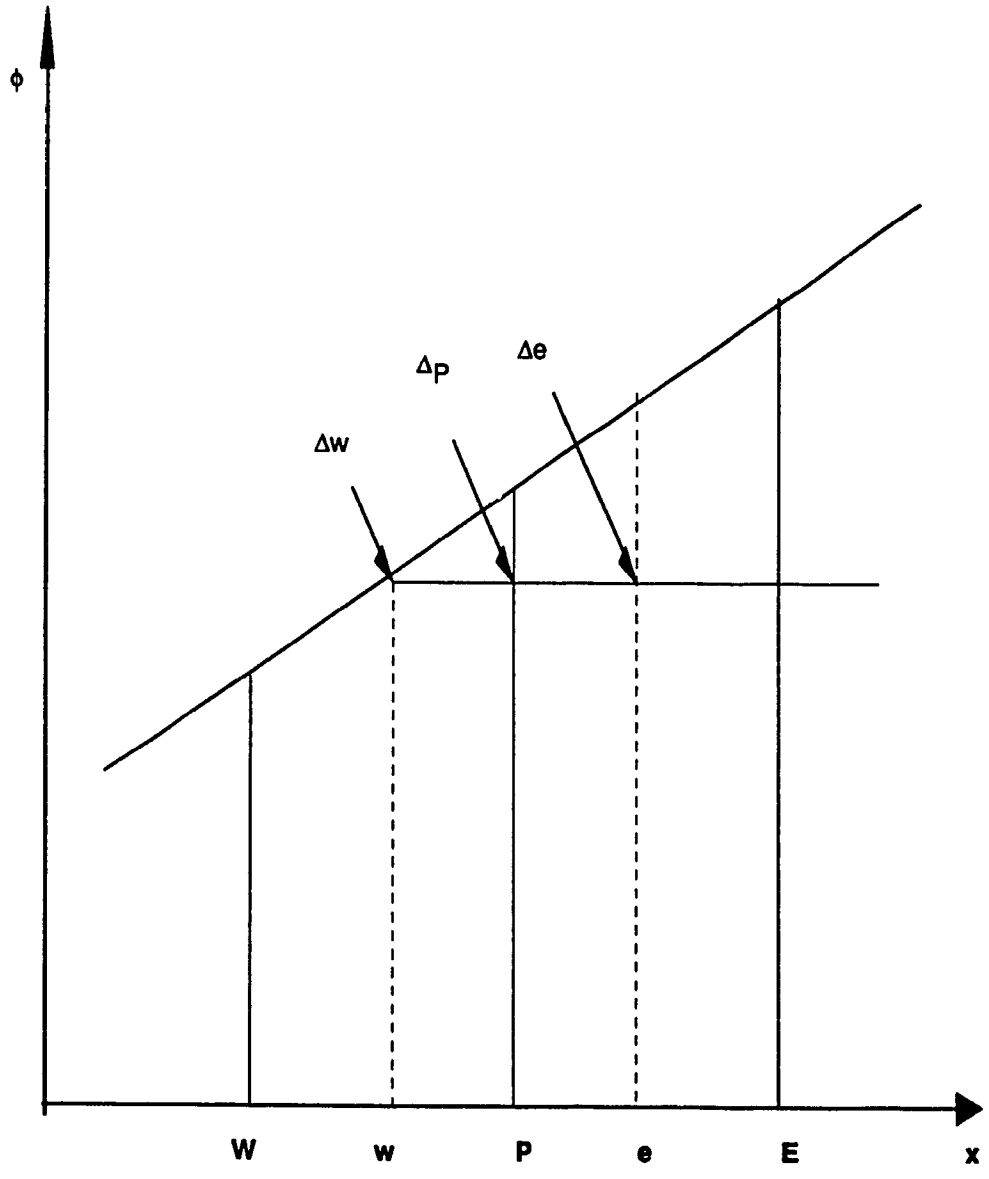

Fig.A.1.2: Piece-Wise Linear Profile for the Variation of the variable

F stands for the strength (Force) of convection of the flow whereas D stands for the Diffusion conductance. It should be noted that D always remains positive, but F can take either positive or negative values depending on the direction of the flow. With the new symbols the discretization equation becomes:

$$\frac{F_e}{2}(\phi_E + \phi_P) - \frac{F_w}{2}(\phi_P + \phi_W) = D_e(\phi_E - \phi_P) - D_w(\phi_P - \phi_W) + \bar{S}\Delta x \qquad \text{(A.1.7)}$$

Rearranging and using the continuity condition ($F_e = F_w$) yields:

$$a_P\phi_P = a_E\phi_E + a_W\phi_W + \bar{S}\Delta x \qquad \text{(A.1.8)}$$

where:

$$a_E = D_e - \frac{F_e}{2}$$
$$a_W = D_w + \frac{F_w}{2}$$
$$a_P = a_E + a_W \qquad \text{(A.1.9)}$$

Often the source term is a function of the dependent variable ϕ itself and it is then desirable to construct the discretized equations by assuming that

$$\bar{S} = S_1 + S_2\phi \qquad \text{(A.1.10)}$$

where S_1 stands for the constant part of S while S_2 is the coefficient of ϕ_P.

Using Eq. A.1.10 in Eq. A.1.8 and rearranging:

$$a_P\phi_P = a_E\phi_E + a_W\phi_W + S_L \qquad \text{(A.1.11)}$$

where:

$$a_P = a_W + a_E - S_2\Delta x$$
$$a_E = D_e - \frac{F_e}{2}$$
$$a_W = D_w + \frac{F_w}{2}$$
$$S_L = S_1\Delta x \qquad \text{(A.1.12)}$$

The discretization equations represent the implication of the piece-wise profile for ϕ. This form is also known as the Central Difference Scheme (CDS) due to the fact that P is assumed as the centre node for the determination of the ϕ value. If another scheme is used - say Upwind Difference Scheme (UDS) or Hybrid Difference Scheme (HDS), then the above discretization equations need more treatment. An excellent review of the various schemes are given in Raithby (1976.a) and Patel, (1982). The essence of UDS is given as follows "The value of ϕ at an interface is equal to the value of ϕ at the grid point on upwind side of the face." Thus

$$\phi_e = \phi_P \quad \text{if} \quad F_e > 0$$
$$\phi_e = \phi_E \quad \text{if} \quad F_e < 0 \qquad \text{(A.1.13)}$$

The value of ϕ_w can be defined similarly. Based on these considerations the parameters of Eq. A.1.11 are defined as:

$$a_P = a_E + a_W - S_2\Delta x$$
$$a_E = D_e + [[-F_e, 0]]$$
$$a_W = D_w + [[\ F_w, 0]]$$
$$S_L = S_1\Delta x \qquad \text{(A.1.14)}$$

(Note: The new operator [[A, B]] denotes the bigger value of A and B.)

In UDS, always the diffusion value of the node in the forward direction is assigned to P and thus it overestimates the diffusion (ref: Fig A.1.2, $\Delta P = \Delta e$). On the other hand the CDS does the reverse (ref: Fig A.1.2 $\Delta P = \Delta e/2$). So a new scheme by combining

the CDS and UDS, named the Hybrid Difference Scheme (HDS), has been formulated by Spalding (1972). The new equation set which is formed by blending Eqs. A.1.9 and A.1.14 can be written as follows:

$$a_E = \left[\left[-F_e, D_e - \frac{F_e}{2}, 0 \right]\right]$$
$$a_W = \left[\left[F_w, D_w + \frac{F_w}{2}, 0 \right]\right] \qquad \text{(A.1.15)}$$

It should be remembered that this formulation is valid for any arbitrary location of the interfaces between the grid points and it is not limited only for mid-way interfaces. Then the parameters of Eq. A.1.11 become:

$$a_P = a_E + a_W - S_2 \Delta x$$
$$a_E = \text{Max}\left(\tfrac{1}{2}|F_e|, D_e\right) - \frac{F_e}{2}$$
$$a_W = \text{Max}\left(\tfrac{1}{2}|F_w|, D_w\right) + \frac{F_w}{2}$$
$$S_L = S_1 \Delta x$$
$$F_e = U_e * 1$$
$$F_w = U_w * 1$$
$$D_e = \frac{\Gamma_e * 1}{(\delta x)_e}$$
$$D_w = \frac{\Gamma_w * 1}{(\delta x)_w} \qquad \text{(A.1.16)}$$

By following a similar procedure, the 3-D difference equation can be written as follows:

$$a_P \phi_P = a_E \phi_E + a_W \phi_W + a_N \phi_N + a_S \phi_S + a_T \phi_T + a_B \phi_B + S_L \qquad \text{(A.1.17)}$$

where:

$$a_P = a_E + a_W + a_N + a_S + a_T + a_B - S_2 \Delta x \Delta y \Delta z$$

$$a_E = \text{Max}\left(\tfrac{1}{2}|F_e|, D_e\right) - \frac{F_e}{2}$$

$$a_W = \text{Max}\left(\tfrac{1}{2}|F_w|, D_w\right) + \frac{F_w}{2}$$

$$a_N = \text{Max}\left(\tfrac{1}{2}|F_n|, D_n\right) - \frac{F_n}{2}$$

$$a_S = \text{Max}\left(\tfrac{1}{2}|F_s|, D_s\right) + \frac{F_s}{2}$$

$$a_T = \text{Max}\left(\tfrac{1}{2}|F_t|, D_t\right) - \frac{F_t}{2}$$

$$a_B = \text{Max}\left(\tfrac{1}{2}|F_b|, D_b\right) + \frac{F_b}{2}$$

$$F_e = U_e * \Delta y \Delta z$$

$$F_w = U_w * \Delta y \Delta z$$

$$F_n = U_n * \Delta x \Delta z$$

$$F_s = U_s * \Delta x \Delta z$$

$$F_t = U_t * \Delta x \Delta y$$

$$F_b = U_b * \Delta x \Delta y$$

$$D_e = \frac{\Gamma_e * \Delta y \Delta z}{(\delta x)_e}$$

$$D_w = \frac{\Gamma_w * \Delta y \Delta z}{(\delta x)_w}$$

$$D_n = \frac{\Gamma_n * \Delta x \Delta z}{(\delta y)_n}$$

$$D_s = \frac{\Gamma_s * \Delta x \Delta z}{(\delta y)_s}$$

$$D_t = \frac{\Gamma_t * \Delta x \Delta y}{(\delta z)_t}$$

$$D_b = \frac{\Gamma_b * \Delta x \Delta y}{(\delta z)_b}$$

$$S_L = S_1 \Delta x \Delta y \Delta z \qquad \text{(A.1.18)}$$

APPENDIX 2

TRI DIAGONAL MATRIX (TDM) ALGORITHM

The solution of the sets of discretized equations along a particular direction can be obtained using Tri Diagonal Matrix Algorithm which is algebraically equivalent to the Gaussian Elimination method. It requires computer storage and time proportional to number of equations, NE, rather than NE^2 or NE^3 which is needed for other matrix methods (Peacman and Rachford 1955, Spalding 1972 and Patankar 1980). However, the diagonal element has to be the dominant element of the matrix and equations which are arranged in a suitable form can only be solved. This counts for the pay-off of this procedure. The details of the derivations are given as follows:

Consider the general discretized equation:

$$a_P \phi_P = a_E \phi_E + a_W \phi_W + a_N \phi_N + a_S \phi_S + a_T \phi_T + a_B \phi_B + S_L \qquad \text{(A.1.17)}$$

When this equation is swept along x direction (East to West) the contributions from other directions are assumed to be known - say a constant "d" . Therefore the above equation becomes:

$$a_P \phi_P = a_E \phi_E + a_W \phi_W + d \qquad \text{(A.2.1)}$$

Letting the grid " P " as 'i', its L.H.S and R.H.S becomes 'i-1' and 'i+1' respectively as shown below:

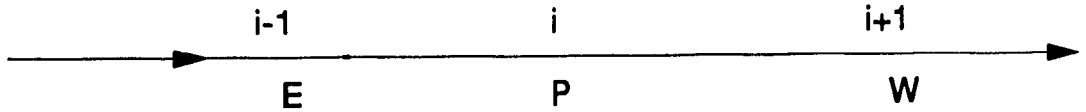

Having that in mind equation A.2.1. can be transformed as

$$a_i \ \phi_i = b_i \ \phi_{i-1} + c_i \ \phi_{i+1} + d_i \qquad \text{(A.2.2)}$$

where:

a_i is the value at P

b_i is the value at E

c_i is the value at W

Moreover, these coefficients are constant for a particular sweep. Moving from the grid point P to W in the forward direction a relation between the value at P to that at W can be written as :

$$\phi_i = k_i \phi_{i+1} + l_i \qquad \text{(A.2.3)}$$

Again k and l's are constants and letting i = i-1 in Eq. A.2.3

$$\phi_{i-1} = k_{i-1} \phi_i + l_{i-1} \qquad \text{(A.2.4)}$$

Using Equation A.2.4 in A.2.2 and rearranging

$$\phi_i \{a_i - b_i k_{i-1}\} = c_i \phi_{i+1} + d_i + b_i l_{i-1}$$

i.e.,

$$\phi_i = \left\{\frac{c_i}{a_i - b_i k_{i-1}}\right\} \phi_{i+1} + \left\{\frac{d_i + b_i l_{i-1}}{a_i - b_i k_{i-1}}\right\} \qquad \text{(A.2.5)}$$

Equation A.2.5 resembles equation A.2.3 where the new k and l's have different values as follows:

$$k_i = \frac{c_i}{a_i - b_i k_{i-1}}$$

$$l_i = \frac{d_i + b_i l_{i-1}}{a_i - b_i k_{i-1}} \qquad \text{(A.2.6)}$$

Equation (A.2.5) is a recurrence relation as it gives the values at 'i' in terms of 'i-1'.

Steps involved in the TDM are grouped as follows:

1) find the value of k_1 and l_1 by using , i = 1 in Eq. A.2.6

2) form the recurrence relations for various k & l's by letting i = 2,3,.... (n-1) and n (where n is the last grid node).

3) refering Eq. A.2.3, for the boundary node i.e., i = n, $k_n = 0$ and hence $l_n = \phi_n$.

4) using the value of ϕ_n in Eq. A.2.3, solve for i = n-1, n-2,....3, 2, 1 which give the values of $\phi_{n-1}, \phi_{n-2} \ldots \phi_1$.

Same procedure can also be followed while moving along y and z directions. However, it is understood that when one moves along y, it is assumed that ($a_E\phi_E + a_W\phi_W + a_T\phi_T + a_B\phi_B + S_L$) is a known constant, whereas for the z direction the term ($a_E\phi_E + a_W\phi_W + a_N\phi_N + a_S\phi_S + S_L$) is assumed to be a known constant.

APPENDIX 3

LIST OF SYMBOLS AND NOTATION

a_p	hybrid difference scheme coefficient at node P
B	building width
Cp	mean pressure coefficient
$C_\mu, C_2, C_1^1, C_1^{11}$	turbulence model constants: 0.09,1.92,2.24,0.8
d_P	distance from node P to the solid boundary
d_e, d_w, d_n, d_s, d_t,d_b	proportionality factors for pressure correction
D	wall dissipation
e, w, n, s	velocity nodes surrounding P
E, W, N, S	scalar locations
E_L	constant used for log-log formula: 9.0
G	turbulence generation term
h	probe height
H	building height
i, j	components in tensor notation
k	turbulence kinetic energy
K_1 ,K_2	constants: 0.27 and -0.47
k_e, k_s	turbulence kinetic energy at the edge and within VSL
k_P	turbulence kinetic energy at node P
l	Prandtl's mixing length scale of turbulence
l_R	recirculation length from leeward side of the building
L	building length
m_ε	modified rate of dissipation term
n	streamline co-ordinate
n_P	number of nodes surrounding P
NE	number of equations

NX, NY, NZ	total nodes on x, y and z directions
p	fluid pressure
p^*	guessed pressure
p'	pressure correction
R_c	radius of curvature of streamline
Re	Reynolds number
Rp	imbalance in the conservation of mass
R_ϕ	residual source
s	streamline co-ordinate
S	source term of the differential equation
S1, S2	constant used for discretation
S_L	linearized source term
S_{ns}	shear strain
t	time
u, v, w	mean velocity components along x, y, z direction
u', v', w'	fluctuating velocity components along x, y, z direction
u_g	velocity at gradient height
u_s	mean velocity along streamline coordinate
U_H	velocity at roof height
U_j	velocity vector
U_P	velocity at node P
U^*	friction velocity
U_S	velocity vector
U_iU_j	Reynolds stress
x,y,z	distance along the co-ordinate axis
Y+	normalized wall distance
z_g	height of the boundary layer
$\propto$	power law exponent
α, β	constants: 1.5 and 0.6
γ_{ij}	rate of production of Reynolds stress

Γ_ϕ	diffusion proportionality factor of ϕ
$\delta x, \delta y, \delta z$	grid distances between nodes
δ_{ij}	Kronecker delta
Δt	time step
$\Delta x, \Delta y, \Delta z$	cell dimensions
ε	dissipation of turbulent kinetic energy
ε_s	dissipation of turbulent kinetic energy within VSL
θ	flow inclination to the x-axis
κ	Von-Karman constant: 0.4
ρ	density of the fluid
ν	kinematic viscosity
ν_e	kinematic viscosity at the edge of VSL
ν_t	turbulent viscosity
σ^2	variance
$\sigma_k, \sigma_\varepsilon$	universal constants: 1.0, 1.3
ω	vorticity fluctuations
ζ	scalar vorticity
ϕ	dependent variable, i.e., u, v, w, k , ε

APPENDIX 4

COMPUTER CODE UTILIZATION

TWIST is developed to compute three - dimensional, turbulent wind effects on buildings. Its present status is more suitable for further research than for commercial design purposes. However, it can be well executed by researchers without prior knowledge of the code. In this appendix instructions are presented to help the usage of TWIST. On screen menus showing the necessary inputs from the user are listed in pages 237 to 239 and the used numerical values are given in Table A.4.1.

The first input needed by TWIST is the building dimensions. It is understood that all the values are given either as full - scale dimensions (m) or as wind - tunnel values (cm). TWIST can read a generated grid arrangement from a file or it can also create its own grid system. For the latter, computational domain values (USD, DSD, DS, DT; ref: Fig. A.4.1) and number of nodes on the building envelope are needed. For an example to get approxmately 50,000 total nodes in the computation, one may use values as 8,4 and 7 for the NH (Number of nodes along the Height), NW (Number of nodes along the Width) and NL (Number of nodes along the Length) respectively. Similary to get about 2,40,000 total nodes, the corresponding values of NH, NW and NL may be 10, 8 and 11 respectively. For the envelope, inputing the same number of nodes as the number of pressure taps on the wind - tunnel model, may be helpful for future possible comparisons.

```
         !! *** WELCOME TO TWIST**** !!

DO YOU WANT SOME HELP WITH THIS PROGRAM
Y

H    =  BUILDING HEIGHT
B/2  =  BUILDING HALF WIDTH
L    =  BUILDING LENGTH

TYPE H,B/2,L

13.75 7.6 15.2

DO YOU WANT TO:

1) USE THE GRID GENERATION ROUTINE
2) READ THE GRID LOCATIONS FROM A FILE
1

USD = DISTANCE FROM BUILDING FRONT TO INLET OF GRID:(3L < USD < 12L)
DSD = DISTANCE FROM BUILDING BACK TO OUTLET OF GRID:(5L < DSD < 15L)
DS  = DISTANCE FROM BUILDING SIDE TO SIDE OF GRID:  (B < DS < 5B)
DT  = DISTANCE FROM BUILDING TOP TO TOP OF GRID:    (H < DT < 7H)

TYPE USD,DSD,DS,DT

100 200 40 90

NH = NUMBER OF GRID NODES ON THE BUILDING IN " z " DIRECTION
NW = NUMBER OF GRID NODES ON THE BUIDING  IN " y " DIRECTION
NL = NUMBER OF GRID NODES ON THE BUILDING IN " x " DIRECTION

TYPE NH,NW,NL
EXAMPLE : TO GET TOTAL NODES AS 54,000  ; USE 8,4,7
          TO GET TOTAL NODES AS 2,40,000; USE 10,8,11

8 4 9

NGF = NUMBER OF GRID NODES IN USD    : NL < NGF < 2NL
NGB = NUMBER OF GRID NODES IN DSD    : NL < NGB < 4NL
NGS = NUMBER OF GRID NODES IN DS     : NW < NGS < 2NW
NGT = NUMBER OF GRID NODES IN DT     : NH < NGT < 2NH

TYPE NGF,NGB,NGS,NGT

8 12 7 8

DGF = DISTANCE FROM BUILDING FRONT TO NEAREST GRID NODE
(L/10NL <DGF< L/2NL)

DGB = DISTANCE FROM BUILDING BACK TO NEAREST GRID NODE
(L/10NL < DGB < L/2NL)

DGS = DISTANCE FROM BUILDING SIDE TO NEAREST GRID NODE

(W/20NW < DGS < B/4NW)

DGT = DISTANCE FROM THE BUILDING TOP TO NEAREST GRID NODE

(H/10NH < DGT < H/2NH)
```

```
TYPE DGF, DGB,DGS,DGT

0.5 1.0 0.5 0.5

DO YOU WANT STORE GRID DETAILS ?
Y

TYPE THE FILE NAME

GRID

DO YOU WANT :

1) CALCULATE THE INITIAL FLOW FIELD
2) READ THE INITIAL FLOW FIELD FROM A FILE

1

POWER LAW VELOCITY PROFILE
ALPHA = POWER LAW EXPONENT,ZREF =  GRADIENT HEIGHT.
UREF  = VELOCITY AT GRADIENT HEIGHT


TYPE ALPHA,ZREF,UREF

0.16 60.0 12.0

DO YOU  TO STORE INITIAL FLOW FIELD
N

MAXIT  = MAXIMUM NUMBER OF ITERATIONS
RESMAX = MAXIMUM NORMALIZED ERROR FOR CONVERGENCE
DIVERG = MINIMUM NORMALIZED ERROR FOR DIVERGENCE

TYPICAL VALUES 200, 0.2, 20.

TYPE MAXIT,RESMAX,DIVERG

200 0.2 20.0

Entre the output file name
The output file is unformatted.  Use "FORMAT" program to get
numerical values.

EXAMPLE

Thanks for Waiting .........

        1   87996.39       42845.70       53371.41       7976.111
35961.00       22113.08
        1   1.000000       0.4869029      0.6065182      1.000000
1.000000       1.000000
        2   79601.56       32392.37       43326.24       7073.164
48730.28       38269.38
        2  0.9046003       0.3681102      0.4923639      0.8867936
1.355087       1.730621
        3   65832.29       23711.75       32646.24       6753.624
26732.04       21349.34
        3  0.7481249       0.2694628      0.3709952      0.8467315
```

```
0.7433621       0.9654620
.............................
.............................
         15  0.1995210       4.5448620E-02  9.3192644E-02  0.3660646
9.3228526E-02  0.1069593
         16   16298.11        3342.137       7289.622       2762.448
 2437.128        1615.002
 .............................
 .............................
         22  0.1856031       3.4403604E-02  5.4187160E-02  0.2335499
6.7771427E-02  7.3033772E-02
         23   16566.51        2915.535       4647.668       1778.448
 2313.398        1584.961
         23  0.1882635       3.3132438E-02  5.2816574E-02  0.2229718
6.4330742E-02  7.1675263E-02
         24   16618.36        2727.798       4725.437       1717.520
 2179.546        1543.186
         24  0.1888528       3.0998977E-02  5.3700346E-02  0.2153330
6.0608599E-02  6.9786087E-02
         25   16502.81        2546.433       4746.468       1653.814
 2047.678        1500.272
         25  0.1875397       2.8937927E-02  5.3939346E-02  0.2073459
5.6941640E-02  6.7845426E-02
         26   16307.31        2407.319       4749.797       1585.560
 1924.954        1465.121
         26  0.1853179       2.7357023E-02  5.3977177E-02  0.1987886
5.3528935E-02  6.6255830E-02
FORTRAN STOP
$ EXIT
  BASS          job terminated at  5-SEP-1990 16:55:28.78

  Accounting information:
  Buffered I/O count:            88      Peak working set size:  2715
  Direct I/O count:             154      Peak page file size:   14920
  Page faults:                 2754      Mounted volumes:           0
  Charged CPU time:     0 00:25:33.78    Elapsed time:     0 00:29:12.79
```

VARIABLE	INPUT VALUES
H, B/2, L	13.75, 7.6, 15.2
USD, DSD, DS, DT	100, 200, 40, 90
NH, NW, NL	8, 4, 9
NGF, NGB, NGS, NGT	8, 12, 7, 8
DGF, DGB, DGS, DGT	0.5, 1.0, 0.5, 0.5
ALPHA, ZREF, UREF	0.16, 60.0, 12.0
MAXIT, RESMAX, DIVERG	200, 0.2, 20

Table. A.4.1: Numerical Values for the Sample Input

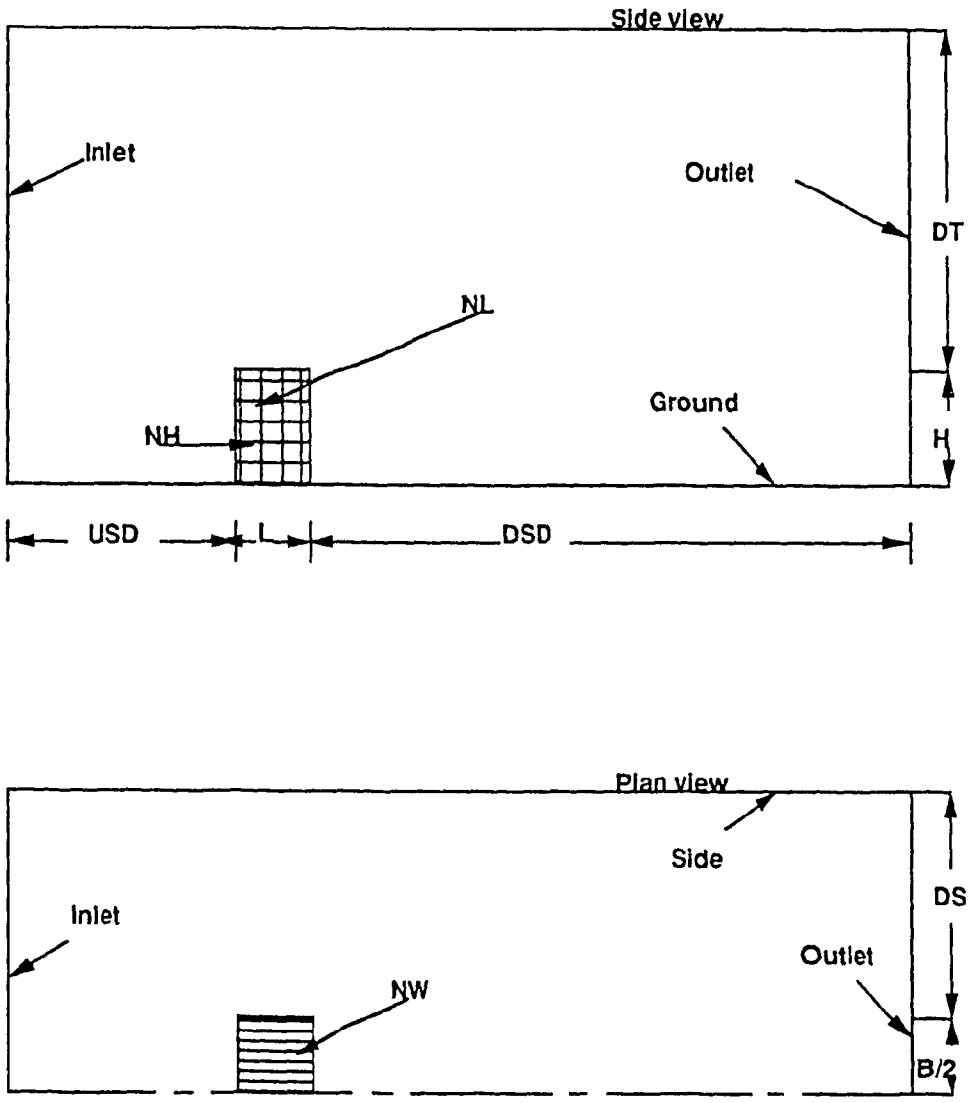

Fig. A.4.1: Parameters of the Computational Domain for Wind Flow Conditions around Buildings

The program also needs the number of velocity nodes on the computational domain for all directions. Normally, more grid nodes (NGB) are used on DSD in comparison to the other places. This will be useful to capture the recirculations and eddies. TWIST uses the following equation for the calculation of nodes for each direction.

x direction: IIMAX = 2*(NGF+NL+NGB+2),
y direction: JJMAX = 2*(NW+NGS+2) and
z direction: KKMAX = 2*(NH+NGT+2).

For computations which require more than 100*100*100 (IIMAX*JJMAX*KKMAX) nodes, the array dimensions has to be increased. This can be easily performed by changing only the "INCLUDE" files without performing changes in the main program. To make the grid distribution denser near solid boundaries, distances of the first grid node from each surface are also needed (ref: Fig. A.4.2). During this inputing, TWIST displays some constraints in order to calculate an optimum grid expansion factor.

A staggered grid arrangement is generated using the above parameters and it may be stored in a file if needed, as listed in Table A.4.2. To compute the initial flow distribution TWIST asks for the conventional parameters of power law velocity profile. These are the power -law exponent value, the free stream velocity and the boundary layer height. Calculated initial distributions can be stored in a file or the program activates Module 2 directly. The criteria for convergence are needed to terminate the iteration process. TWIST displays a set of typical optimum values that are obtained based on the sensitivity analysis carried out in this study.

Based on the above input conditions, the computation process is activated and error levels for all six variables are calculated. The error of the first iteration is used for

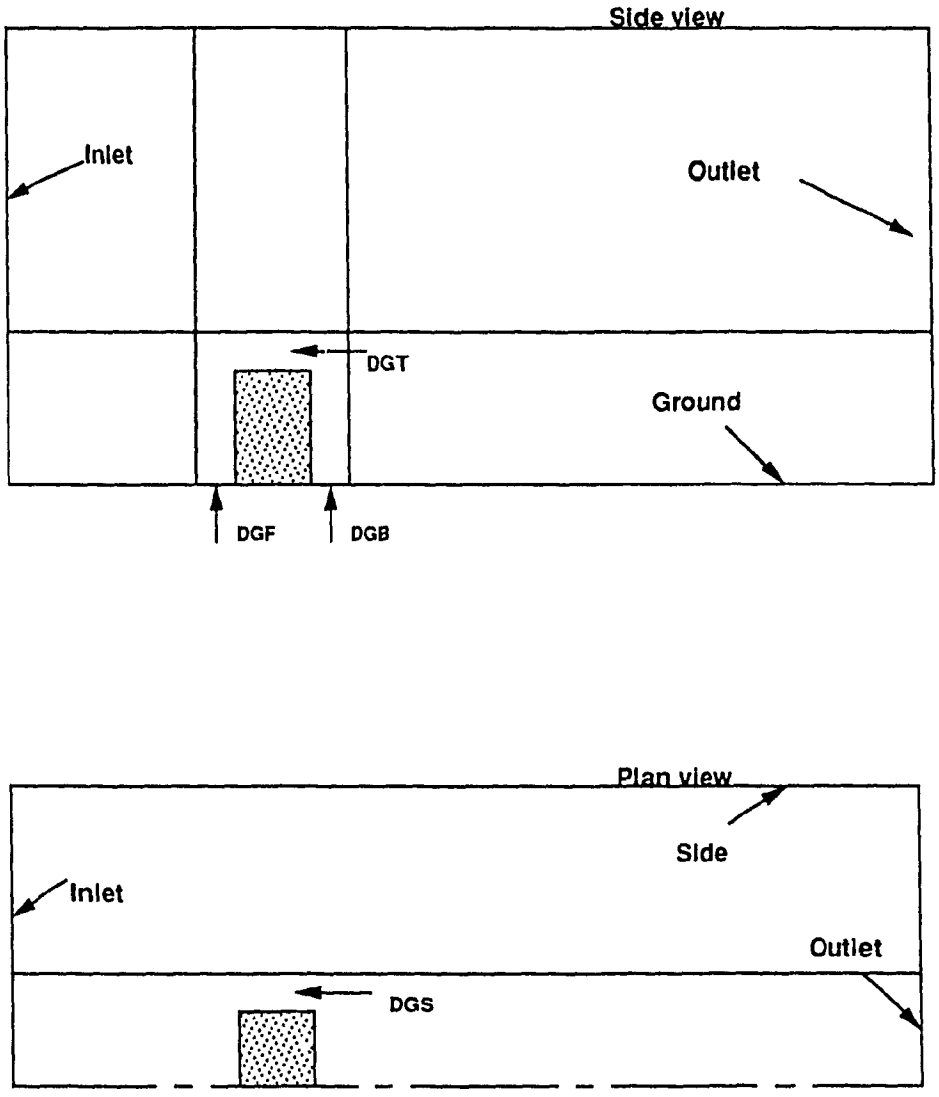

Fig. A.4.2: Distance of the First Grid Node from Solid Boundaries

IIMAX = 62 JJMAX = 26 KKMAX = 36

x coordinate

-163.811	-124.309	-100.000	-75.691	-60.731	-45.772	-36.566	-27.360
-21.694	-16.029	-12.543	-9.056	-6.911	-4.766	-3.445	-2.125
-1.312	-0.500	0.000	0.500	1.000	1.500	2.000	2.500
3.000	3.500	4.000	6.000	7.000	8.000	9.000	10.000
11.000	12.000	13.000	14.000	15.000	16.000	17.323	18.647
20.398	22.149	24.466	26.783	29.849	32.916	36.973	41.031
46.400	51.770	58.875	65.980	75.382	84.785	97.226	109.668
126.132	142.596	164.383	186.170	215.000	243.830		

y coordinate

-3.723	-1.593	0.000	1.593	2.786	3.979	4.871	5.764
6.432	7.100	7.600	8.100	8.849	9.598	10.721	11.844
13.526	15.208	17.728	20.249	24.026	27.802	33.461	39.120
47.600	56.080						

z coordinate

-2.894	-1.357	0.000	1.357	2.554	3.752	4.809	5.866
6.799	7.732	8.556	9.380	10.107	10.834	11.475	12.117
12.684	13.250	13.750	14.250	15.049	15.847	17.123	18.399
20.437	22.476	25.731	28.987	34.188	39.389	47.697	56.006
69.277	82.549	103.750	124.951				

Building Locations: 10 19 1 6 1 10

Table.A.4.2: Computed Grid Distribution Data

normalization. For each iteration, both the normalized factors and the respectively error levels are displayed. The presented test case converged after 26 iterations by taking about a minute of CPU for each iteration. Converged parameters are stored in a file for post -processing. Samples of the outputs for velocities (u, v, w), turbulence properties (k, ε) and pressure (p) are respectively given in Table A.4.3, A.4.4, A.4.5, A.4.6, A.4.7, and A.4.8.

Fig. A.4.3 shows the various options available in Module 3. These are more user friendly than the other two modules and hence easy to use. Examples of the post-processed figures for grid (Fig. A.4.4), u-velocity contours (Fig. A.4.5), turbulence intensity contours (Fig. A.4.6), velocity vectors (Fig. A.4.7) and computed pressure coefficients on the building walls (Fig. A.4.8) have also been appended. Additional technical information for TWIST is provided in Chapter 4, which contains the detailed description of the developed code.

```
      u - velocity
      k = 2
      j = 1
 6.534     6.506     6.487     6.091     5.662     4.440     2.457     0.838
 0.223     0.001     0.001     0.001     0.001     0.001     0.001     0.001
 0.001     0.001     0.001    -0.594    -1.774    -2.523    -2.834    -2.605
-1.634     0.429     1.997     3.091     4.061     5.068     6.537
      j = 2
 6.534     6.506     6.487     6.181     5.688     4.353     2.473     0.867
 0.212     0.001     0.001     0.001     0.001     0.001     0.001     0.001
 0.001     0.001     0.001    -0.567    -1.763    -2.525    -2.849    -2.628
-1.645     0.435     2.001     3.095     4.063     5.070     6.537
      j = 3
 6.534     6.506     6.494     6.198     5.733     4.513     2.750     1.154
 0.361     0.001     0.001     0.001     0.001     0.001     0.001     0.001
 0.001     0.001     0.001    -0.481    -1.645    -2.375    -2.673    -2.413
-1.280     0.820     2.177     3.237     4.190     5.183     6.537
      j = 4
 6.534     6.506     6.504     6.217     5.788     4.695     3.101     1.588
 0.615     0.001     0.001     0.001     0.001     0.001     0.001     0.001
 0.001     0.001     0.001    -0.409    -1.472    -2.128    -2.355    -1.976
-0.408     1.251     2.468     3.464     4.376     5.336     6.537
      j = 5
 6.534     6.506     6.512     6.232     5.837     4.861     3.447     2.102
 1.025     0.001     0.001     0.001     0.001     0.001     0.001     0.001
 0.001     0.001     0.001    -0.344    -1.263    -1.809    -1.918    -1.247
 0.611     1.756     2.840     3.743     4.584     5.489     6.537
```

Table. A.4.3: Samples of the Output for u-velocity

```
        v - velocity
        k = 2
        j = 4
 0.001     -0.041     0.005     0.177     0.477     1.018     1.737     2.332
 1.830      0.001     0.001     0.001     0.001     0.001     0.001     0.001
 0.001      0.001     0.636     0.606     0.356     0.188     0.002    -0.258
-0.340     -0.187    -0.096    -0.051    -0.022    -0.048     0.000
        j = 5
 0.002     -0.050     0.010     0.227     0.603     1.290     2.265     3.257
 2.933      0.001     0.001     0.001     0.001     0.001     0.001     0.001
 0.001      0.001     0.717     0.708     0.392     0.190    -0.054    -0.377
-0.418     -0.234    -0.123    -0.068    -0.031    -0.063     0.000
        j = 6
 0.002     -0.052     0.018     0.260     0.681     1.456     2.605     3.981
 4.228      0.001     0.001     0.001     0.001     0.001     0.001     0.001
 0.001      0.001     0.705     0.706     0.373     0.157    -0.139    -0.466
-0.465     -0.264    -0.140    -0.079    -0.038    -0.077     0.000
        j = 7
 0.002     -0.056     0.027     0.294     0.754     1.590     2.835     4.557
 6.705     -0.070     0.001     0.001     0.001     0.001     0.001     0.001
 0.001      0.001     0.583     0.611     0.325     0.098    -0.255    -0.552
-0.508     -0.291    -0.155    -0.089    -0.045    -0.090     0.000
        j = 8
 0.002     -0.070     0.032     0.346     0.843     1.683     2.806     3.925
 4.534      2.988     2.127     1.620     1.077     0.748     0.504     0.241
 0.061     -0.015     0.152     0.317     0.213    -0.042    -0.431    -0.650
-0.560     -0.324    -0.172    -0.099    -0.051    -0.103     0.000
```

Table. A.4.4: Samples of the Output for v-velocity

```
     w - velocity
     k = 3
     j = 1
 0.001    -0.087    -0.074     0.050     0.163     0.233     0.146    -0.579
-0.872     0.183     0.001     0.001     0.001     0.001     0.001     0.001
 0.001     0.001     0.001     0.639     0.240    -0.015    -0.181    -0.283
-0.342    -0.234    -0.160    -0.111    -0.064     0.019     0.000
     j = 2
 0.001    -0.087    -0.065     0.055     0.154     0.236     0.149    -0.573
-0.866     0.183     0.001     0.001     0.001     0.001     0.001     0.001
 0.001     0.001     0.001     0.646     0.240    -0.016    -0.185    -0.287
-0.346    -0.235    -0.159    -0.111    -0.064     0.019     0.000
     j = 3
 0.001    -0.083    -0.066     0.051     0.151     0.244     0.188    -0.471
-0.854     0.154     0.001     0.001     0.001     0.001     0.001     0.001
 0.001     0.001     0.001     0.675     0.283     0.028    -0.139    -0.223
-0.284    -0.188    -0.132    -0.092    -0.053     0.024     0.000
     j = 4
 0.001    -0.080    -0.066     0.046     0.143     0.236     0.197    -0.384
-0.847     0.106     0.001     0.001     0.001     0.001     0.001     0.001
 0.001     0.001     0.001     0.675     0.321     0.065    -0.112    -0.167
-0.211    -0.143    -0.103    -0.071    -0.040     0.030     0.000
     j = 5
 0.001    -0.078    -0.065     0.044     0.136     0.225     0.203    -0.293
-0.788     0.066     0.001     0.001     0.001     0.001     0.001     0.001
 0.001     0.001     0.001     0.645     0.348     0.092    -0.106    -0.140
-0.160    -0.113    -0.083    -0.057    -0.031     0.035     0.000
```

Table. A.4.5: Samples of the Output for w-velocity

```
     k - kinetic energy
     k = 1
      j = 1
0.576      0.565      0.524      0.389      0.067      0.071      0.235      0.321
0.088      0.000      0.000      0.000      0.000      0.000      0.000      0.000
0.000      0.000      0.103      0.413      0.414      0.412      0.375      0.145
0.050      0.420      0.533      0.564      0.575      0.578      0.578
      j = 2
0.576      0.094      0.089      0.085      0.090      0.106      0.132      0.166
0.182      0.180      0.000      0.000      0.000      0.000      0.000      0.000
0.000      0.000      0.179      0.065      0.074      0.084      0.099      0.114
0.117      0.101      0.092      0.089      0.088      0.093      0.578
      j = 3
0.576      0.094      0.089      0.087      0.096      0.123      0.159      0.186
0.214      0.214      0.000      0.000      0.000      0.000      0.000      0.000
0.000      0.000      0.214      0.067      0.078      0.094      0.112      0.129
0.126      0.108      0.099      0.094      0.091      0.093      0.578
      j = 4
0.576      0.094      0.089      0.087      0.096      0.125      0.167      0.197
0.239      0.239      0.000      0.000      0.000      0.000      0.000      0.000
0.000      0.000      0.239      0.067      0.085      0.110      0.132      0.142
0.133      0.117      0.106      0.099      0.093      0.094      0.578
      j = 5
0.576      0.094      0.089      0.086      0.094      0.124      0.173      0.215
0.259      0.259      0.000      0.000      0.000      0.000      0.000      0.000
0.000      0.000      0.259      0.074      0.099      0.130      0.150      0.151
0.138      0.124      0.111      0.101      0.093      0.093      0.578
```

Table. A.4.6: Samples of the Output for Kinetic Energy

ϵ - dissipation rate of k

k = 3

j = 1

0.056	0.121	0.110	0.106	0.130	0.211	0.368	0.665
0.803	0.347	0.139	0.060	0.035	0.026	0.021	0.019
0.190	0.308	0.388	0.102	0.100	0.132	0.188	0.256
0.256	0.183	0.146	0.131	0.122	0.132	0.057	

j = 2

0.056	0.121	0.110	0.105	0.129	0.210	0.368	0.666
0.774	0.764	0.000	0.000	0.000	0.000	0.000	0.000
0.000	0.000	0.765	0.132	0.101	0.132	0.189	0.256
0.256	0.184	0.146	0.130	0.121	0.131	0.057	

j = 3

0.056	0.121	0.110	0.109	0.148	0.283	0.539	0.865
1.119	1.118	0.000	0.000	0.000	0.000	0.000	0.000
0.000	0.000	1.118	0.152	0.121	0.181	0.264	0.341
0.310	0.219	0.172	0.146	0.129	0.133	0.057	

j = 4

0.056	0.121	0.110	0.108	0.147	0.294	0.610	0.998
1.479	1.479	0.000	0.000	0.000	0.000	0.000	0.000
0.000	0.000	1.479	0.176	0.164	0.268	0.382	0.432
0.360	0.262	0.201	0.162	0.135	0.133	0.057	

j = 5

0.056	0.121	0.110	0.107	0.142	0.287	0.668	1.212
1.846	1.846	0.000	0.000	0.000	0.000	0.000	0.000
0.000	0.000	1.846	0.227	0.248	0.391	0.511	0.501
0.398	0.296	0.222	0.171	0.135	0.131	0.057	

Table. A.4.7: Samples of the Output for Dissipation Rate of k

```
      p - pressure
      k = 1
      j = 1
-0.443    -0.443     3.814     7.758    10.833    17.292    23.878    26.622
27.122    -5.708     0.000     0.000     0.000     0.000     0.000     0.000
 0.000     0.000    -9.104   -10.368   -11.881   -12.298   -10.906    -7.544
-3.809    -1.499    -1.158    -1.209    -1.041    -1.426    -1.426
      j = 2
-0.443    -0.443     3.814     7.758    10.833    17.292    23.878    26.622
27.122    -5.708     0.000     0.000     0.000     0.000     0.000     0.000
 0.000     0.000    -9.104   -10.368   -11.881   -12.298   -10.906    -7.544
-3.809    -1.499    -1.158    -1.209    -1.041    -1.426    -1.426
      j = 3
-0.427    -0.427     3.785     7.619    10.456    16.361    22.368    24.981
25.545    -4.243     0.000     0.000     0.000     0.000     0.000     0.000
 0.000     0.000    -9.439   -10.623   -12.052   -12.452   -11.049    -7.641
-3.871    -1.533    -1.192    -1.228    -1.052    -1.419    -1.419
      j = 4
-0.409    -0.409     3.747     7.440     9.971    15.075    19.900    21.733
22.218    -3.020     0.000     0.000     0.000     0.000     0.000     0.000
 0.000     0.000    -9.953   -10.968   -12.260   -12.638   -11.226    -7.741
-3.917    -1.583    -1.231    -1.250    -1.065    -1.409    -1.409
      j = 5
-0.395    -0.395     3.707     7.269     9.521    13.846    17.300    17.523
17.161    -2.334     0.000     0.000     0.000     0.000     0.000     0.000
 0.000     0.000   -10.439   -11.260   -12.421   -12.787   -11.379    -7.815
-3.939    -1.635    -1.266    -1.269    -1.076    -1.397    -1.397
```

Table. A.4.8: Samples of the Output for Pressure

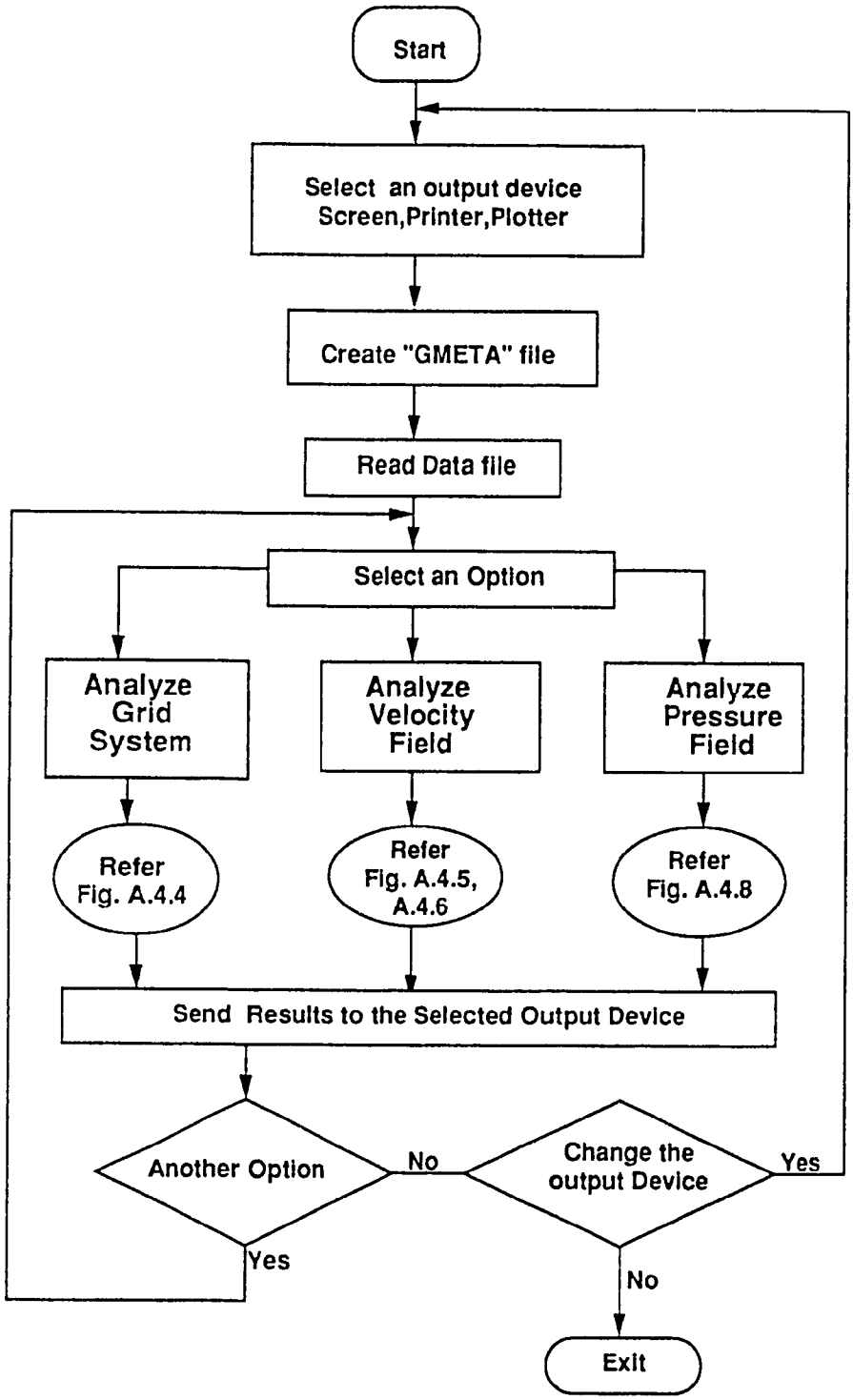

Fig.A.4.3: Available Options for Post-Processing the Numerical Output

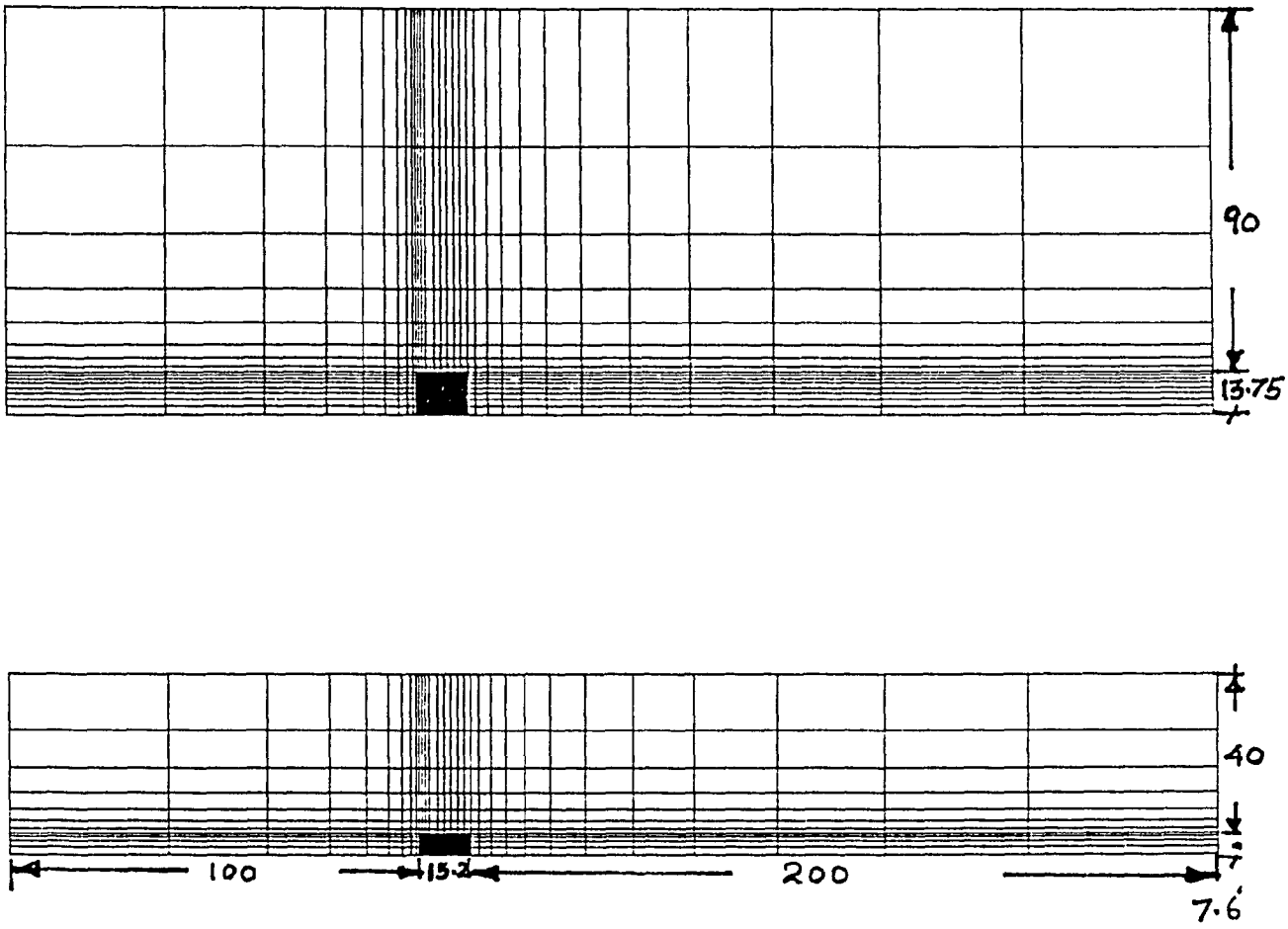

Fig. A.4.4: Post-Processed Views of the Grid Arrangement

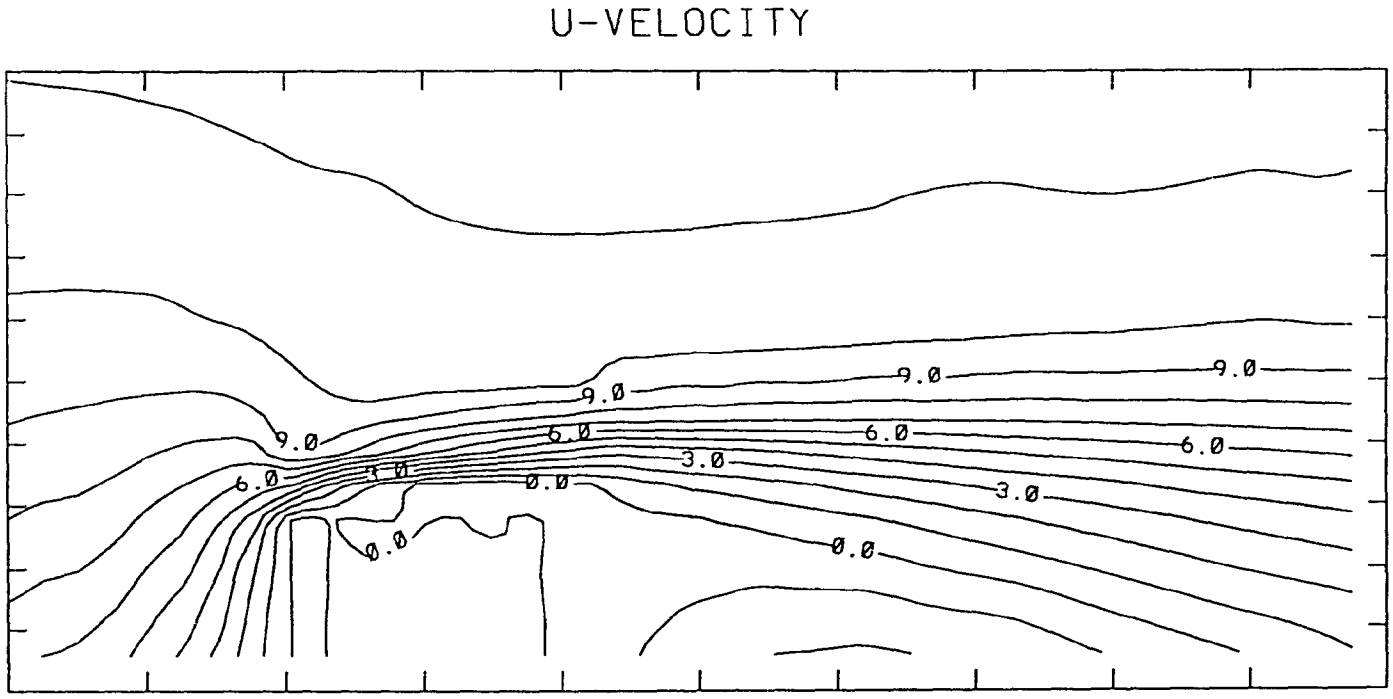

A.4.5 Contour Plots of the u Velocity Values after Post-Processing

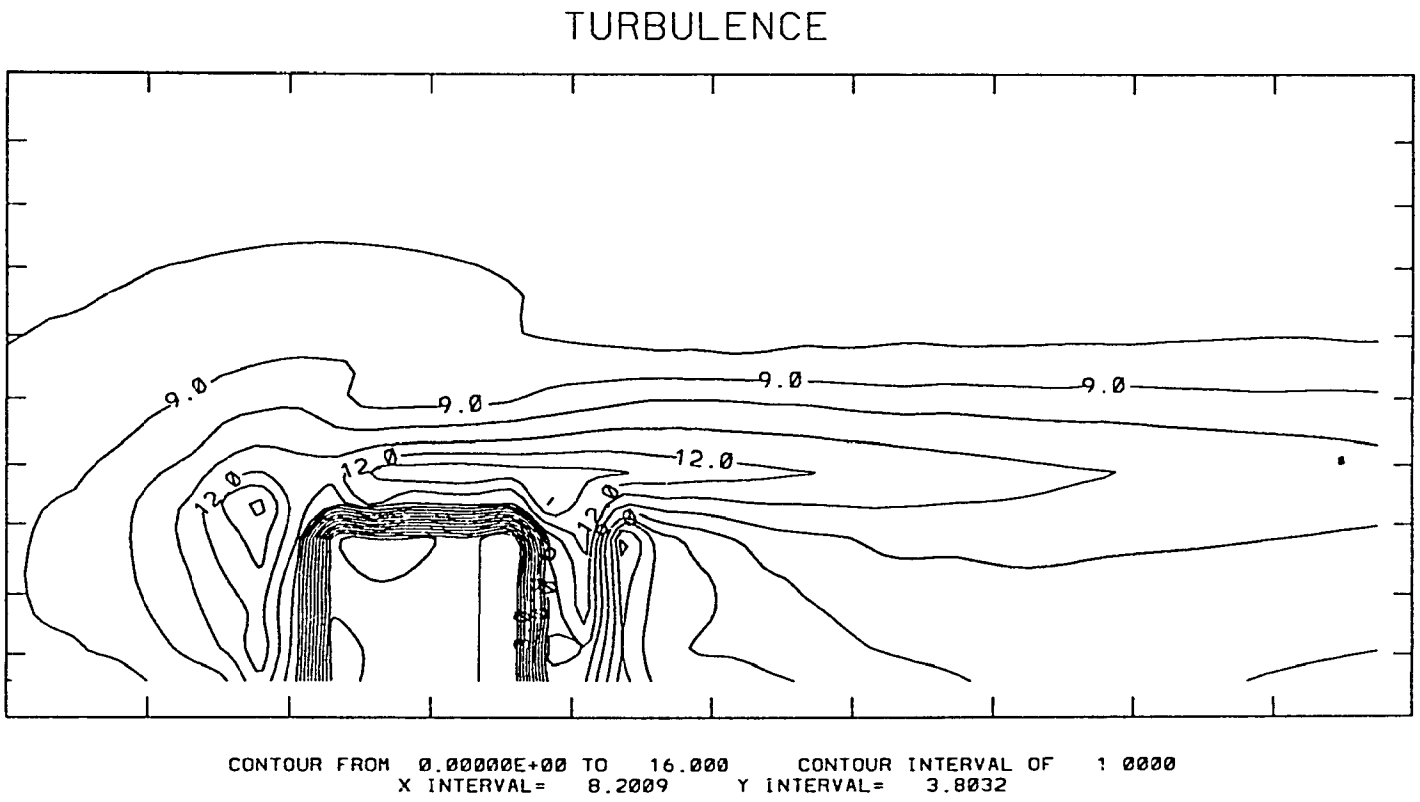

Fig A.4.6: Contour Plots of the Turbulence Intensity Values after Post-Processing

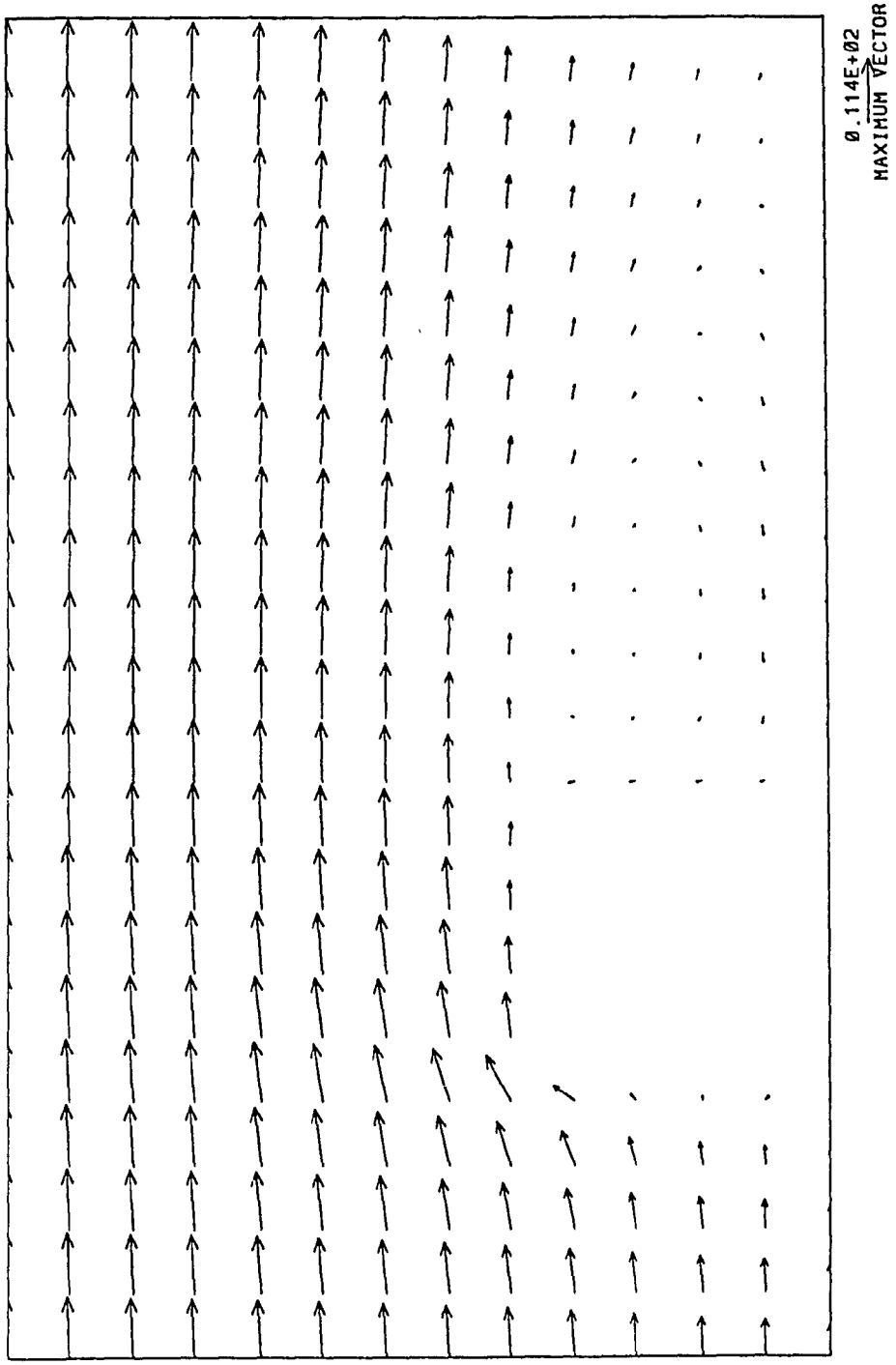

Fig. A.4.7: Vector Plots of the Post-Processed u and w Velocity Components

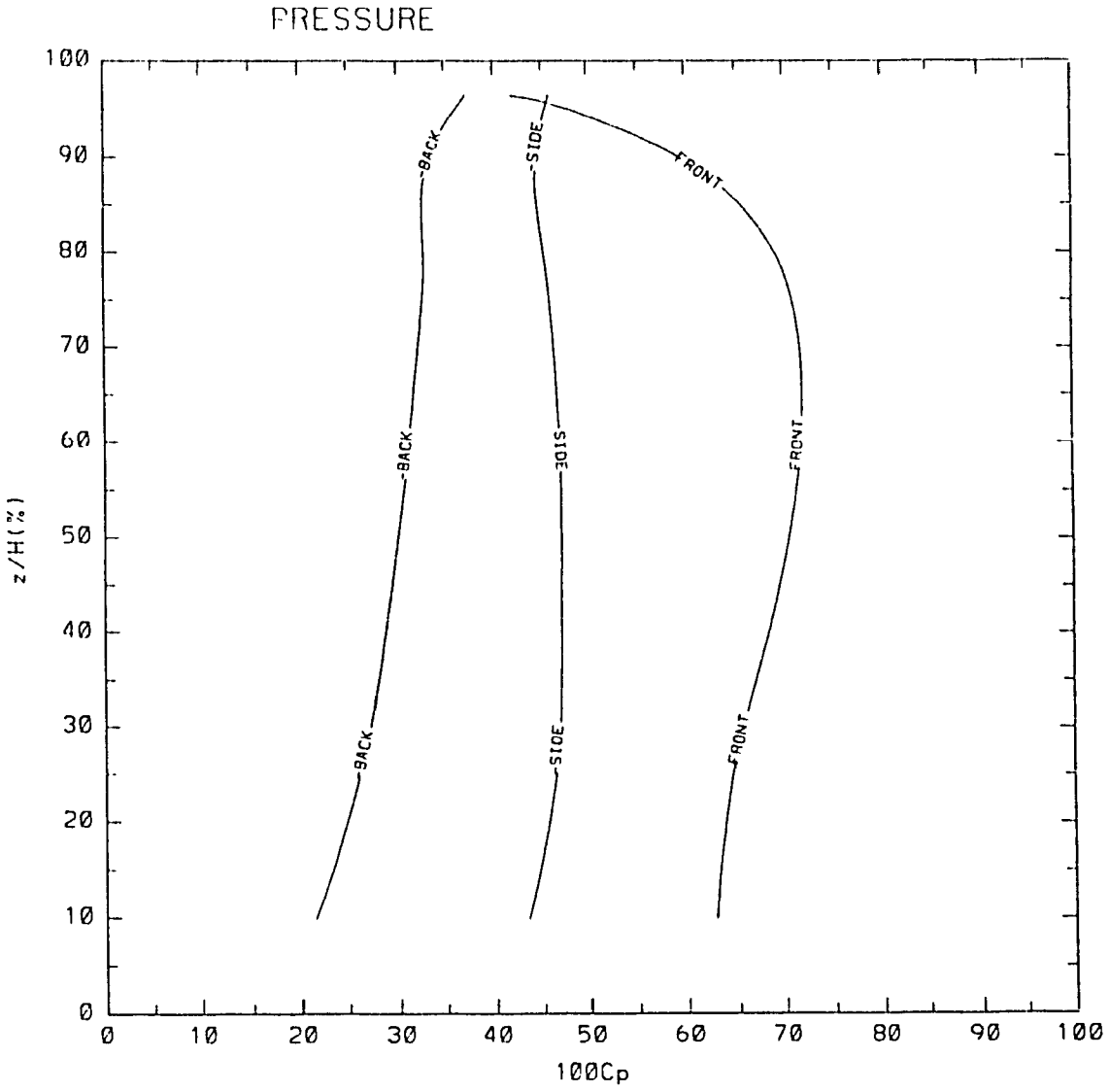

Fig.A.4.8: Post-Processed Pressure Coefficient Values on the Building Envelope